UNIVERSITAT DE BARCELONA

Polycomb and KDM6A Roles in the Epigenetic Dynamics of Ewing Sarcoma Tumorigenesis

Elisabet Figuerola Bou

Universitat de Barcelona

Facultat de Medicina

Doctoral Programme in Biomedicine

Polycomb and KDM6A Roles in the Epigenetic Dynamics of Ewing Sarcoma Tumorigenesis

Dissertation submitted by:

Elisabet Figuerola Bou

This work was performed at the Developmental Tumor Biology Laboratory of Institut de Recerca Sant Joan de Déu (IRSJD) from Hospital Sant Joan de Déu, under the supervision of Jaume Mora, M.D. Ph.D. and Sara Sánchez Molina, Ph.D.

Thesis directors:
Jaume Mora, M.D. Ph.D.
Sara Sánchez Molina, Ph.D.

Thesis tutor:
Neus Agell Jané, Ph.D.

The author:
Elisabet Figuerola Bou

Barcelona, September 2019

"Science and art have that in common that the most ordinary, everyday thing appears to it as something entirely new and attractive, as if metamorphosed by witchcraft and now seen for the first time. Life is worth living, says art, the beautiful temptress; life is worth knowing, says science."

Friedrich Nietzsche

Als meus pares,
A la meva àvia,
A en Joan
I a en Fede.

Acknowledgements

Aquesta és la part que quan vaig començar a escriure la tesis tenia més ganes de fer. Tenia tantes coses a dir que hagués sigut el primer que hagués escrit de la tesis, però vaig pensar que seria molt agosarat començar per aquí. Així que ho vaig deixar per lo últim que escrivís de la tesis i ara, la veritat, em costa molt més que escriure la primera pàgina de la introducció! Perquè no és senzill resumir en un parell de pàgines, tot l'agraïment que tinc cap a la gent que ha contribuït, tant en lo bo com en lo dolent, en el que per mi ha estat aquest llarg aprenentatge, tant a nivell personal com a nivell professional. Dic també en lo dolent, perquè òbviament durant tant de temps n'hi ha hagut d'una de freda i una de calenta, però sóc de les que pensa que també de lo dolent (o del que en un moment concret a un li sembla com a dolent), en surten coses bones que t'empenyen a seguir creixent com a persona.

L'aventura de la tesis per mi va començar amb una de dolenta (en aquell moment, més que dolenta, era com una catàstrofe) i semblava que l'oportunitat de fer la tesis a l'Hospital Sant Joan de Déu era un "xute" d'il·lusió, que era el que em faltava. Per això Jaume i Inma us agrairé sempre que confiéssiu en mi per ser la primera pre-doc del grup de sarcoma d'Ewing. Ara acabo de recordar la Carmen referint-se carinyosament al nostre grup com a "sarcomatoses"; Jaume, durant aquests anys ens has transmès la teva passió a totes i cadascuna de les nostres reunions del divendres i, personalment, t'ho agraeixo moltíssim perquè m'ha donat una visió molt més propera d'aquestes malalties que si hagués estat en qualsevol altre grup de càncer. Després va venir l'Estela al grup i ens va ensenyar de rhabdo i de que era possible passar-se 12 hores al lab amb 4 viatges anar i tornar (en metro) del PRBB. Gracias por todo el cariño y enseñarme que se pueden hacer Western blots cuádruples, extracciones de 50 muestras a la vez y trabajar en el estabulario aun teniendo alergia a los ratones. I per últim, el Pablo i la Maria, que a vegades em feu pensar que potser (només potser) tornaria a començar la tesis si us tingués a vosaltres de companys! Mi Precious, tu siempre tan salá, cuando llegaste fue un flechazo, todo fueron corazones, abrazos y porqué te tengo puesto el freno, que sino… Gracias por ayudarme TANTO, la verdad es que me cuesta mucho imaginar este último año sin el elemento Precious en mi vida. I del grup de Ewing només em queda la Sara, que tendré suerte si cuando abras la tesis no le ves ningún fallo y cuando leas esto no te pones a llorar. Aún me acuerdo cuando te conocí en el PRBB para traerme unas muestras de Hela para hacer extractos de histonas con el kit… desde ese día has sido como una madre en mayúsculas, una amiga, una compañera... Nos hemos hecho un hartón de reír, nos hemos enfadado, hemos llorado, pero, eso sí, no he tocado nunca tu barriga de embarazada (gracias a Dios). Recuerdo llamadas a las 12 de la noche, mandarte audios en inglés en días previos a exposiciones, discusiones tratándome de convencer de algo y acabando con "haz lo que te dé la gana que lo harás igualmente", compartir cafés (es decir, un café partido en dos), virus (de

guardería, que no del laboratorio!), comidas cuando los demás ya hacía una hora que habían ido al bar, ralladas científicas, descomposiciones, ideas, etc etc etc.. Y paro porque si me pongo enserio podría escribir todo un apartado entero de agradecimientos para ti. Ya solo por las tropocientasmil rondas de correcciones que has hecho, te mereces todas las tabletas de chocolate del mundo.

És impossible imaginar aquesta tesis sense el disco ratllat meu taladrant el cap de tothom (i sobretot l'últim any). Des de les amigues d'en Joan, fins als grupis del lab. Fins i tot hi ha algú que diu que el primer any de tesis ja estava taladrant, eh Sole? Yo creo que soy el individuo perfecto para que hagas una segunda tesis sobre "trastornos de la anticipación en el individuo". Gracias por estar siempre ahí desde el minuto 0, cuidándome entre análisis supervisados y no supervisados, porque ¡Ay Sole! (nótese el aire gipsy) has acogido decenas de veces al husky a tu refugio. Le has preparado tuppers, tazas de cola cao, te lo has llevado a la playa, a tus fiestas de cumple, de exposición, a tomar té, de viaje,… y todo esto viniendo de una persona tan antisocial, es todo un privilegio. Mil gracias por todo el apoyo estos años. A mi Isadora (siempre me acordaré que tenía un maquillaje llamado así) que es de lo mejorcito del laboratorio, ya sabes que todos mis Chips aparte de para mí son para ti. Mientras me has enseñado a cuidar a tus niñas también me has cuidado a mí (científica y no científicamente) hasta convertirme en un saltamontes adulto, ¡gracias! Lo de espiralar tesis (yo ya lo he bautizado así) ya es tu segundo oficio, ¡mil gracias! Al meu pollito, que veig com passen els anys per culpa de veure com ell es fa gran. Amb els teus consells viejoven m'has ajudat sempre. Has sigut més que una companya de despatx, una amiga i una bioinfo excel·lent que sé que arribarà molt lluny. A la Mònica, gràcies per unir-nos a tots una mica més amb totes les calçotades i barbacoes a Can Vilà. Gràcies per agafar-me les videollamadas urgents del estabulari, per no trencar-te el genoll al camino (a casa teva em penjarien com pengen als porcs!) i per no tornar a casa amb bicing la nit que vam celebrar el meu 27è cumple (si sabessin això últim potser faria que no em pengessin). A la Marta, per tot el teu suport i per ensenyar-me que és possible ser trimare, cambrera i la més jefaza científica. Gràcies també per posar el Tr@mendu com a punt de trobada. T'admiro moltíssim. Al Carlos, perquè si Déu existeix li hauria de concedir el privilegi del paradís amb exclusivitat masculina. A pesar de no compartir las mismas ideas políticas ni futbolísticas, te admiro y te compadezco por todo lo que has pasado estos años escuchando por partida doble (desayuno y comida) nuestras charlas femeninas y mis dramas. Te has sincronizado seguro con nuestra regla. A la Sonia per encarregar-se de vetllar dels experiments de tots impulsant un potentíssim protocol antifúngic al lab i per encara no haver-me fet cap bronca com a labmanager. A la Merceritas perquè només per ser de Vic ja em vas caure bé; és broma, ets una tia collonuda que, tal com he dit amb el Pablo i la Maria, em fa ràbia no començar la tesis ara per tenir-vos de companys. En definitiva, només per tots vosaltres, compartiria les meves croquetes (i en el fons, molt en el fons, ho sabeu).

A les meves xinxes, que sé que estan allà pel que faci falta. A la Sílvia i a l'Aina per cuidar-me sempre als estius i cada vegada més a l'hivern. A la Paula parisina, que em fa riure i té unes idees tant genials com la de la portada d'aquesta tesis; a la Marina, a la meva altra Paula. A la Nona i a la Magalí, per portar-me a airejar a la natura quan més ho he necessitat. A mi canaria favorita que tengo presente siempre, Elo. Aunque con Fani nos encanta coger un avión y venir a verte a Münster (y por supuesto vendremos a verte en el día de tu tesis), nos morimos de ganas de que vuelvas otra vez a Barcelona. A les #thankyoulinus (Ru, Merichel, Alba, Olga) per les seves noshelocas. Al meu estimat Víctor de la casa dels Hannover i príncep d'Estrasburg, per tot el seu suport abans, durant i sempre. Per intentar que no perdés mai el somriure durant l'escriptura, gràcies de veritat. Als millors amics de la uni que un pot tenir, gràcies per tots els sopars de retrobament de nadal, per tots els riures, amics invisibles, etc. Per ensenyar-me que per molt lluny que estiguem i per molt de temps que passi hi ha coses que mai canvien. A la Fani, la meva companya de viatges, tiberis, penes i glòries, rallades pre-tesis i sé que també post-tesis, la meva amiga incondicional amb la que tant puc parlar de ChIPs com de plantes. El millor que em vaig endur del PRBB. M'encanta haver pogut compartir l'aventura de la tesis amb tu. A les amigues d'en Joan, per escoltar-me atentament explicant mil vegades tot lo de la tesis, en especial a l'Andrea, per la seva assistència durant tot l'embaràs i al part. No saps lo imprescindible que t'has tornat. La meva Tuca i Mel, companyes fidels d'escriptura de la tesis, seminaris, divagacions... els meus ratolinets Jak i Gus, les meves nenes més guapes del món. El meu tamagotchi o telehuevo A2 que m'ha acompanyat durant 10 anys. La meva Kymko, que m'ha donat molta vitallity. Volia acabar la tesis amb els 30.000 km i a hores d'ara encara me'n queden 1000 km per endavant, potser el dia que la llegeixi hi hauré arribat.

Me'n recordo també dels primers passos pel lab, quan era una pequeña saltamontes, com deia la Isa, i de tota la gent que ha anat marxant i arribant nova. La Carmen, la Gemma, el Carles, el Guillem, l'Israel, la Rita, el David, la Txus, el Jose, la Gema, de cadascun d'ells en guardo un bon record. Dels estudiants que he tingut algun estiu, com els bessons més aplicats del món, els Anglada, on amb ells vam veure per primer cop que el MLN4924 tocava el RING1B i pensàvem que era un error de càrrega al Western; la Carla, la meva estudiant gironina que sempre em veia amunt i avall cap al parc científic i feia sempre el possible per ajudar amb els ditxosos MTS. Tots junts hem après molt! També del recolzament amb perspectiva de les Kris Kross (Jump jump!) ha sigut fonamental, gràcies pels consells, cafès, adopcions a l'hora de dinar i d'aguantar-me el rotllo!

Gràcies a tots els membres de l'AECC, en especial a en Dani i la Lourdes, gracias por todo lo que habéis hecho por mí, vuestro punto de vista en determinados momentos de la tesis ha sido fundamental. A Simona y a Stela del grupo de Marian del CSIC por haberme tratado tan bien cuando vine a hacer los experimentos de infecciones de las mesenquimales, y por supuesto a Marian por dejarme ir y por su apoyo científico en todo momento. A tots els

membres d'algun servei científic de Barcelona, que ara sembla com si els hagués patejat tots, per tots els consells, al Jaume Comas, al Nacho Pons, la Raquel Rasal, la Mònica Roldan, i segur que em deixo algú. Als bioinfos, tant de bo sabés (i m'agradés) programar! Però llavors seria tot massa senzill no? La vostra feina en aquesta tesis ha estat fonamental. Gràcies òbviament a la Sole, en especial a en Pol, per la teva total implicació, ajudar-me en moments que anaves a tope, moltes gràcies ho valoro moltíssim i sé que arribaràs molt lluny. Enrique, només et puc dir gràcies, hi ha una bona part de la tesis que sense tu no hagués estat possible.

I el que diré ara és algo que només entendran els del mundillo bio-something i que devem tenir en els gens, però no puc no posar un gràcies també a tot el menjar que bonament algú ha portat al lab en aquests anys. Aquí voldria retre un especial homenatge als tiramisús de la Cinzia, espectaculars. Però també no podem deixar de banda les tones de xocolata, les galetes bombes de la Sole (a veure si aquests agraïments de la tesis serveixen perquè en torni a fer; ahí lo dejo), les botifarres d'ou de la Mònica, els pastissos d'aniversari, les harepas del Carlos, les CROQUETES, l'artemisa, les santes amanides del LIDL, la botifarra congelada-escalfada al microones i barrejada en salsa de tomàquet que no em va matar, etc.

A en Joan perquè ho diré clar i català, sigui el què sigui, tu has estat en gran part d'aquesta història. Les has vist de tots colors i sempre m'has recolzat i el més important, m'has fet riure. La calma que m'has transmès en determinats moments ha sigut clau. Encara que no entenguis (o més aviat no vulguis entendre) de nucleosomes o del RING, aquesta tesis també l'has fet tu i poder compartir les rallades i no tant rallades amb tu ha significat molt per mi. Gràcies també a la Carme, per la seva creativitat, i també a en Joan i a la Berta per escoltar els "rollos" de la tesis.

Als meus pares i a la meva àvia per cuidar-me tant, ja sigui fent tuppers (és del millor que algú pot fer per mi), trucar-me per saber com estic... Papa encara que tot el dia em preguntis on vaig, amb qui estic, si vaig amb moto si no, fins al punt d'arribar a ser pesat, gràcies per preocupar-te tant per mi. Mama, aquest perfeccionisme, aquesta persistència i motivació si els he heretat d'algú només podia ser de tu. M'inspires tot això i mil coses més. Aquesta tesis també és una part teva. Pere, si algú em va fer tirar cap a una carrera científica aquest vas ser tu segur. Les nostres inacabables xerrades sobre el per què de les coses han fet que avui hagi escrit una tesis. Àvia, a part d'alimentar-me m'has cuidat molt. Sé que no vols venir perquè no entendràs res però em faria molta il·lusió que vinguessis a la defensa de la tesis! Sé que tots esteu molt orgullosos i us estimo molt. Fede, no pots arribar-te a imaginar lo MOLT que m'has ajudat amb el disseny de la tesis. Mil gràcies. Us estimo molt a tots.
Per últim i com deia al començament, normalment la part freda va acompanyada d'una

calenta. Doncs a la part calenta, a part d'haver-hi la gent i tots els bons moments que m'han acompanyat aquests anys, hi ha tot l'aprenentatge que cada dia ens transmeten les famílies. A ells els vull donar les gràcies i també als voluntaris, crec que no es coneix prou la feina que feu (jo la primera) i em considero molt afortunada d'haver-ho pogut veure. A la Mireia Espinet i totes les persones del Hospital, per la seva implicació que m'ha ajudat a fer possible una idea tant boja com va ser fer la portada de la tesis. Però sobretot, sobretot, el meu agraïment a l'Estela, per tots la mare d'en Pol, i fa poquet la Laura, la mare de l'Albert. Gràcies per ensenyar-nos que d'una part molt freda en pot sortir una de preciosa com són, per exemple, les curses de la Nit de la Lluna Plena, o tots els actes que organitzeu des de xocolatades solidàries, curses populars, trobades com la del Vi solidari, etc. Gràcies per ensenyar-me que no s'ha de perdre mai la il·lusió. És impressionant TOT el que arribeu a moure. Ens feu pensar que si les dones movem el món som imparables. I em considero molt afortunada d'haver-ho pogut viure aquests anys. I per últim als nens de la planta d'oncologia que amb tota la vostra il·lusió al mes de setembre heu posat el vostre gra de sorra a la tesis amb els vostres dibuixos del que a mi m'inspira un nucleosoma. Aquesta paraulota que per a vosaltres pot arribar a significar un ànec, però d'això es tracta l'art i, de passada la ciència, que està en un racó de la imaginació de cadascú. Gràcies de tot cor Ana, Dario, Jan, Javier, Maria Elisa, Nerea...

TABLE OF CONTENTS

LIST OF FIGURES

I. INTRODUCTION

III. MATERIALS AND METHODS

IV. RESULTS

V. DISCUSSION

LIST OF TABLES

I. INTRODUCTION

III. MATERIALS AND METHODS

LIST OF ABBREVIATIONS

ALL	Acute Lymphoblastic Leukaemia
AML	Acute Myeloid Leukaemia
AMP	Adenosine Monophosphate
ATM/ATR	ATM / ATR Serine/Threonine Kinase
ATP	Adenosine Triphosphate
AYA	Adolescence And Young Adults
BET	Bromodomain And Extra Terminal Domain
BRD	Bromodomain
BSA	Bovine Serum Albumin
CGI	CpG Island
CHD	Chromodomain Helicase DNA Binding Domain
ChIP	Chromatin Immunoprecipitation
ChIP-seq	Chromatin Immunoprecipitation Sequencing
COMPASS	Complex Proteins Associated With Set1
CpG	Cytosine Guanine dinucleotide
CRL	Cullin Ring Ligase
CT	Computed Tomography
D	Aspartate Aminoacid
DDR	DNA Damage Response
DEG	Differentially Expressed Genes
DIPG	Diffuse Intrinsic Pontine Glioma
DLBCL	Diffuse Large B Cell Lymphoma
DPX	Dibutylphthalate Polystyrene Xylene
DUB	Deubiquitinating Enzymes
DZNep	3-Deazaneplanocin A
E	Glutamate Aminoacid
EAD	EWSR1 Transactivation Domain
ES	Ewing Sarcoma
ESC	Embryonic Stem Cell
ETS	Erythroblast Transformation-Specific
EXIT	Escape From X-Chromosome Inactivation
FAD	Flavin Adenine Dinucleotide
FBS	Fetal Bovine Serum
FC	Fold Change
FDG-PET	Fluorine-18-Fluorodeoxyglucose Positron Emission Tomography
FISH	Fluorescence In Situ Hybridization
GH	Growth Hormone
GO	Gene Ontology
H	Histidine Aminoacid
H&E	Haematoxylin and Eosin

HAT	Histone Acetyltransferases
HDAC	Histone Deacetylases
HDM	Histone Demethylases
HECT	Homologous To E6-AP Carboxy Terminus
HFD	Histone Fold Domain
HMT	Histone Methyltransferases
hpMSC	Human Paediatric Mesenchymal Stem Cells
HUVEC	Human Umbilical Vein Endothelial Cells
ICP	Infancy Childhood-Puberty model
IGF	Insulin-Like Growth Factor
IHQ	Immunohistochemistry
iPSC	Induced Pluripotent Stem Cells
iRNA	Interference RNA
JmjC	Jumonji C
K	Lysine Aminoacid
LDH	Lactate Dehydrogenase
lncRNA	Long Non-Coding RNA
MBD	Methyl-Cpg Binding Domain
miRNA	Micro RNA
MRD	Minimal Residual Disease
MRI	Magnetic Resonance Imaging
mRNA	Messenger RNA
MSC	Mesenchymal Stem Cells
NAD	Nicotinamide Adenine Dinucleotide
NAE	Need-8 Activating Enzyme
NB	Neuroblastoma
NCI	National Cancer Institute
ncRNA	Non-Coding RNA
NCSC	Neural Crest Stem Cells
NuRD	Nucleosome Remodelling And Deacetylase Complex
OGS	Osteogenic sarcoma or Osteosarcoma
OS	Overall survival
PARP	Poly ADP-Ribose Polymerase
PBS	Phosphate Buffered Saline
PcG	Polycomb Group Complex
PCR	Polymerase Chain Reaction
PdX	Patient-derived Xenograft
PFA	Paraformaldehyde
PNET	Peripheral Primitive Neurectodermal Tumour
PRC	Polycomb Repressive Complex

PRE	Polycomb Responsive Elements
PTM	Post-Translational Modification
qPCR	Quantitative PCR
R	Arginine Aminoacid
RING	Really Interesting New Gene
RMS	Rhabdomyosarcoma
RNAPII	RNA Polymerase II
rRNA	Ribosomal RNA
RT	Reverse Transcriptase or Retrotranscriptase
RT-qPCR	Quantitative Reverse Transcription PCR
S	Serine Aminoacid
SAH	S-Adenosyl-L-Homocysteine Hydrolase
SAM	S-Adenosyl Methionine
SEM	Standard Error Of The Mean
SET	Su(Var)3-9, Enhancer Of Zeste, Trithorax
shRNA	Short Hairpin RNA
siRNA	Short Interfering RNA
SIRT	Sirtuin
snoRNA	Small Nucleolar RNA
snRNA	Small Nuclear RNA
SS	Synovial Sarcoma
SWI/SNF	Switch/Sucrose Non-Fermentable Complex
T	Threonine Aminoacid
T-ALL	T-Cell Acute Lymphoblastic Leukaemia
TCGA	The Cancer Genome Atlas
TET	Ten-Eleven Translocation
TF	Transcription Factor
TPR	Tetratricopeptide
tRNA	Transfer RNA
TrxG	Trithorax Group Complex
TSS	Transcription Start Site
UBD	Ubiquitin-Binding Domains
UBL	Ubiquitin-Like Protein
UPS	Ubiquitin Proteasome System
VDC	Vincristine, Doxorubicin And Cyclophosphamide
VID	Vincristine, Ifosfamide And Doxorubicin
VIDE	Vincristine, Ifosfamide, Doxorubicin And Etoposide
WHO	World Health Organization
XLID	X-Linked Intellectual Disability
Y	Tyrosine Aminoacid

SUMMARY

Ewing sarcoma (ES) is a highly aggressive tumour of the bone and soft tissue that typically affects children, adolescents, and young adults. The fusion protein EWSR1-FLI1 is the main genetic alteration found that acts as a pioneer factor during early ES tumorigenesis. EWSR1–FLI1 binds GGAA microsatellites causing remodelling of enhancers and genome reprogramming. Among the proteins cooperating with EWSR1-FLI1 at enhancers, our group has described that the Polycomb subunit RING1B co-localizes genome-wide and promotes oncogene recruitment and transcriptional activation of key enhancer genes.
In this thesis, we show that RING1B is a critical factor for ES tumour growth and, together with other E3 ubiquitin ligases, is deregulated by the neddylation pathway inhibitor MLN4924 (pevonedistat). Treatment of ES cell lines with the inhibitor promotes RING1B loss from EWSR1-FLI1–activated targets as well as eviction of EWSR1-FLI1, thereby deregulating gene expression. Lack of neddylation caused by the drug appears to be the mechanism behind the in vitro and in vivo degradation of RING1B.

We also study how introduction of EWSR1-FLI1 to a putative cell-of-origin deregulates distribution of the histone repressive mark H3K27me3. Although the global levels of this histone modification are maintained, we observe a perturbed distribution. Specifically, gain or loss of H3K27me3 occurs in some EWSR1-FLI1–repressed or –activated regions, respectively, which coincide with enrichment of its writer, EZH2, and its eraser, KDM6A, in a transformed ES cell line. Finally, we demonstrate that targeting the tumorigenic distribution of H3K27me3 by combined inhibition of EZH2 (with GSK126) and KDM6A (with GSKJ4) causes a synergic cytotoxic response in ES cell lines.

Altogether, our data provide further insight into the epigenetic mechanisms underlying EWSR1-FLI1–mediated transformation and reveal new targets for future clinical trials.

I. INTRODUCTION

1. A BRIEF INTRODUCTION TO PAEDIATRIC CANCER

1.1 Definition

The term paediatric cancer has classically referred to a heterogeneous group of solid and haematological neoplasms occurring predominantly during childhood. However, this is a wide period of life, which spans from birth to adolescence. We and others have proposed the designation of these tumours as developmental cancer from a biologically-oriented definition, as these tumours arise during, and as a consequence of, the complex process of development of an individual (Mora, 2012). Due to the terminological disparities in the field, many epidemiological studies have restricted paediatric cancer to children aged 0–14 years. It was not until two years ago that a more extended worldwide study was published that included the 15–19 year age group (Steliarova-Foucher et al., 2017). This study presented an overall worldwide incidence rate of 140.6 per million person-years for the age group 0–14 years, 155.8 per million person-years for the age group 0–19 years, and 185.3 per million person-years specifically for the age group 15–19 years (from 2001–2010 registries). Such incidence rates were overall slightly higher for boys and varied with age, region, and diagnostic group. Paediatric cancer encompass a large variety of entities, including leukaemia, lymphomas, central nervous system tumours, sarcomas of bone and soft tissue, neuroblastoma (NB), retinoblastoma, rhabdoid tumours, liver tumours, renal tumours, germ cell tumours, and other rare cancers.

One of the main biological features of paediatric tumours is that they resemble progenitor tissue in all ways. In agreement with this, gene expression studies comparing various stages of normal tissue development have demonstrated a close relationship between these cancer cells and the immature cells of the developing organs from which these tumours originate (De Preter et al., 2006; Rivera and Haber, 2005; Xia et al., 2002). However, critical factors are not only the tissue or the cell of origin, but also the developmental time in which these tumours appear. Accordingly, evidence from genetically engineered mouse models suggest that paediatric tumours originate from stem or progenitor cells during a particular developmental time window (Cozzio et al., 2003; Funato et al., 2014; Han et al., 2016; Huntly et al., 2004; Li et al., 2005; Ng et al., 2015; Pathania et al., 2017; Vitte et al., 2017).

Normal postnatal development is mathematically described by the infancy–childhood–puberty (ICP) model proposed by Karlberg (1989). This model defines growth as an additive function of three biological processes, distinguishing infancy, childhood, and puberty growth. Infancy shows a rapidly decreasing growth curve, as it is largely nutrition-dependent, yet with the fastest growth rate observed in postnatal life. Childhood is represented as a polynomial regression curve and mainly depends on the initial influence

of growth hormone (GH). Finally, puberty is a rapid phase of growth that culminates the growth and development of an individual, and it is driven by collision of GH and sex hormones. Considering all these governing forces and the fact that every tissue matures in pre-specified growth periods during development, it is not surprising that paediatric cancers can be classified according to the developmental period in which they appear **(Figure I. 1).** For instance, retinoblastomas are typical infancy tumours, while in contrast bone sarcomas are puberty tumours that rarely occur before adolescence (Mora, 2012). Thus, understanding the forces that drive the appearance of these tumours has been a matter of debate and is analysed in the next section.

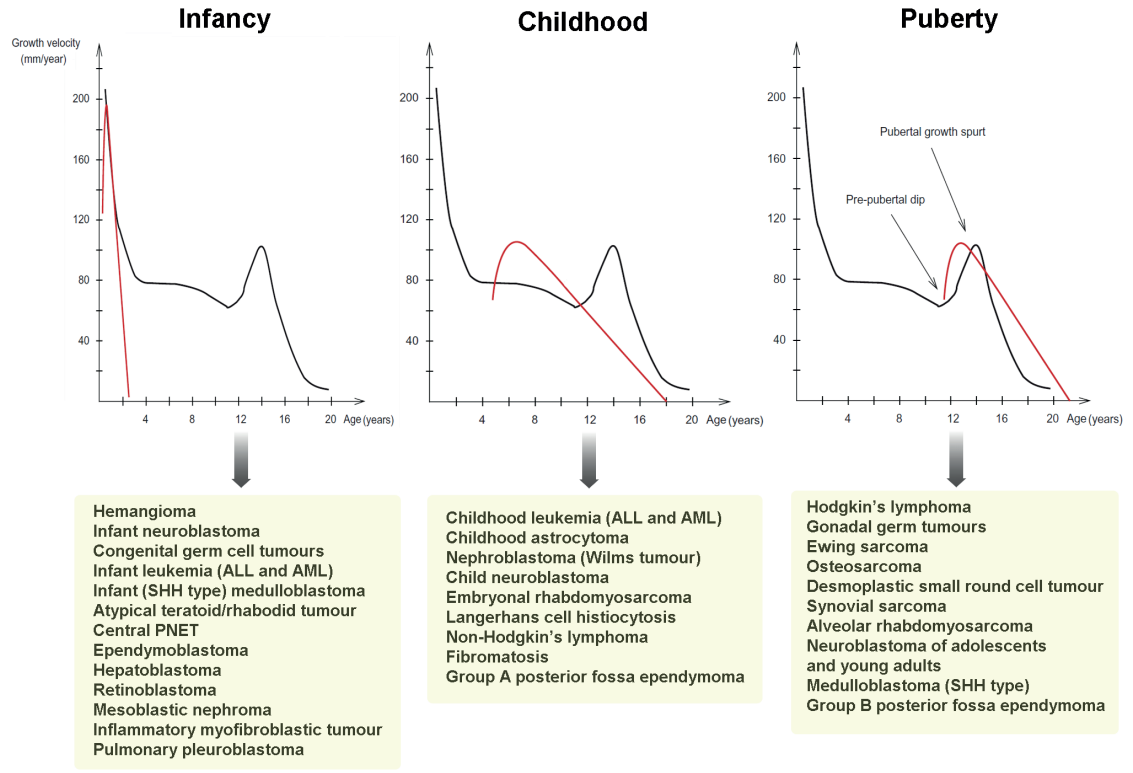

FIGURE I. 1 ***Growth velocity curve of normal human growth overlaps with the age curve presentation of paediatric tumours.***
Each graph shows the overlap between the age curve presentation (red) and the growth velocity curve during 0–20 years of postnatal life. In the mathematical model described by Karlberg (1989), called ICP model, three additive and partly superimposed components characterized by different types of growth can be distinguished: infancy (left), childhood (middle) and puberty (right). In this regard, the first 2 years of postnatal life are characterized by a deceleration growth phase, followed by a stable and slow growth phase from 4–11 years of age. Finally, there is a growth spurt from 12–18 years of age, coinciding with puberty. These growth stages overlap with age presentation of paediatric tumours, as indicated in the yellow boxes below each graph. ALL, acute lymphoblastic leukaemia; AML, acute myeloblastic leukaemia; PNET, primitive neuroectodermal tumour; SHH, sonic hedgehog homolog. Adapted from Mora (2012).

1.2 Origins of paediatric cancer: hypothesis of embryonal tumorigenesis

During the prenatal and postnatal periods of development, tissue growth and differentiation are regulated by complex cellular processes that involve precise regulation of cell division and apoptosis. Defects in any of the pathways that control these processes could promote transformation, making these developing cells particularly prone to tumorigenesis (Scotting et al., 2005). Prenatal life is the highest proliferative stage of any individual lifetime, characterized by an exponential growth phase that will accomplish, in 38 weeks, 42 cell divisions to fully form the 2×10^{12} cells of a newborn. It has been reported that two-thirds of all spontaneous mutations accumulate as a result of cell division during the growth and developmental stages of life (Paashuis-Lew and Heddle, 1998). Therefore, the most accepted theory is that initiation of paediatric tumours with evidence of a prenatal origin (such as leukaemia) require an "accidental" (chance) mutation aberration in the embryonic tissue of origin (known as first hit). Although this is a necessary condition, it is not sufficient to produce full-blown cancer. The following required events, named the precancer-to-cancer transition, might be cell-intrinsic mechanisms to survive the hostile early postnatal environment (second hit) and an accelerated pathway towards genomic instability (third hit) (Marshall et al., 2014). Acute lymphoblastic leukaemia (ALL) has been described as a paradigmatic two-step leukaemogenic process: a first premalignant lesion formed in utero, and a second postnatal acquisition of genetic events that cooperate with microenvironmental forces during maturation of the immune system (Greaves, 2018).

1.3 Why is paediatric cancer so different from adult cancer?

Adult and paediatric cancers usually have been wrongly understood as the same disease. Despite sharing an uncontrolled division of abnormal cells, they differ in a substantial way: adult cancer demonstrates an increasing incidence worldwide, whereas paediatric cancer has a stable incidence. Moreover, adult cancer is mathematically defined as a function of ageing, with increasing incidence over the lifetime of an individual. These data suggest very different malignant transformation mechanisms for adult versus paediatric cancers. Consistently, the adult tumorigenic process is understood as a linear process of accumulation of mutations over years or decades, influenced by environmental factors, following the Vogelstein colorectal carcinoma model (Fearon and Vogelstein, 1990). In contrast, paediatric cancer is mostly independent of environmental cues and rather is based solely on the growth and developmental forces governing development of each organ (see **Figure I. 1**).

Genomic sequencing studies of paediatric tumours have recently demonstrated a

substantially lower mutational burden for them as compared to adult cancers (Grobner et al., 2018; Ma et al., 2018). The genomic events central to childhood oncogenesis include mutations that most frequently occur in epigenetic modifiers or translocations, resulting in fusion oncoproteins (Filbin and Monje, 2019). Striking examples of the most frequently mutated epigenetic regulators in paediatric cancer are H3 histone family member 3A (*H3F3A*) and other epigenetic regulators, including PHD finger protein 6 (*PHF6*), ATRX chromatin remodeler (*ATRX*), lysine demethylase 6A (*KDM6A*), SWI/SNF related, matrix associated, actin dependent regulator of chromatin, subfamily A, member 4 (*SMARCA4*), ASXL transcriptional regulator 1 and 2 (*ASXL1* and *ASXL2*, respectively), CREB binding protein (*CREBBP*), enhancer of zeste 2 (*EZH2*), lysine methyltransferase 2D (*MLL2*), ubiquitin specific peptidase 7(*USP7*), nuclear receptor binding set domain protein 2 (*NSD2*), SET domain containing 2, histone lysine methyltransferase (*SETD2*), structural maintenance of chromosomes 1A (*SMC1A*) and zinc finger MYM-type containing 3 (*ZMYM3*) (Huether et al., 2014). The number of epigenetic alterations suggests a locked-in epigenetic state during development that contributes to the final gene expression and phenotype of the resulting childhood cancers (Filbin and Monje, 2019). Given the importance of epigenetics in these malignancies, a more detailed explanation on epigenetics is provided in the next chapters.

Another distinguishing fact is that 85% of adult cancers occur in the self-renewing epithelia of various organs (including breast, lung, colon, and prostrate), in contrast to paediatric tumours, of which 50% originate in the hematopoietic and central nervous system and only 9% in epithelia (Mora, 2012). The prevalence of epithelial cancers in adults may be due to the cumulative cell division during lifetime homeostasis. Even with exceedingly low endogenous rates of mutations, tumorigenesis in these epithelial cancers increases with age (Hinck and Näthke, 2014).

Finally, for paediatric cancer, the five-year survival rates have significantly increased in the last two decades and now exceed 80% in developed countries. Efforts are currently concentrated on optimizing the quality of longterm survival for diseases that respond to cytotoxic agents (Hudson et al., 2014). In comparison, the 5-year combined relative survival rate for all adult cancers is now approximately 68%, as reported by the National Institute of Health (2010).

2. EWING SARCOMA

2.1 General background on paediatric sarcomas

Sarcomas account for over 20% of paediatric solid malignant cancers but less than 1% of adult solid malignant tumours (Burningham et al., 2012). They include diverse types

of malignancies that arise from bone, cartilage, or connective tissues, such as muscle, fat, peripheral nerves, and fibrous or related tissues (Taylor et al., 2011). In line with the diverse nature of tissues evolving from the mesenchyme, more than 50 histologic sarcoma subtypes have been described, such as osteosarcoma (OGS), Ewing sarcoma (ES), rhabdomyosarcoma (RMS), liposarcoma, synovial sarcoma (SS), and chondrosarcoma.

One of the main characteristics of paediatric sarcomas is their genetic make-up. These tumours are composed of near-diploid cells with few genetic alterations, such as translocations, or cells with complex and unbalanced karyotypes displaying multiple genomic aberrations. Interestingly, the group of translocation-associated sarcomas display recurrent chromosomal aberrations that are shared between different sarcoma subtypes, suggesting that some regions of the genome are recurrent rearrangement breakpoints (Taylor et al., 2011) (**Figure I. 2**). For instance, desmoplastic small round cell tumour and ES share same translocated chromosomes but differ in the chromosome arms involved in the rearrangement. Accordingly, some sarcoma subtypes share dysregulated biological pathways. For instance, the insulin-like growth factor (IGF) pathway plays an important role in ES, SS, and OGS (McKinsey et al., 2011; Rikhof et al., 2009; Xie et al., 1999).

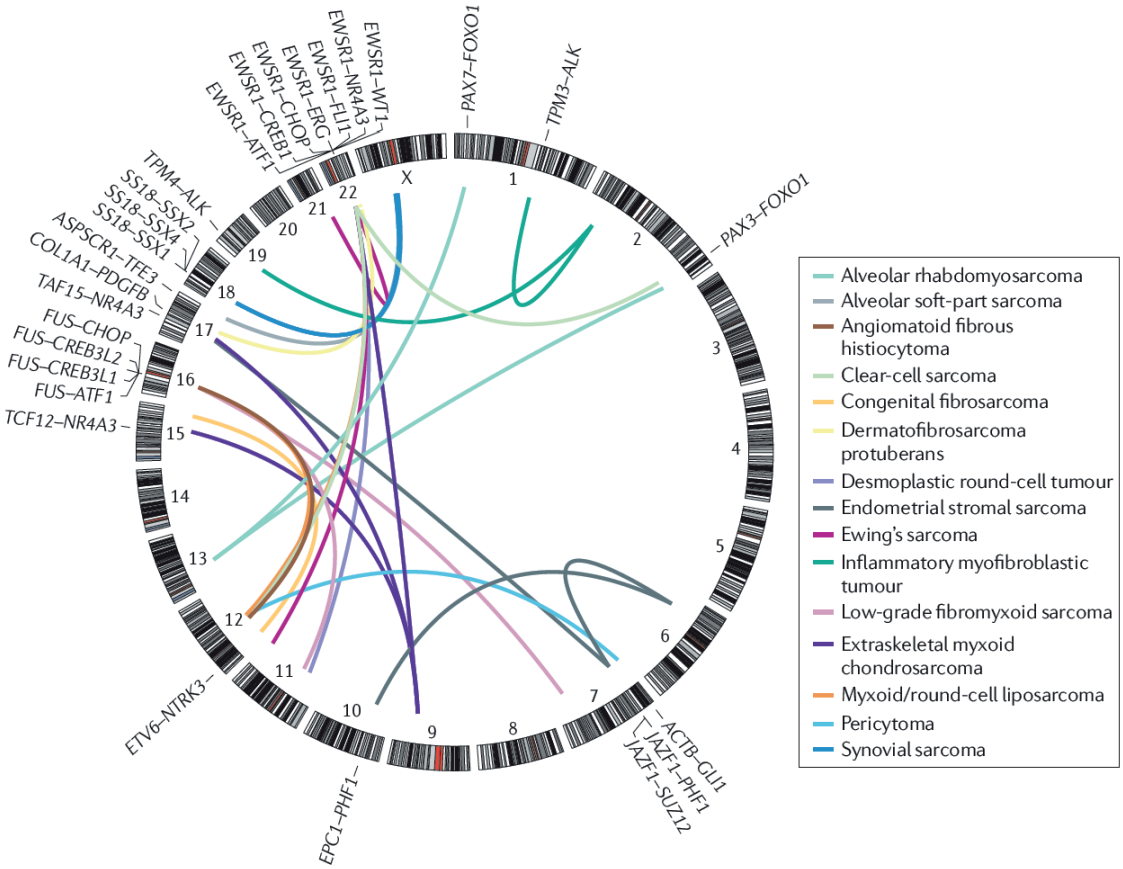

FIGURE I. 2 ***Genomic landscape of the recurrent rearrangements in sarcomas.***
Chromosome-based circos plot showing a summary of recurrent translocations in a variety of sarcomas. Of

note, similarities in the fusion rearrangement partners between the different subtypes can be observed. The outer ring represents genomic location (as labelled); cytobands are shaded, the centromere is in red, and coloured curves join fusion partners (each colour defines a sarcoma subtype as indicated in the right panel legend). Adapted from Taylor et al. (2011).

The question of how and why these translocations occur during sarcomagenesis has recently been a matter of interest. In sarcomas, as in many leukemias, translocations seem to be fundamentally random events that become fixed through natural selection within the precursor cell (Taylor et al., 2011). Recently, it has been reported that some sarcoma translocations might arise in complex loop-like rearrangements called chromoplexy, rather than by simple reciprocal translocations. This event might occur as bursts in early replicating DNA, as a primary event in the development of various sarcomas, including ES (Anderson et al., 2018). Consistent with the embryonal tumorigenesis hypothesis, chromoplexy in ES represents a primary event that may occur years before diagnosis.

Despite having common mesenchymal origin, each type of paediatric sarcoma has unique features with respect to biology, epidemiology, clinical behaviour, and response to treatment. The work in this thesis focuses on ES.

2.2 Defining Ewing sarcoma

ES is a malignant neoplasm of bone and soft tissue that mainly affects children and adolescents and young adults (AYA)[1], representing 2.9% of all paediatric cancers (Howlader et al., 2013). This tumour was previously known as "Ewing sarcoma family of tumours" and included extraosseous ES, peripheral primitive neuroectodermal tumour (PNET), and Askin's tumour, due to common morphological, immunophenotypic, and genetic features (Kovar, 1998). However, the World Health Organization (WHO) classification of sarcomas in 2013 uniformly defined this group as "Ewing sarcoma" (de Alava et al., 2013). This classification also created the term "Ewing-like sarcomas", for those tumours morphologically similar to ES but with different fusion genes as well as distinct clinical and pathological features. Recent data have demonstrated that Ewing-like sarcomas are indeed biologically distinct from ES (Watson et al., 2018).

2.3 Epidemiology

ES is the second most common bone malignancy affecting children and AYA after OGS, with a global incidence of approximately 1.5 cases per million population (Grunewald et al., 2018). However, according to the national Spanish paediatric tumour registry, the annual incidence rate of ES in Spain is 5.2 cases per million population between the age of

1 Although there is so much controversy in the definition, and indeed even in the terminology, used to describe the AYA cancer population between countries, the standard age used by the National Cancer Institute (NCI) uses the 15 to 39 age range to define this group of patients (Aubin, 2011).

0 and 14 years; this is almost twice as high as OGS, which is 3.5 cases per million (Mora et al., 2017). ES tumours are aggressive malignancies mainly presenting during puberty, when rapid bone growth occurs in normal development, with a median age at diagnosis of 15 years (Cotterill et al., 2000; Paulussen et al., 2001). Males are more affected than females with a sex ratio of 3:2. In addition, ethnicity also affects incidence, as ES is predominantly observed in European descendants (Caucasians), with a very low incidence in Asian or African descendants and with a global annual rate of 0.8 and 0.2 cases per million children, respectively (Fraumeni and Glass, 1970; Jawad et al., 2009; Jensen and Drake, 1970).

ES tumours are predominantly bone lesions, presenting preferentially in the pelvis, extremities, and axial skeleton. Differing from other sarcomas of the bone such as OGS, ES affects the diaphysis of the long bones rather than the metaphysis. Only 15% of these malignancies are extraosseus, including deep soft paravertebral, thoracic and proximal limb tissues, kidney, bladder, lung, prostrate, and meninges (Ushigome et al., 2002). Similar to other sarcomas, ES display an aggressive behaviour with tendency toward recurrence following surgical resection and a pronounced proclivity to early haematogenous metastasis primary in lung (38%), bone (including spine; 31%) and bone marrow (11%), being rare in the central nervous system (Pizzo P. A. and Poplack, 1996; Postovsky et al., 2003; Riggi et al., 2009). Currently, patients with localized disease generally have a 5-year overall survival (OS) rate of 70%–80%, which is lower for those presenting pelvic tumours, large tumours, and/or incomplete tumour regression after neoadjuvant or adjuvant chemotherapy. Patients presenting with systemic metastasis have a 5-year OS rate of less than 30%. For the subgroup of patients with isolated pulmonary metastasis, the 5-year OS rate is approximately 50% (Gaspar et al., 2015). Therefore, metastasis is an important prognostic factor but is not unique. Recent evidence shows that age is associated with poor OS (Lee et al., 2010; Miller et al., 2017; Verma et al., 2017). The largest multicentre study of ES in Spain has shown age at diagnosis is an independent prognostic factor superior to metastases, with 18 years as the strongest cut-off (Mora et al., 2017).

2.4 Histopathology

ES was first described by James Ewing in 1921 as an undifferentiated bone endothelioma appearing in the diaphysis of long bones that was radiosensitive but highly recurrent (Ewing, 1972). Histologically, ES harbours sheets of small round haematoxylin-stained cells (blue), usually with extended areas of tumour necrosis and haemorrhage that typically lack immune cells or other inflammatory cell infiltrates. Tumour cells display high nuclear-to-cytoplasmic ratio with stipple chromatin and usually lack nucleoli. In many cases, deposits of glycogen can be observed in the form of positive periodic acid Schiff staining; due to the lack of matrix in tumour cells, they have negative reticulin staining. In ES cases showing more differentiation traits (e.g. PNET tumours), tumour

cells cluster in ill-defined groups of up to ten cells oriented towards a central space (or rosette-like arrangements). They show higher expression of neuron-specific enolase and neuroectodermal markers such as beta-1,3-glucuronyltransferase 1 (B3GAT1 or CD57) than conventional ES (de Alava et al., 2013). A "large cell" or "atypical" variant of ES has been reported (Nascimento et al., 1980); these cells mainly differ from typical ES cells by having larger-size nuclei with irregular contours and conspicuous nucleoli with usually negative periodic acid-Schiff staining (Grunewald et al., 2018) (**Figure I. 3**).

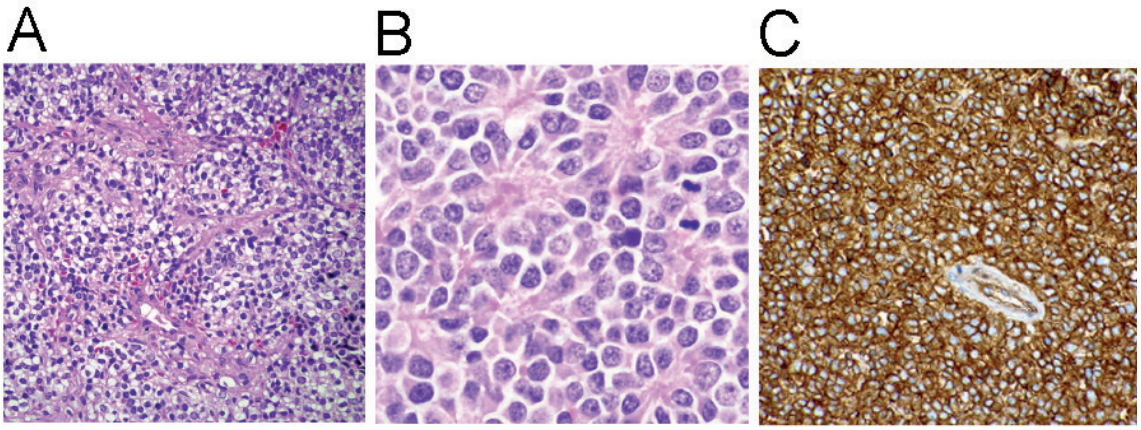

FIGURE I. 3 ***Histologic and immunohistochemical features of ES.***
A) Hematoxylin and eosin (H&E) staining of ES, which appears as sheets of monotonous small round blue cells with lack of matrix and regular round nuclei occupying the whole cell with fine chromatin (magnification 10×). ***B)*** H&E staining showing an ES case with atypical morphology displaying a rosette-like arrangement of tumour cells. These structures provide evidence of neural differentiation in a minority of cases (magnification 40×). ***C)*** CD99 staining showing positivity for this ES tumour with diffuse and intense plasma membrane expression. Images with an original magnification 20×. Adapted from Grunewald et al. (2018).

Notably, the morphological description reported for ES is not exclusive and can be observed in many developmental tumours, like NB, or in other sarcomas, such as Ewing-like sarcomas or other small round cell sarcomas. Hence, distinguishing each tumour type would depend on the identification of specific histological markers and genetic traits. The CD99 molecule (CD99) is a cell-surface glycoprotein used as a diagnostic marker for ES (Ambros et al., 1991) and is expressed in 95% of ES cases (de Alava et al., 2013)). However, it has very low specificity as it is also present in a large group of normal tissues and tumour types, including other round cell sarcomas, lymphoblastic lymphomas, and leukaemia. Characterization of the ES histopathology is essential for diagnostics as well as for the assessment of tumour necrosis during treatment, as it correlates with patient OS (Gaspar et al., 2015).

2.5 Diagnosis

An accurate diagnosis of ES is crucial for being able to precisely categorize and treat

patients. Clinical diagnosis of ES is complex, as it may present with a very unspecific history of intermittent pain, sometimes nocturnal, which tends to worsen over time. As ES presents during the period of life characterized by skeletal growth, and as children and adolescents commonly have injuries from sports or daily life activities, the clinical suspicion is often blurred. Furthermore, as this disease can present in such a variety of sites, symptoms are very diverse and only some patients have a palpable mass. Therefore, the median time from initial symptoms to final diagnoses is 3–9 months (Widhe and Widhe, 2000). This time delay, however, is not associated with clinical outcome (Alonso et al., 2014).

The diagnostic process usually begins with imaging evaluation of the primary tumour. X-ray generally shows a tumour-related osteolytic lesion in the metaphyseal-diaphyseal bone with a multi-layered appearance, known as "onion skin" lesion. Computed tomography (CT) scans can detect smaller lesions and identify bone destruction and periosteal involvement in the lesion, while magnetic resonance imaging (MRI) provides higher definition of the soft tissue component of the lesion. Finally, a metabolism-based method, fluorine-18-fluorodeoxyglucose positron emission tomography (FDG-PET) is used to evaluate evolution of the lesion and gives information about tumour regression or progression with treatment (Kuleta-Bosak et al., 2010) (**Figure I. 4**). Definitive diagnosis eventually only comes from the analysis of tumour biopsy, which allows for histopathological orientation of a small round blue cell tumour with an immunohistochemical pattern compatible with ES. The final molecular diagnostic confirmation is obtained by detection of the specific translocation by different techniques, including fluorescence *in situ* hybridization (FISH) technique and quantitative reverse-transcription PCR (RT-qPCR).

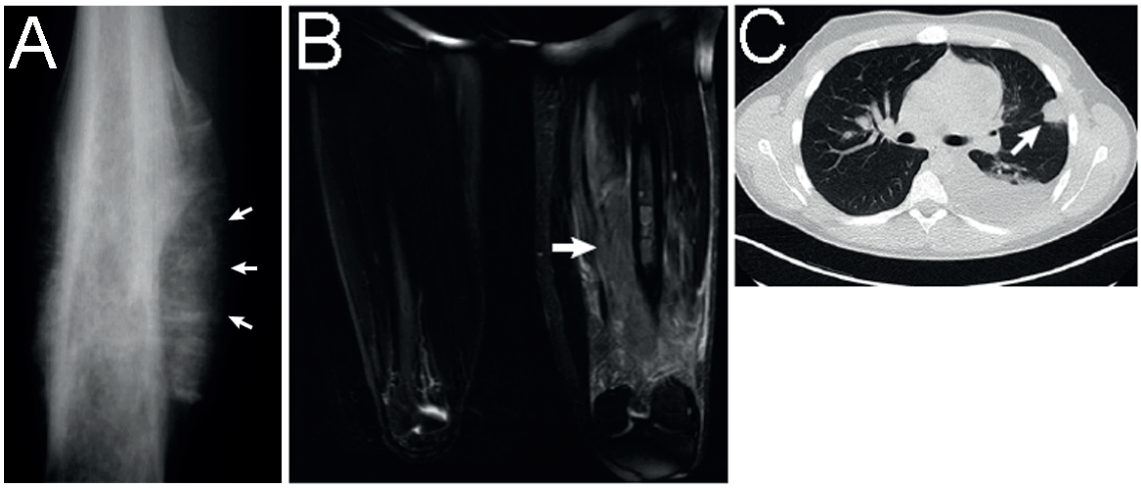

FIGURE I. 4 ***Characteristic radiological images of ES.***
A) X-ray images in the right femur of a 14-year-old boy showing an anterioposterior osteolytic lesion with involvement of the periosteal soft tissue that is indicative of ES (arrows). ***B)*** MRI scan (T2-weighted) of the same patient showing a primary tumour with an infiltrated ES lesion with involvement of soft tissue and changes in the bone marrow in the right femur with soft-tissue edema involvement (arrow). ***C)*** CT scan

images of a 19-year-old male showing a pulmonary metastasis in the left lung (arrow). Adapted from Grunewald et al. (2018).

2.6 Treatment

Patients with newly diagnosed ES are usually treated with chemotherapy before local treatment is applied, to reduce the size of the primary tumour as well as more importantly to prevent metastatic disease progression. Local control includes surgery and/or radiation, depending on the feasibility of tumour resection. Surgery in some cases may imply amputation with or without reconstruction with endoprosthesis or allogenic or autologous bone grafting. ES is radiosensitive, and many studies have demonstrated the benefits of combining radiotherapy with chemotherapy (Foulon et al., 2016). Treatment is finally completed with postoperatively multi-agent cytotoxic chemotherapy to eradicate microscopically disseminated disease, the so-called minimal residual disease (MRD), that could lead to metastatic progression, which is the major cause of death. Notably, 20% of localized ES cases at diagnosis have disseminated tumour cells in bone marrow and blood (Schleiermacher et al., 2003).

Cooperative group clinical trials have reported that treatment intensity and multidrug treatment are relevant factors for outcome. Modern protocols consist of intense induction chemotherapy with vinca alkaloids, alkylating agents, and anthracyclines. Three general strategies for initial chemotherapy are most commonly used, which depend in part on institutional preferences and patient age (Van Mater and Wagner, 2019). In North America patients typically receive the combination of compressed regimens of vincristine, doxorubicin, and cyclophosphamide (VDC), alternating with ifosfamide and etoposide (VP-16), using an intensive time schedule with planned administration every two weeks (Womer et al., 2012). In Europe, cyclophosphamide is omitted, and intensive treatment with the aforementioned chemotherapeutics including ifosfamide (VIDE) is the initial regimen used, which is administered for up to 14 total cycles (Juergens et al., 2006). For adult patients, some centres have simplified the regimen to vincristine, ifosfamide, and doxorubicin (VID) (Wagner et al., 2017). High-dose chemotherapy followed by autologous haematopoietic stem cell rescue remains a controversial matter in the field and has not been formally proven to help patients (Whelan et al., 2016).

Despite extensive therapies, at least one-fourth of patients with initially localized disease will relapse after completing planned therapy. The recurrence rate is even higher for those with initially metastatic disease, with treatment failure seen in 50–80% of patients depending on the site of metastasis (Gaspar et al., 2015). For those patients, the chance of long-term survival is very low, and there is an urgent need for better treatments. To improve the outcome of these patients, many treatments have been proposed, such as the addition of a gemcitabine and docetaxel regimen (Mora et al., 2017; Mora et al.,

2009), or high-dose busulfan and melphalan chemotherapy with autologous stem cell transplantation (Oberlin et al., 2006). However, the superiority of one regimen over another has not yet been established. Many randomized clinical trials are currently investigating the efficacy of new agents. Some ongoing trials include the addition of monoclonal antibodies against the receptor of insulin-like growth factor 1 (IGF1) (trials with both R1507 and robatumumab) to dose-compressed chemotherapy (Anderson et al., 2016; Pappo et al., 2014). Therapies that inhibit the mTOR pathway (temsirolimus), topoisomerase (irinotecan) or the DNA repair mechanism (temozolamide) are also under research (Bagatell et al., 2014). Adjuvant immunotherapy with autologous lymphocytes, tumour lysate, or keyhole limpet hemocyanin-pulsed dendritic cell vaccination with or without recombinant human interleukin 7 (IL-7) has been shown to improve survival in patients with metastatic paediatric sarcomas including ES (Merchant et al., 2016).

2.7 Genetic alterations in ES

2.7.1 ES translocation

ES is characterized by a recurrent and balanced chromosomal translocation (Aurias et al., 1984; Becroft et al., 1984; de Chadarevian, 1984; Turc-Carel, 1983; Vigfusson et al., 1986; Whang-Peng et al., 1984; Whang-Peng et al., 1986). In approximately 85% of ES cases, translocation involves chromosomes 11 and 22, t(11;22)(q24;q12) (Delattre et al., 1992). It fuses the EWSR1 RNA-binding protein 1 *(EWSR1)* gene of the FET (*FUS*/*TLS*, *EWSR1*, *TAF15*) family (previously called TET) of RNA-binding proteins with a member of the erythroblast transformation-specific (ETS) family, i.e. the Fli-1 proto-oncogene gene *(FLI1),* leading to an *EWSR1-FLI1* fusion gene. In approximately 15% of ES cases, chromosomal rearrangements involving other members of these two families have been reported, such as variants containing *EWSR1* fused to another ETS member like the ETS transcription factor *ERG (ERG*) (Zucman et al., 1993). Finally, other still less frequent translocations, found in approximately 1% of cases each, involve *EWSR1* rearrangements with the ETS variant 1 *(ETV1)* or -4 (*ETV4),* or with FEV transcription factor gene (*FEV*) (Jeon et al., 1995; Peter et al., 1997; Urano et al., 1998). Similarly, alternative variants have also been described between ETS genes and *EWSR1* paralogues of the FET gene family, for instance, the FUS RNA-binding protein gene *(FUS)* or the TATA-box binding protein associated factor 15 gene *(TAF15)* (Ng et al., 2007; Watson et al., 2018). **Table I. 1** summarizes all the FET-ETS fusions found in ES.

Table I. 1 ***Chromosomal alterations frequently found in ES.***
The most common rearrangements found in the clinics of TET/FET with ETS members are shown. Frequency and chromosomal translocations are also included. (Adapted from Grünewald et al., 2018).

FET part (5')	ETS part (3')	Fusion Gene	Chromosomal translocation	Frequency (%)
EWSR1	FLI1	*EWSR1-FLI1*	t(11;22)(q24;q12)	≈85%
	ERG	*EWSR1-ERG*	t(21;22)(q22;q12)	≈10%
	ETV1	*EWSR1-ETV1*	t(7;22)(p22;q12)	<1%
	ETV4	*EWSR1-ETV4*	t(17;22)(q21;q12)	<1%
	FEV	*EWSR1-FEV*	t(2;22)(q33;q12)	<1%
FUS	ERG	*FUS-ERG*	t(16;21)(p11;q22)	<1%
	FEV	*FUS–FEV*	t(2;16)(q35;p11)	<1%

The *EWSR1-FLI1* fusion gene contains the ubiquitously active promoter of *EWSR1* from the FET family, which is constitutively expressed. Considering that the t(11;22)(q24;q12) translocation is reciprocal, it also leads to the reverse fusion protein, *FLI1-EWSR1*, whose expression is regulated by the tissue-restricted *ETS* promoter and thus is commonly loss or lowly expressed in ES (Zucman et al., 1993). Adding a layer of complexity to genetic studies of ES tumours, at least 12 subtypes of in-frame chimeric transcripts with different combinations of exons have been found in clinical specimens. The most common subtype, designated as type 1, accounts for approximately 60% of *EWSR1-FLI1* translocations and consists of exon 7 from *EWSR1* fused to exon 6 of *FLI1*. Type 2 includes the exon 5 of *FLI1* and is present in 25% of *EWSR1-FLI1* translocations (Zoubek et al., 1996). Although it was initially believed that these fusion subtypes influenced prognosis, posterior data revealed no association with patient outcome (Le Deley et al., 2010; van Doorninck et al., 2010).

All predicted fusion proteins for *EWSR1-FLI1* have the potent SYGQ (serine-tyrosine-glycine-glutamine-rich) region at the N-terminus that contains the transactivation domain of *EWSR1* fused to the C-terminal DNA-binding domain of *FLI1*. This generates a fusion protein capable of binding DNA that acts as an aberrantly active transcription factor (TF) (Lessnick et al., 1995; May et al., 1993; Thompson et al., 1999). Due to the similar DNA-binding domains of all ETS fusion rearrangements, these fusions have almost the same binding specificity (Wei et al., 2010), suggesting a genetic redundancy for such driving lesions. Consistently, EWSR1-FLI1 and EWSR1-ERG translocations have same phenotypical and clinical alterations (Ginsberg et al., 1999). **Figure I. 5** shows in detail the domains of the FET-ETS fusions focused on EWSR1-FLI1 translocation.

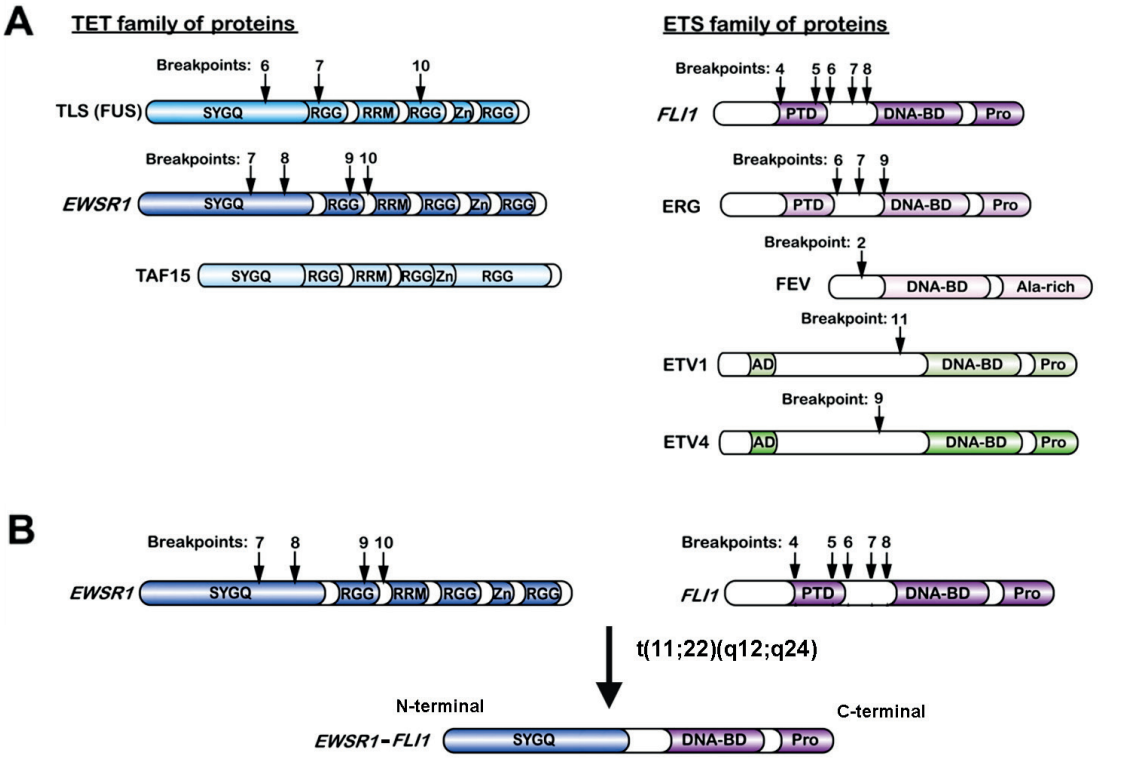

FIGURE I. 5 ***Domain structures of the FET-ETS members and EWSR1-FLI1 in detail.***
A) Domain structures of the FET family of RNA binding proteins (including *TLS/FUS, EWSR1, TAF15*) (left) and the ETS family of TF (including *FLI1*, *ERG*, *FEV, ETV1*, and *ETV4*) (right). ***B)*** Wild-type *EWSR1* and *FLI1* and the resulting *EWSR1-FLI1* fusion protein. The fusion protein conserves the SYGQ transactivation domain of the FET family as well as the DNA-BD and Pro domains from the ETS family that permit DNA binding as a TF. SYGQ, the serine-tyrosine-glycine-glutamine rich transactivation region; RGG, arginine-glycine-glycine rich region; RRM, RNA-recognition motif; Zn, putative zing finger; PTD, pointed domain; DNA-BD, DNA-binding domain; Pro, proline-rich activation domain; AD, alanine-rich region involved in transcriptional repression. Arrows indicate breakpoints, which occur in the introns of wild-type genes; after splicing, exons are joined to generate various chimeric fusions, including EWSR1-FLI1. Adapted from Sankar and Lessnick (2011).

2.7.2 Additional recurrent mutations and copy number variations

In addition to key reciprocal translocation, ES have recurrent structural chromosomal aberrations. Usually, they involve parts of chromosome arms or even whole chromosomes, with chromosomal gains the most frequent alterations. These include trisomy of chromosome 8 (found in 50% of cases) as well as gain of chromosome 2 and the long arm of chromosome 1 (1q) (in 25% of cases) and gain of chromosome 20 (in 10–20% of cases) (Kullendorff et al., 1999; Mugneret et al., 1988). Additional structural aberrations are less common than numerical changes, although unbalanced rearrangements involving chromosomes 1 and 16 have also been described. In the majority of these cases, the net imbalance is gain of 1q with simultaneous loss of 16q, t(1;16), which is associated with poor clinical outcome (Kullendorff et al., 1999; Mugneret et al., 1988; Stark et al., 1997). The most frequent chromosomal deletions involve the small arm of the chromosome 9

(9p), producing the loss of the tumour suppressor cyclin-dependent kinase inhibitor 2A *(CDKN2A)*, which has been associated with poor prognosis (Brohl et al., 2014; Crompton et al., 2014).

Next-generation sequencing studies have demonstrated that these tumours, as most developmental cancers, have a very low mutational burden (0.15 mutations/Mb) (Brohl et al., 2014). Nevertheless, frequent loss-of-function mutations were found in the cohesin complex family member stromal antigen 2 gene *(STAG2)* and tumour protein p53 (*TP53)*, in 20% and 5–20% of ES, respectively (Brohl et al., 2014; Crompton et al., 2014; Tirode et al., 2014). Moreover, alterations in *STAG2* alone or in combination with *TP53* have been reported to be associated with poor clinical outcome (Tirode et al., 2014). Less frequent recurrent somatic mutations (2.7% of ES cases) were found in epigenetic regulators, including *EZH2*, the BCL6 corepressor gene *(BCOR)*, and *ZMYM3*. In addition, 12% of ES cases had a mutated *CDKN2A*, suggesting that it is an important target to silence in ES, as it is alternatively lost throughout deletion of chromosome 9p (Brohl et al., 2014; Brownhill et al., 2007; Crompton et al., 2014; Tirode et al., 2014). Considering that these tumours have very low mutational burdens, and that mutations are in epigenetic regulator genes, epigenetics is thought to play a critical role in ES initiation and progression.

2.8 The enigma of the cell-of-origin

While other sarcomas, such as OGS and fibrosarcoma, present some lineage-specific differentiation traits with a known lineage precursor, the cell-of-origin for ES is still unknown. The uniformly and poorly differentiated phenotype of ES, together with the fact that it can arise from either bone or soft tissue, has complicated the identification of its histogenesis and has been a topic of research for decades. Novel DNA methylation studies suggest that ES might arise from a specific cellular lineage, with different epigenetic states at the time of cellular transformation (Sheffield et al., 2017).

In 1921, James Ewing proposed an endothelial origin based on cellular morphology and the rareness of stroma (Ewing, 1972). Later, in 1971, a myelogenous origin was suggested according to the structural features that resembled developing myelocytes (Kadin and Bensch, 1971). Since then, several hypotheses regarding the histogenesis of ES with neural crest stem cells (NCSC) and mesenchymal stem cells (MSCs) as the putative cells of origin have been presented. A NCSC origin was purposed consistent with the potential of ES cells to differentiate into neuronal lineage *in vitro* (Cavazzana et al., 1987), and some observational studies have revealed that ES display some neural lineage markers (Franchi A. et al., 2001) as well as neurosecretory granules (Suh et al., 2002). Furthermore, ectopic expression of EWSR1-FLI1 in NCSC can be well-tolerated and lead to an altered expression of well-known ES target genes. In further support for a neuroectodermal origin, genome

expression studies have revealed proximal genetic traits of ES tumours to NCSC (von Levetzow et al., 2011).

In contrast to this hypothesis, emerging evidence in the last years has pointed to a mesenchymal origin. Initial studies showed that knockdown of the ES translocation drives the ES transcriptome towards MSC (Tirode et al., 2007). In parallel, other reports showed that introduction of EWSR1-FLI1 into MSCs *in vitro* and *in vivo* increases their ability to transform into sarcoma-like cells (Lin et al., 2011; Miyagawa et al., 2008; Rodriguez et al., 2012). In further support of these data, CD99 is detected at low levels in MSCs and is upregulated upon introduction of ES translocation into mouse MSCs (Castillero-Trejo et al., 2005; Riggi et al., 2005). Moreover, ectopic expression of EWSR1-FLI1 in bone marrow-derived MSCs lead to cell transformation and engraftment of ES-like tumours *in vivo* (Riggi et al., 2005). Moreover, they display a transcriptional signature resembling that of MSCs (Hancock and Lessnick, 2008; Riggi et al., 2010; Riggi et al., 2008). Considering that MSCs can be derived from the neural crest (Nagoshi et al., 2008), and that ES translocation induces a neural program (Hu-Lieskovan et al., 2005; Rorie et al., 2004; Staege et al., 2004), the most accepted theory is a mesenchymal origin within a neural crest-derived progenitor that is at transition to mesenchymal endothelial development (Staege et al., 2004).

2.9 Disease models

A large number of studies have used ES cell lines to investigate biological pathways and testing drug efficacy *in vitro* and *in vivo* in xenograft models in immunodeficient mice or zebrafish embryos, yet a faithful genetically engineered mouse model is still lacking in the field (Minas et al., 2017). For the preclinical drug testing studies, one model that shows promising results is the patient-derived xenografts (PdX) (Geier et al., 2015). Other alternatives have been focused on creating orthotopic xenograft or patient-derived models of the disease (Stewart et al., 2017; Wang et al., 2009).

Much effort has centred on overexpressing the fusion oncoprotein (traditionally using EWSR1-FLI1) in a multiplicity of embryonic cells, such as NCSCs, MSCs, and allographs of embryonic osteochondrogenic progenitors, giving rise to tumours that display most of the characteristics of ES (Castillero-Trejo et al., 2005; Riggi et al., 2005; Riggi et al., 2010; Tanaka et al., 2014; von Levetzow et al., 2011). However, the very restricted spatial-temporal tolerance to the expression of this oncogene in development suggests that this protein is not sufficient to induce ES tumorigenesis. Furthermore, ectopic expression of EWSR1-FLI1 fails to activate similar genetic programs or transform most human cell lines, indicating that cell specificity is a major determinant of the fusion oncogene (Lessnick et al., 2002; Miyagawa et al., 2008; Riggi et al., 2008). Thus, many models have performed concomitant p53 deficiency or forced expression of antiapoptotic family members, such

as the BCL2 apoptosis regulator (BCL2), to overcome oncogene toxicity (Javaheri et al., 2016; Leacock et al., 2012; Lin et al., 2008).

In our studies, we have used human paediatric-derived MSCs (hpMSCs). After introduction of EWSR1-FLI1, these cells undergo a transcriptional program that resembles ES with high fidelity (Riggi et al., 2010). Furthermore, many relevant chromatin studies have been performed in these cells (Boulay et al., 2017; Boulay et al., 2018; Riggi et al., 2014; Tomazou et al., 2015).

3. EPIGENETICS

3.1 Definition of epigenetics: a trip to its origins

The most commonly accepted definition of epigenetics comes from a back-translation of "epi", which means upon, above, or beyond, and "genetic", which assigns a DNA sequence. Thus, epigenetics refers to the layer of information beyond what is encoded in the DNA sequence (Greally, 2018).

Epigenetics is a very old term that has drastically changed its meaning over time (Bird, 2007; Deans and Maggert, 2015; Felsenfeld, 2014). The first definition was formulated in 1650 by the physician and physiologist William Harvey. Although he used the term "epigenesis", he defined it as the developmental and gradual process of increasing complexity of the formation of an individual, in contrast with the organism preformation theories of that period. It was not until 1942 that the term "epigenetics" was used by the embryologist Conrad Waddington, defining it as the "whole complex of developmental processes that lie between genotype and phenotype". To explain his theory, he developed an "epigenetic landscape" model, represented as a marble on the top of a hillside, in which cell fate determination of a developing cell triggers a cascade of decisions or branching pathways (named creodes). In 1942, he speculated that the choice of a path / creode that determined cell fate was due to the actions of genes, thereby allowing a mutation to alter cell fate (Waddington, 1942). Sixteen years after Waddington's definition of the term, David Nanney reformulated Waddington's theory to propose that genetic components were responsible for maintaining and perpetuating a library of genes, relating epigenetics with cellular memory.

Our current definition of epigenetics bears no resemblance to Waddington's original concept. Epigenetics, from a molecular biology point of view, is commonly understood as the heritable and reversible mechanisms that underlie the modification of DNA without changing the sequence itself, determining whether, when, and how much of a gene is expressed (Nichol et al., 2016).

3.2 Chromatin structure

The 2-m long human genome is highly packaged into a macromolecular dynamic polymer, known as chromatin. It is constituted by DNA, histones, and non-histone proteins, which interact to condense the chromatin fibre down to 2-10 μm.

3.2.1 Histones

Histones are among the most evolutionary conserved proteins in eukaryotic cells. Five different histone types are known: H1/H5, H2A, H2B, H3, and H4. Core histones (H2A, H2B, H3, and H4) are essential small basic proteins with a common structure of a histone fold domain (HFD) that consists of three α-helices separated by two loops (Arents and Moudrianakis, 1995). They also have a short N-terminal tail that is highly positively charged and disordered in solution. In contrast, histone H1/H5 (also known as the linker histone) has a conserved tripartite structure with a globular domain with a preference for recognition of the nucleosome throughout its winged helix fold (Ramakrishnan et al., 1993; Singer and Singer, 1976).

Genes encoding canonical histones are located in clusters, and their transcription is tightly coupled to DNA replication in order to restore duplicated chromatin during the S cell cycle phase. Dysregulation of histone gene expression leads to defects in cell cycle progression, genome stability, DNA damage response (DDR), and transcriptional regulation (MacAlpine and Almouzni, 2013). Besides the canonical histones, many variants of the core histones as well as of the linker histone H1 have evolved, which differ in their primary amino acid sequences from their canonical paralogues. Genes encoding these variants are typically found singly in the genome and are expressed at low levels during cell cycle (Banaszynski et al., 2010; Weber and Henikoff, 2014). Histone variants have roles in a range of processes including DNA repair, meiotic recombination, transcription initiation and termination, sex chromosome condensation, and chromatin packaging in sperm cells (Talbert and Henikoff, 2010).

3.2.2 The nucleosome

The basic unit of chromatin is the nucleosome, consisting of ~147 base pairs of DNA wrapped 1.75 times in a left helix manner around a cylindrical octamer core of histone proteins. Such an octamer comprises two heterodimers of histone H3-H4 associated as a tetramer and is surrounded on both sides by a histone H2A-H2B dimer (Luger et al., 1997). Further incorporation of the linker histone H1 by binding at the entry and exit at the dyad axis stabilizes the nucleosome structure, forming the chromatosome (Woodcock et al., 2006). Within the nucleosome particle, each core histone forms a histone fold structure,

with their N-terminal flexible tail external to the nucleosome. Chemical modification of these external tails constitutes one of the main points of epigenetic regulation, which will be explained in the next sections.

3.2.3 The chromatin fiber

Linker DNA connects adjacent nucleosomes (each one spaced 10–60 bp). In low salt conditions, nucleosomes adopt an extended beads-on-a-string conformation. However, in physiological conditions, they organize in a much more complex structure constituted by nucleosome-nucleosome interactions, leading to folded and oligomeric structures forming a higher order condensed structure of the DNA fibre of 30 nm. It has been reported that core histone tails mediate condensation of the fibre with the H4 tail having a particularly critical role (Dorigo et al., 2003; Gordon et al., 2005; McBryant et al., 2009) (**Figure I. 6**). The maximum level of chromatin condensation is achieved when the chromatin fibre measures from 700 nm to 1.4 μm of depth during mitosis, leading to the easily recognized X-shaped chromosomes (Woodcock and Dimitrov, 2001). In contrast, when cells are in interphase and non-dividing, the genome is organized into discrete bodies.

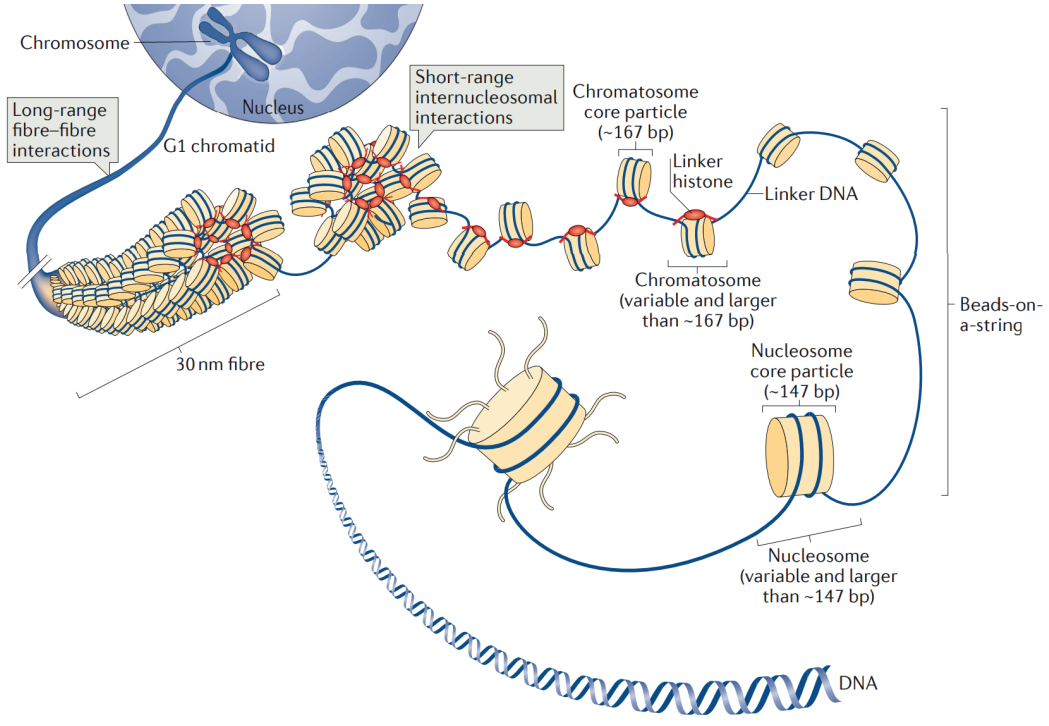

FIGURE I. 6 ***Levels of chromatin organization.***
DNA compaction in the cell nucleus implies the formation of a hierarchy of histone-dependent interactions, including the formation of the nucleosome, constituted by an octamer of histone proteins. Strings of nucleosomes in a bead-on-a-string disposition are stabilized by linker histone H1 interactions with the nucleosome particles, which constitute the chromatosome. Higher-order chromatin structures are performed by short-range internucleosomal interactions leading to 30 nm fibres. The association of individual fibres by long-range fibre–fibre interactions produces tertiary highly packaged structures that will be visualized as a

chromosome in metaphase of the cell cycle; these can measure from 1.5 to 700 μm. Adapted from Fyodorov et al. (2018).

Chromosomes are relaxed and compartmentalized into nuclear domains that are known as chromosome territories, constituting a basic feature of nuclear architecture (Cremer and Cremer, 2001). Two major chromatin structures can be classified according to their level of condensation: heterochromatin and euchromatin. Heterochromatin resembles a condensed structure that is characterized by lower levels of expression, whereas euchromatin is transcriptionally permissive and displays a relaxed organization (Li and Reinberg, 2011; Zhou et al., 2010).

3.3 Chromatin regulation

Chromatin is a highly ordered and dynamic structure. A precise regulation of chromatin packaging will alter the accessibility of many DNA interacting protein complexes, such as the transcriptional machinery complex (Kouzarides, 2007). Different epigenetic mechanisms modulate access to DNA in response to upstream or external signals including DNA methylation, nucleosome remodelling, histone post-translational modifications (PTM), incorporation or replacement of histone variants and non-coding RNA (ncRNA) (**Figure I. 7**). Remarkably, none of these mechanisms operates in isolation but rather work together to create a complex interconnected epigenetic network that regulates gene expression. Due to the critical role of these mechanisms in transcription, it is not surprising that over the past decade epigenetic dysregulation has emerged as a prominent and recurrent theme in cancer (Berdasco and Esteller, 2013). We will briefly describe all these epigenetic processes with a specific focus on histone modifications and the enzymatic activities behind them.

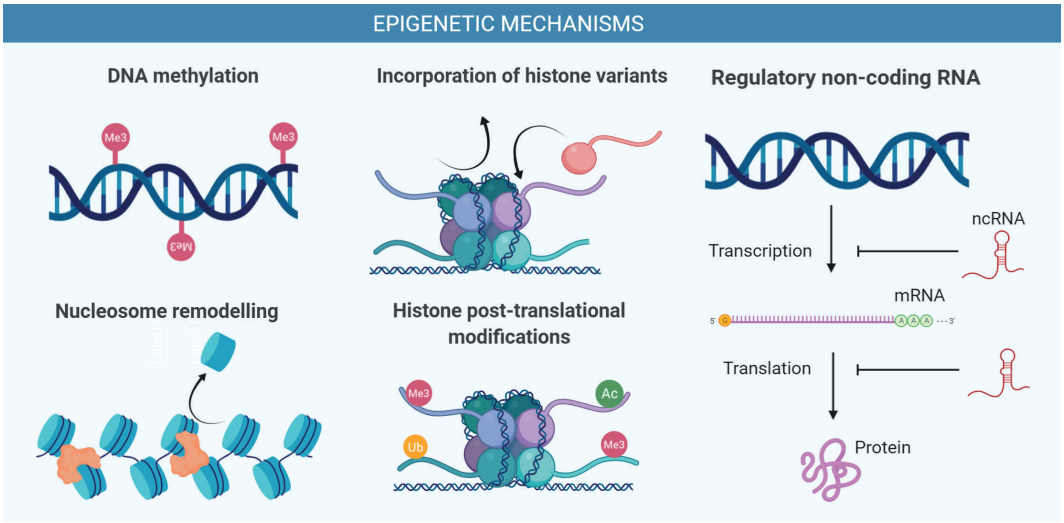

FIGURE I. 7 ***Epigenetic mechanisms regulating chromatin.***
Five main epigenetic mechanisms control chromatin structure and thus the accessibility of transcriptional machinery leading to changes on gene expression: *i*) modification of DNA nucleotides by methylation, which is associated to transcriptional repression; *ii*) incorporation or replacement of histone variants of the nucleosome core, mediated by chaperone proteins; *iii*) regulatory non-coding RNA, such as microRNA, that

can block gene transcription or translation of coding genes; *iv*) nucleosome remodelling, which promotes sliding, eviction or incorporation of nucleosomes into chromatin; and *v*) post-translational modification of histones on the N-terminal tail, which are exposed at the external soluble part of the nucleosome, providing a further level of chromatin regulation. (Created with Biorender.com)

3.3.1 DNA methylation

DNA methylation is a chemical epigenetic modification that occurs at the fifth carbon of the pyrimidine ring of the DNA nucleotide cytosine, forming the modified nucleotide of 5-methylcytosine (5mC). This modification mainly occurs at cytosine followed by guanine dinucleotides (CpG) of the genome and is much less commonly observed at non-CpG sites, such as cytosine followed by adenine, thymine or another cytosine (CpA, CpT and CpC) (Gruenbaum et al., 1981; Woodcock et al., 1987). The human genome contains about 30,000 CpG islands (CGI), which are areas full of such CpG dinucleotides that are defined as 0.5 kb stretches of DNA with a GC content superior of 55%, typically found in the promoter region (Goldman, 2001). *De novo* methylation of DNA is catalysed by DNA methyltransferase 3 alpha and beta (DNMT3A and DNMT3B, respectively) and is then maintained by the major DNA methyltransferase 1 (DNMT1), with participation from DNMT3A and DNMT3B (Jones and Liang, 2009). The identification of 5mC oxidases of the ten-eleven translocation (TET) family led to the discovery that DNA methylation can be reversibly modified (Wu and Zhang, 2010). Methylated CpG are recognized by a family of proteins harbouring a methyl-CpG–binding domain (MBD) that recruits chromatin remodellers or histone modifiers associated with gene repression. Thus, this modification is fundamentally associated to the heritable transcriptional repression of transposable elements in the genome, monoallelic expression of imprinted genes, inactivation of X chromosome in female cells, and the selective exposure of promoters to TFs.

DNA methylation has been reported to be altered in many cancers. In particular, tumour cells display an abnormal pattern of methylation characterized by a widespread loss of DNA methylation that contrasts with the starkly CGI hypermethylation of tumour suppressors (Baylin et al., 1986; Jones and Baylin, 2002). These alterations have been associated to age (Maegawa et al., 2010; Teschendorff et al., 2010), consistent with the age-incidence association of adult cancer (see section 1.3). In paediatric tumours, DNA methylation alterations have also been described, for instance in posterior fossa group A ependymomas, which exhibit CpG-island hypermethylation compared to other ependymomas subtypes (Bayliss et al., 2016).

3.3.2 Incorporation or replacement of histone variants

Histone variants have the potential to displace the canonical histones from the nucleosome octamer, altering its nature either by inducing structural changes or by perturbing its

interaction with other factors (e.g. remodelling complexes, transcription machinery, or other nucleosomes). Incorporation or replacement of histone variants relies on the activity of histone chaperones. Five H3 variants have been identified in mammals with very different functions: centromere protein A (CENP-A), H3.1, H3.2, H3.3 and H3.1t. The H3.1 and H3.2 variants mediate gene repression (Hake et al., 2006), while H3.3 is associated with transcriptionally active regions (Bernstein and Hake, 2006). Other examples are found on the variants of canonical H2A, including H2A.X, H2A.Z, macroH2A and H2A.Bbd. H2A.X, for instance, has an important role during DNA double-stranded breaks, whereas H2A.Z has been implicated in the formation of heterochromatin (Jin et al., 2005).

3.3.3 Nucleosome remodelling

Nucleosomes are relatively stable entities due to the cumulative effect of many weak DNA-histone interactions, occurring in approximately every 10 bp of DNA (Luger and Richmond, 1998). However, three essential movements control its positioning in chromatin: sliding along the DNA molecule, exchange by another nucleosome, and eviction from the DNA fibre. These movements are critical for gene expression, as they can inhibit access of DNA-binding proteins to DNA, facilitate transcription, or bring distal regulatory sites into proximity (He et al., 2010; Thomas and Elgin, 1988). Chromatin remodelling requires biochemical coupling to adenosine triphosphate (ATP) hydrolysis. Nucleosome remodellers involve multiprotein complexes that are organized into four subfamilies according to their ATPase catalytic subunit and flanking domains. They include the switch/sucrose non-fermenting (SWI/SNF) complex, imitation switch (ISWI), chromodomain helicase DNA binding (CHD) and inositol requiring 80-like (INO80) families. All remodelling enzymes have unique flanking domains that serve as platforms for chromatin effectors. For instance, the SWI/SNF ATPases contain bromodomains (BRD) for recognising acetylated histones; ISWI ATPases contain a HAND/SANT/SLIDE domain for recognizing internucleosomal DNA; the CHD ATPases contain chromodomains that specifically interact with methylated lysines, and the INO80-like ATPases have a long peptide chain between their two helicase domains that has been proposed to fit DNA junctions during replication (Giles et al., 2019).

Nucleosome remodellers play important roles in regulating the initiation and elongation of transcription. They are often recruited to target genes through interactions with sequence-specific TF to serve as coactivators or corepressors. Once recruited to target gene promoters, chromatin remodellers alter the local chromatin organization by nucleosome movement or displacement, which can facilitate either gene activation or repression (Becker and Workman, 2013). For example, the SWI/SNF complexes have transcriptional activating roles, whereas the nucleosome remodelling and deacetylase complex (NuRD; also known as Mi-2) belongs to the CHD family of nucleosome remodellers and is

involved in transcription repression (Denslow and Wade, 2007). Given the determinant role of these complexes on nucleosome remodelling and consequently on gene expression, mutations in these complexes have been reported in many cancers in the last years. The SWI/SNF complex is the most frequently mutated chromatin regulator observed in adult cancers. At least nine genes encoding this complex are recurrently mutated, with a collective frequency nearing that of the "master" tumour suppressor p53 (Kadoch et al., 2013). This is in agreement with sequencing studies of paediatric tumours, in which the SWI/SNF complex was one of the eight recurrently mutated epigenetic nodes, including mutations in SWI/SNF-related, matrix associated, actin dependent regulator of chromatin, subfamily 4 and 1, member A and C (*SMARCA4* and *SMARC1*, respectively*)*, actin-like 6B *(ACTL6B)* and AT-Rich interaction domain 1A and 1B (*ARID1A* and *ARID1B*, respectively) (Huether et al., 2014).

3.3.4 Regulatory non-coding RNA

Non-coding RNA (ncRNA) represents a subclass of RNA that is not translated into protein. Based on function, ncRNAs can be classified as either housekeeping or regulatory ncRNAs. Housekeeping ncRNAs are constitutively expressed and include messenger, transfer and ribosomal RNA (mRNAs, tRNAs and rRNAs, respectively), which are involved in transcriptional and translational regulation, and small nuclear RNA (snRNAs) and small nucleolar RNA (snoRNAs), with essential roles on RNA biogenesis and maturation. The second group, regulatory ncRNAs, can be subdivided in two major groups based on an arbitrary threshold of 200 nucleotides length, namely short ncRNAs (sncRNAs) and long ncRNAs (lncRNAs). Short ncRNAs include microRNAs (miRNAs), small interfering RNAs (siRNAs) and P-element-induced wimpy testis (PIWI)-associated RNAs (piRNAs), all of which regulate gene expression. lncRNAs are a group of large, heterogeneous ncRNAs that represent an important point for epigenetic regulation, as they can interact with genes to alter gene transcription, silence translation or guide methylation. They exhibit a wide range of secondary and tertiary structures, have introns and display epigenetic marks, indicating their ability to be differentially expressed (Srijyothi et al., 2018). An emerging number of studies have begun to elucidate particular ncRNAs dysregulated across multiple cancer types (Huarte, 2015). However, due to their relatively low abundance and reduced conservation across species as compared to coding RNA, studying ncRNAs is quite difficult.

3.3.5 Histone post-translational modifications (PTM)

Post-translational modifications (PTM) of histones occur in the N-terminal tails that protrude from the nucleosome. These are dynamic and reversible covalent modifications that include acetylation, methylation, phosphorylation, ubiquitylation, neddylation,

sumoylation and ADP-ribosylation. Such modifications influence chromatin accessibility, providing binding platforms for chromatin remodellers, histone chaperones, DNA/histone modifying enzymes and general TFs (Allis and Jenuwein, 2016; Kouzarides, 2007). Consequently, PTMs have a crucial role in DNA transcription, replication and repair. Dysregulation of histone PTMs has been related to developmental defects and cancer (Chi et al., 2010).

Currently, 18 different PTMs on at least 400 residues that can affect both canonical and histone variants, have been described (Bannister and Kouzarides, 2011; Huang et al., 2014). Indeed, histone PTMs act in a combinatorial way influencing one another so that one modification can activate or recruit chromatin-modifying complexes to generate another histone PTM. This is referred to "histone crosstalk" and can lead to thousands of combinations that occur along the N-tail of the same histone (named "*in cis*") or affect histones of different nucleosomes ("*in trans*"). Such complex functional links between PTM modifications constitute the so-called "histone code" that considerably extends the information potential of the genetic code (Bannister and Kouzarides, 2011; Jenuwein and Allis, 2001). Combinations of various histone PTMs, together with TFs and RNA polymerase II (RNAPII), are referred as chromatin states and have been used to define regulatory elements of the genome such as promoters or enhancers (Ernst and Kellis, 2010). For example, H3K4me1 combined with H3K27ac mark active enhancers. Active promoters are characterized by a detectable level of H3K4me3 coupled with a high ratio of H3K4me3 to H3K4me1, whereas the presence of H3K27me3 or H3K9me3 is associated with repressive chromatin states. Poised or bivalent promoters show occupancy of H3K4me3 together with H3K27me3 (**Figure I. 8**).

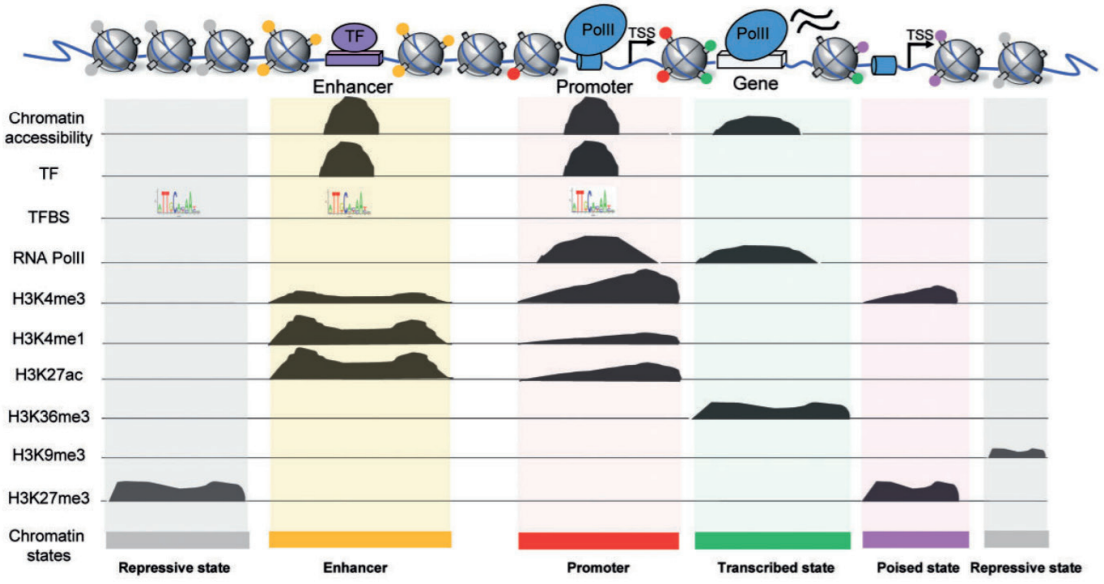

FIGURE I. 8 ***Chromatin states involve recurrent histone PTM combinations that define regulatory elements of the genome.***
Chromatin states are defined by different combinations of histone modifications, TFs, and RNA Pol II

binding. In this example, a typical repressive state (gray) is characterized by high H3K27me3 signal or H3K9me3 signal; an enhancer state (yellow) shows a high occupancy ratio of H3K4me1 to H3K4me3, as well as high H3K27ac; the promoter state (red) shows a high occupancy ratio of H3K4me3 to H3K4me1 and of RNA Pol II binding at the promoter; and the poised promoter state (magenta) shows the occupancy of H3K4me3 and H3K27me3, which combination of both constitute the bivalent domains. Actively transcribed regions (green) are characterized by a high occupancy of H3K36me3 with some RNAPII binding along the gene body. TFBS indicates the sequence of TF binding sites. Retrieved from Jiang and Mortazavi (2018)»Щ.

A large number of histone modifiers have been identified. According to their function they can be classified as "writer", "eraser" and "reader" (**Figure I. 9**). Writers are those proteins or protein complexes that place the epigenetic histone PTM, whereas erasers remove them. Readers have a domain that is able to recognize a histone PTM, or a combination of them, leading to the recruitment of additional chromatin-modifying complexes to transduce the epigenetic signal. Numerous reader proteins have been identified that display characteristic domains that enable the epigenetic signal to be recognized and transduced (Giles et al., 2019).

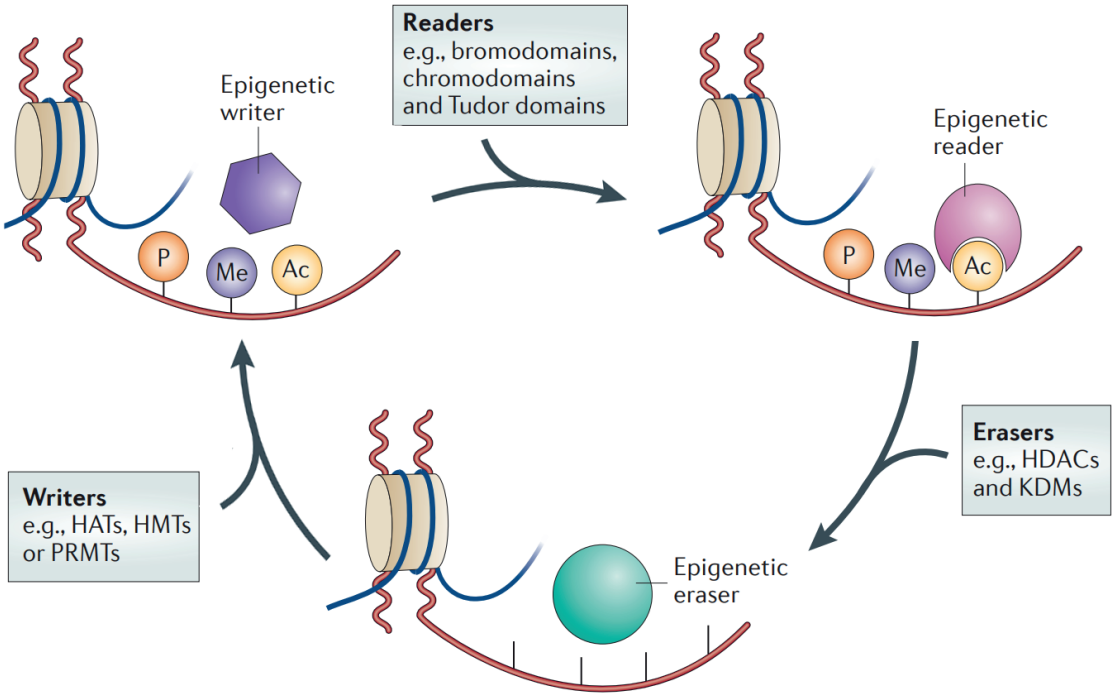

FIGURE I. 9 ***Writers, erasers, and readers of histone PTMs.***
Histone PTMs includes a wide range of modifications, such as methylation (Me), acetylation (Ac), and phosphorylation (P). In general, three enzymatic activities regulate histone PTM: epigenetic writers set the corresponding histone PTMs and include histone acetyltransferases (HAT), methyltransferases (HMT), and protein arginine methyltransferases (PRMT); epigenetic readers recognize PTMs throughout their particular domain and include bromodomains (BRD), chromodomains, and Tudor domains; and epigenetic erasers are responsible for the removal of the histone marks and include histone deacetylases (HDAC), lysine demethylases (KDM), and phosphatases. The reading process of the histone modification recruits epigenetic effectors that can lead to local structural changes on chromatin affecting gene expression. Addition and removal of these PTMs on histone tails may affect other histone PTMs in a highly complicated histone code. Adapted from Falkenberg and Johnstone (2014).

The most common histone PTMs are as follows.

a) Histone acetylation

Histone acetylation was the first histone PTM described, showing a strong association with actively transcribed genes (Allfrey et al., 1964; Pogo et al., 1966). This modification is highly dynamic and typically occurs in the lysine (K) residues of histones. In a few cases, it can be found at serine (S), threonine (T) and tyrosine (Y) residues (Huang et al., 2014; Rothbart and Strahl, 2014). Acetylation neutralizes the positive charge of K residues, so that charge-dependent interactions between histones and chromatin, linker DNA or adjacent histones are weakened, which leads to an increased accessibility of the DNA to the transcription machinery. Consequently, this modification is associated with cellular processes that require DNA access, such as prior to DNA replication (Unnikrishnan et al., 2010), during transcription or during DNA repair (Xu and Price, 2011). Specifically, histone acetylation can be found at cis-regulatory regions, such as active promoters and enhancers, and it is present in some cases within gene bodies of active genes (Dawson and Kouzarides, 2012; Rajagopal et al., 2014). For instance, acetylation of H3K27 is typically found in active enhancers.

Histone acetyltransferases (HAT) include all the enzymes responsible for catalysing acetylation of histones, by transferring acetyl group from acetyl-CoA. Besides histones, a variety of non-histone substrates are acetylated by HATs. Based on their cellular location in the nucleus or cytoplasm, HATs are classified as type A or B, respectively. Type A HATs are further subdivided into five families according to their homology and acetylation mechanisms and include the Gcn5-related N-acetyltransferase (GNAT) family, the MYST family (according to the acronyms of their members) and several steroid receptors and transcription co-activators families (Bowers et al., 2010; Chen et al., 1997; Spencer et al., 1997; Voss et al., 2009). The GNAT family includes the CREB binding protein (CBP) and E1A binding protein P300 (p300), which are the main writers responsible for setting H3K27ac (Jin et al., 2011; Raisner et al., 2018). Type B HATs also have cytoplasmic substrates and can acetylate the newly synthesized histones (Blanco-García et al., 2009). On the other hand, histone deacetylases (HDAC) antagonize the enzymatic activity of HATs by removing histone acetylation (**Figure I. 10**). In humans, 18 HDAC enzymes can use either zinc or nicotinamide adenine dinucleotide (NAD) to deacetylate histone residues (Seto and Yoshida, 2014). Sirtuins (SIRT) are the classic example of NAD-dependent deacetylases that have been related to longevity, aging-related diseases and metabolic homeostasis (Guarente, 2011). Acetylated lysine residues are “read” by a large number of histone effectors containing BRD domains, which is an extensive area of research.
Altered global levels of histone acetylation through mutation or dysregulation of HATs or HDACs is a common event in cancer including paediatric cancer (Grobner et al., 2018;

Ma et al., 2018; Ropero and Esteller, 2007). Loss of acetylated K16 and trimethylated K20 in histone H4, for instance, has been linked to a variety of tumours (Fraga et al., 2005) with potential prognostic value (Seligson et al., 2009). In addition, some fusion partners in leukaemia are rearranged with CBP or physically interact with other HATs leading to an aberrant acetylation pattern that is essential for the leukemogenic process (Ayton and Cleary, 2001; Perez-Campo et al., 2013).

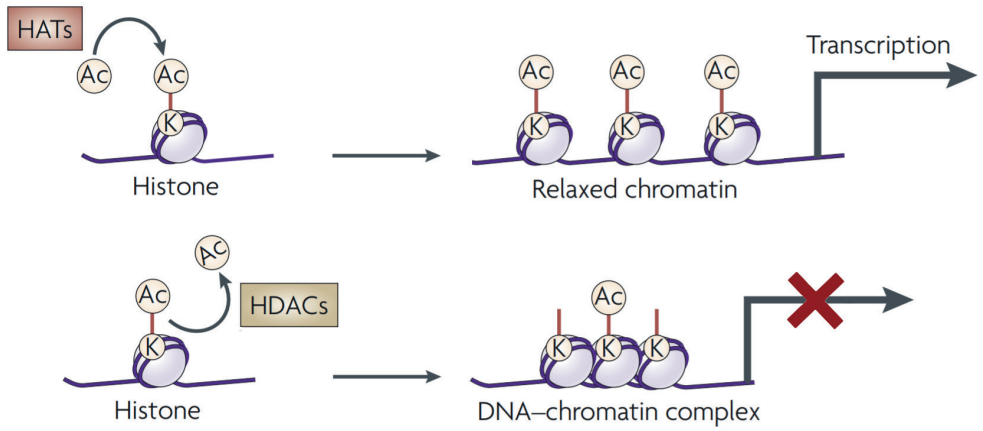

FIGURE I. 10 ***Histone acetylation and its effects on gene transcription.***
Histone acetyltransferases (HAT) settle acetylation residues on lysine residues (K) leading to a more accessible chromatin fibre and thus promoting gene activation. In contrast, histone deacetylases (HDAC) remove such acetyl groups from histone proteins, leading to a more compacted structure and hence blocking gene transcription. The red cross indicates transcriptional repression. Adapted from Kazantsev and Thompson (2008).

b) Histone phosphorylation

Phosphorylation is a histone PTM that occurs in the S, T, Y or histidine (H) residues, imparting a negative charge to the histone tail. This modification, together with the negative charge of the phosphates of the DNA backbone, creates charge repulsion between histones and DNA. Thus, phosphorylation of histones, similarly to acetylation, increase chromatin opening (Banerjee and Chakravarti, 2011). Histones are phosphorylated in a variety of biological contexts. For instance, phosphorylation of H2A.X in S139 (producing γH2A.X) by ATM Serine/Threonine Kinase (ATM) or ATR Serine/Threonine Kinase (ATR) kinases during DDR, leads to more accessible chromatin facilitating the recruitment of the DNA repair machinery (Paull et al., 2000).

c) Histone ADP-ribosylation or PARylation

ADP-ribosylation or PARylation is a reaction catalysed by most members of the poly-ADP-ribose polymerase (PARP) family that comprises 17 proteins in humans (Barkauskaite et

al., 2015). With the exception of PARP9 and PARP13, PARP proteins transfer a single mono-ADP-ribose group from NAD^+ to their target proteins on arginine (R), aspartate (D), glutamate (E), K and S residues. This modification is thought to act similarly to acetylation and phosphorylation, leading chromatin to adopt a more relaxed structure (Messner and Hottiger, 2011). During DDR ADP-ribosylation is catalysed by PARP1-3 near sites of DNA damage which promotes recruitment of DNA repair factors via recognition of the ADP-ribose (PAR) domains. The DNA-dependent activity of these DDR PARPs requires the presence of a conserved Tyr-Gly-Arg (WGR) domain, which is present in PARPs 1–3 (Barkauskaite et al., 2015).

d) Histone ubiquitylation

Ubiquitin is a small, highly conserved, mainly globular protein consisting of 76 amino acids that controls a multitude of biological processes including protein degradation, endocytosis, autophagy, immunity, DNA repair, inflammation, and transcription (Husnjak and Dikic, 2012).

Ubiquitination is the process that leads to the activation and transfer of ubiquitin to target proteins in a coordinated three-step enzymatic cascade (**Figure I. 11**). Ubiquitin is first activated by an ATP-dependent reaction by E1 enzymes, followed by a transferring step to an ubiquitin-conjugating enzyme, or E2. The final step is carried out by an ubiquitin ligase E3, which first recognizes and recruits a target protein (designated as the substrate) and then transfers and conjugates ubiquitin from the E2 onto a K residue of the substrate. Ubiquitin itself contains seven K residues, which serve as acceptors for the second ubiquitin molecule, leading to polyubiquitylation of the substrate after multiple rounds of this reaction. There are two known E1 enzymes (including the ubiquitin activating enzyme or UAE), 38 known E2 enzymes and more than 600 known E3 ubiquitin ligases. E3 ligases are classified into three families according to their functional domain: homologous to E6-AP carboxy terminus (HECT) type, a really interesting new gene (RING) type or U-box domain-containing (U-box) type (Ardley and Robinson, 2005). The family of RING/U-box-type E3 ligases can be either single-subunit proteins or multi-subunit complexes. For example, the RING-finger protein 2 (RING1B) and the cullin-containing RING-finger E3s (CRLs) are both RING-type E3 ligases; but for the first, the RING-finger and substrate binding domain are contained on the same polypeptide, whereas for CRL, these are separated into different subunits acting as a scaffold (explained in more detail in Section 4.4.2). The ubiquitinated substrates are recognized by a variety of ubiquitin-binding domains (UBD) or ubiquitin receptors that contain at least one UBD within their structure (Dikic et al., 2009). The activity of the E1-E2-E3 ubiquitinating enzymes in the cell is counterbalanced by the activity of 100 identified deubiquitinating enzymes (DUB), which remove ubiquitin from the targeted proteins (Amerik and Hochstrasser, 2004).

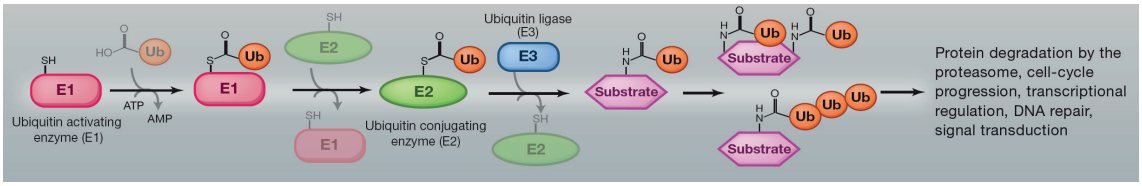

FIGURE I. 11 ***Ubiquitination cascade.***
Ubiquitination of proteins, including histones, requires the sequential action of three enzymes: E1, E2, and E3. E1, or ubiquitin-activating enzyme, catalyzes the ATP-dependent activation of ubiquitin and formation of a thioester bond between the ubiquitin C-terminus and the catalytic cysteine on E1. Ubiquitin is then transferred to a catalytic cysteine of E2 (ubiquitin-conjugating enzyme) and through the E3 (ubiquitin ligase) to the substrate. Ubiquitin is covalently attached through its C-terminus to the lysine's ε-amino group or (less frequently) to the N-terminus of proteins by forming an isopeptide bond. This modification is required for many cellular processes, including protein degradation by the proteasome, cell cycle progression, transcriptional regulation, DNA repair, and signal transduction. Retrieved from Morreale and Walden (2016).

As histones are the most abundant ubiquitinated proteins, their ubiquitination plays critical roles in many processes in the nucleus, including transcription, maintenance of chromatin structure, and DNA repair. This PTM occurs at all four histones, but it has been well characterized in H2A and H2B, especially in the context of DDR. Ubiquitination of H2A on residues K13/15, K119 and K127/129 by RING-finger protein 168 (RNF168), RING1B and BRCA1 DNA repair–associated (BRCA1), respectively, defines regulatory zones during DDR, preventing transcription as well as conditioning the repair pathway choice (through homologous or non-homologous recombination responses) (Uckelmann and Sixma, 2017). Consistently, deregulation of H2A variants as well as their PTMs has been linked to tumorigenic processes. For instance, deubiquitination of histone H2A.Z mediates androgen-receptor oncogenic gene activation in prostate cancer (Corujo and Buschbeck, 2018).

e) Histone modification by ubiquitin-like proteins: neddylation

Ubiquitin-like proteins (UBL) are related by sequence and structure to include the small ubiquitin-like modifier (SUMO) and the neural precursor cell expressed, developmentally down-regulated 8 (NEDD8). UBL are conjugated to substrates via biochemical mechanisms that are homologous to the ubiquitination cascade, each one having its specific E1, E2, and in some cases E3. The functional consequences of the modification are distinct depending on the UBL and substrate involved. For NEDD8, the neddylation cascade starts with an activation step that involves its cleavage by cell hydrolases, such as ubiquitin C-terminal hydrolase L3 (UCHL3) and SUMO peptidase family member NEDD8 specific (SENP8). After this processing, NEDD8 is activated in an ATP-dependent reaction by an E1, leading to its transfer to an E2 NEDD8 conjugating enzyme, which shuttles it to an E3 ligase that will conjugate NEDD8 to its specific substrate. In contrast to the ubiquitination cascade, very few enzymes in the NEDD8 pathway have been identified so far: only one E1 (the NEDD8-activating enzyme (NAE)) and two E2 (ubiquitin conjugating enzyme E2 M

(UBE2M) and ubiquitin conjugating enzyme E2 F (UBE2F)). Very few E3 are known, and most of them contain a RING-finger domain, for instance RING-finger protein 111 (RNF111) or RING box 1 (RBX1) (Zhao et al., 2014).

Certain neddylated substrates are E3 enzymes, and it has been reported that conjugation of NEDD8 regulates their ligase activity (Flotho and Melchior, 2013; Kerscher et al., 2006). For instance, activation of the CRL E3 ligases requires the conjugation of NEDD8 at a certain K residue (Zhou et al., 2019). On the other hand, most substrates can be both ubiquitylated and neddylated. Furthermore, overexpression of NEDD8 leads to conjugation to substrates of the ubiquitin pathway (Hjerpe et al., 2012). Thus, neddylation and ubiquitylation pathways appear to be connected.

Histones are frequently neddylation substrates (Li et al., 2014). During DDR, poly-neddylation of histone H4 functions as a signal for amplification of the DDR cascade through its recognition by RNF168 (see histone ubiquitination) (Ma et al., 2013). Since DDR is an important dysregulated pathway in cancer, the role of histone neddylation during DDR highlights potential new roles for NEDD8 in cancer.

f) Histone methylation

Histone methylation is based on the transfer of a methyl group from a molecule of S-adenosyl methionine (SAM) to a K or R residue of histone tails (Shi and Whetstine, 2007). There are three different methylation states: mono- (me), di- (me2, which can be symmetric or asymmetric) and tri- (me3) methylation. Commonly methylated sites are K4, -9, -27, -36 and -79 of histone H3, and K20 of histone H4. Since none of the methylation states change the electronic charge of the amino acid chain (Taverna et al., 2007), these PTM lead to different outcomes in the regulation of chromatin structure and function (Martin and Zhang, 2005). In general, H3K4, H3K36 and H3K79 methylation is considered to mark active transcription, whereas H3K9, H3K27 and H4K20 methylation is associated with silenced chromatin states (Black et al., 2012) (**Figure I. 12**). Nevertheless, promoters of some developmental genes in ESCs are marked simultaneously by activating H3K4me3 as well as repressing H3K27me3 marks; these are known as bivalent domains. The coexistence of these two marks is believed to play a decisive role in the maintenance of pluripotency, poising genes for subsequent activation during cell-fate decision (Bernstein et al., 2006; Di Croce and Helin, 2013).

Histone methyltransferases (HMT) catalyse the addition of methyl groups donated from SAM molecules to histones and non-histone proteins. Three families of HMT have been identified so far, including the Su(var)3-9, Enhancer of Zeste, Trithorax (SET)-domain-containing proteins, DOT1-like proteins and protein N-methyltransferase family (PRMT).

While SET-domain and DOT1-like HMT methylate K residues, members of the PRMT family have been shown to methylate R residues (Martin and Zhang, 2005).

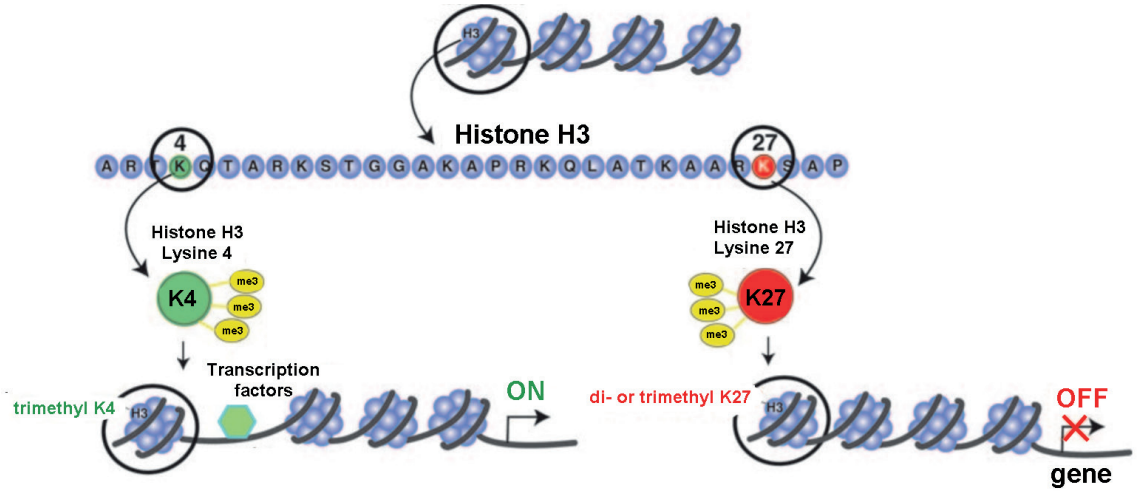

FIGURE I. 12 ***Transcriptional effects of histone methylation on residues K27 and K4 of histone H3.*** Methylation of histone H3 has different effects on gene activation depending on the methylated residue. For example, methylation of K27 residue, which is mediated by the Polycomb repressive complex 2 (PRC2), leads to a more compact chromatin structure that prevents binding of TFs to promoter region, thus the gene is silenced. In contrast, methylation of K4 in the same histone, which is mediated by mixed lineage leukaemia (MLL) complex (containing MLL, WDR5, RbBP5, and Ash2L), relaxes the chromatin structure, and then TFs have access to the promoter, resulting in transcriptional activation. Adapted from Wen et al. (2008).

Methylation of histone residues was thought to be relatively permanent and only removed by histone exchange or by dilution during cell division. Thus, it was not until 2004 that the first histone demethylase (HDM) activities were published. Two evolutionary conserved families of HDMs have been described according to the enzymatic reaction used to remove methylation marks: the flavin (FAD) and the Jumonji C (JmjC) families (Black et al., 2012). FAD-demethylases were the first identified that perform an amine oxidation with FAD-dependant reduction. FAD-demethylases include the lysine demethylase 1A (KDM1A), also known as LSD1, which catalyses demethylation of H3K4me1 and H3K4me2. It has the ability to additionally demethylate H3K9me1 and H3K9me2 but cannot demethylate tri-methyl residues. In contrast to FAD demethylases, the second family of demethylases, JmjC, perform a dioxygenase reaction that is dependent on iron and α-ketoglutarate for demethylating mono-, di- and trimethylated residues. This family consists of 30 homologous members, of which 18 display HDM activity, including lysine demethylases -2 to -6 (KDM2–6) (Kooistra and Helin, 2012). Readers of histone methylation contain a wide variety of domains including chromodomains, PHD finger domains, WD40, Tudor, double/tandem Tudor, MBT, Ankyrin repeats, zf-CW and PWWP, among a long list that is continually growing. **Table I. 2** summarizes the principal HMT and HDM identified regarding histone H3 and H4 as well as their reader proteins.

In this thesis, we focus on H3K27me3, and especially on its writers and erasers, which are presented in detail on the next section.

TABLE I. 2 ***Principal HMT and their HDM and readers on histones H3 and H4.*** The star symbol (*) indicates that the HMT subunit constitutes part of the complex associated with Set1 or COMPASS complexes, with ASH2L, RBBP5, and WDR5 components. SET1A/1B-containing complexes additionally contain WDR82 and CXXC1; MLL1/2 complexes contain Menin, and the MLL3/4 COMPASS complexes contain PTIP, PA-1, and NCOA6. Domain indicates the reader domain to recognize the histone PTM. Chromo, chromodomain; PHD, PHD finger domain; TTD, Tandem Tudor domain, BAH, bromo-adjacent homology domain; MBT, malignant brain tumor domain. Adapted from Hyun et al. (2017).

Residue	HMT (writer)	HDM (eraser)	Reader	Domain	Biological roles of K methylations
H3K4	SET1A/KMT2E*	LSD1/KDM1A	CHD1	Chromo	Chromatin remodeller
	SET1B/KMT2F*	LSD2/KDM1B	BPTF	PHD	NURF complex subunit
	MLL1/KMT2A*	NO66/MAPJD	TAF3	PHD	Transcription initiation factor subunit
	MLL2/KMT2B*	JARID1A/KDM5A	Sgf29	Tudor	Crosstalk between H3K-4me2/3 and H3 acetylation
	MLL3/KMT2C*	JARID1B/KDM5B	ING4	PHD	G/M cell cycle arrest
	MLL4/KMT2D*	JARID1C/KDM5C	CFP1	PHD	Binds to unmethylated CpG
	SMYD1/KMT3D	JARID1D/KDM5D	PHF2/KD-M7C	PHD	Oxygen sensor in normoxia
	SMYD2/KMT3C	-	SPIN1	PHD	Senescence and apoptosis
	SET7/9/KMT7	-	PHF23	PHD	Autophagy
	PRDM9/KMT8B	-	PYGO2	PHD	Self-renewal of mammary progenitor cells
H3K9	SUV39H/KM-T1A–B	JHDM2A/KDM3A	HP1α/β	Chromo	Heterochromatin formation
	G9a/KMT1C	JHDM2B/KDM3B	HP1γ	Chromo	Transcription elongation
	GLP/KMT1D	JHDM2C/KDM3C	UHRF1	TTD	DNA methylation
	SETDB1/KMT1E	JHDM3A/KDM4A	-	-	-
	PRDM family	JHDM3B/KDM4B JHDM3C/KDM4C JHDM3D/KDM4D PHF8/KDM7B PHF2/KDM7C	-	-	-
H3K27	EZH1/KMT6B	UTX/KDM6A	CBX7	Chromo	Transcriptional depression of PRC complex target gene
	EZH2/KMT6A	UTX/KDM6A			
		UTY/KDM6C	EED	WD40	Spreads H3K27 methylation
		JMJD3/KDM6B	BAHD1	BAH	Facultative heterochromatin formation
		KIAA1718/KDM7A	NSD2	PWWP	Transcription elongation
		PHF8/KDM7B	-	-	-
H3K36	SETD2/KMT3A	JHDM1A/KDM2A	DNMT3A	PWWP	DNA methylation
	NSD1/KMT3B	JHDM1B/KDM2B	LEDGF	PWWP	DNA repair
	NSD2/KMT3G	JHDM3A/KDM4A	NBS1	-	DNA repair
	NSD3/KMT3F	JHDM3B/KDM4B	Ku70	-	DNA repair

H3K36	SMYD2/KMT3C	JHDM3C/KDM4C	MRG15	Chromo	RNA splicing
	ASH1L/KMT2H	JHDM3D/KDM4D	ZMYND11	PWWP	RNA splicing
	SETD3	-	-	-	-
	SETMAR	-	-	-	-
H3K79	DOT1L/KMT4	-	TP53BP1	Tudor	DDR
H4K20	SET8/KMT5A	PHF8/KDM7B			
	SUV4-20H1/ KMT5B	PHF2/KDM7C	L3MBTL1	MBT	Chromatin compaction
	SUV4-20H2/ KMT5C	LSD1	ORC1	BAH	Replication
			ORCA	WD repeat	
			Pdp1	PWWP	-

3.4 Polycomb group and KDM6 histone modifiers

3.4.1 Polycomb and their role in development with Trithorax

Polycomb proteins (PcG) are transcriptional regulatory factors that control gene expression, being a paradigmatic model of epigenetic regulation of gene silencing (Aranda et al., 2015). They were first identified in *Drosophila melanogaster,* when in 1942, Slifer described a mutation that caused the development of partial sex combs (a specialized row of distinctive bristles in the thoracic legs of adult males flies and named the mutation *extra sex combs (esc)*. In 1947, a dominant mutation with a similar phenotype conferring additional sex combs was described and named *Polycomb (Pc)*. Later, all these genes were termed PcG. In 1978, Lewis postulated that PcG negatively regulates a set of developmental genes named as BX-C, which would explain why mutations on these regulators cause such pronounced developmental defects, known as homeotic phenotypes. It was further discovered that homeotic genes controlled by PcG (in mammals known as *HOX* genes) are multiple, clustered and very conserved from arthropods, such as fly, to mammals, due to their role in the generation of different body segments, regulating morphogenesis and organogenesis (Kassis et al., 2017).

Once the idea of a global repressor of the BX-C genes was proposed, the suggestion of a global activator soon followed. Consistently, the identification of *trithorax* (*trx)*, was identified as a positive regulator of such developmental genes (Schuettengruber et al., 2011). Similar as PcG, the wide number of subunits was grouped into the Trithorax group of proteins or TrxG. Given the numerous steps required for transcriptional activation, TrxG involves many DNA-binding, histone-modifying and chromatin remodelling proteins. Such TrxG-associated proteins group into complexes such as the complex protein associated with Set1 (COMPASS) or COMPASS-like complexes. They all generally include HMT with a SET domain (see **Table I. 2**) and a variety of protein members, such as the WD repeat domain 5 (WDR5), ASH2 like, histone lysine methyltransferase complex subunit (ASH2L), that dictate the function of the complex (Geisler and Paro, 2015). For instance,

a complex with lysine methyltransferases MLL3/MLL4 and KDM6A (see Section 3.4.6) targets methylation of H3K4 through its SET domain to some hormone-responsive genes, whereas a COMPASS complex with MLL1/MLL2 and menin 1 (MEN1) orchestrates activation of HOX genes (Schuettengruber et al., 2011).

Both PcG and TrxG are critical for maintaining cellular identity required for normal cell differentiation (Di Croce and Helin, 2013). Cell fate identity is regulated by differential spatiotemporal genetic programs that become activated or repressed by a cascade of maternal and zygotic TF in the early stages of development. At later developmental stages, these factors disappear and PcG and TrxG maintain such predetermined transcriptional patterns (for example in HOX genes) to stably transmit them during cell division or replication (Schuettengruber et al., 2011).

3.4.2 Polycomb complexes and their recruitment to chromatin

Since the discovery of PcG in flies, 18 PcG genes have been identified in *Drosophila*. In mammals this number has expanded during evolution, most likely by multiple duplication events, with a total of 37 members (Aranda et al., 2015). PcG proteins associate into two functional transcriptional repressive complexes (PRC), known as PRC1 and PRC2. PRC1 complexes have the core subunit RING-finger protein 1 (RING1A) or RING1B, which displays a E3 ligase activity that monoubiquitinates histone H2A at lysine 119 (H2Aub). The second complex PRC2, contains the core subunit enhancer of zeste homolog 1 (EZH1) or EZH2 with HMT activity, which is mainly involved in generating H3K27me2/3.

It is intriguing how PRC complexes are recruited to chromatin. In *Drosophila*, the PcG binding regions, called Polycomb responsive elements (PRE), were identified as DNA motifs for sequence-specific DNA binding proteins such as TF (Müller and Kassis, 2006). Consistently, a classical or hierarchical recruitment model was proposed in which (i) PRC2 might be recruited to these PREs through interactions with TFs, (ii) recruitment stimulates H3K27 methylation that (iii) provides a docking site for the PRC1 complex to bind. However, this model does not explain why PRC1-bound regions are devoid of H3K27me3. Therefore, an alternative model proposes that context-dependent interactions between TF, PRC1 and PRC2 are cooperative rather than hierarchical (Aranda et al., 2015; Schuettengruber et al., 2017) (**Figure I.13**).

In certain genomic contexts, both PRC complexes can be recruited independently of each other to chromatin. Therefore, additional factors have been found to mediate PcG recruitment to chromatin, including sncRNA or lncRNA, cooperative interactions with TF and histone PTMs, such as the recognition of H3K9me3 that induces PRC2 recruitment (Schuettengruber et al., 2017).

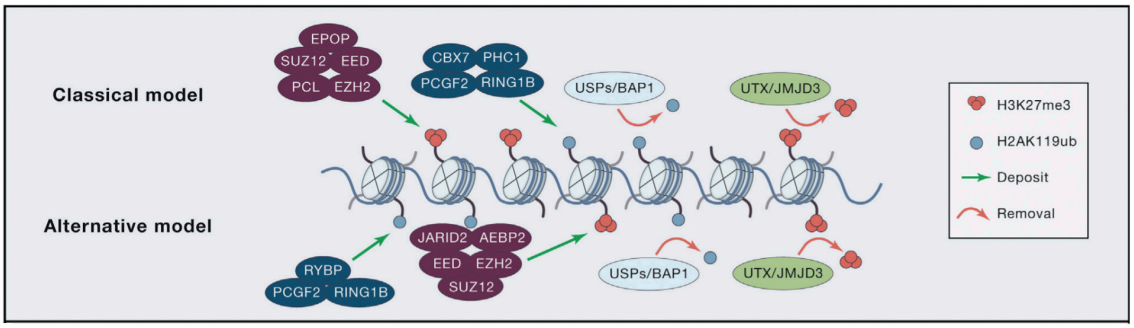

FIGURE I. 13 ***Models for PcG recruitment to chromatin.***
Two models explaining PcG recruitment to chromatin have been proposed: the classical and the alternative models. The first model suggests that PRC2 first binds chromatin and deposits H3K27me3. This modification is then recognized by the CBX subunit of the canonical PRC1 complex, which in turn catalyses monoubiquitination of H2A on K199 (H2AK119ub). Thus, recruitment of PRC to chromatin by this model is hierarchical. The alternative model, however, points to a coordinated recruitment in which ncPRC1 is targeted to unmethylated CpG islands (CGI) through its FBXL10/KDM2B subunit. ncPRC1 seems to be responsible for the majority of the H2AK119ub modifications present at PcG-target sites, which might facilitate the recruitment of PRC2. H3K27 methyl marks can be erased by histone demethylases, such as UTX/KDM6A and JMJD3/KDM6B, while several deuquibitinases (including BAP1, USP16, and USP21) can remove the monoubiquitin moiety from histone H2A. Adapted from Schuettengruber et al. (2017).

3.4.3 Polycomb and transcriptional regulation

PcG complexes mediate transcriptional regulation by altering the chromatin environment through its catalytic dependent and independent activities. First, through its enzymatic activities, PcG complexes impose monoubiquitination of H2A on K119 and the di-/tri-methylation of H3K27 at the gene bodies, which directly block gene transcription. In addition, in bivalent promoters marked by H3K27me3 and H3K4me3, PcG complexes hold the poised RNAPII at the transcriptional start site, thereby inhibiting its release. PRC1-mediated H2A ubiquitination was initially suggested to play an important role in PcG-mediated repression by interfering with multiple steps of the transcription process. However, more recent data have demonstrated that it is not required for PcG repression in flies and mammals (Illingworth et al., 2015; Pengelly et al., 2015), suggesting that the catalytic activity of PRC2 might be a key effector for such silencing. Secondly, PcG can induce chromatin condensation in a catalytic independent manner, rendering chromatin inaccessible to transcriptional machinery and inhibiting the SWI/SNF chromatin remodelling complexes (Aranda et al., 2015; Schuettengruber et al., 2017). Additional mechanisms exist for PcG-mediated gene repression, for instance by inhibiting the acetyltransferase activity of CBP, thereby favouring H3K27 methylation of the same K by PRC2 (Tie et al., 2016).

In recent years, a radically contrasting scenario has emerged that places PcG complexes as activators of gene expression (Cohen et al., 2018; Creppe et al., 2014; Frangini et al., 2013; Gao et al., 2014; Morey et al., 2013; Morey et al., 2015; Schaaf et al., 2013). For instance, during ESC differentiation toward an ectodermal fate, PRC1 is required for the

initial activation of developmental genes (Creppe et al., 2014). Another example of PRC1 mediating transcriptional activation is found in quiescent lymphocytes, where PRC1 is recruited to actively transcribed genes independently of PRC2, enabling the processivity of RNAPII (Frangini et al., 2013). A component of the PRC1 complex, activator of transcription and developmental regulator (AUTS2), triggers the recruitment of p300 to the complex, which acetylates histone tails favouring transcription activation (Gao et al., 2014). This switch from PRC1's role from repressor to activator has been proposed to be related to a change in the subunits conforming the complex (Creppe et al., 2014) or due to a phosphorylation of the catalytic subunit of PRC1 that severely reduces its enzymatic activity (Gao et al., 2014). Finally, a PRC1 role facilitating long-range promoter-enhancer interactions in the developmental gene Meis homeobox 2 (MEIS2) has been shown to promote gene activation (Kondo et al., 2014).

3.4.4 The PRC1 complex

PRC1 complexes have diverse compositions and can be divided into canonical and non-canonical complex. All share a conserved protein core composed by the catalytic activity of RING1A/B and one of the six Polycomb group RING-finger (PCGF1-6) proteins. Thus, six different groups of PRC1-containing PCGF complexes can be found, named PRC1.1–6 (**Figure I. 14**). PRC1-containing PCGF2/4 (known as MEL18 and BMI-1, respectively) subunits constitute the canonical PRC1 complex 1.2 and 1.4 (cPRC1.2 and cPRC1.4, respectively). These complexes are specified by the presence of one chromobox protein (CBX2,4,6-8) that binds to H3K27me3, and of a polyhomeotic homolog 1-3 (PHC1-3) that contains a sterile alpha motif domain essential for PcG-mediated repression. These accessory proteins regulate the recruitment of the complex to specific chromatin domains and/or modulate the catalytic activity of the core complex. The group of non-canonical complexes of PRC1 (ncPRC1) contain RING1B Yy1-binding protein (RYBP) or its homolog YY1 associated factor (YAF2). These subunits associate with PCGF1, PCGF3, PCGF5 or PCGF6 to form ncPRC1.1, ncPRC1.3, ncPRC1.5 and ncPRC1.6 complex, respectively. PRC1.1 complex contains the H3K36-specific demethylase lysine demethylase 2B (KDM2B) and BCL6 co-repressor (BCOR). However, this classification excludes the complexes containing RYBP and RING1B that are associated with PCGF2 and PCGF4 (Aranda et al., 2015).

At the molecular level, cPRC1 and ncPRC1 complexes co-occupy common as well as distinct subsets of target genes, with cPRC1-CBX correlating with higher H3K27me3 binding as compared to ncPRC1-RYBP. Furthermore, genes occupied by ncPRC1-RYBP are moderately expressed as compared to the robust gene silencing imposed by cPRC1-CBX complexes (Morey et al., 2013).

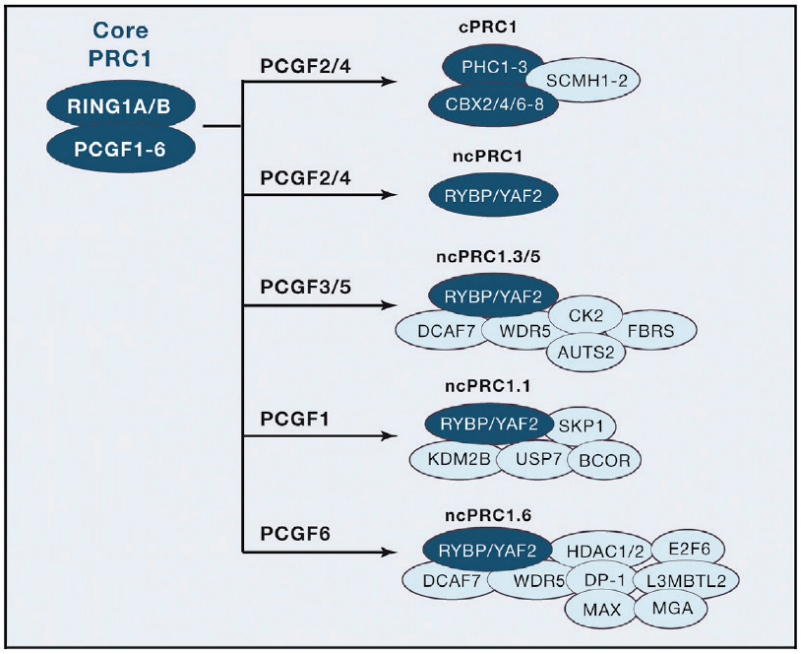

FIGURE I. 14 ***PRC1 complexes.***
Different compositions of the PRC1 complex are shown. The core of PRC1 (RING1A/B and PCGF1-6) can associate to a variety of proteins, thereby defining the canonical or the non-canonical PRC1 complexes (cPRC1 and ncPRC1, respectively). Both cPRC1 and ncPRC1 contain the PCGF2/4 subunit, but while cPRC1 contains PHC and CBX proteins, ncPRC1 complex is defined by the presence of RYBP/YAF2. The different subtypes of ncPRC1 are named according to the PCGF recruited. In this regard, PCGF1 constitutes the ncPRC1.1, PCGF6 the ncPRC2.6, and PCGF3/5 the ncPRC1.3/5. Adapted from Schuettengruber et al. (2017).

a) RING1B in cancer

Overexpression of RING1B is commonly associated with tumorigenesis in many cancers, including liver, uterine, cervical, lung breast, prostate, bladder and colon cancers (Bosch et al., 2014; Hernández-Ruiz et al., 2018; Sánchez-Beato et al., 2006). As ES is a developmental tumour, it is not surprising to find many alterations in developmental regulators, such as PcG proteins, in this disease. In this regard, the PRC1 PcG subunit PCGF2 (or BMI1) was reported to be overexpressed in the vast majority of ES tumours (Cooper et al., 2011; Douglas et al., 2008). BMI-1 promotes ES tumorigenicity independently of *CDKN2A* repression, a major target of PcG complexes, but blocks differentiation and cell-matrix adhesion pathways (Douglas et al., 2008). Likewise, our group has shown that RING1B is highly expressed in primary ES tumours, contributing to ES development through sodium channel, voltage gated, type VIII, alpha subunit (Nav1.6), and NF-κB-mediated repression (Hernandez-Muñoz et al., 2016).

According to the new activating roles in transcription for RING1B, emerging evidence suggests a tumorigenic activating function of this PcG subunit in cancer (Chan et al., 2018; Rai et al., 2015). In melanoma, RING1B exerts an oncogenic and prometastatic role that

is dependent on both transcriptional activation and repressive functions. Mechanistically, E3 ligase activity of RING1B is necessary for the invasive behaviour of the tumour through repression of the latent transforming growth factor beta binding protein 2 (*LTBP2)* promoter. On the other hand, RING1B drives proliferation of melanoma cells through direct transcriptional upregulation of the cell cycle regulator cyclin D2 (*CCND2*) (Rai et al., 2015). Moreover, recent evidence shows that RING1B regulates enhancer activity and gene transcription in breast cancer cells, by promoting the expression of oncogenes but also by regulating chromatin accessibility (Chan et al., 2018). Furthermore, high levels of RING1B in these studies correlate with lower survival of breast cancer patients. In further support with these data, in *Drosophila*, PRC1 redistributes genome-wide to sites decorated with active enhancer marks, such as H3K27ac, during oncogenesis (Loubière et al., 2016). Further evidence for RING1B being involved in tumorigenesis came from our group, which recently found that RING1B co-localizes genome-wide with EWSR1-FLI1 in ES cells. While retaining its repressive canonical activity, we found RING1B to be necessary for the recruitment of the fusion oncogene to key activated targets including *NK2 Homeobox 2* (*NKX2-2)*, *SRY-Box 2* (*SOX2)* or *IGF1* (Sánchez-Molina et al., 2019).

b) Targeting RING1B

There is currently a lack of small molecule inhibitors that can prevent RING1B recruitment to specific genomic sites. These drugs would be especially important for tumours in which RING1B exerts an oncogenic transcription activation role. The only specific inhibitor available currently for RING1B is PRT4165, which inhibits the E3 enzymatic activity of RING1A and RING1B. This inhibitor thus seems to be valuable in studying the contribution of H2A ubiquitylation to gene repression (Ismail et al., 2013), rather than the contribution of RING1B on enhancer activation. Therefore, development of RING1B-specific inhibitors is currently an area of active research.

3.4.5 The PRC2 complex

The PRC2 complex is an essential chromatin modifier that is conserved in organisms from plants to flies and humans that mediates mono-, di-, or trimethylation of H3K27 (Schuettengruber and Cavalli, 2009). This complex comprises the HMT EZH1 or EZH2, the embryonic ectoderm development (EED), suppressor of Zeste (SUZ12), and the histone binding proteins RB binding protein 4 (RBBP4) or -7 (RBBP7). EZH1/2 are the core subunits that contain the conserved SET domain, which permits the HMT activity of the complex. Importantly, EZH1 and EZH2 are mutually exclusive in the complex. EZH1 has only a minor HMT activity *in vitro* and *in vivo* as compared to EZH2 and is mostly expressed in adult tissues and non-dividing cells. In contrast, EZH2-containing complexes are closely associated with embryonic tissues and actively dividing cells (Margueron et al., 2008; Shen et al., 2008).

Similar to PRC1, a diversity of accessory proteins can associate to the core complex, modulating the HMT activity or chromatin target sites. Two fundamental alternative assemblies linked to PRC2 can be found, namely PRC2.1 and PRC2.2 (**Figure I. 15**). The first complex, PRC2.1, is defined by its mutually exclusive binding of one of the three Polycomb-like homologs (PCL), named PHD finger protein 1 (PHF1), -19 (PHF19), or metal response element binding transcription factor 2 (MTF2), which stimulate efficient enzymatic activity for methylating the H3K27me2 substrate. PRC2.2 is defined by the presence of AE binding protein 2 (AEBP2) and Jumonji and AT-Rich interaction domain containing 2 (JARID2), which also enhance the enzymatic activity and regulate chromatin binding of the PRC2 complex. Finally, the elongin BC and Polycomb Repressive Complex 2 associated protein (EPOP) and ligand dependent nuclear receptor corepressor (LCOR) can be additionally recruited to PRC2 complexes (Schuettengruber et al., 2017). Despite efforts to identify all PRC2-related subunits, the functional importance of many of them in a developing organism has yet to be determined.

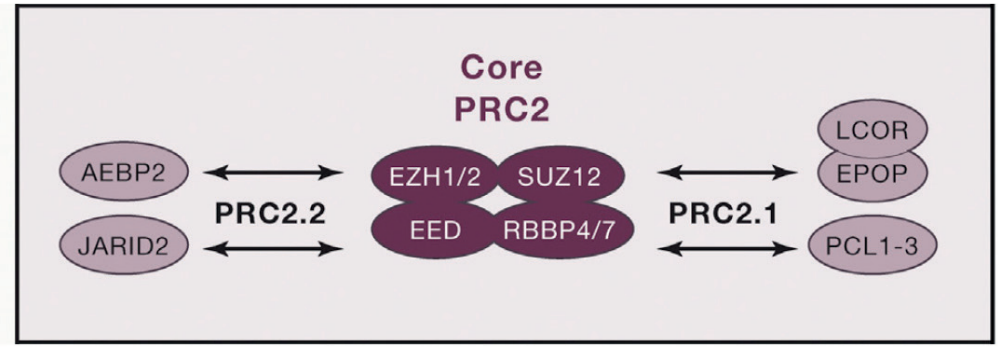

FIGURE I. 15 ***PRC2 complexes.***
Different compositions of the PRC2 complex are shown. The core of the PRC2, constituted by EZH1/2, SUZ12, EED, and RBBP4/7, can associate with a variety of accessory proteins. PRC2.1 is formed by association of PCL1-3, EPOP, and LCOR, while PRC2.2 is formed by association of AEBP2 and JARID2. Adapted from Schuettengruber et al. (2017).

a) EZH2 in cancer

First evidence suggesting PRC2 may have a role in cancer was the observation that there was a positive correlation between the level of EZH2 and poor prognosis in prostate and breast cancer (Kleer et al., 2003; Varambally et al., 2002). This data was subsequently corroborated by identification of somatic mutations in the catalytic domain of EZH2 (e.g. mutations in Y641) in patients with non-Hodgkin's lymphoma, follicular lymphoma, and diffuse large B-cell lymphoma (DLBCL), which lead to hyper-activation of its catalytic activity. Additional somatic mutations and amplifications have been related to non-small-cell lung cancer, prostate cancer, colon cancer, and melanoma (Kim and Roberts, 2016).

Whole-genome sequencing studies of paediatric tumours have found PRC2 complex as one of the eight recurrently mutated epigenetic nodes. In this regard, genes encoding the subunits *EZH2, EED, AEBP2, ASXL1* and *ASXL transcriptional regulator 2 (ASXL2)* are highly frequently mutated (Huether et al., 2014). Over half of the mutations found in this study within PRC2 complexes occurred in paediatric leukaemia. Consistent with these results, loss-of-function mutations of EZH2 have been reported in T-ALL, in which EZH2 acts as a tumour suppressor (Ntziachristos et al., 2012). Even though gain-of-function mutations in EZH2 are rare in paediatric tumours, EZH2 overexpression has been found in several of these malignancies, including high-risk NB and ES (Chen et al., 2018; Staege et al., 2004). In ES, *EZH2* is a directly activated target of EWSR1-FLI1, which drives tumour growth and metastasis *in vivo* (Richter et al., 2009). This study proposed that EZH2 exerts its oncogenic role in ES by blocking endothelial and neuroectodermal differentiation programs. Likewise, in high-risk NB, EZH2 is a critical factor repressing neuronal differentiation programs as well as critical tumour suppressors, such as the insulin-like growth factor binding protein 3 (*IGFBP3*) (Chen et al., 2018).

DIPG represents a paradigmatic model of EZH2 exerting a tumorigenic role due to perturbed distribution of its enzymatic activity. In this disease, a mutation in histone H3 that converts the lysine 27 to methionine (K27M) leads to a global decrease in H3K27me3, causing dysfunction of the HMT activity of EZH2. This in turn prevents methylation of the wild-type H3K27, resulting in de-repression of gene expression that promotes gliomagenesis (Bender et al., 2013; Lewis et al., 2013). Recent data have shown that the PRC2 complex is redistributed to poised enhancers in H3.3K27M mutant cells, contributing to tumorigenesis in part by locally increasing H3K27me3 in tumour suppressor genes and thereby leading to its repression (Fang et al., 2018).

Overall, in paediatric cancer EZH2 can have a either tumour suppressor or, in stark contrast, an oncogenic role, indicating a context-dependent functional switch.

b) Targeting EZH2

Given the gain-of-function mutations or overexpression of EZH2 in a wide range of cancers, development of EZH2-specific inhibitors has been an active area of investigation. In general, HMTs transfer a methyl group from the SAM universal methyl donor to the K side chain of histones, forming S-adenosyl-L-homocysteine (SAH) as a product. Consistently, many EZH2 inhibitors have been developed exploiting such enzymatic activity. 3-deazaneplanocin A (DZNep) was the first inhibitor developed that was widely used for experimental work. However, despite its potentially promising results *in vitro* and *in vivo*, DZNep has a very short plasma-life, confers nonspecific inhibition of histone methylation, and is toxic in animal models (Miranda et al., 2009). In an attempt to reduce

the toxicity and improve the specificity of EZH2 inhibitors, several SAM-competitive inhibiting compounds were released in 2012, including GSK126. This inhibitor had a 1000-fold selectivity for EZH2 as compared to the other 20 HMTs, and 150-fold selectivity as compared to EZH1 (Kim and Roberts, 2016). Promising preclinical results with GSK126 led to the development of a phase I clinical trial in B-cell lymphoma. However, disappointing data have been published for this trial proposing a combinatorial strategy for future developments (Huang et al., 2019). Novel, more potent EZH2 inhibitors have been released, such as EPZ-6438 or tazemetostat, which have a more than 4500-fold selectivity for EZH2 over 14 other HMTs, and 35-fold over EZH1. Promising results were reported with this inhibitor for rhabdoid tumours, resulting in decreased levels of H3K27me3 and a dose-dependent tumour regression (Knutson et al., 2013). Derived from preclinical studies, tazemetostat is currently in 10 phase II clinical trials, including rhabdoid, DLBCL, and non-Hodgkin's lymphoma (National Institute of Health, 2019).

3.4.6 Histone lysine demethylases of the KDM6 family

KDM6 is a subfamily of HDMs tightly linked to gene activation that, through their JmjC domain, specifically demethylates H3K27me2 and H3K27me3, with preference for H3K27me3 *in vitro* and *in vivo* (Agger et al., 2007; Lee et al., 2007; Van der Meulen et al., 2014). It consists of three members: KDM6A (or UTX), lysine demethylase 6B (KDM6B), and ubiquitously transcribed tetratricopeptide repeat containing, Y-linked (UTY or KDM6C). KDM6 members contain a zinc-binding domain that provides specificity toward H3K27, excluding the near-cognate H3K9. Although all KDM6 members display a JmjC domain, only *KDM6A* and *UTY* transcripts show high homology (with 88% sequence similarity). In contrast, KDM6B has low homology with the other members (with only 29%), which is suggestive of very different functions. As the name implies, both *KDM6A (UTX)* and *UTY* genes are located on the X and Y chromosomes, respectively. Thus, it was first thought that *UTY* was an inactive degenerate form of the *KDM6A* gene with no functional activity. However, recent studies suggest that UTY catalyses demethylation of H3K27 *in vitro*, analogously to KDM6A and KDM6B, but with reduced activity due to point substitutions involved in substrate binding (Walport et al., 2014).

KDM6A plays an important role in activating HOX gene expression during development, regulating body patterning (Agger et al., 2007). Moreover, its histone demethylase catalytic activity facilitates formation of induced pluripotent stem cells (iPSC) (Mansour et al., 2012). This study reported a unique requirement for KDM6A in the induction of pluripotency, as this function was not reconstituted by overexpressing other KDM6 family members, such as KDM6B or UTY. On the other hand, KDM6B is induced upon inflammation or viral stimuli, differing from other KDM6 members (Anderton et al., 2011; De Santa et al., 2007). Furthermore, KDM6B mediates the inflammatory response by inducing genes

important for the activation of macrophages (De Santa et al., 2007) (**Figure I. 16**).

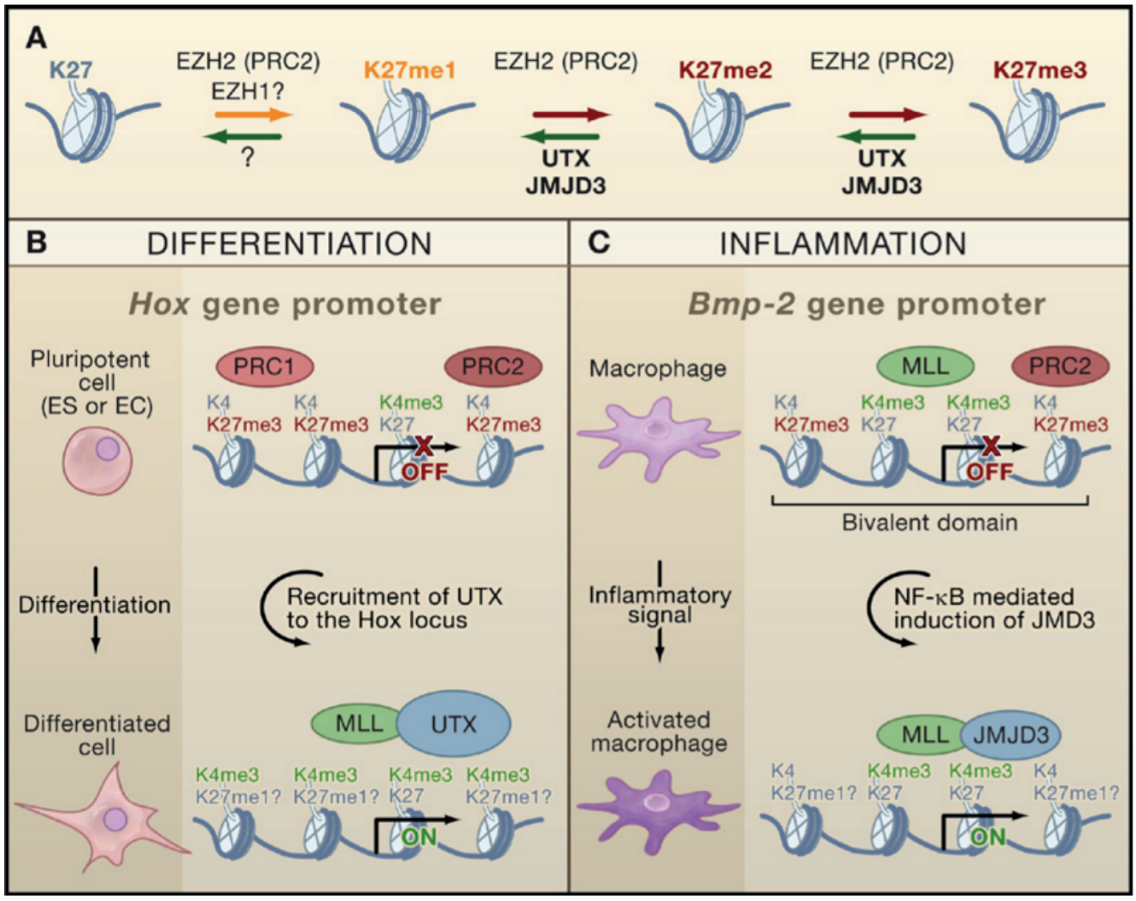

FIGURE I. 16 ***KDM6A and KDM6B antagonize PRC2 HMT activity in various contexts.***
A) KDM6A and KDM6B are specific H3K27 di- and trimethyl demethylases that antagonize the activity of the core subunit of the PRC2 complex, EZH2, that methylates this residue. ***B)*** During development, MLL and PRC2 maintain the poised state of bivalent genes, which are decorated with both H3K27me3 and H3K4me3 marks. Upon a differentiation stimulus, KDM6A participates on resolving these poised genes by removing H3K27me3. In parallel, MLL methylates H3K4, and as a result these genes become transcriptionally activated. ***C)*** KDM6B is induced upon activation of macrophages by inflammatory stimuli. In macrophage activation, the enzyme has the capacity to resolve bivalent domains, for example at the promoter of *BMP-2*, to enhance expression of target genes. Retrieved from Swigut and Wysocka (2007).

KDM6A constitute the H3K4 HMT complexes containing MLL2-MLL4 (Cho et al., 2007; Lee et al., 2007), which together with RBBP5, ASH2L, and WDR5 is known as COMPASS-like complex. Additional demethylase independent activities for KDM6 members have been reported; for instance, KDM6A has been recently linked to drive a feedforward regulatory loop, setting up active enhancers by facilitating recruitment of MLL4 and p300 in a demethylase-independent manner (Wang et al., 2017).

Recent work revealed a sex-dependent effect after *KDM6A* knock-out in ESC and mice. Some male *KDM6A*-deleted littermates survived to birth, probably due to UTY compensating activity. In contrast, females with *KDM6A* deletion did not survive

(Shpargel et al., 2012; Welstead et al., 2012). Interestingly, *KDM6A* is also known to escape X chromosome inactivation, resulting in a dosage imbalance between males and females (Greenfield et al., 1998).

a) KDM6A in cancer

In 2009, somatic loss-of-function mutations and deletions affecting KDM6A were identified. Since then, a broad range of mutations or deregulation affecting this protein have been described in several malignancies. Consistently, loss-of-function mutations have been identified in multiple myeloma, oesophageal, renal, and bladder cancer (Van der Meulen et al., 2014). Indeed, together with different PcG subunits, KDM6A is in one of the eight epigenetic nodes most frequently mutated in paediatric tumours (Huether et al., 2014). Although KDM6A represents a *bona fide* tumour suppressor gene in most cancers, its role in some tumours is more ambiguous. Such disparities are well studied in T-ALL, in which KDM6A was initially described as a tumour suppressor (Ntziachristos et al., 2014). However, new data show that in a small group of T-ALL, KDM6A acts as a coactivator, thereby supporting oncogenic reprogramming (Benyoucef et al., 2016). The fact that KDM6A is located on the X-chromosome yet escapes from X-chromosome inactivation adds another layer of complexity to such studies. For instance, in medulloblastoma, subgroups 3 and 4 are marked by a disturbed gender distribution towards males. Mutations affecting KDM6A might partially explain the higher prevalence of males in these medulloblastoma subgroups. Moreover, female patients harbouring *KDM6A* defects showed bi-allelic *KDM6A* inactivation, suggesting that complete loss of *KDM6A* is required for malignant transformation (Robinson et al., 2012).

b) Targeting KDM6A

Generic inhibitors of JmjC demethylases have been identified, including N-oxalyglycine, methylstat, and 2,4-dicarboxypyridine, which mimic the α-ketoglutaric acid necessary for the demethylation reaction. Other inhibitors include the iron-chelating agent deferoxamine or the pyridine hydrazine JIB-04 and catechols. However, all these compounds are selective against some or all the JmjC enzymes, and hence highly unspecific for the KDM6 family. In this regard, the development of GSK-J4 inhibitor and its ethyl ester derivative GSK-J1 represents a significant improvement to selectively targeting these demethylases (Van der Meulen et al., 2014). GSK-J4 is a prodrug that is converted *in vivo* to GSK-J1, which has been shown to increase cellular H3K27 methylation as a result of inhibiting KDM6A and KDM6B. However, Heinemann et al. (2014) showed that GSKJ1 is only 5–10-fold more potent against KDM6B and KDM6A as compared to other JmjC demethylases, like the lysine demethylase 5 (KDM5) family. Furthermore, they demonstrated that GSK-J4 also inhibits the catalytic activity of KDM5 demethylases with similar potency. Nevertheless,

this is the only pharmacological tool currently available to inhibit KDM6 proteins. In fact, GSK-J4 has proven to be pre-clinically active in malignancies such as NB, DIPG, T-ALL, and AML (Hashizume et al., 2014; Li et al., 2018; Lochmann et al., 2018).

4. CHROMATIN REMODELLING AND EPIGENETIC MECHANISMS IN ES

4.1 GGAA repeats in ES

EWSR1-FLI1, FLI1, and other ETS family members can bind DNA at a specific motif, the "ACCGGAAGT" also known as GGAA repeats, through a conserved ETS high-affinity DNA binding domain (Bailly et al., 1994; Lamber et al., 2008). It has been demonstrated that both FLI1 and EWSR1-FLI1 display similar DNA binding affinity and specificity towards this motif (Mao et al., 1994); however, EWSR1-FLI1 is a more potent transactivator than wild-type EWSR1 (Gangwal et al., 2008). Indeed, binding of EWSR1-FLI1 may not be limited to *bona fide* ETS binding sites as it also binds to multimeric repeats of GGAA with high affinity (**Figure I. 17**).

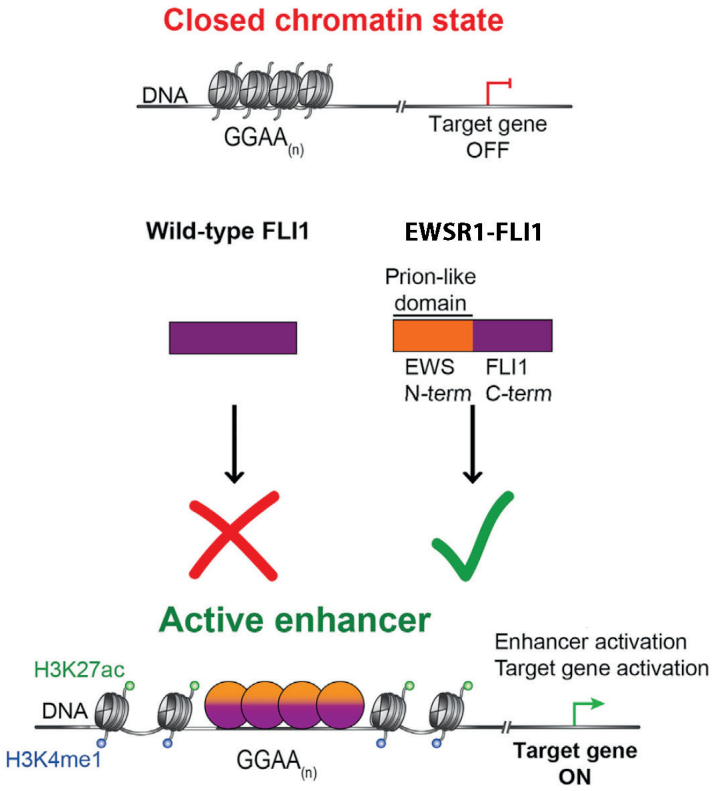

FIGURE I. 17 ***EWSR1-FLI1 binds GGAA repeats leading to transcriptional activation.***
EWSR1-FLI1 and FLI1 have similar DNA binding affinities. Due to the prion-like domain conferred from *EWSR1*, which has a potent activation domain, only EWSR1-FLI1 has the ability for transcriptional activation, leading to aberrant activation of ES target genes. Adapted from Boulay et al. (2017).

Johnson et al. (2017) reported that approximately 3.5 million of GGAA repeat regions exist in the human genome, of which 99% have only 2 motifs. These motifs have likely happened by chance and consequently might have no function, but a subset of these regions serve as EWSR1-FLI1 response elements. Given that there is a poor cross-species conservation of these repetitive elements, recruitment of EWSR1-FLI1 to its target genes might not be conserved between human and mice, although they have similar EWSR1-FLI1 targets. This might explain in part why development of an ES mice model has not been developed yet (Minas et al., 2017). Moreover, the GGAA microsatellite regions are interestingly very polymorphic between European and African genetic backgrounds (Beck et al., 2012), probably explaining the rareness of ES in African descendants that was reported long ago (Jensen and Drake, 1970).

In the ES genome, the GGAA repeats are sufficient to induce EWSR1-FLI1–mediated activation of their adjacent targets (Gangwal et al., 2008; Guillon et al., 2009; Patel et al., 2012; Riggi et al., 2014; Tomazou et al., 2015). Moreover, silencing of a specific repeat controlling the expression of a key gene in ES is sufficient to impair the growth of ES xenografts (Boulay et al., 2018). Hence, these are critical regulatory elements of ES where EWSR1-FLI1 can bind to exert its oncogenic activity. These data are in agreement with previous studies showing that a minimum of 4 consecutive repeats are necessary for EWSR1-FLI1 to bind (Gangwal et al., 2008), whereas a maximum of approximately 18–26 repeats allow for an optimal configuration of EWSR1-FLI1 at these sites providing maximal transcription function (Johnson et al., 2017). Some of these EWSR1-FLI1-bound multiple GGAA repeats are *de novo* super-enhancers created by the fusion oncoprotein. De novo super-enhancers function in long-range regulation with open chromatin areas depleted of nucleosomes, reduced DNA methylation, and enrichment of activating histone marks such as H3K27ac and H3K4me1 (Boulay et al., 2017; Riggi et al., 2014; Sheffield et al., 2017; Tomazou et al., 2015). 78% of EWSR1-FLI1 binding sites display H3K27ac in ES cell lines and primary tumours, both harbouring highly concordant chromatin states (Riggi et al., 2014). Indeed, this enhancer mark is significantly lost when performing EWSR1-FLI1 knockdown experiments in ES cell lines (Tomazou et al., 2015). Furthermore, essentially all (99%) promoters bound by EWSR1-FLI1 in ES cell lines and primary tumours carried the active transcription initiation histone mark H3K4me3 (Riggi et al., 2014). Moreover, these studies also indicated no overlap between EWSR1-FLI1-binding sites with the PcG repressive mark H3K27me3 and neither H3K9me3, in agreement with the active transcriptional state of these regions (Patel et al., 2012; Riggi et al., 2014; Tomazou et al., 2015).

Studies from Patel et al. (2012) showed that, in HUVEC cells and other cell lines tested as part of the ENCODE consortium, repressive marks such as H3K27me3 were commonly present at the GGAA repeats bound by EWSR1-FLI1. Moreover, promoters containing

GGAA repeats in MSC are enriched in H3K27me3 and following introduction of EWSR1-FLI1 loss this histone modification, resulting in a marked gene activation (Boulay et al., 2018). Likewise, in other cellular models, such as NCSC, overexpression of EWSR1-FLI1 leads to loss of H3K27me3 in developmentally repressed loci, such as homeobox D11 *(HOXD11)* (Svoboda et al., 2014). Overall, the transition of such GGAA repeats from a basal H3K27me3-enriched repressive state to an active chromatin state (i.e. H3K27ac, H3K4me3 or H3K4me1) following EWSR1-FLI1 introduction in MSC remains to be elucidated. Indeed, the mechanistic basis of such loss in developmental loci such as the *HOX* genes upon overexpression of EWSR1-FLI1 is currently missing as well.

4.2 Epigenetic reprogramming in ES

EWSR1-FLI1 is considered a pioneer factor of ES tumorigenesis (Braun et al., 1995). By binding the GGAA repeats, EWSR1-FLI1 drives a widespread epigenetic reprogramming that leads to altered transcriptional programs consisting of activation as well as repression. Although the mechanism by which EWSR1-FLI1 activates or represses its targets is still unknown, it is hypothesized that distance and overall chromatin landscape may be contributing factors in EWSR1-FLI1-mediated active or repressive functions (Johnson et al., 2017) .

Several chromatin-remodelling complexes and transcriptional partners have been related to the transcriptional activation of EWSR1-FLI1. At the GGAA repeats, EWSR1-FLI1 interacts with members of the COMPASS and SWI/SNF chromatin remodelling complexes, such as WDR5 and BRG1/BRM associated factor (BAF), respectively, and the acetyltransferase p300. This leads to chromatin remodelling, promoting chromatin opening and subsequent activation of ES transcriptional programme (Boulay et al., 2017; Riggi et al., 2014). In addition, a member of the bromodomain and extraterminal (BET) family of proteins, BRD4, a reader of histone acetylation, binds to H3K27ac in addition to other acetylated K residues on histone H4, thereby regulating enhancer activity and gene expression in ES cells (Gollavilli et al., 2018).

A transcription repressive function for EWSR1-FLI1 is also required for the transformed phenotype of ES (Sankar et al., 2013). Riggi et al. (2014) proposed a mechanism by which EWSR1-FLI1 binds active enhancers in mesenchymal contexts to promote repression. These sites might be non-repeat canonical ETS binding sites at which EWSR1-FLI1 might compete and displace wild-type ETS to promote gene repression and thus block differentiation. Bilke et al. (2013) described that the interactions of EWSR1-FLI1 with the E2F transcription factor 3 (E2F3) at the promoter region generally has an activation effect, whereas EWSR1-FLI1-complexes lacking E2F3 might be responsible for repression. A more detailed mechanism proposed by Sankar et al. (2013) suggests that the NuRD

repressive complex might help through direct binding with EWSR1-FLI1 to mediate repression, with the histone deacetylase LSD1/KDM1A playing a key role. They also speculated that part of the repressive mechanism mediated by EWSR1-FLI1 might be indirect, through upregulation of transcriptional repressors. The classical example of such type of regulation is NKX2-2, an EWSR1-FLI1–induced TF known to mediate oncogenic transformation via transcriptional repression (Owen et al., 2008). Likewise, other studies point to the PRC2 enzymatic subunit EZH2, which is upregulated by EWSR1-FLI1 and blocks neurectodermal and endothelial differentiation (Richter et al., 2009). Nevertheless, additional studies are required to elucidate the exact mechanisms by which EWSR1-FLI1-mediates repression, either direct or indirect.

4.3 Genetic programs and key targets in ES

EWSR1-FLI1 plays a critical role in establishing and maintaining the tumorigenic phenotype of ES (Ouchida et al., 1995; Prieur et al., 2004). Nevertheless, ectopic expression of the fusion oncogene fails to activate similar genetic programs or transform most human cell lines (Lessnick et al., 2002; Miyagawa et al., 2008; Riggi et al., 2008). Furthermore, ectopic expression of EWSR1-FLI1 in adult MSC as compared to hpMSC revealed that ES target genes were generally induced in the paediatric models as compared to the adult counterparts (Riggi et al., 2010). Therefore, cellular background is crucial for the establishment of transcriptional ES signature.

In the last years, suppression of EWSR1-FLI1 by antisense technologies has led to the identification of several hundred EWSR1-FLI1 target genes that act in key molecular pathways involved in ES pathogenesis (**Figure I. 18**).

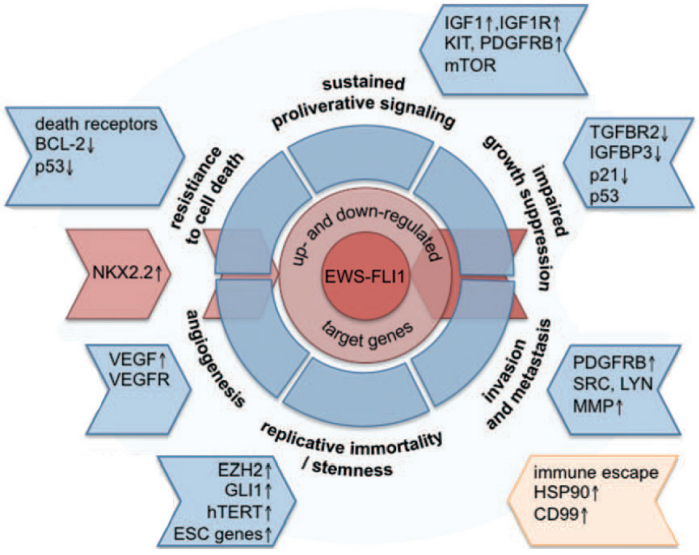

FIGURE I. 18 ***Genetic reprogramming of ES mediated by EWSR1-FLI1.***
The EWSR1-FLI1 fusion oncoprotein acts as an aberrant TF that is considered to be the driver of ES. It

deregulates many cellular processes, including angiogenic, metastatic, and proliferative pathways, as well as resistance to cell death, leading to a tumorigenic genetic program that is crucial for ES cell survival. Tumour biology is thus highly dependent on the action of EWSR1-FLI1, leading to the term "oncogene addiction". Adapted from Potratz et al. (2012).

A larger number of EWSR1-FLI1-activated targets have been described than repressed targets. Among such upregulated targets, many TF have been identified, resulting in the activation of multiple pathways that maintain the ES tumorigenic program (Kauer et al., 2009). These include known mediators of transformation as well as genes involved in cellular differentiation, cell-cycle regulation, cell migration, signal transduction, chromatin architecture, telomerase activity and many other pathways. **Table I.3** summarizes many of the EWSR1-FLI1 targets that have been studied in this thesis.

TABLE I. 3 ***EWSR1-FLI1 target genes and their associated function in ES.*** List of EWSR1-FLI1 target genes transcriptionally activated (A) or repressed (R) in ES. Function of the targets in ES is indicated together with the reference publication.

EWSR1-FLI1 target gene	(A/R)	Reported function in ES	References
CAV1	A	Modulates the ES ability to metastasize	Tirado et al. (2006)
Nuclear receptor subfamily 0 group B member 1 *(NR0B1)*	A	Required for ES transformed phenotype	Kinsey et al. (2006)
NKX2-2	A	Blocks mesenchymal genetic programs	Smith et al. (2006)
Fc fragment of IgG, receptor, transporter, alpha *(FCGRT)*	A	-	Gangwal et al. (2008)
Calcium voltage-gated channel auxiliary subunit Beta 2 *(CACNB2)*	A	-	Monument et al. (2012)
Cyclin D1 *(CCND1)*	A	Dysregulation of G1/S cell cycle transition	Kennedy et al. (2015)
IGF1	A	Regulates cell growth and survival	Cironi et al. (2008)
Jumonji and AT-rich interaction domain containing 2 *(JARID2)*	A	-	Riggi et al. (2010); Riggi et al. (2008)
SOX2	A	Regulates ES cell differentiation and tumorigenicity	Riggi et al. (2010)
VRK serine/threonine kinase 1 *(VRK1)*	A	Cell cycle dependent kinase involved in G2-M transition	Riggi et al. (2014)
EZH2	A	Blocks neuroectodermal differentiation	Richter et al. (2009)
Insulin-like growth factor binding protein 3 (*IGFBP3*)	R	Related to IGF1 pathway	Prieur et al. (2004)

4.4 Experimental therapies in ES targeting chromatin remodelling

Novel therapeutic approaches are clearly needed in ES to, first, increase survival of patients with relapsed or metastatic disease, whose outcome is especially low; and second, to improve survival of patients with localized disease by decreasing toxicity and secondary

effects derived from the traditional cytotoxic treatments. The first therapeutic option one might think of is to target EWSR1-FLI1. A rationale behind such therapies is consistent with the fact that synthetic RNA interference (RNAi) targeting the fusion oncoprotein, leads to inhibition of tumour growth *in vitro* and *in vivo* (Ouchida et al., 1995; Takigami et al., 2011). Although these results were encouraging, *in vivo* delivery of RNAi has been proven to be a difficult process (Ramon et al., 2013). Moreover, the difficulty of targeting the EWSR1-FLI1 fusion protein is further supported by the fact that it is currently not druggable, as it lacks any enzymatic activity. An indirect approach to inhibit its TF activity is disruption of the transcriptional complex recruited by EWSR1-FLI1, with an inhibitor of the RNA helicase A (RHA), such as YK-4-279. This compound reduced tumour growth in orthotopic xenografts (Erkizan et al., 2009) and is currently under investigation in phase I clinical trials.

Given the importance of chromatin remodelling in ES, novel preclinical and experimental therapies targeting this process will be presented.

4.4.1 Targeting DNA damage pathways with PARP inhibitors

ES tumours are highly sensitive to alkylating agents that promote DNA damage. Consistent with the role of PARP proteins in DNA repair (see Section 3.3.5c), ES cells are also highly sensitive to PARP-1 inhibitors such as olaparib (Brenner et al., 2012; Ordóñez et al., 2015). Furthermore, homologous recombination DDR is impaired in ES (Gorthi et al., 2018). However, studies extending the use of olaparib or other PARP inhibitors as monotherapy in xenograft models have reported limited effectiveness, consistent with no objective responses from a phase II study of olaparib. Nonetheless, studies testing combinatorial treatments of PARP inhibitors with other drugs, such as the DNA alkylating agent temozolamide, have reported enhanced sensitivity in ES with several clinical trials ongoing (Vanden Heuvel et al., 2018). Furthermore, a combination of olaparib with trabectedin enhances the activity with relevant antitumor activity in preclinical models (Ordóñez et al., 2015). Therefore, combination therapies with olaparib represent a promising therapeutic tool for ES treatment.

4.4.2 Ubiquitination pathway inhibitors: MLN4924

The ubiquitin proteasome system (UPS) is a major clearance system for maintaining protein homeostasis by degrading unwanted proteins, including misfolded, damaged, and short-lived proteins (Ciechanover, 1998). This system is perturbed in many diseases, including cancer (Ciechanover and Schwartz, 2004).

The successful development of the first-in-class proteasome inhibitor bortezomib for the

treatment of multiple myeloma and relapsed mantle cell lymphoma (Orlowski and Kuhn, 2008) has demonstrated that UPS is an attractive anticancer target. More specific inhibitors of the system, associated with reduced secondary effects, have been developed in the last years, including MLN4924 (Pevonedistat). MLN4924 is a potent first-in-class selective inhibitor of the NAE enzyme (see Section 3.3.5e) that resembles adenosyl monophosphate (AMP) and consequently binds preferentially to the adenylation site of NAE, forming a sulphamate adduct that inhibits NEDD8 activation. As a result, the first steps of the neddylation cascade are blocked (**Figure I. 19**).

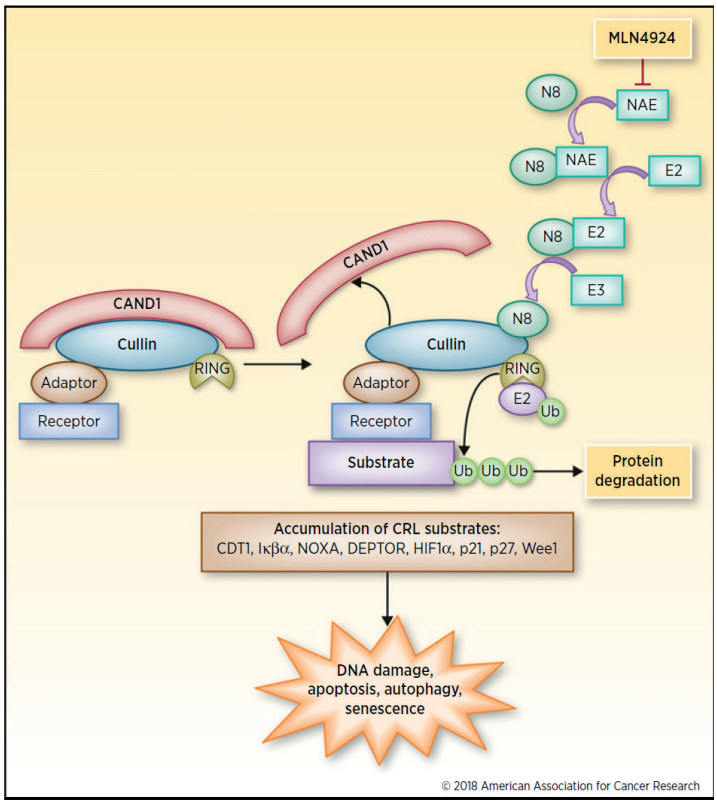

FIGURE I. 19 ***Inhibition of neddylation by MLN4924 and its effects on CRL.***
Activation of CRLs requires the covalent addition of a NEDD8 (N8) molecule to the cullin protein. NEDD8 is activated by an E1 NEDD8-activating enzyme (NAE), transferred to an E2 NEDD8-conjugating enzyme and ultimately shuttled to an E3 ligase that tags NEDD8 to its specific substrate, in this case cullins, a subunit of CRL. Cullin neddylation disrupts inhibitory binding by CAND1 (Cullin-associated and NEDD8-dissociated-1), thereby maintaining CRLs in an active conformation to enable ubiquitination (Ub) and degradation of CRL substrates. MLN4924 inhibits NAE and prevents downstream cullin neddylation and CRL activity, leading to an accumulation of CRL substrates that are involved in key cellular processes. This triggers the induction of DNA damage, apoptosis, autophagy and senescence, all of which inhibit tumour growth. CRLs are composed of a cullin protein tightly bound to a RING-finger–containing protein and various adaptor and receptor components that permit substrate recognition. Retrieved from Yang et al. (2018).

The best characterized and fully validated neddylation targets of MLN4924 are the cullin component of the E3 ligases CRL (see Section 3.3.5d). As neddylation of cullins is necessary for CRL activity, CRLs are entirely inactivated by this drug, and their substrates

accumulate. As CRL control the ubiquitination and turnover of many key substrates with important roles in cell cycle control, DNA replication and repair, cell survival, oxidative stress response, and hypoxia, their accumulation by MLN4924 triggers DNA damage, senescence, or apoptosis (Soucy et al., 2009).

ES cell lines and xenografts are highly sensitive to MLN4924 (Mackintosh et al., 2012; Smith et al., 2012). Furthermore, MLN4924 has been demonstrated to be preclinically highly active against several paediatric cancers, such as AML, ALL and lymphoma, being currently in phase I clinical trials (Soucy et al., 2009; Zhao et al., 2014). In ES, specifically, it has been shown that MLN4924 alters the cell cycle causing a delay in G2/M and S-phase progression triggering apoptosis. In addition, the cell cycle arrest is thought to be related to an accumulation of the WEE1 G2 Checkpoint Kinase (WEE1), a CRL substrate (Mackintosh et al., 2012).

4.4.3 Targeting chromatin erasers and readers

The chromatin remodelling process mediated by EWSR1-FLI1 to create *de novo* enhancers requires BRD4 proteins (Gollavilli et al., 2018). Consistently, the BET inhibitor JQ1 has shown *in vitro* and *in vivo* activity against ES cell lines and other EWSR1-ETS-driven sarcomas (Bid et al., 2016).

Other efforts have focused on inhibiting HDAC with generic inhibitors such as vorinostat (SAHA), but these have demonstrated limited activity in patients (Keshelava et al., 2009). Recent *in vitro* studies with the sodium butyrate inhibitor (NaB) have been reported to impair cell growth, improve survival, and induce differentiation in ES tumours (Souza et al., 2018).

Inhibition of HDM is apparently an additional promising epigenetic strategy in this tumour. KDM1A/LSD1 is highly expressed in ES tumours, as one of the molecules together with the NuRD complex that is recruited by EWSR1-FLI1 to mediate transcriptional repression (Sankar et al., 2013). Inhibition of this demethylase with HCI-2509 is effective in multiple xenografts models of ES (Sankar et al., 2014). Additional studies with the reversible inhibitor SP-2509 also show promising cytotoxic results in ES (Pishas et al., 2018). LSD1 inhibitors are currently in phase I clinical studies. Finally, in contrast to the enzymatic activity of KDM1A/LSD1, HMT of H3K4 KMT2A/MLL1, was shown to be highly expressed in ES (Svoboda et al., 2017). Indeed, the same study revealed that inhibition of the MEN1-MLL1 interaction to chromatin by MI-503 leads to loss of tumorigenicity.

II. HYPOTHESIS AND OBJECTIVES

ES represents a paradigm of a pathognomonic chromosomal translocation operating as an aberrant transcription factor that is necessary for the tumorigenic process. Considering the simplicity of the ES genome, more recent efforts have focused on studying the complex epigenetic mechanisms underlying EWSR1-FLI1-mediated transformation, to identify potential drug targets that could improve patient outcome, especially for patients with metastasis or recurrence.

In this context, our overall hypothesis is that future therapeutic strategies in ES might be improved by the identification of novel epigenetic targets. Consistently, we hypothesize that RING1B and the enzymatic activities underlying H3K27me3, i.e. EZH2 and KDM6, might be potential targets involved in the chromatin remodeling process mediated by EWSR1-FLI1. To fulfill this, we have the following aims:

- **Aim 1:** Analyze the contribution of RING1B to ES tumorigenesis in ES xenografts.

- **Aim 2**: Characterize the potential inhibition of the transcriptional activating role of RING1B upon MLN4924 treatment in ES cell lines.

- **Aim 3**: Analyze the genome-wide distribution of H3K27me3 and the enzymatic activities setting this mark, and their roles in transcriptional programs in ES models and cell lines.

- **Aim 4**: Evaluate the potential targeting of aberrant H3K27me3 distribution using the epigenetic inhibitors GSK126 and GSKJ4.

III. MATERIALS AND METHODS

1. MATERIALS

1.1 Oligonucleotide sequences

All oligonucleotides (primer) sequences used in this work were synthetized by Sigma Aldrich. For gene expression analysis, oligonucleotides were developed by KiCqStart SYBR Green from Sigma Aldrich. Primers targeting the promoter and enhancer region of a particular gene (genomic primers) were designed with the UCSC Primer3 online tool (Rozen and Skaletsky, 1999) using the DNA sequence downloaded from the Eucharyotic Promoter Database (EPD) (Kuleshov et al., 2016) or directly from the region of interest in the Genome Browser. All primer sequences shown in **Table III. 1** satisfy the conditions to be properly amplified by quantitative PCR.

TABLE III. 1 ***Genomic and cDNA primers used for RT-PCR.***
A list of the type and direction (forward or reverse) of the sequences of each primer is *shown*. Type indicates if the primer sequence targets a region of the cDNA or a genomic region, for gene expression or for ChIP techniques, respectively.

Primer	Forward (5'-3')	Reverse (5'-3')	Type
AURKB	ATTGGAGTGCTTTGCTATG	TTTAGGTCCACCTTGACG	cDNA
B4GALT6	GATGATGACCTTTGGAACAG	CTATGGTGATGAGGAATTGAC	cDNA
CACNB2	TACTCCAGTAAATCAGGAGG	TGATGGAGGTGTTGATTTTC	cDNA
CAMK2N1	ATTCTGTATGTTGCACCTTG	TTGAGACACAGGAACAATTC	cDNA
CAV1	CAGGGACATCTCTACACC	TCAAAGTCAATCTTGACCAC	cDNA
CDH13	AAGATCAACAATACACACGC	CTGAGATCTGTGATATTCGTC	cDNA
EGFR	AGTGCCTGAATACATAAACC	GTAGTGTGGGTCTCTGC	cDNA
EWSR1-FLI1	CCAAGTCAATATAGCCAACAG	GGCCGTTGCTCTGTATTCTTA	cDNA
EZH2	AAGAAATCTGAGAAGGGACC	CTCTTTACTTCATCAGCTCG	cDNA
FCGRT	TATTGGGAGAAAGAGACCAC	GAAATTCATGAACTCCTCGC	cDNA
FOXD1	ACAACTAAGCCTTTTTGAGG	AAAAGTACACCAGACAAGTG	cDNA
GAPDH	CTTCAACAGCGACACCCACT	GTGGTCCAGGGGTCTTACTC	cDNA
IGF1	CCCAGAAGGAAGTACATTTG	GTTTAACAGGTAACTCGTGC	cDNA
JAM3	AACATTGGCGGAATTATTGG	GGTTCTTGTAACTTTCTCCATC	cDNA
JARID2	CTCAGGAAAAAGAAGTGGTC	CTTCCCTTATAGATGCACTTG	cDNA
KCNK9	AAGTCCGTTTAGGGGAAC	CACTTGAGAAGGCAGAAATC	cDNA
KDM6A	GTGGGCAATTAAAGCATTTC	TTCACTTTGAACATAAGCCC	cDNA
KDM6B	CAGGAGAATAACAACTTCTGC	CACAGGAATATTGGATGCATAG	cDNA
NKX2-2	CTTCAGTACTCCCTGCAC	CTTGGAGAAAAGCACTCG	cDNA
NR0B1	CAGTCAGCATGGATGATATG	CACAGCTCTTTATTCTTCCC	cDNA
NRXN1	AGAACTGCATATACACCAGG	GATTCTTCAATGGCGATGTC	cDNA
RING1B	CAGACAAACGGAACTCAACCATT	CTGTTATTGCCTCCTGAGGTGTT	cDNA
SH3RF3	TACGTGGAGCTCAATGAC	CTGCTTAAAGTGGGACTTG	cDNA
SOX2	ATAATAACAATCATCGGCGG	AAAAAGAGAGAGGCAAACTG	cDNA
TBP	TTCGGAGAGTTCTGGGATTGTA	TGGACTGTTCTTCACTCTTGGC	cDNA
TLE1	TATTCCAGTCCAAAGAGTCC	AGATGACTTCATAGACTGTAGC	cDNA

VRK1	AGGTGTACTTGGTAGATTATGG	ATCTTTTGGGGTCTTCTTTG	cDNA
AURKB	TATGCATGTAGAGGCTCAACAAT	TCTGGAAGTGAGGGAAGCAT	Genomic
CACNB2	GCAAGACTGTAAGCCCCATGG	CTAGGACACATTCAGAATCTGGC	Genomic
CAMK2N1	AAGAAGGGATTCCGTCAGGT	TGTCTGACACCCCCTTTTTC	Genomic
CAV1	GGTTCAAGAGTACATGTGCAGG	GGGAGTAGGCTTTGTAGCTGG	Genomic
CAV2	TTTTGCTGACCCATGCTTCTC	GCTCTATACCCCAACATTTTCTGTG	Genomic
CCND1	GAGACAAGGTCCCACTCTGTCG	GAGACAAGGTCCCACTCTGTCG	Genomic
CDH13	TATCTGCCATGCAAAACGAG	AAGCATTGGGTAGAGGCTGA	Genomic
DICER	TCTTTTCCCCGATCTGTTGC	TTGCTTCAGCCCAGGATTTC	Genomic
ENC1	GCTGACACTGGTCCCCAAAG	AGCAGATGCCTTGGGTTTGA	Genomic
EZH2	GACACGTGCTTAGAACTACGAACAG	TTTGGCTGGCCGAGCTT	Genomic
FCGRT	GAAAGCAGATGAATGGTTGCCAGG	CTGTCACCTCTATCCGAGTTCC	Genomic
FEZF1	GTGCGGCTAACCTGTTCTACG	GGTCTGGCTCCTGTGTGC	Genomic
FOXD11	CGGGATTCCTACCTTCTTCC	CCCTGTCCAGTGTCGAGAAC	Genomic
HOXA1	GTGTGGGGAAAGAACTGAGC	GCCCTTCTCCGCTTACTGTT	Genomic
HOXD11	TTGGCGAGCGTTGATATAGA	CTTGGGCCAGGATCAACTAA	Genomic
IGF1	TCTATTTTCAGCATTGCAGGGG	GGATCCCTGCTGTTTTGGC	Genomic
IGFBP3	CCTGCCTGGATTCCACAG	CTGCATGACGCCTGCAAC	Genomic
JARID2	TGGTTTACATGGGGCCTGTT	TGGATGGCCAGATTTATGTGC	Genomic
KCNA5	GCTGAAGGTTGCATCTGCT	GGCCCTGACGTCAAGAAG	Genomic
KCNK9	AGCTGGAGCTGGTGATCCT	TGACCGTGATCGCAAAGTAG	Genomic
KIAA1797	GTAGGTGACCTAGAGGGCC	GAAGGCAGGTGGTAAAGCAGG	Genomic
NKX2-2	AAGGATGGAAACTTGGCCTCA	AAGAGTTAGTGGTCTTCCCATCCA	Genomic
NR0B1	GATTCTGTATCAGCTGGTATATACC	GCATCAGGAAGCCTGGATCC	Genomic
NRXN1	ATGGAAATGGTGGATGTGGT	CTTTGGATAGTCCCGCTCAC	Genomic
SOX2	GAAGTGCACCCTATGCCAGT	CAAGTCCTCTGTGGGGGTTA	Genomic
TAL1	GGACACAACGAAATCAGTCAAAC	GTTCTCAGCAGGGATCTGATTCT	Genomic
TLE1	GGATATGGCTGCAGGAGAGA	CCTTTGGGCTCCTTCCTACT	Genomic
VRK1	TGGCTCAGGCCTTTGTCATC	TGAAGACCATTGCCCCATCT	Genomic

Primer sequences used for sequencing experiments are listed in **Table III. 2.**

TABLE III. 2 ***Sequencing primers used for EWSR1-FLI1-pLIV amplification.***
Information related to the sequence and the melting temperature of the primers used in the sequencing experiments.

Primer	Sequence (5'-3')	Melting Temperature
pLIV A	GCCTCGAGGTTTGTAATACGAC	49ºC
EF B	CCAAGTCAATATAGCCAACAG	46ºC

1.2 Interference RNA oligonucleotides

Knockdown experiments were performed with interference RNA using either small interfering RNA (siRNA) or short hairpin RNA (shRNA) sequences, as shown in **Table III. 3**.

TABLE III. 3 ***Interference RNA sequences used.***
Information about the sequence, source and type of interference RNA used in this work.

Primer	Type	Sequence (5'-3')	Source
Luciferase control	siRNA	CUUACGCUGAGUACUUCGA	Sigma Aldrich
NEDD8 seq#1	siRNA	GUGGCAAGCAGAUGAAUGA	Sigma Aldrich
NEDD8 seq#2	siRNA	GCUUCCCUCUCUUAUGACU	Sigma Aldrich
KDM6A sh78	shRNA	AAGTTTCACATCTATGGTA	Dharmacon
KDM6A sh99	shRNA	GGGAAGTACAGACACTATT	Dharmacon
Non target control	shRNA	Patented	Dharmacon

1.3 Plasmids

DNA plasmids used are listed in **Table III. 4**.

TABLE III. 4 ***DNA plasmids used.***
Detailed information about the type, the selection marker and the source of the DNA plasmids used in this work.

Plasmid	Type	Resistance	Source
EWSR1-FLI1-pLIV	Lentiviral	Ampicillin	From Dr Nicolo Riggi
EWSR1-FLI1-pEGFPN1	Recombinant DNA plasmid	Ampicillin	Generated in our lab
KDM6A-Flag-pCS2	Recombinant DNA plasmid	Ampicillin	From Dr Marian Martinez Balbas
PAX8	DNA plasmid	Ampicillin	From Dr Marian Martinez Balbas
VSV-G	DNA plasmid	Ampicillin	From Dr Marian Martinez Balbas

1.4 Antibodies

Primary antibodies and the specific technique used are listed in **Table III. 5**. Western blot antibodies were diluted in PBS with 0.1% Tween 20 (Sigma Aldrich) and 0.01% bovine serum albumin (BSA) (Sigma Aldrich) and stored at –20˚C.

TABLE III. 5 ***Primary antibodies used for Western blot (WB) and antibodies used for chromatin immunoprecipitation (ChIP), immunofluorescence (IF) and immunoprecipitation (IP) experiments.***
Table provides detailed information relative to the dilution, use, source and the reference of each antibody.

Antibody	Use	Working Dilution	Reference	Source
RING1B	WB; CHIP; IHQ	1:1000; 5-10 µL; 1:500	D139-3	MBL
	IP	5 µL	5694	Cell Signalling
KI67	IHQ	1:50	PA0230	Leica
CD99	IHQ	1:20	187-L-CE	Leica
p53	WB	1:1000	sc-126	Santa Cruz
p27	WB	1:1000	554069	BD Pharmigen
ACTIN	WB	1:30.000	A2228	Sigma Aldrich

TUBULIN	WB	1:30.000	T6199	Sigma Aldrich
FLI1	WB; ChIP	1:250; 25 µL	MBS373012	MyBiosource
	WB	1:250	sc-356	Santa Cruz
EZH2	WB	1:1000	5246	Cell Signalling
	ChIP	10 µL	pAb-039-050	Diagenode
H2Aub	WB	1:1000	D27C4	Cell Signalling
H4	WB	1:1000	ab10158	Abcam
NEDD8	WB	1:1000	ab81264	Abcam
H3K27me3	WB; IF	1:1000; 1:250	07-449	Millipore
	CHIP	5 µL	ab6002	Abcam
H3K27ac	WB	1:1000	ab4729	Abcam
H3K4me3	CHIP	5 µL	ab8580	Abcam
KDM6A	WB	1:500	A302-374	Bethyl
	ChIP; IF; IHQ	10 µL; 1:250	33510	Cell Signalling
KDM6B	WB	1:500	ab38113	Abcam
GFP	WB	1:500	A-11122	Invitrogen
Cleaved PARP	WB	1:1000	5625	Cell Signalling

Secondary antibodies are listed in **Table III. 6.**

TABLE III. 6 ***Secondary antibodies used for Western blot(WB) or Immunofluorescence experiments(IF).*** Information about the usage, dilution, reference and source is detailed for each antibody.

Antibody	Use	Dilution	Reference	Source
IRDye 680LT donkey anti-rabbit IgG	WB	1:10000	925-68023	LI-COR
IRDye 800CW donkey anti-mouse IgG	WB	1:10000	926-32212	LI-COR
IRDye 800 CW goat anti-rabbit IgG	WB	1:10000	926-32211	LI-COR
IRDye 680RD goat anti-mouse IgG	WB	1:10000	926-68070	LI-COR
Alexa Fluor 647 goat anti-rabbit IgG (H+L)	IF	1:500	10123672	Thermo Fisher Scientific
Alexa Fluor Plus 488 goat anti-mouse IgG (H+L)	IF	1:500	15626746	Thermo Fisher Scientific
Alexa Fluor® 594 conjugate goat anti-rabbit IgG (H+L)	IF	1:500	A-11012	Applied Biosystems
Alexa Fluor® 594 conjugate goat anti-mouse IgG (H+L)	IF	1:500	A-11032	Applied Biosystems

2. SAMPLES

2.1 ES tumour samples

Paraffin blocks from 18 ES tumour samples from patients of our institution at the debut were provided by the Biobank of Hospital Infantil per a la Recerca (BHISJDI) from Hospital Sant Joan de Deu (HSJD, Barcelona) following the guidelines and approval of the local ethics committee (Clinical Research Ethics Committee from Fundació Sant Joan de Deu). Clinical information regarding to these samples is available under request.

2.2 Animal samples

In vivo studies were performed with approval from the Institutional Animal Research Ethics Committee. Nude Hsd: Athymic Nude-Foxn1^{nu} mice (Envigo) were injected subcutaneously with 5 x 10^6 cells for SK-ES-1 shCTRL in 100 µL of Matrigel (Becton Dickinson) and PBS each flank (5 mice; n = 10). The same procedure was performed in parallel for the SK-ES-1 shRING1B cell line. Tumour growth was monitored three times a week by measuring tumour volume with a digital calliper. Mice were sacrificed when tumours reached a size of 1.5 cm in any dimension. At the end of the experiment, tumours were excised, and half of each specimen was frozen in liquid nitrogen for RNA experiments and the other half was fixed in 10% formalin for immunohistochemistry experiments.

ES xenograft samples treated with MLN4924 at 30 mg/kg, 60 mg/kg, or 90 mg/kg (as published in Mackintosh et al. (2012), provided by Dr Enrique de Alava's group (Instituto de Biomedicina de Sevilla [IBIS], Sevilla). Samples from ES PdX models treated with 60 mg/kg or 90 mg/kg of MLN4924 in monotherapy (unpublished results) were also provided by Dr. Enrique de Álava and Dr. Ángel Montero (Insitut de Recerca Hospital Sant Joan de Deu [IRSJD], Barcelona). Both ES xenografts and PdX were embedded in OCT cryostat medium.

3. CELL CULTURE TECHNIQUES

3.1 Cell culture

ES cell lines were purchased from the American Type Culture Collection (ATCC), having distinct types of EWSR1-FLI1 translocation such A4573 (type III), SK-ES-1 (type II), A673, and TC-71 (both type I). Human embryonic kidney cells immortalized with the SV40 Large T-antigen (HEK 293T) were also purchased from ATCC. All cell lines were cultured in RPMI 1640 medium (Gibco) supplemented with 10% fetal bovine serum (FBS) (HyClone, Lonza), 5 mM of L-glutamine, and 10,000 U/mL of penicillin-streptomycin (both from Gibco). Cells were frozen in fetal bovine serum (FBS) with 10% DMSO (Sigma Aldrich).

Primary human umbilical vein endothelial cells (HUVEC) were also purchased from ATCC. These cells were grown at low confluence in endothelial basal medium (EBM) (Lonza, Cultek) supplemented with 10% FBS and growth factors of the EGM SingleQuots kit (Lonza, Cultek). These factors include human epithelial growth factor (hEGF), hydrocortisone, ascorbic acid, and bovine brain extract. A stock of frozen vials of cells at a very low passage number was generated in FBS with 10% of DMSO for these experiments.

All cell cultures were sub-cultured using Trypsin-EDTA (0.25%), phenol red (Gibco) before the cells reach confluence, and washed with phosphate buffered saline (PBS) pH 7.4 (Gibco). Cell cultures were maintained at 37˚C in a humidified atmosphere containing 5% CO_2.

3.2 Isolation and characterization of hpMSCs

3.2.1 Isolation and cell culture

hpMSCs extracted from the healthy bone marrow of paediatric donors were provided by Dr. Mireia Camos from the Haematology Unit of our institution (HSJD, Barcelona) following the guidelines and approval of the hospital's Ethics Committee for Clinical Investigation. Dr. Cinzia Lavarino's group performed all isolation and immunocharacterisation experiments in collaboration with Dr. Montserrat Torrebadell from the Haematology Unit of our institution (HSJD, Barcelona), according to previously described protocols (Riggi et al., 2008; Suva et al., 2004; Suva et al., 2008). hpMSC cells were cultured at low confluency with Iscove's Modified Dulbecco's Medium (Thermo Fisher Scientific, Gibco), supplemented with 10% fetal newborn calf serum (Thermo Fisher Scientific, Gibco), 1% penicillin-streptomycin (Thermo Fisher Scientific, Gibco), and 10 ng/mL of recombinant human platelet derived growth factor BB (PDGF-BB) (PeproTech). Cells were maintained at 37˚C in a humidified atmosphere containing 5% CO_2; after growing several days in T-25 flasks, they were trypsinized and expanded into T-75 flasks. A stock of frozen vials of cells at a very low passage number was generated in fetal bovine serum (FBS) with 10% of DMSO for use in all experiments.

3.2.2 Characterization of the mesenchymal stem cell features by their differentiation potential

The MSC signature was evaluated based on their differentiation potential to osteogenic, chondrogenic, and adipogenic lineages, according to the Mesenchymal and Tissue Stem Cell Committee of the International Society for Cellular Therapy (ISCT) (Dominici et al., 2006). For this purpose, MSCs were exposed to three different differentiation media, including the StemMacs AdipoDiff, the StemMACS OsteoDiff Media, and the StemMACS ChondroDiff Media (Miltenyi Biotec). Cells were seeded in two 6-well plates containing 5 x 10^4 cells/well and grown with the adipogenic or the osteogenic differentiation media, which was replaced every 3 days. After 10 days, cells cultured with the osteogenic media were fixed in 4% paraformaldehyde (PFA) (Sigma Aldrich) and stained for 10 min at room temperature with 1 tablet of a buffered solution containing 5-bromo-4-chloro-3-indolylphosphate (BCIP)/nitro blue tetrazolium (NBT), pH 9.5 (Sigma Aldrich), which is the substrate for alkaline phosphatase whose blue-purple product can be visually observed.

For the adipogenic culture, cells were fixed at day 21 in 4% PFA and stained with 0.5% Oil Red O solution in isopropanol (Sigma Aldrich). To evaluate the chondrogenic ability, 2.5 x 10^5 cells were pelleted and grown in suspension with the chondrogenic differentiation media. At day 21, the generated chondrogenic cellular nodule that was visibly without aid was formalin fixed, embedded in paraffin, and processed according to standard protocols. Alcian blue with nuclear fast red (BHD Chemicals) staining was used to detect positive chondrogenic cells. Staining of chondrogenic, adipogenic, and osteogenic lineages for hpMSCs is shown in **Figure III. 1**.

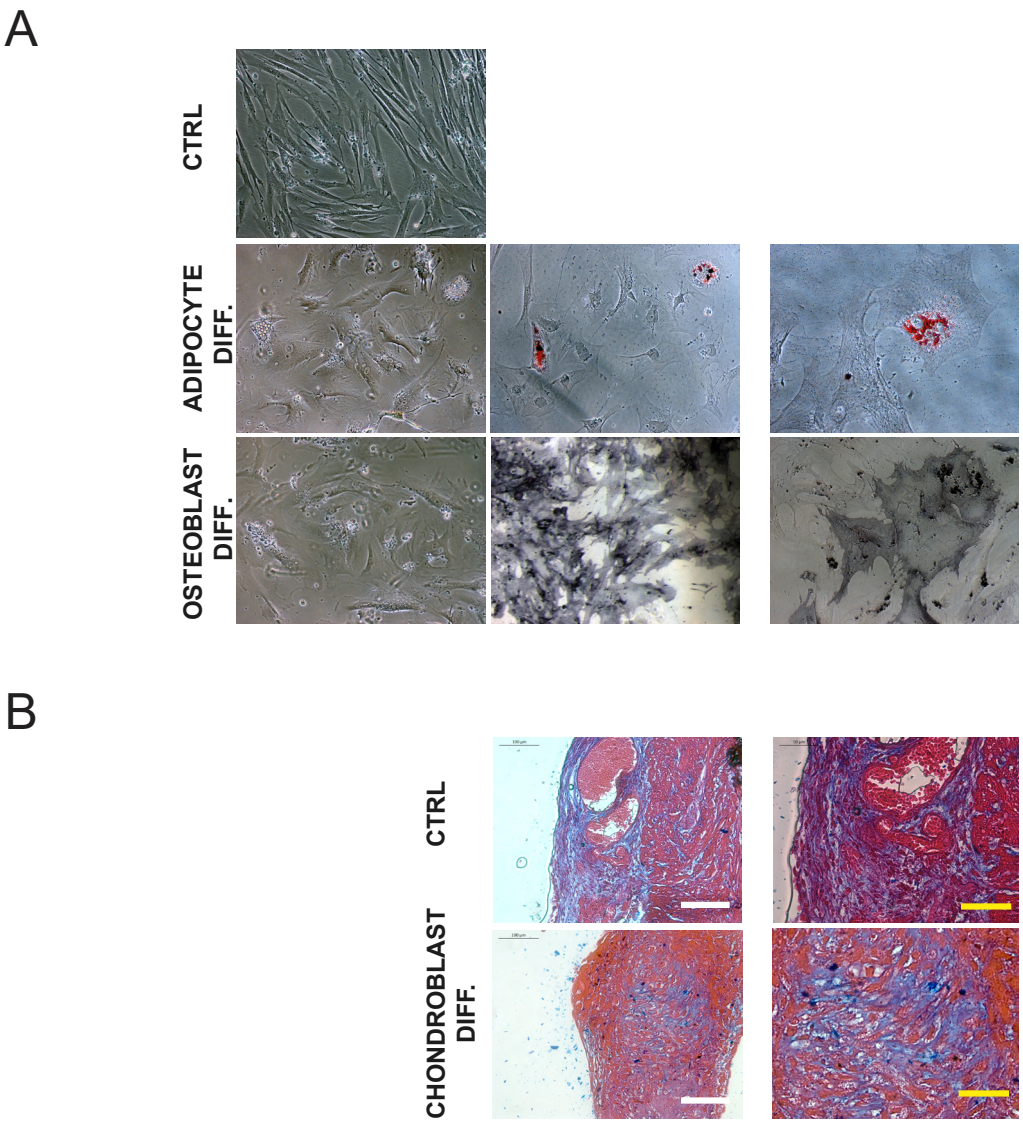

FIGURE III. 1 ***Differentiation of hpMSCs into adipogenic, osteogenic, or chondrogenic lineages***
A) Phase-contrast images showing hpMSCs grown adherent and cultured with adipogenic, and osteogenic differentiation media and control media (left columns). At 21- or 10-days incubation with adipogenic or osteogenic differentiation media, respectively, differentiated cells were further stained with oil red and alkaline phosphatase. All images were captured at 10× magnification except for the far-right images, which were captured at 40×. ***B)*** Microscope images of paraffin embedded tissue from hpMSCs cultured with chondrogenic media after 21 days and stained with Alcian blue and nuclear fast red showing positivity for chondrocytes. A control colon tissue was used in parallel to evaluate positivity of Alcian blue staining. Scale bar represents 100 (white bar) and 50 μm (yellow bar).

3.3 Transfection and infection techniques

Transfection is the process of introducing nucleic acids into cells by non-viral methods, whereas infections imply the use of virus to introduce such material.

3.3.1 Transient transfections

In transient transfections, cells express the foreign gene transiently, as it cannot be integrated in the genome and is lost through cell division.

a) Transfection of plasmid DNA

In order to transiently overexpress a transgene of a DNA plasmid (see **Table III. 4**), 1.5×10^6 cells of HEK 293T cells were seeded in 10-cm dishes and incubated for 24 hours at 37˚C in a humidified incubator. Cell transfection was performed the following day by incubating a multi-component non-liposomal reagent, such the X-tremeGENE HP transfection reagent (Roche), with 7.5 µg of total DNA, and diluted in 1 mL serum-free OPTIMEM media (Thermo Fisher Scientific). To induce formation of the transfection complex, diluted DNA was incubated for 20 min at room temperature. The transfection complex was then transferred dropwise to the cell culture and incubated for 48 hours, at which point cells have had enough time to express the transfected transgene. Then, cells were harvested and collected for further experiments.

b) Transfection of siRNA

Transient transfection of a particular siRNA (see **Table III. 3**) was performed in 6-well dishes containing 3.5×10^4 cells per well. The siRNA-lipid complex was produced by diluting 25 pmol of siRNA in OPTIMEM media with 10 µL of Lipofectamine RNAiMAX Reagent (Invitrogen) following the protocol guidelines of the manufacturer. The transfection complex was then added dropwise to the culture media and incubated for 72 hours, and then cells were collected for further experiments. All quantities refer to well.

3.3.2 Generation of stable cell lines by infection

a) Infection of ES cell lines

Transient transfection of Lenti-X 293T cells (Cultek) was used to produce the lentiviral particles expressing the transgene (in this case, the shRNA sequence). Cells were grown in 10-cm dishes containing 3×10^6 cells at very low passage number. X-tream gene HP DNA transfection reagent (Roche) was used to transfect cells with 7.5 µg of the shRNA plasmid

(see **Table III. 3**) and the lentiviral packaging vectors (see **Table III. 4** for the packaging vectors). In this regard, two vectors manage the production of the lentivirus, including the envelope plasmid PAX8 and the packaging plasmid vesicular stomatitis G protein (VSV-G). PAX8, with the lentiviral *env* gene, encodes for the viral surface glycoprotein gp160, essential for the virus entry into the host cell as they enable binding to cellular receptors and fusion with cellular membranes. VSV-G plasmid contains *gag* and *pol* genes, which encode structural proteins and enzymes required for viral reproduction; it also contains *tat* and *rev,* both of which are essential for the expression of the viral genome. Using two vectors to produce the lentiviruses is known as a second-generation system. More information about this system is given in **Figure III. 2**.

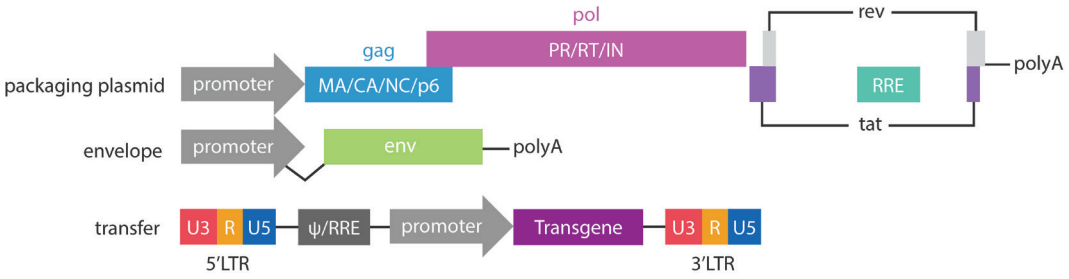

FIGURE III. 2 ***Schematic representation of the second generation of lentiviral plasmids***
In addition to the transfer plasmid containing the transgene (e.g., the empty and EWSR1-FLI1-pLIV plasmids), two plasmids were used in this second generation system to produce the virus: the packaging and the envelope plasmids. Packaging plasmids contain the *gag*, *pol*, *rev*, and *tat* genes necessary for the virus to be functional when transfected into packaging cells. The envelope plasmid (VSV-G) contains the *env* gene, which is necessary to encapsulate the viruses produced. The viral accessory genes *vif, vpu, vpr*, and *nef* were removed in this system. R*ev*-responsive elements (RRE) and long terminal repeats (LTR) are present in the viral genome. U3, R, and U5 are different regions inside such LTR sequences. The polyadenylation (poly A) tail stabilizes the genomic structure. (Adapted from Second generation recombinant lentiviral vectors (2019).

The supernatant of lentiviruses expressing the shRNA sequence was collected at 48-hours post-transfection. Then, it was transferred to the ES cell line culture at 3:1 ratio in the presence of 10 µg/mL hexadimethrine bromide (Polybrene) (Sigma-Aldrich), a cationic polymer that promotes binding of the viral envelope with cell membrane increasing infection efficacy. Cell media containing lentiviruses was removed after 15–18 hours, and cells were washed 3 times with PBS and replaced with fresh media containing antibiotic. Given that shRNA vectors contain an antibiotic-resistance gene to puromycin it is possible to positively select infected cells. Thus, different puromycin (Sigma Aldrich) concentrations were used to select transduced cell lines with 1 µg/mL for A673 cells, and 0.5 µg/mL for SK-ES-1 cells, for 72 hours. A control dish was selected with puromycin in parallel to ensure that non-transduced cells were killed. Cells were then expanded and frozen in liquid nitrogen in aliquots of FBS with 10% DMSO.

The A673 and SK-ES-1 ES cell lines expressing stable knockdown for RING1B were published in Hernandez-Muñoz et al. (2016). Stable knockdown of EZH2 in the A4573 and

A673 ES cell lines was kindly provided by Dr. Inma Hernández-Muñoz (Institut Hospital del Mar d'Investigacions Mèdiques IMIM, Barcelona). Stable knockdown of KDM6A in A673 and SK-ES-1 ES cells was generated in our laboratory.

b) Infection of primary cell cultures

In primary cells, such as hpMSC and HUVEC, the efficient delivery of DNA or RNA with standard transfection protocols is typically challenging. For this work, the viral transduction method was used to overexpress EWSR1-FLI1 in target cells by using lentiviruses, which can productively infect non-dividing cells, which is a critical point for primary cell cultures.

Empty and EWSFLI1-pLIV expressing lentiviruses were produced in 10-cm dishes containing 3×10^6 cells of Lenti-X 293T packaging cells (Cultek) at a low passage number. For each plate, 7 µg of the lentiviral plasmid, 5 µg of VSV-G, and 6 µg of PAX8 were prepared and introduced by calcium phosphate transfection, according to standard protocols. Over the next 12–18 hours, the cellular media was replaced and supernatant containing lentiviruses was collected at 48 hours post-transfection and filtered with 0.45 µm filters. One day prior to infection, target cells were seeded at low confluence (5500 cells/cm^2 for hpMSC; 3000 cells/cm^2 for HUVEC) and transduced with 3:1 of the lentiviral supernatant with fresh media containing Polybrene (Sigma Aldrich) at 6 µg/mL and incubated for 15–18 hours. Then, cells were washed 3 times with PBS and incubated with fresh growth media containing puromycin (0.3 µg/mL in HUVEC; 0.75 µg/mL in hpMSC) and selected for 72 hours, when cells were collected for further experiments. A control dish without the transduction media was also treated with puromycin to ensure killing of cells. After selection step, cells resembled no phenotypical differences between control and EWSR1-FLI1+ cells (see **Figure III. 3**).

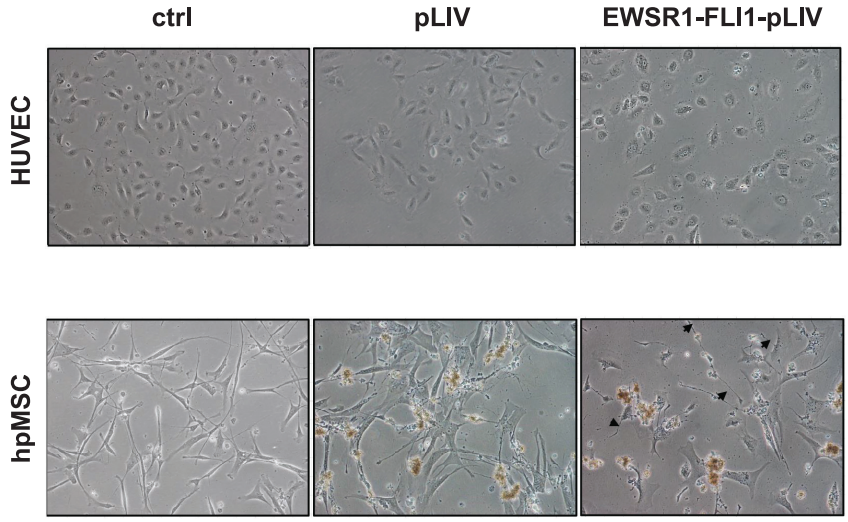

FIGURE III. 3 ***Phenotypic traits of HUVECs and hpMSCs infected with empty or EWSR1-FLI1-pLIV***
Phase-contrast images showing no phenotypical differences between control and EWSR1-FLI1 cells in HU-

VEC cells. Despite lower numbers of cells at 5 days post-infection, hpMSCs infected with EWSR1-FLI1-pLIV resemble a subtle elongated phenotype, as indicated by arrows, in comparison to cells infected with empty pLIV; and HUVEC cells infected with EWSR1-FLI1-pLIV show a rounder phenotype compared to control. Images were captured with a 10× magnification.

3.4 Pharmacological treatments of cell cultures

Pharmacological treatments and drugs used *in vitro* in this work are summarized in **Table III. 7.** All treatments and combinations were evaluated at 72 hours, except for MG132 and aphidicolin treatments; specifically, MG132 was added 8 hours before the end of the experiment, and aphidicolin treatment lasted 48 hours. Doxycycline hyclate (Sigma Aldrich) was added to A673 and SK-ES-1 cell cultures at 0.5 and 2 μg/mL for 72 hours to induce the expression of the shRNA sequences targeting KDM6A.

TABLE III. 7 ***In vitro inhibitors used in this work.***
Table provides information regarding to the inhibitors used in this thesis with information about the concentration, vehicle, and source.

Inhibitor	Concentration used (μM)	Vehicle	Source
Aphidicolin	0.5	ethanol	Sigma Aldrich
GSK126	10	DMSO	Selleck Chemicals
GSK-J4	1.5 – 2.5 - 5	DMSO	Selleck Chemicals
MG132	10	DMSO	Sigma Aldrich
MLN4924 (Pevonedistat)	0.05 – 0.1 – 0.125	DMSO	From Dr. de Álava group

3.5 Cell viability studies

3.5.1 MTS assays

Cell viability experiments were performed in 96-well plates and analysed by The CellTiter 96® AQueous One Solution (Promega), which contains the tetrazolium compound [3-(4,5-dimethylthiazol-2-yl)-5-(3-carboxymethoxyphenyl)-2-(4-sulfophenyl)-2H-tetrazolium,inner salt; MTS] and a stable electron-coupling reagent (phenazine ethosulfate; PES). 10 μL of this solution was added per well to the cell culture and incubated for 2 hours in a humidified incubator (37˚C, 5% CO_2). The principle of this assay is that the tetrazolium compound (Owen's reagent) can be reduced by dehydrogenase enzymes of metabolically active cells (viable cells), forming a yellow coloured product named formazan that is soluble in the culture medium. The absorbance reading after this incubation period at 490 nm with a 96-well plate reader (Infinite M Nano+, Tecan) is directly proportional to the number of living cells in culture.

3.5.2 Clonogenic assays with crystal violet staining

Plates (6-well) were seeded with 3000 or 6000 cells per well, treated the following day, and

incubated for a minimum of 6 days in a humidified cell incubator (37˚C, 5% CO_2) until colonies in the control were clearly visible without aid. Cells were then washed with PBS, fixed for 10 min with 4% PFA, washed with PBS, and then incubated at room temperature with a crystal violet solution (2% W/V, 20% methanol, in PBS) until cell colonies visibly stained. After several washes to remove crystal violet excess, plates were dried upside down at room temperature. Images from the stained dishes were captured in the Audiovisuals unit of HSJD to obtain the proper image quality.

3.6 Flow cytometry studies

3.6.1 Cell cycle studies with propidium iodide staining

Evaluation of the cellular DNA content by flow cytometry is a rapid and precise method to study the cell cycle phases of different experimental conditions. It is based on the ability of a fluorogenic compound (such as propidium iodide) for intercalating into the nucleic acids of the cell stoichiometrically, so that fluorescence emission is proportional to the DNA content of a cell (Riccardi and Nicoletti, 2006). This assay gives an idea of the different proportion of cells in each phase of the cell cycle as well as ploidies. In this regard, cells in the replication phase or S-phase of the cell cycle because they have more DNA than cells in G1 will therefore take up proportionally more dye and will fluoresce more brightly. Cells in G2 phase will be approximately twice as bright as cells in G1 phase. Advanced apoptotic cells because they loss DNA appear as a subG1 peak. However, this peak is not exclusive to apoptotic cells, as necrotic cells, nuclear fragments, clumps of chromosomes, micronuclei, or nuclei with normal DNA content but different chromatin structure are also represented in this peak.

Cultured cells were collected and fixed in 70% ethanol for at least 30 min at –20˚C. Ethanol was then extracted by two centrifugation cycles at 1800 rpm with PBS washes. Cells were then incubated with 0.5 μg/mL of RNase and 25 μg/mL of propidium iodide for 30 min at 37˚C. After incubation, the cellular RNA is degraded and propidium iodide only binds double-stranded nucleic acids (in this case, DNA). Using a flow cytometer and measuring the fluorescence of propidium iodide with an excitation/emission wavelength of a maximum of 493/636 nm, diploid cells show a narrow peak of intensity. The Gallios (Beckman Coulter) flow cytometer was used for these experiments to study the cell cycle, and the MultiCycle AV Standalone software (see section 8) was used to quantify the proportion of cells in each phase of the cell cycle and the subG1 peak.

3.6.2 Cell death studies with annexin V staining

Annexin V staining reveals the number of apoptotic cells by discriminating the early and

late phase of apoptosis and the necrotic fraction of cells. It is based on the detection of a phosphatidyl serine phospholipid in cells. In normal conditions this phospholipid is present in the inner cytoplasmic surface of the lipid bilayer of the cell membrane; but in apoptotic cells it is translocated to the outer lipid layer, exposing it to the external cellular environment (van Engeland et al., 1998). Annexin V is an anticoagulant particle circulating in blood that has high affinity to phosphatidyl serine molecules exposed in the outer layer of the cell membrane. Incubation of cells to annexin V conjugated to an Alexa Fluor 488 antibody from the Dead Cell Apoptosis Kit (Invitrogen) and propidium iodide staining of DNA enables the number of viable cells versus apoptotic (early or late) and necrotic cells to be measured. Using this kit, 100 µL of 1×10^6 cells/mL resuspended in annexin-binding buffer were labelled with 5 µL of annexin V conjugated antibody and 5 µL of propidium iodide and incubated in the dark for 15 min at room temperature. After incubation, 400 µL of the buffer was added to the cells and rapidly analysed by the Gallios (Beckman Coulter) flow cytometer by measuring the fluorescence with an excitation/emission wavelength of 499/521 for annexin V and 535/617 nm for propidium iodide. By flow cytometry, viable cells are characterized by negative propidium iodide and annexin V staining, whereas apoptotic cells will display high intensity of annexin V fluorophore. The early and late apoptotic fraction can be distinguished by the intensity of propidium iodide, which deeply penetrates the cell membrane when cells are in advanced apoptosis due to a loss of membrane integrity. Necrotic cells show a positive propidium iodide staining with a negative annexin V signal.

4. DNA MOLECULAR BIOLOGY TECHNIQUES

4.1 Obtainment and analysis of plasmid DNA

4.1.1 Bacterial transformation and isolation of DNA plasmid

DNA plasmids (**Table III. 4**) were amplified using the *Escherichia coli* DH5α strain (Invitrogene, Life Technologies). The EWSR1-FLI1-pLIV lentiviral vector was amplified by the One Shot Stbl3 chemically competent bacteria cells derived from the HB101 *Escherichia coli* strain (Invitrogen, Life Technologies), which is recommended for unstable inserts such as lentiviral DNA–containing repeats. All plasmids were transformed by heat shock following the manufacturer's instructions. An outgrowth step was introduced by adding 500 µL of S.O.C. medium (Thermo Fisher Scientific) without antibiotic to the cells, which were grown for 45 min at 37˚C in a shaking incubator. Two different volumes of transformed bacteria were spread in Lysogeny broth (LB) agar plates in the presence of 100 µg/mL of ampicillin, to ensure growth of well-spaced colonies and incubated overnight at 37˚C. The following day, single colonies were picked and grown in suspension in 5 mL LB with ampicillin for 12–18 hours in a shaking incubator at 37˚C. Two millilitres of the

mini-culture was transferred to 200 mL of LB with antibiotic and grown overnight at 37˚C. Bacteria were then pelleted at 4000 rpm for 15 min, and plasmid DNA was extracted using the NucleoBond Xtra-plasmid midi/maxi plus kit (Macherey Nagel) and eluted in 500 µL of Tris buffer supplied with the kit. Isolated plasmid DNA was quantified with Nanodrop 1000 spectrophotometer (Thermo Fisher Scientific).

4.1.2 Validation of amplified DNA plasmid by Sanger sequencing

Polymerase chain reaction (PCR) was originally developed in 1983 by Kary Mullis and is a molecular biology technique used to make multiple copies of a particular DNA region (Mullis et al., 1986). The PCR reaction relies on a thermostable DNA polymerase that would synthesize the new strands of DNA from a DNA template, and DNA primers designed specifically for the DNA region of interest. The reaction is repeatedly cycled through a series of temperature changes, which allow many copies of the target region to be produced. Following the PCR amplification step a concrete region of DNA can be sequenced by Sanger sequencing. This technique was developed by Fred Sanger in 1977 and is still used to sequence regions of DNA up to about 900 base pairs in length (Sanger and Coulson, 1975). The Sanger sequencing reaction consists of a DNA template, a DNA polymerase enzyme, a primer sequence that is the template for the polymerase to start sequencing, and dideoxy or chain-terminating nucleotides, which are versions of all four nucleotides but each labelled with a different dye. The Sanger reaction adds normal nucleotides as well as these terminating nucleotides to the amplification chain. Terminating nucleotides lack a hydroxyl group on the 3' carbon of the structure, blocking the addition of subsequent nucleotides. This will be repeated several round of amplification cycles, and by the time reaction is completed, sample will contain fragments with different lengths, all labelled with a specific colour dye of the terminal nucleotide. The sequencer will then transform the colour signal and the fragment length information to a genomic sequence.
Isolated and quantified plasmid DNA from bacterial colonies was amplified with specific primer sequences, targeting regions outside the multicloning site of the vector and inside the insert. PCR mixes and reactions using such primers were performed as shown in **Table III. 8**.

TABLE III. 8 ***Sanger sequencing mix preparation.***
Detailed information about the reagents as well as the quantity used of each in the sequencing mix preparation prior to Sanger sequencing. The final volume was adjusted with nuclease-free water. All reagents were from Applied Biosystems.

Mix	**Quantity (V_f = 12 µL)**
BigDye	0.25 µL
BigDye Buffer 5x	2 µL
Primer 10 µM	0.38 µL
Template 250 ng	-
DMSO 5% 0.6 µL	0.6 µL

Amplification of the template was performed in the GeneAmp PCR System 9700 Fast Thermal Cycler (Applied Biosystems) by denaturing the DNA 3 min at 94˚C, followed by 40 cycles amplification at 96˚C for 15 seconds, using melting temperature of each primer (see **Table III. 2**) for 15 seconds, and 60˚C extension for 4 min. PCR products were cleaned up with ExoSAP-IT PCR Clean-up Kit (GE Healthcare) and sequenced using the 96-capillary 3730xl DNA Analyzer of the Genomics core facility of the Universitat Pompeu Fabra (UPF, Barcelona). Sequencing results were visualized with Bioedit software, and sequence alignment was performed with Blastn online tool from National Institute of Health (NIH). Sequences obtained from amplification of different regions of the empty and EWSR1-FLI1-containing vectors are shown in **Figure III. 4**.

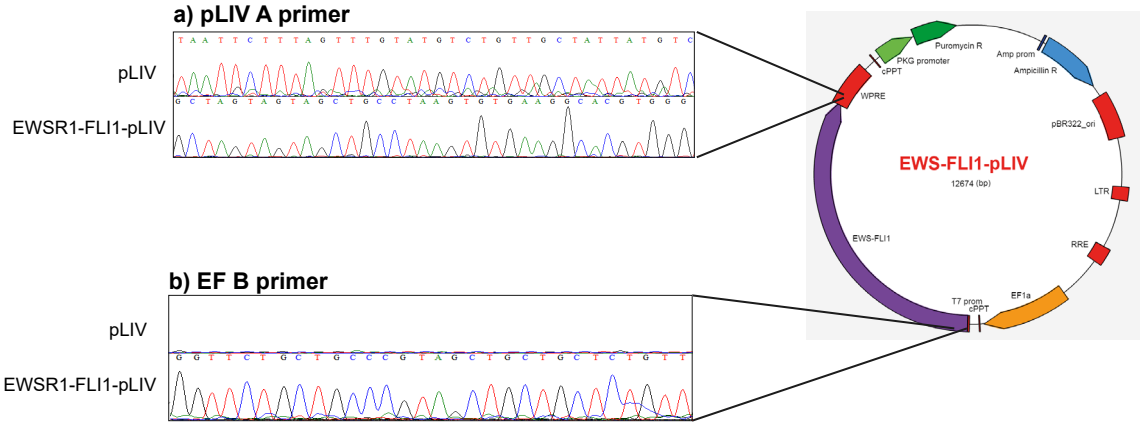

FIGURE III. 4 ***Schematic images representing the sequences obtained by Sanger sequencing using two different pair of primers in empty and EWSR1-FLI1-pLIV vectors***
Example of a sequenced plasmid vector. Images were obtained in Chromas Lite software and show amplified sequences for pLIV and EWSR1-FLI1-pLIV using two different primers (a and b) designed close to the multicloning site (MCS) region of the vector and in the EWSR1-FLI1 sequence, respectively. Amplification with the pLIV A primer (a) shows differences in the sequences obtained for pLIV and EWSR1-FLI1-pLIV, whereas amplification of the vectors using the EF B primer (b), designed to amplify a region of *EWSR1-FLI1*, only amplifies in the sample containing EWSR1-FLI1-pLIV sample, hence indicating the presence of the EWSR1-FLI1 insert.

4.2 Chromatin immunoprecipitation

Chromatin immunoprecipitation (ChIP) technique identifies interactions between DNA and the proteins interacting with it, including TFs, coactivators, and histones. After fixation of DNA, an antibody targeting a protein of interest is used to pull down the DNA associated to that protein and to amplify a suspected region by quantitative PCR. This information gives a direct snapshot of specific protein-DNA interactions in a cell at a specific moment or experimental condition.

ChIP assays were performed as previously described (Sánchez-Molina et al., 2014). Cultured cells were fixed using 1% of methanol-free formaldehyde (Thermo Fisher Scientific) for 10 min at room temperature, and crosslinking was stopped by adding 500

µL glycine (1.25 M). For ES cell lines, lysis was performed in soft lysis buffer (0.1% sodium dodecyl sulfate [SDS], 0.15 M NaCl, 1% Triton X-100, 1 mM Ethylenediamine tetraacetic acid [EDTA], and 20 mM Tris pH 8) supplemented with 1 mg/mL of protease inhibitors (Roche). For hpMSCs, a stronger lysis buffer (1% SDS, 10 mM EDTA, and 50 mM Tris pH 8) with 1 mg/mL of protease inhibitors was used. Lysates were sonicated in a Bioruptor Pico (Diagenode) in 10 cycles until chromatin was sheared to an average fragment length of 200 bp. After centrifugation, a small fraction of eluted chromatin was measured with Qubit dsDNA HS kit (Thermofisher Scientific) and checked for chromatin fragments using Bioanalyzer (Agilent) or by loading 1 µg of fragmented DNA in 1% SeaKem LE agarose (Lonza) diluted in TAE buffer (40 mM Tris, 20 mM acetic acid, and 500 mM EDTA) with 1:10000 dilution of SYBR Safe Gel DNA Stain (Thermo Fisher Scientific) and run for 30 min at 100V. The 1 kb DNA ladder and the 5X GoTaq green loading dye (Promega) were also used. Starting with 30 µg of sample, immunoprecipitations for each antibody (see **Table III. 5**) were performed overnight. The following day, 50 µL of Dynabeads Protein A (Invitrogen) were added to samples, and the slurry was incubated for 2 hours to capture the chromatin fragments bound to the antibody. Immunoprecipitates were washed with buffers TSE I (0.1% SDS, 1% Triton X-100, 2 mM EDTA, 20 mM Tris-HCl pH 8, 150 mM NaCl), TSE II (the same as TSE I but with 500 mM NaCl), and TSE III (0.25 M LiCl, 1% Nonidet P-40, 1% deoxycholate, 1 mM EDTA, 10 mM Tris-HCl pH 8) and two times with Tris-EDTA buffer. All incubation and washing steps were performed in a rotating wheel at 4˚C to avoid protein degradation. DNA captured by the beads was eluded by adding 120 µL of a solution containing 1% SDS, 0.1 M $NaHCO_3$ in a decrosslinking step that heats the samples at 65˚C for 5 hours with gentle shaking. Genomic DNA fragments from ChIP samples were purified with QIAquick PCR Purification kit (Qiagen) and eluted in 50-100 µL.

Quantitative PCR (qPCR) permits to determine absolute or relative quantities of a known sequence that is amplified in a PCR reaction. By using a fluorescent reporter (e.g. SYBR green) in the reaction that intercalates with DNA, amplified DNA would emit a fluorescence intensity that is proportional to the amount of DNA. Thus, it is possible to monitor the reaction in real time and measure the synthesis of DNA. Differences in DNA content from ChIP assays were determined by qPCR using the 7500 Real Time PCR System (Applied Biosystems) and SYBR Green master mix. qPCR was performed in 96- or 384-well plates (Themo Fisher Scientific) in 7500 Real Time PCR (Applied Biosystems) for the 96-well plates or QuantStudio 6 Flex (Applied Biosystems) for the 384-well plates. Reaction was carried out with 2 µL of DNA from ChIP samples 5 µL SYBR Green PCR Master Mix (Applied Biosystems), and 0.2 µL each of forward and reverse primer pairs at 10 µM (for primer sequences, see **Table III. 1**) in a final volume of 10 µL per well. Every immunoprecipitation was done in triplicate and qPCRs were carried out using fixed amounts of input and immunoprecipitated DNA. The reported data represent qPCR values normalized to input DNAs with the percentage of input method of the bound/input signal.

For experiments with more than one condition, data were calculated with the percentage of input method subtracting the corresponding IgG value to the immunoprecipitated samples.

4.3 ChIP sequencing and bioinformatic analysis

DNA from ChIP can be used to study genome-wide all DNA fragments bound to the protein of interest by sequencing techniques. Library preparation and quality controls of ChIP material was performed by the Functional Genomics Service of the Institut for Research in Biomedicine (IRB) and the Genomics Unit of Centre for Genomic Regulation (CRG). Libraries were prepared using the NEBNext Ultra DNA Library Prep for Illumina (New England Biolabs) according to manufacturer's protocol. In brief, this protocol uses 2–5 ng of input and ChIP for end repair and addition of the "A" bases to 3' ends, ligation of adapters, and excision. All purification steps were performed using Agen Court AMPure XP beads (Qiagen). Library amplification was performed by PCR using NEBNext Multiplex oligonucleotides for Illumina (New England Biolabs). Final libraries were analysed using Agilent High Sensitivity Chip to estimate the quality and check size distribution, and quantified by qPCR using the KAPA Library Quantification Kit (KapaBiosystems). Finally, they were amplified with Illumina's cBot, and libraries were loaded onto the flowcell sequencer 1 × 50 on Illumina's Hiseq 2500.

ChIP-seq data was analysed by Dr. Enrique Blanco from Dr. Luciano Di Croce's group (CRG, Barcelona) in collaboration with Pol Castellano (Biomarkers and Nutritional and Food Metabolomics from University of Barcelona, Barcelona). ChIP-seq samples were mapped against the hg19 human genome assembly using BowTie with the option -m 1 to discard reads that could not be uniquely mapped to just one region (Langmead et al., 2009). MACS was run with the default parameters but with the shift-size adjusted to 100 bp to perform the peak calling against the corresponding control sample (Zhang et al., 2008). The genome distribution of each set of peaks was calculated by counting the number of peaks fitted on each class of region according to RefSeq annotations. Promoter region was the region within 2.5 Kb upstream and downstream the transcription start site (TSS). The rest of the gene, excluding the promoter region, was considered as a genic region. Peaks that did not belong to promoter or genic regions were classified into intergenic regions, and peaks that overlapped with more than one genomic feature were proportionally counted the same number of times. Each set of target genes was retrieved by matching the ChIP-seq peaks in the region 2.5 Kb upstream of the TSS until the end of the transcripts as annotated in RefSeq. The UCSC genome browser was used to generate the screenshots of each group of experiments along the thesis (Kent et al., 2002). Publicly available ChIP-seq tracks from the gene expression omnibus (GEO2R) accession number GSE106925 (samples GSM2857585, GSM2857586, GSM2857578, GSM2857579) and

GSE61944 (samples GSM1517562, GSM1517565) were used in this thesis.

5. RNA MOLECULAR BIOLOGY TECHNIQUES

5.1 RNA extraction

Cell pellets were collected and subsequently lysed for RNA extraction or stored frozen at –20˚C. Total RNA from cellular pellets was isolated and purified using the RNAeasy Mini Kit (Qiagen) following manufacturer's instructions and eluted in 50 µL of the RNase-free water supplied with the kit. For *in vivo* samples, tumours of sacrificed animals were frozen at –80˚C. RNA was extracted from 20–30 mg of the tumour using the same kit as for cell lines but including 2-mercaptoethanol in the cellular lysis step and a hand tissue grinder for homogenization. RNA quantification of samples was performed using the Nanodrop 1000 spectrophotometer (Thermo Fisher Scientific).

5.2 Quantitative reverse transcription PCR (RT-qPCR)

Purified RNA (1 µg) was reverse transcribed using 0.5 µg of random hexadeoxynucleotides or random primers (Promega) in a total volume of 12 µL of water. The mix was run for 3 min at 85˚C in GeneAmp PCR System 9700 Fast Thermal Cycler (Applied Biosystems) to induce the annealing with the template, and then 4 µL reverse transcriptase buffer, 2 µL dNTPs (10 mM), 1 µL RNase inhibitor (2500 U/µL), and 1 µL Moloney Murine Leukemia Virus Reverse Transcriptase (M-MLV RT) (200 U/µL) (all from Promega) were added to a final volume of 20 µL. The retrotranscriptase (RT) reaction was performed in the thermocycler for 1 hour at 44˚C followed by 10 min amplification at 92˚C to inactivate the enzyme. The cDNA obtained (approximately 10 ng/µL) was diluted 1:5 with 80 µL of RNase free water and then stored at –20˚C or analysed by quantitative PCR (qPCR). qPCR was performed in 96- or 384-well plates (Themo Fisher Scientific) with 2 µL diluted cDNA, 5 µL SYBR Green PCR Master Mix (Applied Biosystems), and 0.2 µL each of forward and reverse primer pairs (for primer sequences, see **Table III. 1**) in a final volume of 10 µL per well. Each cDNA sample was run in triplicate, and its levels were analysed using the 7500 Real Time PCR (Applied Biosystems) for the 96-well plates or QuantStudio 6 Flex (Applied Biosystems) for the 384-well plates. The obtained qPCR data was analysed using the comparative 2-ΔΔCT method with GAPDH or TBP as housekeeping genes.

5.3 PCR amplification of cDNA and resolution in agarose gels

cDNA obtained from RNA samples was amplified with specific primer sequences (**Table III. 1**) and amplified by PCR with the PCR mixes shown in **Table III. 9**.

Table III. 9 ***PCR mix preparation.***
Detailed information about the reagents as well as the quantity used of each before PCR amplification. The final volume was adjusted with nuclease-free water. All reagents were purchased in Promega.

Mix	Quantity (V_f = 20 µL)
10X Buffer	2 µL
25 mM $MgCl_2$	1.2µL
10 mM dNTPs	1.2µL
10 µM primer Fwd	0.4 µL
10 µM primer Rv	0.4 µL
Taq-polymerase	0.2 µL
DNA template (1 µg)	4 µL

Templates were amplified in the GeneAmp PCR System 9700 Fast Thermal Cycler (Applied Biosystems) by denaturing the DNA 10 min at 94˚C, followed by 40 cycles amplification at 94˚C for 30 seconds, 62˚C for 30 seconds and 72˚C for 59 seconds, followed by an extension step at 72˚C for 7 min. Subsequently, amplified material was run in 2% agarose gels with SYBR Safe Gel DNA Stain (Thermo Fisher Scientific) at 100V for 30 min. Sample (5 µL) and the 1 kb DNA ladder (Promega) were loaded into the gel with 3 µL of 5· GoTaq green loading dye (Promega). Visualization of the DNA bands in the gel was performed by UV light exposure by using the Gel Doc EZ Imager (BioRad). An agarose gel with EWSR1-FLI1 fusion type I amplification from cDNA samples of infected HUVEC cells with EWSR1-FLI1-pLIV vector, as compared to ES cell lines fusions, is presented in **Figure III.5**.

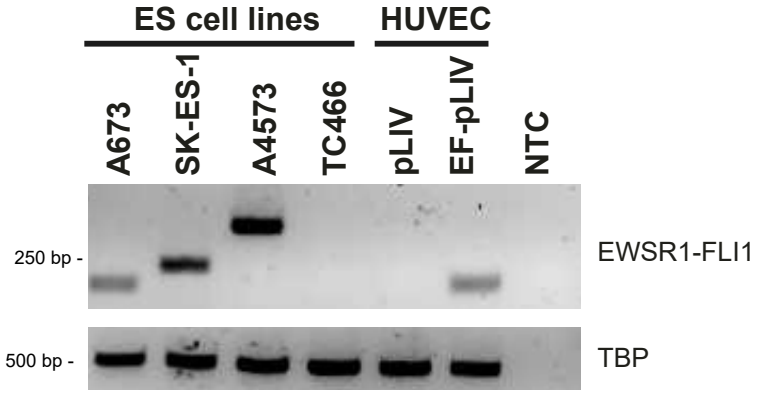

FIGURE III. 5 ***Detection of EWSR1-FLI1 in HUVEC cells infected with the EWSR1-FLI1-pLIV vector***
Image showing the agarose gel result after amplification of EWSR1-FLI1 and TBP in HUVEC cells infected with control and EWSR1-FLI1-pLIV, compared to ES cell lines. A standard PCR protocol of the Molecular Diagnostics Unit of HSJD was used to detect expression of *EWSR1-FLI1* from cDNA samples. A673, SK-ES-1, and A4573 ES cells amplify EWSR1-FLI1 fusion type 1, 2, and 3, respectively, represented in the gel as bands with different lengths. HUVEC cells infected with EWSR1-FLI1 display the type I fusion protein. TC466 does not amplify with EWSR1-FLI1 primers since it harbours EWSR1-ERG fusion. TBP was used as an amplification control. NTC is the non-template control.

5.4 Expression microarrays and functional analysis

A gene expression microarray was performed at the Microarray Analysis Service of Insitut Hospital del Mar d'Investigacions Mèdiques (IMIM, Barcelona). RNA samples were amplified and labelled according to GeneChip WT PLUS Reagent kit and hybridized to Human Gene 2.0 ST (Affymetrix) in a GeneChip Hybridation Oven 640. Washing and scanning were performed using the Expression Wash, Stain and Scan Kit and the GeneChip System of Affymetrix (GeneChip Fluidics Station 450 and GeneChip Scanner 3000 7G). After quality control of raw data, they were background corrected, quantile-normalized, and summarized to a gene-level using the robust multi-chip average (RMA); a total of 26599 transcript clusters, excluding controls, were obtained, which roughly corresponds to genes and other RNAs, such lincRNAs and miRNAs. NetAffx 36 annotations based on human genome 19 were used to summarize data into transcript clusters and to annotate analysed data. Linear Models for Microarray (LIMMA) (Smyth, 2004), a moderated *t*-statistics model, was used for detecting differentially expressed genes between conditions. Microarray Analysis Service (IMIM, Barcelona) and Pol Castellano (Biomarkers and Nutritional and Food Metabolomics from University of Barcelona, Barcelona) performed all microarray analyses. All data analyses were performed in R (version 1.42.0) with limma (version 3.34.9), genefilter, gplots, Vennerable, and hugene20sttranscriptcluster.db packages. The cut-off for considering significant differentially expressed genes was settled with 0.32 log fold change with P-value less than 0.05. For functional analysis, EnrichR (Kuleshov et al., 2016) or DAVID Bioinformatic Resources (Huang et al., 2008) were used to study enriched pathways from MLN4924 and shRING1B data.

5.5 Supervised analysis of expression database from ES tumours

Public available gene expression data from 184 debut ES tumours and reference 73 adult MSC and 17 embryonal stem cell (ESC) analysed by Affymetrix Human Genome U133 Plus 2.0 Array were downloaded from Gene Expression Omnibus data base (GEO2R) (https://www.ncbi.nlm.nih.gov/geo/) (ES tumours accession numbers: GSE17679, GSE34620 and GSE37371; Reference Accession Numbers: GSE13828, GSE7896, GSE8884, GSE9440, GSE9510, GSE10315, GSE13604, GSE6460, GSE7637, GSE9451, GSE9520 and GSE9593). All microarray analysis was performed by Dr. Soledad Gómez (HSJD DAI-Omics unit). Data were imported using the oligo package (R/Bioconductor) and normalized using the RMA algorithm (Irizarry et al., 2003). A correlation heatmap was used to ensure quality control of the data. Unsupervised analysis of data was performed using a standard deviation cut-off of 1.5 (n=2702 of total 54675 probes). Supervised analysis of KDM6A using the limma package was performed using the 203992_s_at probe, displaying a binomial distribution with 7.023 log2 mean in ES tumours (adjusted P-value >0.05; log FC =1; FDR method). R packages oligo, limma, rgl, ggplot, and RColorBrewer were used for this analysis.

6. PROTEIN MOLECULAR BIOLOGY TECHNIQUES

6.1 Protein extraction from cell cultures

Cultured cells were collected using the cell scraper or with trypsin-EDTA (0.25%) with phenol red (Gibco), and centrifuged to obtain the cell pellet, which was immediately processed or stored at –20˚C. Total cellular extracts of such pellets were prepared in RIPA buffer (10 mM Tris-HCl pH 8, 1 mM EDTA, 0.5 mM EGTA, 1% Triton X-100, 0.1% sodium deoxycholate, 0.1% SDS, and 140 mM NaCl) containing the phosphatase and the EDTA-free Protease Inhibitor Cocktail (Roche). Cell lyses were incubated on ice for 30 min, and samples were then centrifuged at 12,000 rpm for 15 min at 4˚C. Histone extracts of cultured cells were isolated using the EpiQuick Histone Extraction kit (Epigentek) by following the manufacturer's instructions. Protein supernatants were collected and quantified by Bradford assay (Sigma Aldrich) at 575 nm in the Infinite M Nano+ (Tecan) spectrophotometer.

6.2 Protein extraction from mouse samples

ES xenografts and PdX tumour samples treated with MLN4924 were stored at –80˚C. Small pieces of tumours were smashed in dry ice and weighed in AS R analytical balance (Radwag). RIPA protein extraction buffer with protease inhibitor mixture was subsequently added according to the weight of the tumour piece. Stainless-steel beads (0.2 mm diameter) were added, and samples were homogenized in the Bullet Blender (Nex Advance) at 12,000 rpm for 1 minute. Supernatant was collected, and samples were lysed by three cycles of cooling in ice for 15 min and vortex. Samples were centrifuged at 12,000 rpm for 15 min at 4˚C, and protein supernatants were collected and quantified by Bradford assay in the same way as proteins from cell cultures.

6.3 Western blot

About 30–50 μg of protein extracts, or 5 μg of histone extracts, were mixed with 5× Laemmli sample buffer (0.6 M Tris-HCl pH 6.8, 0.5 mM DTT, 25% glycerol, 2% SDS, and 0.1% Bromophenol blue) and boiled at 95˚C in a digital dry block heater to denature the protein structure. Samples were then loaded in sodium dodecyl sulfate polyacrylamide gel electrophoresis (SDS-PAGE) with different concentrations of acrylamide (8–15%), according to the weight of the protein sample to be detected. Acrylamide gels were prepared in two sections: the stacking and the resolving part. Electrophoresis was performed at 35 mA/gel during approximately 1 hour in running buffer (1% SDS, 25 mM Tris, and 192 mM glycine) using a Mini-PROTEAN Tetra Cell electrophoresis chamber connected to a PowerPac Basic power supply (all from Biorad). The PageRuler Plus Prestained Protein

Ladder (Bio-Rad) was used as a molecular weight. Gels were then blotted in 0.45 µm pore nitrocellulose membranes (GE Healthcare Life Sciences) for 1.5 hours in transfer buffer (20% methanol, 25 mM Tris, and 192 mM glycine) using Mini Trans-Blot Cell blotting chambers and a PowerPac Basic power supply at 250 mA at 4˚C. Non-specific binding was blocked by incubating the membranes with 3% BSA or 5% skim milk powder (Sigma Aldrich) in PBS for 1 hour at room temperature. Membranes were then washed in PBS with 0.1% Tween 20 (PBST) (Sigma Aldrich) and incubated overnight at 4˚C with the primary antibody (see **Table III. 5**). Actin, tubulin, or histone H4 were used as loading controls and were incubated at room temperature for 1 hour. After primary antibody hybridization, membranes were washed in PBST 3 times for 10 min each and incubated 1 hour at room temperature with the corresponding secondary antibody, whose type depends on the host species of the primary antibody (see **Table III. 6**). Membranes were washed 3 times as previously described and visualized using the near infrared fluorescence-based imaging system Odyssey CLx (LI-COR Biosciences).

6.4 Protein immunoprecipitation

Protein immunoprecipitation (IP) is used to identify physiologically relevant protein-protein interactions. The principle of this assay is the usage of specific antibodies targeting the proteins of interest of a whole cell lysate. Capturing the immunocomplex with high-affinity beads, such as agarose protein A or G beads, allows all the unbound material to be discarded. Finally, the immunocomplex is denaturalized, and the antigens are analysed by SDS-PAGE and Western blot. Here, a soft lysis buffer without SDS, such as IPH buffer (50 mM Tris-HCl pH 8, 150 mM NaCl, 5 mM EDTA, and 0.5% NP-40) with protease inhibitors, was added into the cell pellets to preserve the interactions between proteins in the lysate. Cells were lysed for 30 min on ice and centrifuged at 12,000 rpm for 15 min. The protein supernatant was then precleared by adding 40 µL of Protein A/G plus agarose beads (Santa Cruz Biotech) for 1 hour. Samples were centrifuged at 1,800 rpm for 2 min to precipitate the beads, which were discarded, as they contained the non-specific binding fraction of the lysate. 10% of the cell lysate was collected in 5× Laemmli sample buffer and stored at –20˚C for the input fraction. Supernatant was transferred into a new tube and incubated overnight with the antibodies targeting the protein of interest (see **Table III.5**). IgG was used as the negative control of the immunoprecipitation step. The following day, the same amount of beads was added to the samples, and the slurry was incubated for 2 hours at 4˚C. The supernatant was then discarded, and beads containing the immunocomplex with the protein of interest were washed three times with IPH buffer with protease inhibitor and incubated for 10 min at 4˚C. All centrifugations of beads were done at 1,800 rpm for 2 min at 4˚C, and incubations were performed in a rotating wheel at 4˚C. Supernatants were discarded, and beads were mixed with 5× Laemmli sample buffer and 2 µL of 2-mercaptoethanol (Sigma Aldrich). Input samples and immunoprecipitated

samples were then boiled at 95˚C for 5 min to denature protein structure and protein binding to the beads.

For GFP-tagged proteins, the GFP-Trap magnetic beads (Chromotek) were used to immunoprecipitate the protein complex. As GFP-Trap magnetic beads have a small recombinant alpaca antibody with high affinity to GFP covalently bound to the surface of agarose magnetic beads, the antibody incubation step is shorter, and isolation of the beads from the non-bound protein fraction can be done using a magnet. Immunoprecipitation was performed following manufacturer's instructions. For all immunoprecipitation experiments, protein-protein interactions were evaluated in gradient SDS-PAGE 8–16% MINI Protean TGX Precast Gels (BioRad) to ensure detection of proteins with very different weights.

6.5 Microscopic image techniques

6.5.1 Immunohistochemistry staining

For immunohistochemistry (IHC) studies, paraffin block samples were cut into sections of 2 μm with the microtome and heated at 56˚C for 45 min. A deparaffining and rehydration step in an alcohol battery with xylene and ethanol baths was performed, according to standard protocols. After washing slides with distilled water, an antigen retrieval step with a pressure cooker and the Epitope Retrieval Solution pH 6 Novocastra (Leica Biosystems) was performed for 3 min at 100˚C. Subsequently, slides were washed with distilled water and then endogenous peroxidase was blocked with the Peroxidase Block Novocastra (Leica Biosystems) for 5 min, following manufacturer's instructions. Slides were next washed with Wash buffer containing 1× dilution of Bond Wash Solution 10× Concentrate (Leica BioSystems) and incubated with Protein Block Novocastra (Leica Biosystems) for 5 min. The primary antibody was then added in a 1:400 dilution with the Bond Primary antibody diluent (Leica Biosystems) and incubated overnight at 4˚C (see **Table III. 5**). The following day, slides were washed with Wash buffer and incubated with the Post Primary component of the Polymer Kit (Post Primary Block + Polymer) Novocastra Novolink (Leica Biosystems) for 30 min. After washing, they were incubated with the Novolink Polymer component of the kit for 30 min. The DAB (Polymer) Kit (Buffer + Chromogen) Novocastra (Leica Biosystems) was incubated for 3–5 min until tissue was visually stained. Slides were then washed and counterstained in haematoxylin for 20–40 seconds, washed again, and then dehydrated with alcohol and xylene according to standard protocols. Slides were finally cover slipped with dibutylphthalate polystyrene xylene (DPX) and dried at room temperature. As negative controls, some sections were processed in the absence of primary antibody; no signal was detected. For the positive control, human placenta sections from HSJD biobank were used and stained as previously described. Slides were

scanned using the Leica Ariol system (Leica Biosystems) and quantified using the Ariol software by the Molecular Pathology Service of the Instituto Universitario de Biología Molecular y Celular del Cáncer (IBMCC) of University of Salamanca (USAL-CSIC, Salamanca). IHC images were captured by Leica DM5500B and digital camera DFC000T (Leica Biosystems) of the Microscopy Unit of HSJD.

6.5.2 Immunocytochemistry staining

For immunocytochemistry (ICC) experiments, cells were grown on coverslips or in 4 chamber Millicell EZ Slide (Sigma Aldrich) and fixed for 10 min in 4% PFA. An incubation step with PBS containing 0.1% of Tween 20 (PBST) for 5 min at room temperature was done to ensure permeabilization and accessibility of the antibody to the nuclear compartment in the next steps. To block for non-specific binding, 3% bovine serum albumin (BSA) in PBS was added to the samples for 1 hour at room temperature, and then primary antibody was incubated overnight in a wet chamber at 4˚C. The following day, cells were washed 3 times with PBST for 10 min each and labelled with secondary antibodies (for dilutions of primary and secondary antibodies, see **Tables III. 5** and **III. 6,** respectively). Cell nuclei were stained using 1:500 dilution of Hoescht dye in PBST for 1 hour, and slides were mounted with ProLong Gold (Thermo Fisher Scientific). Confocal images from three different channels were collected with a Leica SP8 confocal microscope equipped with a HC PL APO CS2 100×/1.40 oil immersion objective using a step size of 1 μm, in the Microscopy Confocal Unit of HSJD. Super-resolution images were captured using the HyVolution tool from Leica Microsystems, which combines optical super-resolution at sub-airy pinhole sizes with subsequent computational analysis by image deconvolution. Combination of both allows for simultaneously image multiple fluorophores and capture intracellular details, such as the nuclei compartment, with a resolution up to 140 nm. Confocal images were processed and analysed with Image J software (Schindelin et al., 2012). For colocalization experiments, representative images from 6 different nuclei with a minimum of 6 stacks per nuclei were used to quantify each prove. Colocalization was calculated by Pearson's correlation method (Manders et al., 1993) and Li's intensity correlation method using JaCop pluggin in Image J (Bolte and Cordelières, 2006).

7. STATISTICAL ANALYSIS

Statistical analyses were performed using GraphPad. All data are expressed as mean ± SEM. Student's *t*-test and Mann-Whitney *t*-test (for non-normally distributed data) were used for nonpaired comparisons of two groups. Two-way analyses of variances (ANOVA) and Kruskal-Wallis (for nonnormally distributed data) were applied to determine differences between multiple groups. $\chi 2$ test was used to compare proportions. Median survivals were calculated using the Kaplan–Meier method, and curves were compared using the log-rank

test. The appropriate post-hoc tests are indicated in the figure legends. Values for n and P are also specified in each figure legend. A 95% confidence interval was used, and values of $P < 0.05$ were considered as statistically significant.

8. SOFTWARE

TABLE III. 10 ***List of the software used in this thesis.***

Software	Source
7500 Fast Real-Time PCR System Software	Applied Biosystems
Adobe Photoshop CS5	Adobe
Adobe Illustrator CS5	Adobe
BioEdit	BioEdit
Chromas Lite	Technelysium Pty Ltd
Endnote X7	Clarivate Analytics
Fiji (ImageJ)	National Institute of Health
Graphpad Prism7	Graphpad software
Image Lab software Suite	Biorad Laboratories
Leica LAS X LifeScience	Leica Microsystems
Li-Cor Image Studio Suite v.5.0	Li-Cor Biosciences
MultiCycle AV Standalone	Phoenix Flow Systems
NIS-Elements Software	Nikon
Primer 3	Steve Lincoln, Mark Daly, and Eric S. Lander
QuantStudio 6 & 7 Flex Real-Time PCR System	Applied Biosystems
Tecan i-Control v. 2.0	Tecan Life Sciences

IV. RESULTS

1. ROLE OF RING1B IN ES TUMORIGENESIS

Previous work from our group has identified the PcG subunit RING1B as highly expressed in primary ES tumours as compared to other sarcomas. We reported protection of ES cells from apoptotic cell death by RING1B-mediated repression (Hernandez-Muñoz et al., 2016). Increasing evidence indicates that PRC1 complexes containing RING1B have potential for transcription activation, via catalytic-independent association with KDM6A, an H3K27me3 demethylase, and p300 (Rai et al., 2015). In agreement with this new role, we have recently described that RING1B co-localizes with EWSR1-FLI1 at enhancers, while retaining its repressive activity at PcG developmental-regulated genes. We demonstrated that RING1B is necessary for the expression of key EWSR1-FLI1 targets by facilitating the recruitment of the fusion oncoprotein to key enhancers (Sánchez-Molina et al., 2019).

To investigate the *in vivo* relevance of RING1B in ES tumorigenesis, we subcutaneously injected SK-ES-1 cells with a shRNA targeting RING1B and a control shRNA sequence into nude athymic mice. Each mouse carried ES inoculum in two flanks with the same shRNA sequence. At 19 days post-injection, tumours derived from shRING1B xenografts were significantly smaller than controls, with median values of 166.8 mm^3 (n=10) and 534.9 mm^3 (n=10), respectively (P-value < 0.05) (**Figure IV. 1A**). Importantly, the median

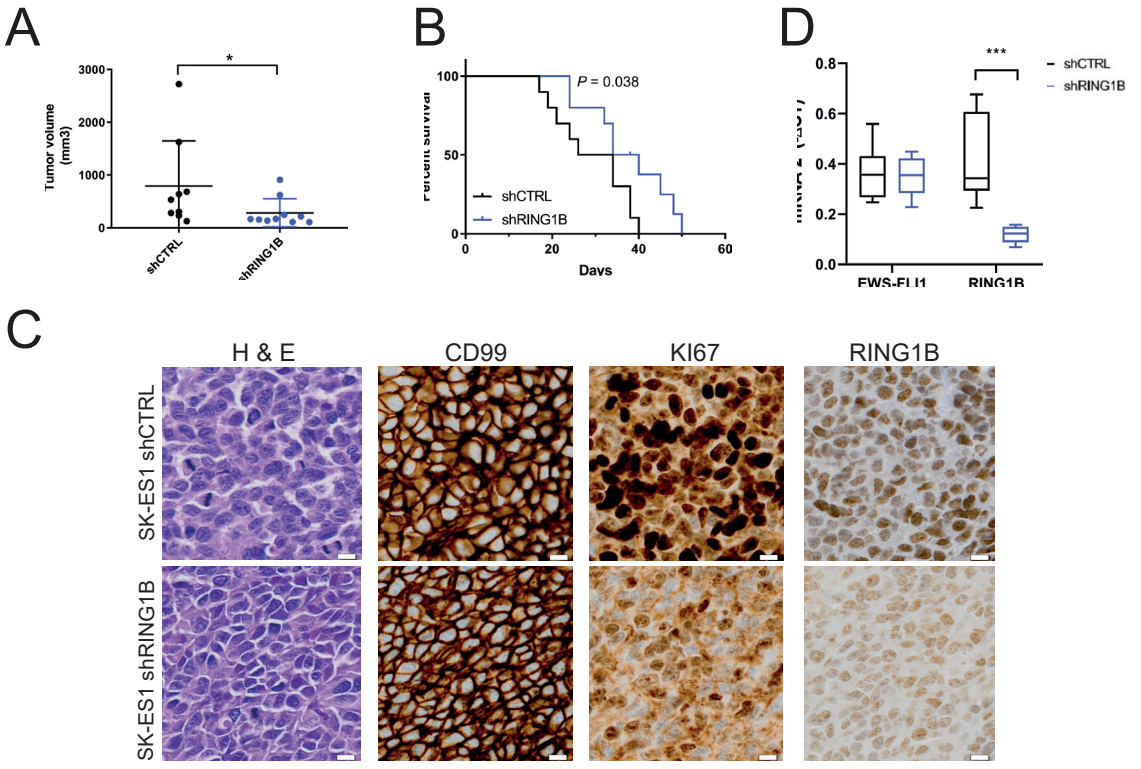

FIGURE IV. 1 ***RING1B knockdown in SK-ES-1 xenografts impairs tumour growth in vivo.***
A) Boxplot summarizing the tumour volume distribution of xenografts established by subcutaneous injection of SK-ES-1 shCTRL versus shRING1B cell lines in athymic nude mice at 19 days post-injection. Median volume was 534.9 mm^3 and 166.8 mm^3, respectively. *P < 0.05. ***B)*** Kaplan–Meier survival curves of mice

with shCTRL versus shRING1B xenografts. P value was calculated using the log-rank statistical test. *P < 0.05. ***C)*** Immunohistochemistry study of RING1B, EWSR1-FLI1, and CD99 antibodies in sections of excised tumours from shCTRL and shRING1B xenografts. Proliferation was assayed by immunohistochemistry staining of Ki-67. Section tissue morphology was controlled with H&E staining of tumours. All images were captured at 40× magnification. Scale bar represents 20 μm. ***D)*** RT-qPCR analysis of mRNA expression for *RING1B* and *EWSR1-FLI1* in tumours. mRNA expression levels were calculated with the ΔΔCT method and normalized to *GAPDH*. Data represent the mean ± SEM (n = 9–10 animals per group). *P < 0.05 and ***P < 0.001 as compared to control.

survival of mice was 30 days for those with shCTRL and 37 for those with shRING1B (**Figure IV. 1B**), demonstrating that genetic knockdown of RING1B caused delay in tumour growth. This result was further confirmed by immunohistochemical studies showing shCTRL tumours displayed higher proliferation rates than shRING1B, according to KI-67 staining (**Figure IV. 1C**). We also confirmed a lower expression of RING1B in knockdown xenografts as compared to controls. The ES marker CD99 remained essentially unchanged. These data agreed with the mRNA expression levels observed for RING1B and EWSR1-FLI1 in tumours at the endpoint (**Figure IV. 1D**). In brief, all pieces of evidence highlight the importance of RING1B in ES tumorigenesis and further support RING1B as an attractive pharmacological target to test.

2. TARGETING RING1B BY MLN4924 (PEVONEDISTAT)

The NAE inhibitor MLN4924 has been reported to be remarkably active in a panel of ES cell lines and xenografts, harbouring a mean IC50 of 31 nM (Mackintosh et al., 2012; Smith et al., 2012). Members of the large CRL family of E3 ubiquitin ligases, which mediate protein turnover, are among the most altered substrates described by MLN4924. Full activation of CRL requires neddylation of the cullin subunit (Zhou et al., 2019). By inhibiting the first steps of the neddylation cascade, MLN4924 triggers an accumulation of many CRL substrates involved in multiple crucial cellular processes, including cell cycle arrest, apoptosis, senescence, and autophagy (Soucy et al., 2009). RING1B, the enzymatic subunit of PRC1, has E3 ubiquitin ligase activity on histone H2A, which has been primarily linked to gene repression (Wang et al., 2004). Given the striking sensitivity of ES cells to MLN4924, together with the mechanistic basis reported for MLN4924 to functionally perturb E3 ubiquitin ligases, we asked whether this drug could alter RING1B in ES.

2.1 The strong sensitivity of ES cells to MLN4924 correlates with an accumulation of CRL substrates

In order to validate if MLN4924 functionally modifies E3 ligases, we first characterized the IC50 concentration for MLN4924 in ES cells, as compared to a non-tumoral cell line (HEK 293T), by exposing the cells to different concentrations of the inhibitor for 72 hours. By MTS viability assays we reproduced the high vulnerability reported for ES cell lines to MLN4924, showing mean IC50 of 80 nM, 86 nM and 114 nM for A4573, A673 and SK-ES-1, respectively (**Figure IV. 2A).** In contrast, HEK 293T cells displayed

a more resistant pattern, lacking the delay in cell viability observed for ES cells at such concentrations. These results were further confirmed by crystal violet staining (**Figure IV. 2B**). We subsequently studied the activity of CRL upon MLN4924 treatment by analysing the expression of p27 and p53 substrates by Western blot. We observed that p27 and p53 CRL substrates accumulated in ES cells following MLN4924 treatment, in agreement with literature (**Figure IV. 2C**). Specifically, A673 cells displayed an early accumulation of proteins at 50 nM, while SK-ES-1 cells required a higher concentration of the drug, at 100 nM. Despite the sensitivity of these cells to MLN4924, levels of EWSR1-FLI1 remained invariable. In contrast, CRL substrates in HEK 293T cells showed no changes at these concentrations of MLN4924.

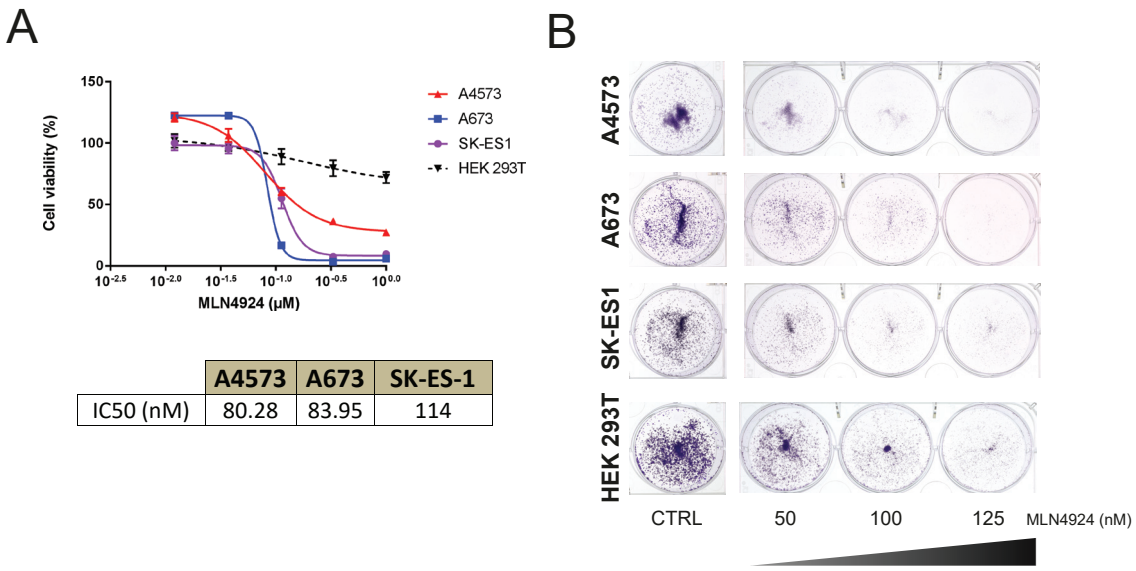

	A4573	A673	SK-ES-1
IC50 (nM)	80.28	83.95	114

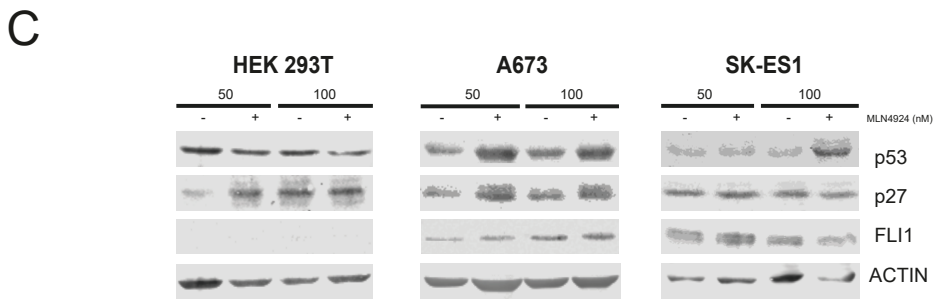

FIGURE IV. 2 ***ES cell lines are especially sensitive to MLN4924 treatment, correlating with an accumulation of CRL substrates.***
A) MTS cell proliferation curves expressed in percentage of viable cells in A4573, A673 and SK-ES-1 ES cell lines after different concentrations of MLN4924 treatment for 72 hours. HEK 293T was used as a control. Represented values are means of five technical replicates per condition. Best-fit curves of three biological replicates were built in GraphPad Prism. Table below shows the IC50 values calculated with the same program. ***B)*** Images of crystal violet staining of ES cells and HEK 293T treated at the indicated concentrations of MLN4924 taken 6 days later. ***C)*** Western blot analysis of a representative experiment showing protein levels of p27 and p53 CRL substrates upon MLN4924 treatment at 50 and 100 nM in ES cell lines and HEK 293T. FLI1 antibody detects levels of EWSR1-FLI1 fusion oncoprotein in ES cells. Actin was used as a loading control.

Altogether, these results reproduce the striking sensitivity reported for ES cell lines to MLN4924, independently of EWSR1-FLI1 protein changes. Furthermore, our data indicate that CRL substrates accumulate, showing specific perturbation of these E3 ligases in ES cells.

2.2 MLN4924 deregulates gene expression profiling of E3 ubiquitin ligases in ES cell lines

To elucidate to which extent MLN4924 alters the expression of E3 ligases in ES cells, we performed a genome-wide gene expression analysis of A673 and SK-ES-1 cells treated with the drug. We used a sub-IC50 concentration of MLN4924 to avoid maximal contribution of cell-death effects, i.e. 50 nM for 72 hours in both cell lines. Consistent with the higher sensitivity to MLN4924 observed in A673 cells as compared to SK-ES-1 cells, gene expression data revealed significantly more genes altered in A673 than in SK-ES-1 with 3116 and 1698 deregulated targets, respectively (log fold change (FC) 0.32 and P-value < 0.05) (**Figure IV. 3A**). Functional analyses of these data by DAVID Bioinformatics Resources revealed enrichment in gene ontology (GO) terms in A673 cells that were principally involved in cell death in response to DNA damage and stress, such as the release of cytochrome C from mitochondria, DNA damage checkpoint, and apoptosis, among the top-10 biological processes. These data are consistent with the induction of apoptosis described for MLN4924 in ES cells (Mackintosh et al., 2012). In contrast, SK-ES-1 cells showed enrichment in pathways closely related to cell response to stress, such as interferon (IFN) signalling, response to virus, and oxidation-reduction processes (**Figure IV. 3B**). We suggest that enrichment of such stress-related pre-apoptotic pathways displayed by SK-ES-1 cells were due to the less sensitive phenotype shown for this cell line at the drug concentration used in this study.

In order to explore whether E3 ubiquitin ligases were significantly altered in the differential expressed genes (DEG) list, we crossed our data with a public dataset comprising 377 human E3 ubiquitin ligases (Medvar et al., 2016). We found that 70 E3 ligases in A673 cells, and 20 in SK-ES-1 cells, were among the significantly deregulated genes by MLN4924, representing 18.5% and 5.3%, respectively, of the total E3 ligases (**Figure IV. 3C**). This result indicates that MLN4924 not only alters the enzymatic activity of some E3 ligases such as CRL (seen as an accumulation of CRL substrates in Figure IV. 2C) but also the expression levels of many E3 ligases. Note that at these concentrations of MLN4924, SK-ES-1 cells had almost one-third deregulated E3 ligases as compared to A673 cells. RING1B was not in the list of statistically significant deregulated E3 ligases, although it decreased with drug treatment in both datasets. Accordingly, we confirmed *RING1B* downregulation by MLN4924 by RT-qPCR, which was statistically significant for A673 cells. Moreover, this was specific for *RING1B* and ES cells, as *RING1B* mRNA levels in HEK293T cells remained unaltered (**Figure IV. 3D**).

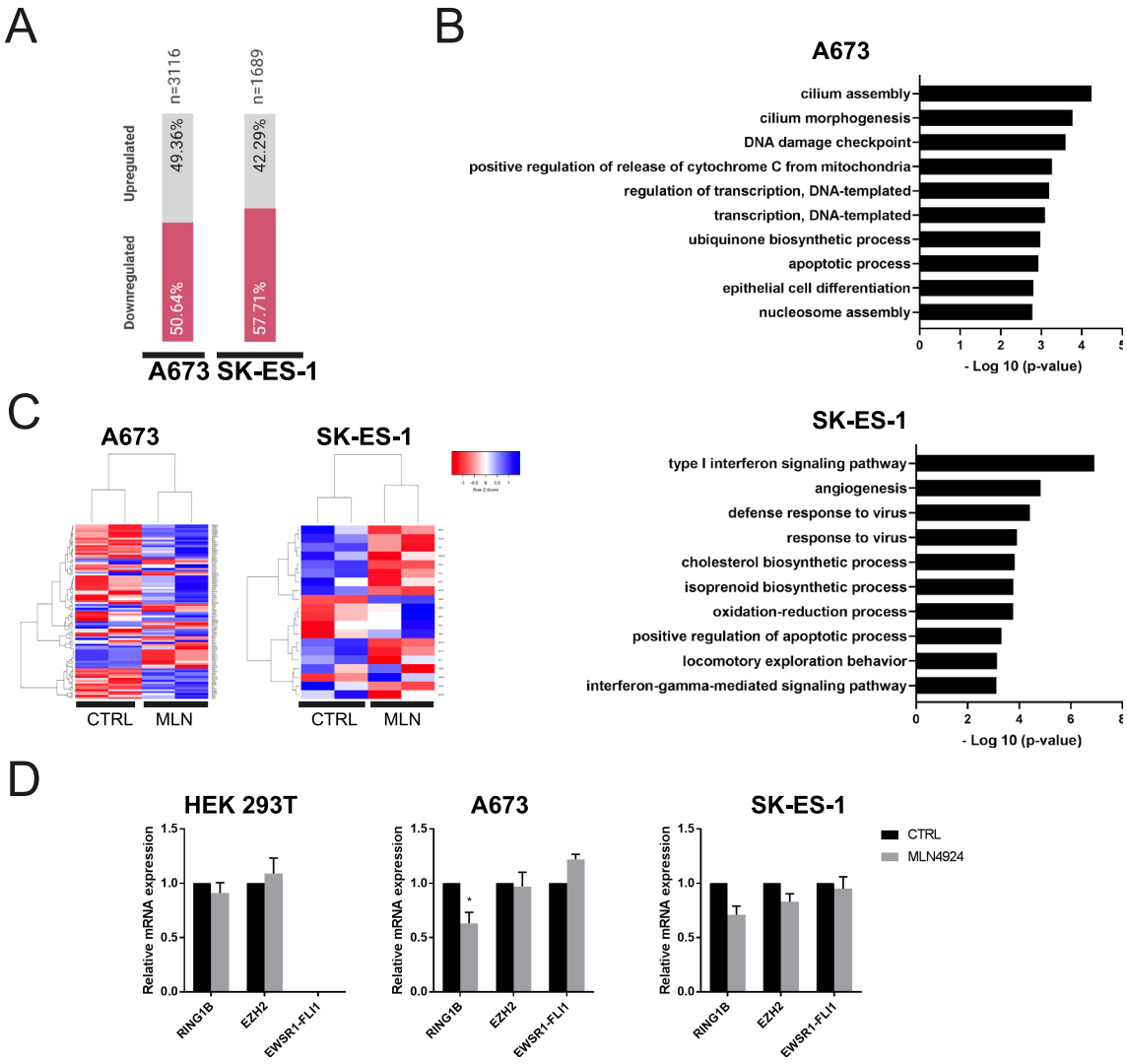

FIGURE IV. 3 ***MLN4924 deregulates E3 ubiquitin ligases including RING1B in A673 and SK-ES1 ES cell lines.***

A) Bars representing percent of DEG from microarray analysis upregulated (grey) and downregulated (pink) in A673 and SK-ES-1 cells treated with 50 nM of MLN4924. A log FC of 0.32 and a P-value < 0.05 cut-off was used for the analysis. ***B)*** GO enrichment analysis of the top-10 biological pathways of DEG upon MLN4924 treatment for A673 (up) and SK-ES-1 (down) ES cells. The statistical significance of the enrichment (-log(P-value)) is shown in the x-axis, and the y-axis shows the GO biological processes. ***C)*** Heatmap visualization of gene expression values of a subset of 70 and 20 E3 ubiquitin ligases significantly deregulated by MLN4924 in A673 and SK-ES-1, respectively. Expression levels are indicated by the shading in the heatmap, with blue indicating a negative log FC value (lower expression) and red indicating a positive log FC (higher expression). Dendrograms show the results of hierarchical clustering of genes (left) and biological samples (up). Control (CTRL) and treated (MLN) replicates are indicated below histograms. ***D)*** RT-qPCR analysis of mRNA levels of RING1B and EZH2, the catalytic subunits of PRC1 and PRC2, respectively, and *EWSR1-FLI1*, in control and MLN4924 treated ES cells. HEK 293T was used as a control. mRNA expression was calculated with ΔΔCT method and normalized to *TBP*. All experimental conditions were calculated relative to the control condition. All data represent mean ± SEM from minimum of three biological replicates. *P < 0.05.

Overall, our data indicate a remarkable deregulation of E3 ubiquitin ligases by MLN4924. The sensitivity of ES cells to MLN4924, together with the decrease of *RING1B* at the mRNA level, prompted us to use this drug to study the effects of RING1B modulation in ES cells.

2.3 RING1B knockdown sensitizes ES cell lines to MLN4924 inducing apoptosis

We have demonstrated MLN4924 causing a decrease of *RING1B* transcript levels. To investigate the pathways involved in *RING1B* deregulation by MLN4924, we crossed the *RING1B* knockdown gene expression data in A673 and SK-ES-1 ES cell lines from Sánchez-Molina et al. (2019) with our data. We first confirmed depletion of RING1B in A673 and SK-ES-1 cells by Western blot, which was associated with invariable levels of EWSR1-FLI1 (**Figure IV. 4A**, left). Interestingly, the RING1B decrease caused no alterations of H2Aub protein levels (**Figure IV. 4A**, right), indicating that RING1B function in ES is

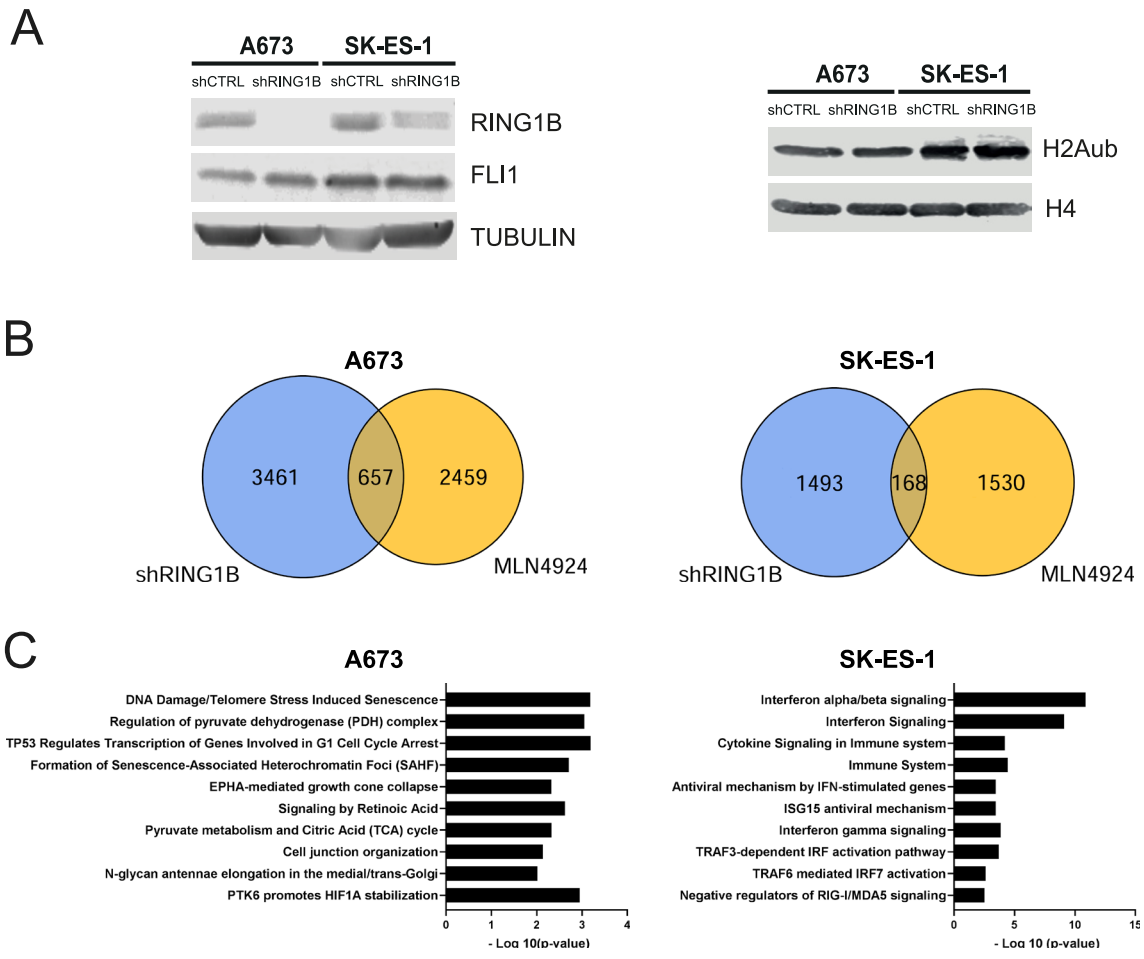

FIGURE IV. 4 ***MLN4924 treatment and RING1B knockdown share DNA damage and cell-stress related pathways in ES cells.***
A) Representative immunoblots showing RING1B (left) and ubH2A (right) levels from whole-cell

protein extracts or histone extracts, respectively, in A673 and SK-ES-1 knockdown cells. EWSR1-FLI1 was detected with FLI1 antibody. Tubulin and histone H4 were used as loading controls. ***B)*** Venn diagrams of the set of DEG generated for RING1B knockdown (shRING1B) and MLN4924 treatment (MLN4924) in A673 (left) and SK-ES-1 (right) using a log FC 0.32 and P-value 0.05 cut-off. Common genes are represented in grey shading. Each diagram contains the number of genes represented. ***C)*** Enrichment analysis of the top-10 biological pathways of the common DEG set between RING1B and MLN4924 in A673 (left) and SK-ES-1 (right). The x-axis shows the statistical significance of the enrichment (-log(P-value)), and the y-axis shows the top-10 enriched pathway categories from Reactome pathway database (2016).

uncoupled from its ubiquitin ligase activity towards H2A, as proposed in Sánchez-Molina et al. (2019). Intersection of the 4118 DEG of *RING1B* knockdown with our gene set of 3116 DEG deregulated with MLN4924 in A673 cells (logFC 0.32 and P-value < 0.05) showed a striking overlap of 657 (16%) of commonly deregulated genes (**Figure IV. 4B**, left). Although SK-ES-1 cells had less deregulated targets upon MLN4924 treatment, they also displayed an overlap of 168 genes (10%) (**Figure IV. 4B**, right). These results indicate that a great part of the effects produced by RING1B knockdown are also observed when treating these cells with MLN4924, supporting our previous observations indicating that RING1B is deregulated by MLN4924. We subsequently investigated the pathways involved in the gene set of commonly deregulated genes for each cell line. Functional enrichment analysis using EnrichR, indicated the DNA damage/telomere stress-induced senescence, or the TP53 in the G1 cell cycle arrest pathway, were among the top-10 most statistically significant representative pathways in A673 cells (**Figure IV. 4C**, left). SK-ES-1 cells, however, displayed pathways related to immune processes, such as IFN or cytokine signalling (**Figure IV. 4C**, right).

Consistent with these observations, exposing control and RING1B knockdown cells to different concentrations of MLN4924 and evaluating cell proliferation, showed that the depleted cells were more sensitive to the drug as compared to control. The IC50 values for control and RING1B-depleted cells were 158 and 85 nM, respectively, in A673 cells, and 138 and 100 nM, respectively, in SK-ES-1 cells (**Figure IV. 5A**). A673 cells, in particular, showed a delay in cell viability that was statistically significant at 100 nM of MLN4924. In order to elucidate if such differences were related to cell death, we analysed cell apoptosis by annexin V staining by flow cytometry. Analyses of different concentrations of MLN4924 in A673 and SK-ES-1 cells showed that lack of RING1B increased the fraction of early and late apoptotic cells upon treatment with MLN4924 (**Figures IV. 5B** and **IV. 5C**). Furthermore, we observed that such induction of cell death was concentration-dependant in both ES cell lines.

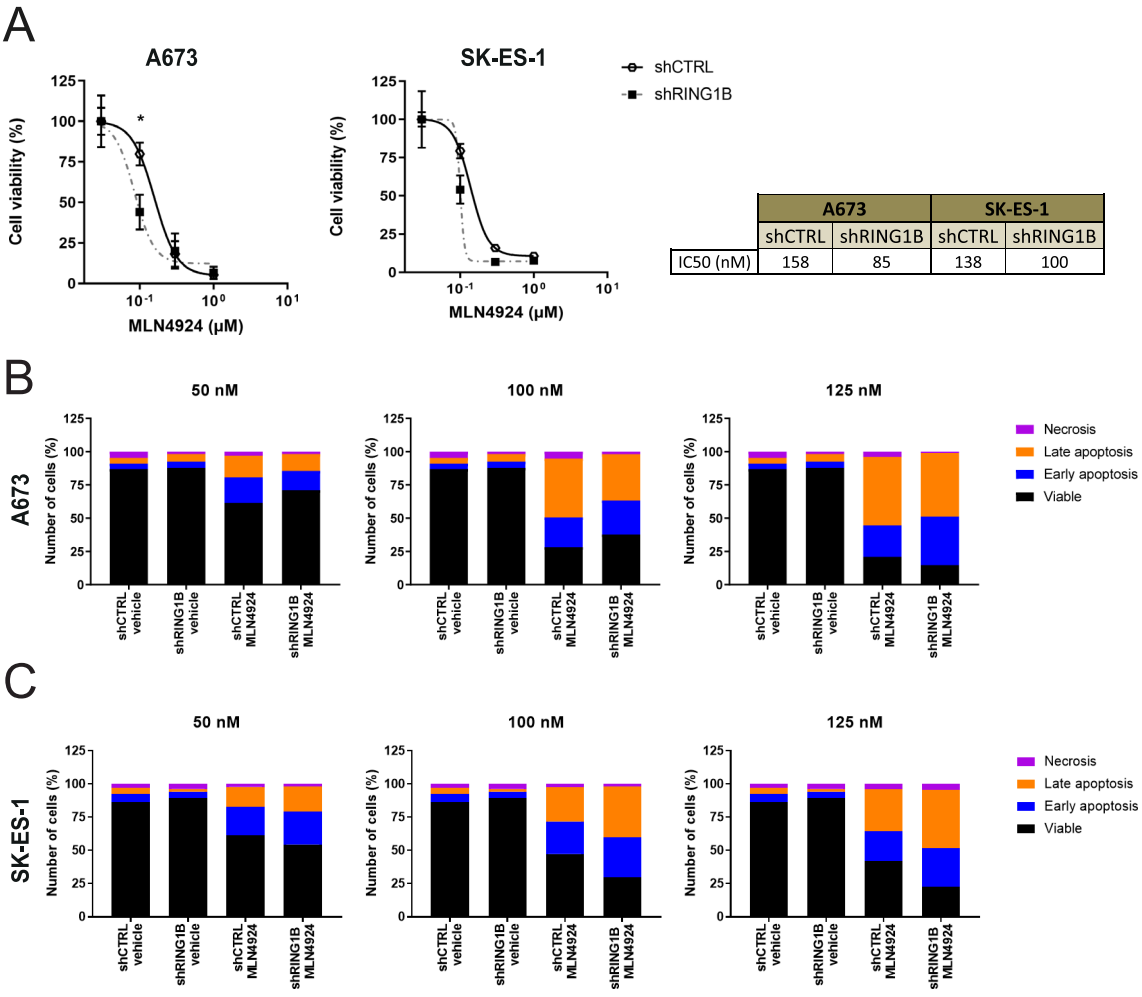

	A673		SK-ES-1	
	shCTRL	shRING1B	shCTRL	shRING1B
IC50 (nM)	158	85	138	100

FIGURE IV. 5 ***RING1B knockdown sensitizes ES cells to MLN4924 and correlates with an increase in the number of apoptotic cells.***
A) MTS cell proliferation curves expressed in percentage of viable cells in RING1B knockdown A673 (left) and SK-ES-1 (right) ES cell lines upon treatment with different concentrations of MLN4924 at 72 hours. Best-fit curves of three biological replicates were built in GraphPad Prism. The right table shows the IC50 values, which were calculated with this program. One-way ANOVA statistical test was used to calculate for statistically significant differences at each concentration point. *P < 0.05. ***B)*** Bar charts representing percentages of viable, early, and late apoptotic and necrotic cells analysed by annexin V staining by flow cytometry in RING1B knockdown in A673 cells upon treatment with different concentrations of MLN4924. Data from a representative experiment performed in parallel with the three experimental conditions are shown. ***C)*** The same results shown in ***B)*** but for SK-ES-1 cells.

Collectively, we have demonstrated a striking relationship between RING1B and MLN4924, indicating DNA damage or IFN signalling as common deregulated pathways in ES cells. Furthermore, we show RING1B knockdown sensitizes these cells to MLN4924 treatment, which is associated to an enhanced apoptosis, demonstrating RING1B dependency in ES cells as previously proposed by our group.

2.4 MLN4924 produces deficient neddylation triggering RING1B proteasome degradation

We next explored if the downregulation observed for *RING1B* at the mRNA level correlated with a decrease at the protein level as well. To do this, we extensively analysed RING1B protein levels in a panel of different ES cell lines treated with different concentrations of MLN4924 as compared to the HEK 293T control cell line. We observed a concentration-dependent decrease of RING1B by Western blot that was evident in all ES cells at 125 nM (**Figure IV. 6A**). Notably, RING1B levels in HEK 293T control cells were unaltered. Correlating with mRNA results, SK-ES-1 cell line was the least responsive to MLN4924 treatment.

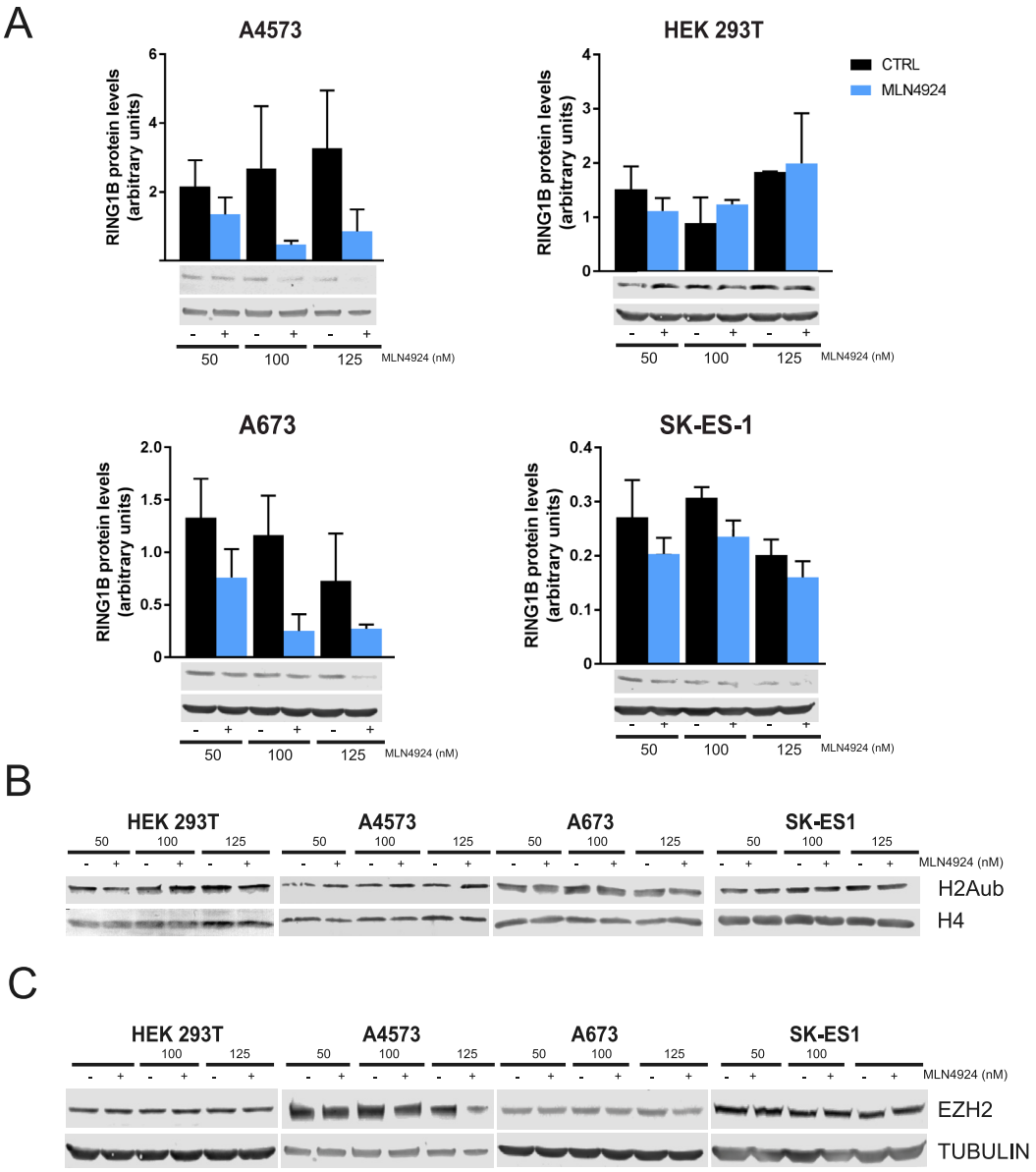

FIGURE IV. 6 ***MLN4924 decreases RING1B at protein level in ES cell lines in a concentration-dependant manner.***
Western blot showing ***A)*** RING1B protein levels in ES cells upon MLN4924 treatment, compared to a control

cell such as HEK 293T. Histograms represent the densitometric values related to loading control obtained in the analysis of three biological replicates of the experiment. All data represent the mean ± SEM. Tubulin was used as loading control; ***B)*** H2Aub levels in ES cells and HEK 293T upon MLN4924 treatment from histone extracts. Histone H4 was used as loading control; and ***C)*** EZH2 levels in ES cells and HEK 293T upon MLN4924 treatment. Tubulin was used as loading control. 50, 100, and 125 nM MLN4924 concentrations were used for these experiments.

We then asked whether the decrease seen on RING1B protein was associated to a defective E3 enzymatic activity by analysing H2Aub by Western blot. Surprisingly, the overall levels of H2Aub were unaltered upon MLN4924 treatment at every concentration tested (**Figure IV. 6B**). The stable levels found for H2Aub upon MLN4924 treatment coincide with data published by other groups (Kim et al., 2011). We additionally investigated whether the decrease of RING1B in ES cells was specific for this PcG protein. Western blot analysis of EZH2, the catalytic component of PRC2, revealed that the levels of this subunit were maintained with all the concentrations tested, consistent with the mRNA results (**Figure IV. 6C**). Thus, the decrease of RING1B upon MLN4924 treatment was specific for this PcG protein, with no repercussion on the overall levels of H2Aub.

We next sought to explore the mechanism by which RING1B was deregulated by MLN4924 in ES cells. To elucidate if the proteasome machinery was behind the RING1B decrease, we treated A673 cells with the proteasome inhibitor MG132, alone or in combination with MLN4924. We used the highest concentration of MLN4924 tested previously (125 nM), to ensure a strong decrease of RING1B levels. If the proteasome machinery was the main factor responsible for its degradation, we would expect that following MG132 treatment in combination with MLN4924, protein levels of RING1B would recover as compared to MLN4924 treatment alone. In agreement with our hypothesis, addition of MG132 to cells treated with MLN4924 almost restored RING1B levels, indicating that the proteasome mediated its degradation by MLN4924 (**Figure IV. 7A**). The incomplete restoration of RING1B protein levels is in agreement with its downregulation at mRNA level by MLN4924.

MLN4924 deregulates S-phase cell cycle proteins in ES cells (Mackintosh et al., 2012). Considering these data, we asked if deregulation of S-phase proteins by MLN4924 might explain the decrease of RING1B protein. To this end, we treated ES cells with aphidicolin, which blocks cell cycle at the early S-phase, and analysed RING1B protein levels. We observed that the accumulation of cells blocked in S-phase upon aphidicolin treatment by flow cytometry did not correlate with a decreased level of RING1B in Western blot (**Figure IV. 7B**). It thus seems that RING1B degradation is not related to the deregulation of S-phase proteins described for MLN4924 treatment.

Neddylation has been extensively characterized in the context of CRL. Reports of non-cullin neddylation in recent years indicate that NEDD8 might have additional biological

functions (Enchev et al., 2015). As MLN4924 is a general inhibitor of neddylation, we hence hypothesized that inhibition of neddylation by MLN4924 could be the mechanism behind RING1B degradation in ES cells. We simulated the suppression of neddylation of MLN4924 by transiently transfecting ES cell lines with a siRNA against NEDD8. Analysis of RING1B by Western blot showed a positive correlation between lower NEDD8 and RING1B levels, confirming that lack of neddylation triggers RING1B degradation in ES cells (**Figure IV. 7C**). Furthermore, RING1B has been described to be neddylated (Li et al., 2014). Consistently, NEDD8 was detected in RING1B immunoprecipitates in A673 cells (**Figure IV. 7D**).

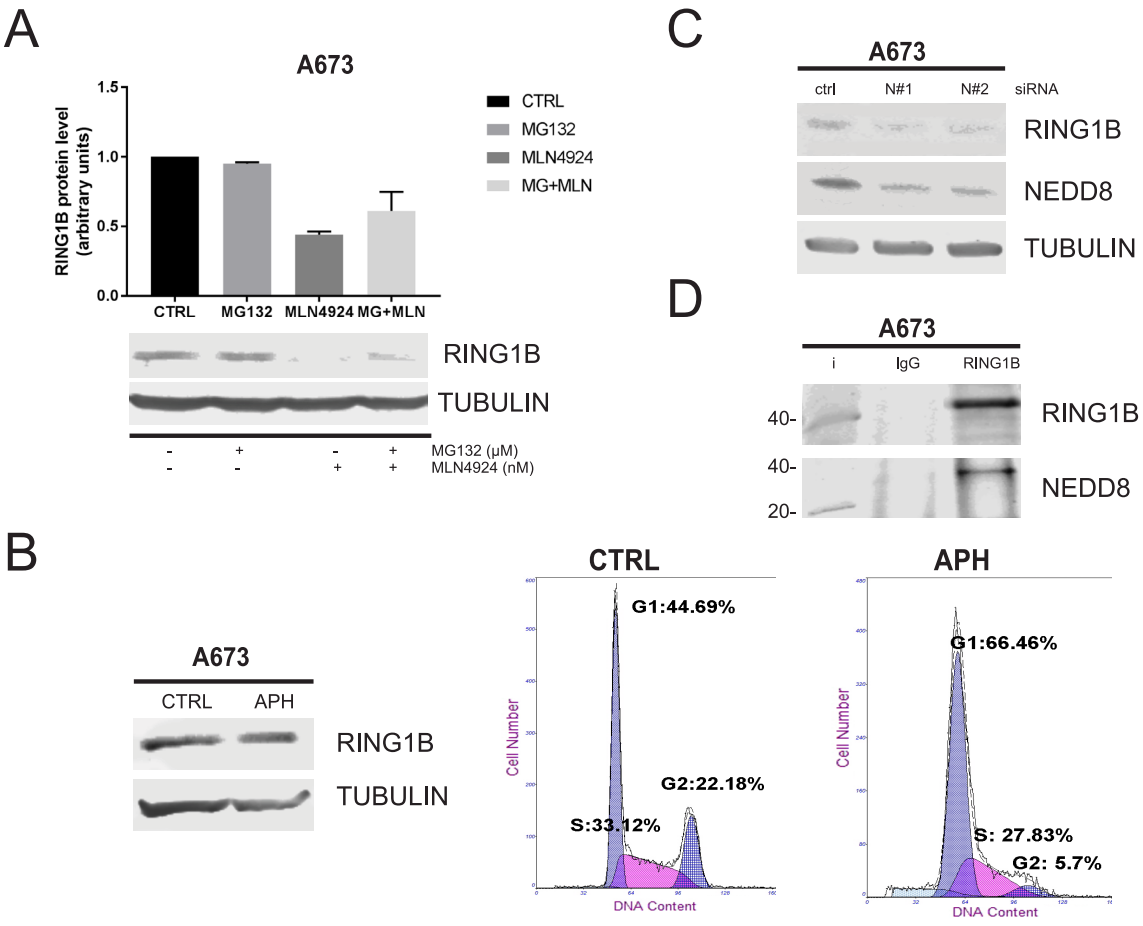

FIGURE IV. 7 ***Lack of neddylation caused by MLN4924 prone RING1B proteasome-degradation in A673 cells.***

A) Western blot representing RING1B protein levels upon treatment with 125 nM of MLN4924, the proteasome inhibitor MG132, and combinatorial treatment (MG+MLN). Treated cells with vehicle is shown as CTRL. Tubulin was used as a loading control. Histogram represents the densitometric values related to loading control and normalized to CTRL. Data obtained from the analysis of three biological replicates of the experiment. All data represent the mean ± SEM. ***B)*** Western blot (left) and cell cycle analysis (right graphs) from flow cytometry experiments of A673 cells treated with vehicle (CTRL) and aphidicolin (APH). Western blot shows RING1B protein levels upon aphidicolin treatment. Tubulin was used as loading control. Graphs represent percentage of cells in G1, S and G2 cell cycle phases, with the x-axis indicating DNA content and the y-axis the cell number. Data from a representative experiment are shown. ***C)*** Western blot of RING1B and NEDD8 protein levels upon NEDD8 knockdown with two siRNA sequences targeting NEDD8 from a representative experiment. Mock control and the two different siRNA are represented as M, N#1 and N#2. ***D)*** Western blot analysis of RING1B immunoprecipitates in A673 showing NEDD8 and RING1B blots. Input represents 10% of whole cell extracts.

Collectively, these results indicate that RING1B is stabilized, at least in part, by neddylation in ES cells. We further showed that MLN4924 perturbs RING1B proteostasis by triggering its degradation via proteasome, as it recovers following treatment with a proteasome inhibitor. Therefore, we conclude that RING1B degradation by MLN4924 in ES cells is related to inhibition of neddylation by the drug, triggering its degradation through the proteasome.

2.5 MLN4924 evicts RING1B and EWSR1-FLI1 from EWSR1-FLI1–activated target genes.

Our group has recently shown that RING1B co-localizes genome-wide with EWSR1-FLI1 in the *de novo* enhancers generated by the oncoprotein, facilitating its recruitment and modulating transcription (Sánchez-Molina et al., 2019). A well-known set of EWSR1-FLI1–activated target regions, co-occupied by RING1B, was also defined in this work.

To further elucidate if the deregulation of RING1B protein levels caused by MLN4924 affected its recruitment to chromatin, we analysed RING1B binding at EWSR1-FLI1 targets by ChIP-qPCR technique upon treatment. We noticed that low concentrations (50 nM) of MLN4924 were enough to lose RING1B from oncogene-activated target sites, especially in the most sensitive cell lines tested, A673 and A4573 (**Figure IV. 8A**). No effect was observed for the more resistant cells of SK-ES-1 (data not shown). As previous data from our group revealed EWSR1-FLI1 recruitment is affected by RING1B knockdown in ES cells (Sánchez-Molina et al., 2019), we next checked whether MLN4924 perturbs binding of the oncogene to its targets. Even though MLN4924 did not alter EWSR1-FLI1 levels at that concentration (see **Figure IV. 2C**), ChIP-qPCR experiments revealed that EWSR1-FLI1 was evicted from its target regions correlating with the loss of RING1B observed at these sites (**Figure IV. 8B**). We next explored whether such eviction from these transactivation regions is associated with transcriptional changes. Interestingly, expression analysis of some EWSR1-FLI1–activated targets by RT-qPCR demonstrated a slight decrease in gene expression by MLN4924 in A673 cells, as compared to control cells (**Figure IV. 8C**). For instance, downregulation of EWSR1-FLI1 enhancer-regulated genes like *CAV1, SOX2,* and *NKX2-2* correlated with the loss of RING1B by qPCR in A673 cells. Overall, these data agree with previous observations by our group (in Sánchez-Molina et al., 2019) indicating that in addition to clear co-localization of RING1B and EWSR1-FLI1 genome-wide at enhancer regions, downregulation of RING1B modulates expression of key oncogene targets, such as *NKX2-2* and *SOX2*.

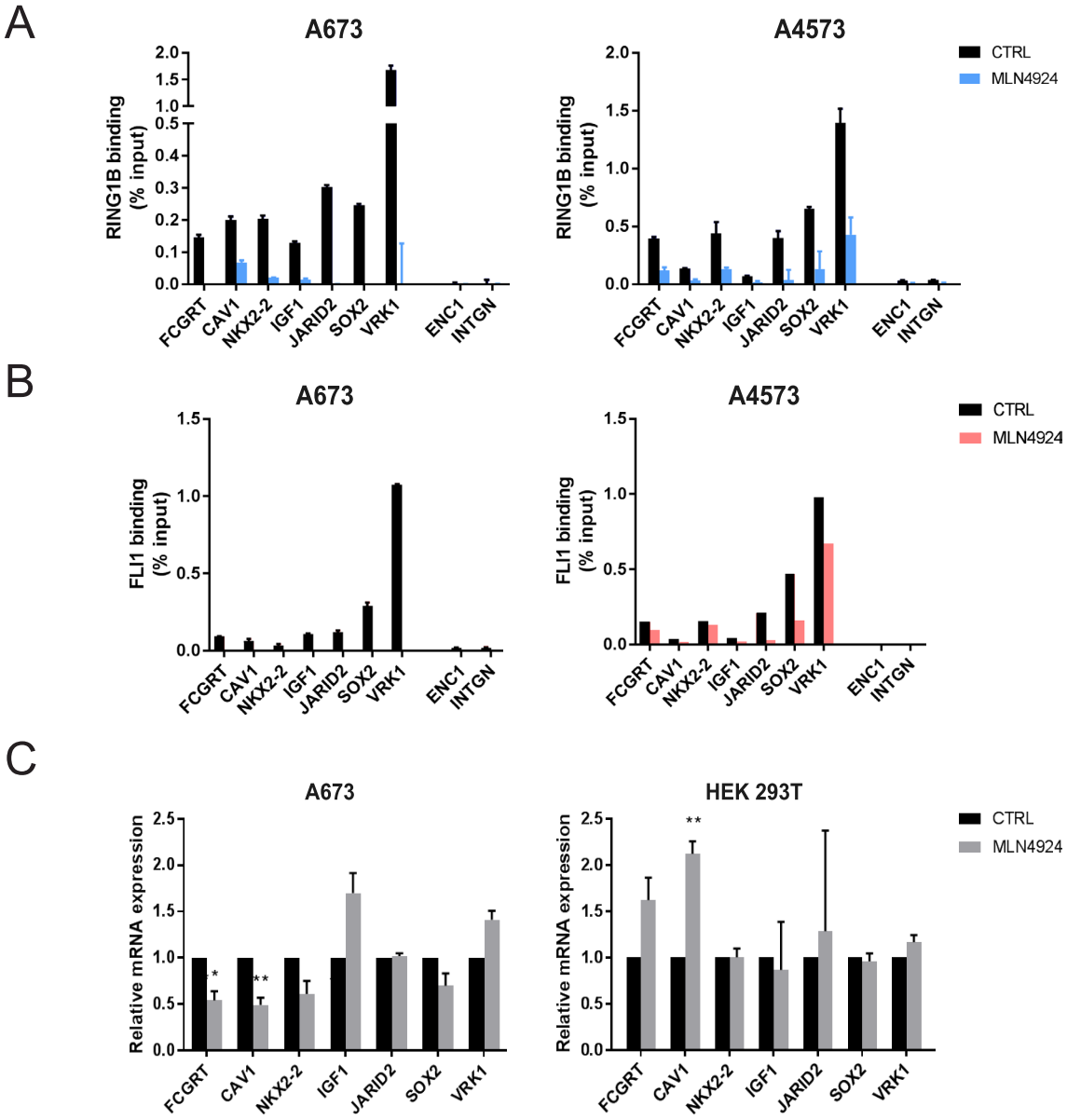

FIGURE IV. 8 ***MLN4924 causes a loss of RING1B from EWSR1-FLI1–activated targets coinciding with an eviction of EWSR1-FLI1.***
A) ChIP-qPCR experiments of RING1B binding in ES cells treated with 50 nM of MLN4924 at 72 hours. Data were calculated with the percent input method, and IgG was subtracted from immunoprecipitated samples. ***B)*** The same experiments as shown in ***A)*** but analysing EWSR1-FLI1 binding in ES cells. The FLI1 antibody was used to immunoprecipitate the fusion oncoprotein. ***C)*** Analysis of EWSR1-FLI1–activated targets by RT-qPCR upon MLN4924 treatment in A673 cells and a control HEK 293T cell line. All data represent mean ± SEM from minimum of three biological replicates. *P < 0.05.

In sum, our results demonstrate that MLN4924 recapitulates the effects of RING1B knockdown in ES cells, including RING1B loss together with an eviction of EWSR1-FLI1 from its activated target regions that correlates with transcriptional consequences.

2.6 RING1B protein levels are downregulated in vivo

To further extend our knowledge of RING1B regulation by MLN4924 *in vivo*, we studied RING1B protein levels in ES xenografts and a PdX treated in monotherapy with this drug. RDES and RM82 ES xenograft samples were kindly provided by Dr. Enrique de Álava and were published in Mackintosh et al. (2012). ES PdX samples from our institution were provided by Dr. Ángel Montero and Dr. Enrique de Álava (manuscript in preparation). Detailed information regarding these experiments is shown in **Figure IV. 9A**. These studies revealed that ES xenografts were sensitive to MLN4924, as assessed by the tumour volume at the end point compared to control. In contrast, monotherapy treatment was not efficacious for a concrete ES PdX, which showed no response to the inhibitor (**Figure IV. 9B**). Evaluation of RING1B protein levels in these samples by Western blot showed a decrease in RM-82 ES xenografts at the highest dose of MLN4924 tested (i.e. 90 mg/kg), corroborating our *in vitro* observations that MLN4924 reduced levels of this protein. In contrast, in ES PdX, this was visibly at a lower dose (60 mg/kg). Nevertheless, decreased RING1B levels were not associated with MLN4924 response, indicating the solely inhibition of RING1B was not critical for tumour survival of this PdX in particular.

A

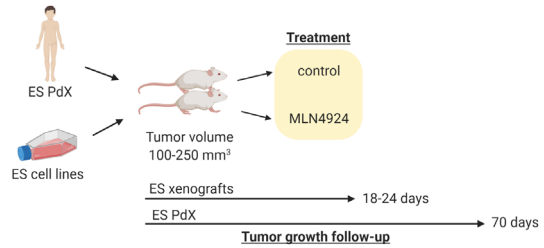

B

Model	Treatment	Mice (n)	Response			
			0	30	60	90
RDES xenograft	Control	9	NR	-	-	-
	MLN4924	9	-	R	R	-
RM82 xenograft	Control	8	NR	-	-	-
	MLN4924	8	-	R	R	R
ES PdX	Control	6	NR	-	-	-
	MLN4924	4	-	-	NR	-

C

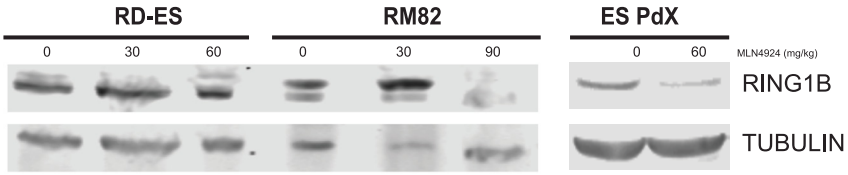

FIGURE IV. 9 ***MLN4924 decreases RING1B levels in vivo in ES xenografts and PdX.***
A) Schematic representation of two *in vivo* studies evaluating tumour response to MLN4924 performed by Dr Enrique de Álava group (published in Mackintosh et al. (2012)) and Dr Angel Montero (article in preparation). Treatment started in both experiments when tumours reached 100–250 mm^3. For ES xenografts, mice were sacrificed when tumours in control group reached 1500 mm^3, which for RDES was at day 16 and for RM82 was at day 21. For ES PdX, mice were treated until day 21, and tumour growth follow-up was performed until the end of the study when tumours measured 2000 mm^3. (Created with Biorender.com) ***B)*** Table showing number of tumours in each group and the MLN4924 response assessed as the tumour volume at the endpoint as compared to control. The ES PdX was evaluated at day 21 at the end of treatment. Three doses of MLN4924 were used for ES xenografts (30, 60 and 90 mg/kg), and one dose of 60 mg/kg was used for ES PdX studies. R indicates regression and NR, non-regression. ***C)*** Western blot of RING1B protein levels at the endpoint in ES xenografts and a PdX. Tubulin was used as loading control.

In conclusion, our data indicate that a NEDD8 inhibitor, such as MLN4924, causes downregulation of the E3 ubiquitin ligase RING1B especially at the protein level, *in vitro* and *in vivo*. Moreover, we show the inhibitor alters the capacity of RING1B to recruit EWSR1-FLI1 to the *de novo* enhancers produced by the fusion oncoprotein. We demonstrated that RING1B knockdown shares many altered pathways with cells treated with MLN4924, explaining the higher sensitivity of RING1B knockdown cells to the inhibitor. Overall, we provide further rationale for RING1B inhibition as a novel target in ES.

3. CHARACTERIZATION OF H3K27me3 AND ITS ENZYMATIC ACTIVITIES IN ES

3.1 H3K27me3 is redistributed in ES

GGAA repeats are DNA sequence motifs implicated in ES due to their overrepresentation as directly bound elements of EWSR1-FLI1 (Gangwal et al., 2008; Guillon et al., 2009). Further experimental evidence identified these elements as sites at where the oncogene operates as a pioneer factor to mediate the transition from closed to open chromatin and to establish an active enhancer state (Riggi et al., 2014). Importantly, no overlap between EWSR1-FLI1–bound GGAA repeats and the PcG-mediated repressive mark H3K27me3 has been reported in either ES cell lines or primary tumours (Riggi et al., 2014; Tomazou et al., 2015). However, data published by other groups demonstrated that in ectopic models overexpressing the fusion protein, this mark is lost from PcG repressed loci, such as *HOXD* (Svoboda et al., 2014). Furthermore, chromatin studies have revealed that the GGAA repeats to which EWSR1-FLI1 is recruited in ES are extensively decorated with H3K27me3 in HUVECs and hpMSCs (Boulay et al., 2018; Patel et al., 2012). Given the relevance of PcG in cell lineage differentiation, and our recent findings about the contributions of RING1B in ES, we decided to further study the H3K27me3 histone modification at a global and gene-specific level during ES tumorigenesis.

3.1.1 Global levels of H3K27me3 are maintained in EWSR1-FLI1–transformed cells

As H3K27me3 has been reported to be absent from EWSR1-FLI1 target regions (Riggi et al., 2014; Tomazou et al., 2015), we next asked whether H3K27me3 was globally lost upon overexpression of EWSR1-FLI1. For this, we used an easy-to-use embryonic cell context, such as HEK 293T cells, to introduce EWSR1-FLI1–pEGFPN1 by conventional transfection techniques. First, we confirmed the expression of EWSR1-FLI1 at the protein (**Figure IV. 10A**) and mRNA (**Figure IV. 10B**) levels in two biological replicates of the transfected cells. We next analysed by Western blot the H3K27me3 and H3K27ac levels in histone extracts of control and EWSR1-FLI1–transfected cells, as global levels of the active enhancer-related histone modification H3K27ac were published as the most altered

histone mark in EWSR1-FLI1–knockdown models (Tomazou et al., 2015). Surprisingly, similar to H3K27ac levels, H3K27me3 levels remained unaltered despite the strong induction of the oncogene (**Figure IV. 10C**). Furthermore, immunofluorescence staining of H3K27me3 revealed a diffused distribution pattern across the nuclei for EWSR1-FLI1-GFP transfected cells in contrast with the focal pattern displayed in cells negative for the GFP-tagged fusion protein (**Figure IV. 10D**).

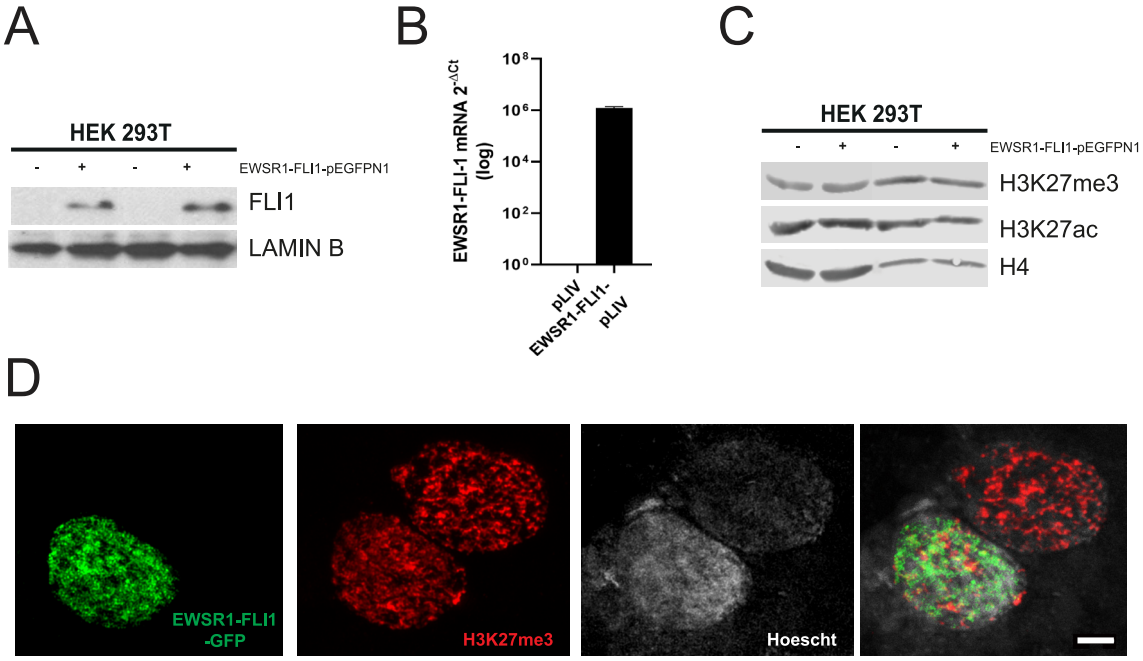

FIGURE IV. 10 ***Overall levels of H3K27me3 are maintained in HEK 293T cells overexpressing EWSR1-FLI1.***

A) Western blot confirming overexpression of EWSR1-FLI1 in two biological replicates of transfection of the oncoprotein in HEK 293T cells. The FLI1 antibody was used to detect EWSR1-FLI1 and Lamin B was used as loading control. ***B)*** RT-qPCR analysis of mRNA levels of EWSR1-FLI1 upon overexpression of EWSR1-FLI1-pEGFPN1 in HEK 293T cells. mRNA expression level was calculated with ΔΔCT method and normalized to *GAPDH*. Data represent the mean ± SEM and presented in a logarithmic scale. ***C)*** Western blot showing levels of H3K27me3 and H3K27ac in histone extracts from HEK 293T overexpressing control and EWSR1-FLI1-pEGFPN1. Histone H4 was used as loading control. ***D)*** Confocal microscope images showing H3K27me3 and EWSR1-FLI1-GFP in HEK 293T cells transfected with EWSR1-FLI1-pEGFPN1. EWSR1-FLI1-GFP was detected in green channel, H3K27me3 was detected in red channel and nuclei were stained with Hoechst and detected in blue channel. Images were processed in Image J to generate an image composite of all channels. Scale bar represents 3 μm.

In order to elucidate to what extent H3K27me3 levels remained invariable upon introduction of EWSR1-FLI1, we performed the same analysis in a cellular background closer to the postulated mesenchymal cell-of-origin of ES (Castillero-Trejo et al., 2005; Riggi et al., 2005; Riggi et al., 2008; Tirode et al., 2007). For this, we overexpressed EWSR1-FLI1 in hpMSCs, currently considered a model that recapitulates the early steps of ES tumorigenesis (Boulay et al., 2017; Riggi et al., 2010). Additionally, given the high similarity of gene expression data reported for human umbilical vein endothelial cells (HUVEC) and ES cell lines (Staege et al., 2004), we included HUVEC cells in our studies.

Overexpression of EWSR1-FLI1-pLIV in HUVEC and hpMSC models by lentiviral transduction and further selection of EWSR1-FLI1 positive cells led to no phenotypical differences as compared to controls in HUVEC. However, the hpMSC model shown more elongated features (see Materials and Methods). We then collected the cells right after the selection step to analyse the immediate changes promoted by EWSR1-FLI1 in these cellular contexts. First, we validated EWSR1-FLI1 expression at both protein and mRNA levels and confirmed a strong induction in the two cellular models (**Figure IV. 11A** and **IV.11 B**, respectively). Analysis of histone marks by Western blot reproduced our previous results in HEK 293T cells for both HUVEC and hpMSC, indicating that introduction of EWSR1-FLI1 does not alter overall levels of either H3K27me3 or H3K27ac at the protein level (**Figure IV. 11C**).

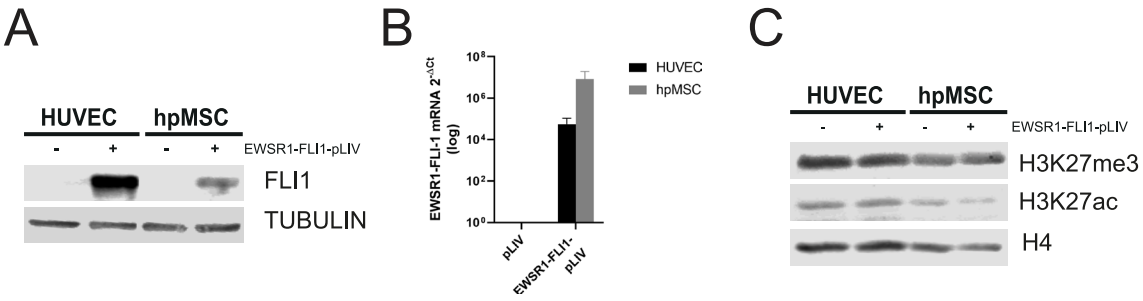

FIGURE IV. 11 ***Overall levels of H3K27me3 are maintained in HUVEC and hpMSC overexpressing EWSR1-FLI1.***
A) Western blot confirming overexpression of EWSR1-FLI1 in HUVEC and hpMSC infected with control and EWSR1-FLI1-pLIV. The FLI1 antibody was used to detect EWSR1-FLI1, and tubulin was used as loading control. Data from representative experiments are shown. ***B)*** RT-qPCR analysis of mRNA levels of EWSR1-FLI1 upon overexpression of EWSR1-FLI1-pLIV in HUVEC and hpMSC. mRNA expression levels were calculated with the ΔΔCT method and normalized to *GAPDH*. Data represent the mean ± SEM and are shown in a logarithmic scale. ***C)*** Western blot showing levels of H3K27me3 and H3K27ac in histone extracts from HUVEC and hpMSC infected with control and EWSR1-FLI1-pLIV. Histone H4 was used as loading control. Data from representative experiments are shown.

Altogether, our data demonstrate that in ectopic models of the fusion protein, global levels of H3K27me3 remain unchanged. Hence, given the loss reported for H3K27me3 at EWSR1-FLI1 binding sites, our results suggest that histone marks are redistributed during ES tumorigenesis.

3.1.2 EWSR1-FLI1 targets H3K27me3-repressed regions

Several groups have described a *bona fide* list of GGAA repeats directly bound by EWSR1-FLI1 to activate transcription (Bilke et al., 2013; Gangwal et al., 2008; Riggi et al., 2014). These regions have been reported to be highly enriched in H3K27me3 in embryonic cells and HUVEC (Patel et al., 2012), in contrast with the absence of this histone mark found in ES cell lines (Riggi et al., 2014; Tomazou et al., 2015). Consistently, we studied whether this mark was present in the GGAA repeats of EWSR1-FLI1-bound promoters by ChIP-

qPCR in hpMSC and HUVEC as compared with the ES cell line A673. Additionally, we checked for H3K4me3, which defines active promoters. Analysis of these regions interestingly revealed that H3K27me3 was especially enriched in HUVEC and hpMSC. In contrast, in A673 cells, these promoters were devoid of this mark and, coinciding with their transcriptional active state, they were strongly enriched for H3K4me3 (**Figure IV. 12A**). This is in agreement with previous observations indicating that H3K4me3 mainly associates with EWSR1-FLI1–bound regions in promoters (Riggi et al., 2014; Tomazou et al., 2015). In contrast, the same regions in HUVEC or hpMSC models lacked H3K4me3.

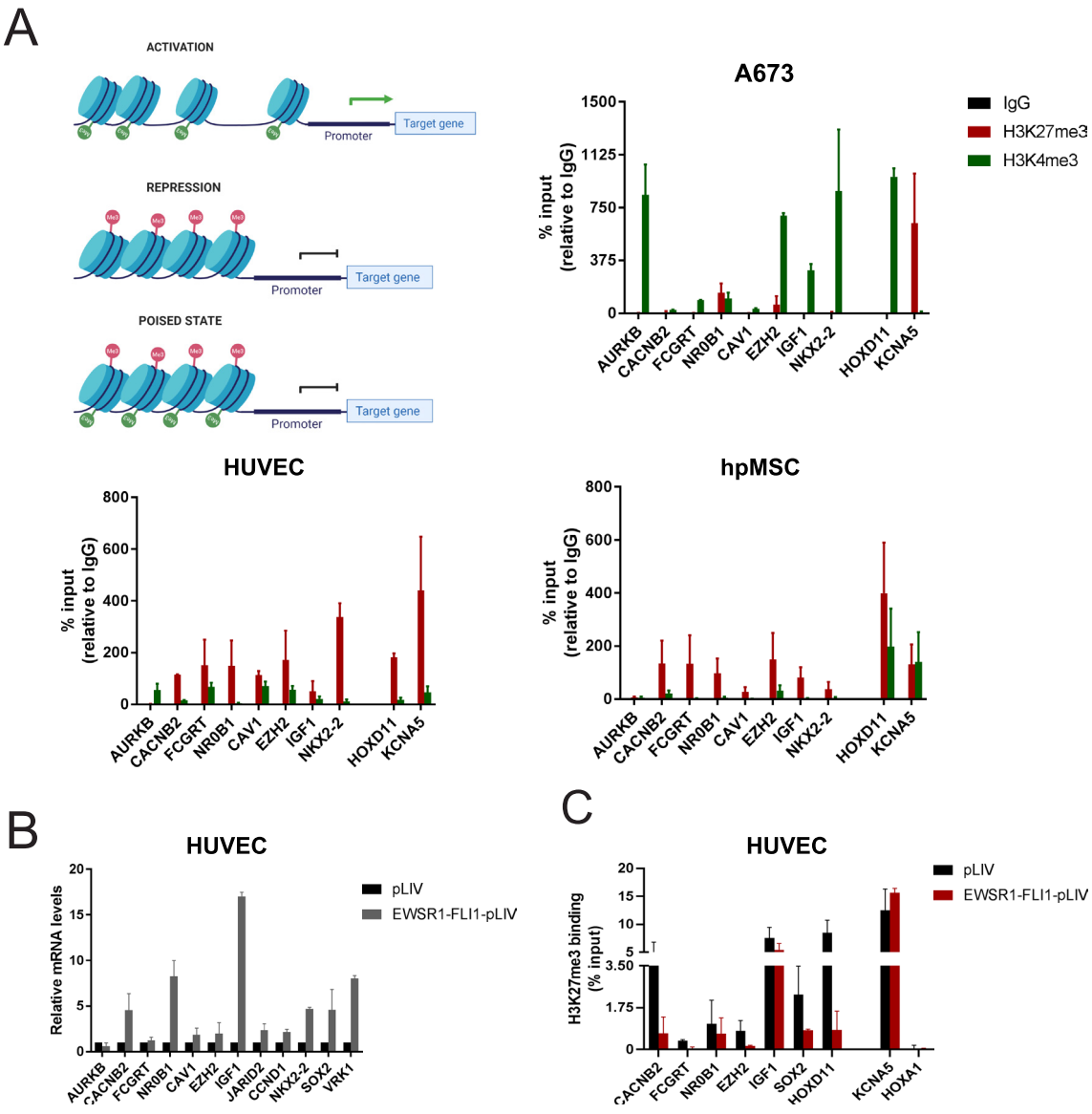

Figure IV. 12 ***EWSR1-FLI1-activated targets are highly enriched in H3K27me3 in HUVEC and hpMSC and lose this mark upon introduction of the oncogene.***
A) ChIP-qPCR experiments showing H3K27me3 and H3K4me3 enrichment in promoters of EWSR1-FLI1–activated targets in A673, HUVEC and hpMSC. Data shown were calculated with percent input method and normalized to IgG. *HOXD11* and *KCNA5* are control positive regions for H3K4me3 and H3K27me3, respectively, in A673 cells. A schematic representation of H3K4me3 (green) and H3K27me3 (red) in the promoter regions of chromatin during transcription is also shown. ***B)*** RT-qPCR analysis of mRNA levels

of EWSR1-FLI1-activated targets upon overexpression of EWSR1-FLI1-pLIV in HUVEC cells. Data were calculated with ΔΔCT method and normalized to *TBP*. Data from EWSR1-FLI1 experimental condition were calculated relative to the control condition (empty pLIV). All data represent mean ± SEM from a minimum of three biological replicates. ***C)*** ChIP-qPCR experiments showing enrichment of H3K27me3 in control and EWSR1-FLI1-pLIV HUVEC cells. Data represented were calculated with percent input method. IgG value was subtracted to immunoprecipitated samples. *KCNA5* was used as a control region positive for H3K27me3 and *HOXA1* was used as a negative region. All data represent the mean ± SEM from a minimum of three biological replicates.

HOXD11 and the potassium voltage-gated channel subfamily A member 5 (*KCNA5)* were used as control regions. *HOXD11* is overexpressed in ES and, following ectopic expression of the fusion oncoprotein in NCSC, loss H3K27me3 from its promoter (Svoboda et al., 2014). Hence, we used this region as a negative control for H3K27me3 in A673. As *KCNA5* is highly repressed in ES (Ryland et al., 2016; Ryland et al., 2015), we used it as a positive region for H3K27me3 enrichment in ES. Altogether, our results demonstrate that EWSR1-FLI1–activated targets display a very different pattern for H3K27me3 in non-transformed cellular contexts as compared to A673.

In an attempt to elucidate whether H3K27me3 is lost from the specific set of promoters activated during ES tumorigenesis, we analysed this mark in HUVEC overexpressing EWSR1-FLI1. First, we checked the induction of various EWSR1-FLI1–activated targets upon the introduction of the oncogene by RT-qPCR (**Figure IV. 12B**). We obtained a prominent overexpression especially for *IGF1, CACNB2, SOX2, NR0B1, VRK1*, and *NKX2-2*. As these regions were initially marked with H3K27me3, we investigated by ChIP-qPCR if such an increase in gene expression was associated with a loss of H3K27me3 at the promoter level. In agreement with the expression data, we found that activation of EWSR1-FLI1 target genes was accompanied with a loss of H3K27me3 from their promoter region, especially for *CACNB2* and *SOX2*, similarly to the control gene *HOXD11* (**Figure IV. 12C**). *KCNA5* was used as a positive control for H3K27me3 and *Homeobox A1 (HOXA1)* was included as a negative region for H3K27me3.

Overall, non-transduced cell models display abundant H3K27me3 in EWSR1-FLI1–activated genes as compared to transformed cellular contexts such as A673. We have demonstrated that introduction of EWSR1-FLI1 in HUVEC causes a necessary loss of this mark from promoters, which allows for gene activation by EWSR1-FLI1.

3.1.3 H3K27me3 is lost specifically in EWSR1-FLI1–activated promoters

The unchanged global levels of H3K27me3, together with the local loss observed in some EWSR1-FLI1–activated promoters following ectopic expression of EWSR1-FLI1, suggests a genome-wide redistribution of the H3K27me3 histone mark. When we checked the expression of EWSR1-FLI1–activated targets upon ectopic expression of the oncogene in hpMSC overexpressing the fusion oncogene, we found even stronger gene activation from

a dozen- to hundred-fold inductions as compared to the HUVEC model (**Figure IV. 13A**). This strong induction is in agreement with data from Riggi et al. (2010). To elucidate which regions gain and loss H3K27me3 at a genome-wide scale during the early steps of EWSR1-FLI1 oncogenic transformation, we performed ChIP-seq of H3K27me3 in hpMSC. We sequenced two biological replicates (R1 and R2) of H3K27me3 ChIP samples from empty pLIV (ctrl) and EWSR1-FLI1-pLIV (EF) hpMSC, yielding an average of 33 million uniquely mapped reads per sample (**Figure IV. 13B**). These reads corresponded to 5194 and 629 peaks associated to 2469 and 429 genes in control and EF hpMSC cells R1 replicates, respectively. According to the repressive role of H3K27me3 classically exerted in the promoter region of genes, analysis of the genomic distribution revealed that the majority of peaks were mainly found in promoters in both experimental conditions (**Figure IV. 13C**). Notably, we observed a slight decrease in the percentage of promoter peaks of H3K27me3 upon EWSR1-FLI1 introduction in hpMSC (from 46.3% to 42% in R1, and from 47.8% to 41.3% in R2), which was associated to a gain of this mark in the genic and intergenic regions. These data further support our previous results, indicating a redistribution process of this mark. We subsequently validated our ChIP-seq by visually

A

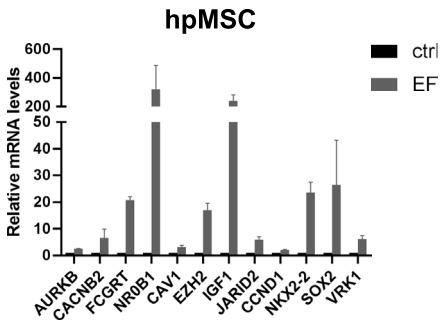

C

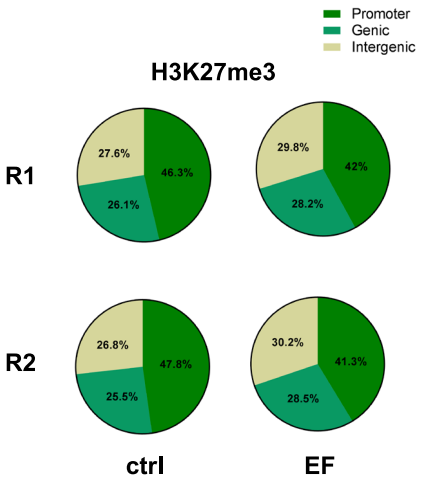

B

	INPUT		H3K27me3			
	ctrl	EF	ctrl		EF	
			R1	R2	R1	R2
Barcode	ATCACG	CAGATC	ACAGTG	TTAGGC	GGCTAC	TAGCTT
Mapped reads	35.779.419	36.381.527	32.900.115	31.481.061	31.181.637	30.635.927
Peaks	-	-	5194	4704	629	442
Genes	-	-	2469	2235	429	311

D

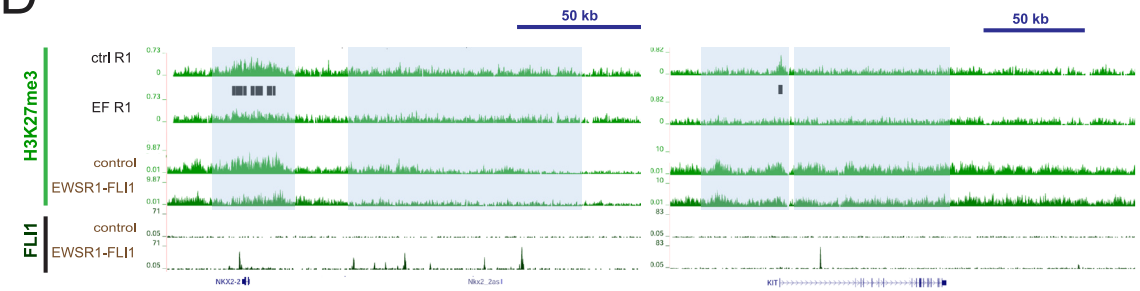

Figure IV. 13 ***Ectopic expression of EWSR1-FLI1 alters the genomic distribution of H3K27me3 in hpMSC, showing a loss at the promoter and enhancer regions of oncogene-activated targets.***
A) RT-qPCR analysis showing mRNA levels of EWSR1-FLI1–activated targets upon overexpression of

EWSR1-FLI1-pLIV in hpMSC cells. Data were calculated with the ΔΔCT method and normalized to *TBP*. Data from EWSR1-FLI1 experimental condition were calculated relative to the control condition. All data represent mean ± SEM from a minimum of three biological replicates. ***B)*** Table providing information of H3K27me3 ChIP-seq from hpMSC cells infected with empty pLIV and EWSR1-FLI1-pLIV. The barcode used and number of mapped reads including number of associated peaks and genes sequenced is shown. Input information is also shown. ***C)*** Pie chart showing the genomic distribution of H3K27me3 ChIP-seq peaks (in promoters, genic or intergenic regions) in control and EWSR1-FLI1-hpMSC samples. ***D)*** Genome browser visualization of H3K27me3 enrichment in EWSR1-FLI1-activated targets, exemplified in *NKX2-2* and *KIT* in control hpMSC and EWSR1-FLI1-hpMSC samples. Peak distribution is represented as black bars under each track. Publicly available ChIP-seq tracks of FLI1 and H3K27me3 in control and EWSR1-FLI1-hpMSC from Boulay et al. (2018), were also included in these studies, which are indicated in brown names. Peak distribution is represented as black bars under each track. Grey boxes frame the promoter and enhancer areas with H3K27me3 loss following EWSR1-FLI1 introduction in hpMSC. Ctrl indicates hpMSC infected with empty pLIV, and EF indicates hpMSC infected with EWSR1-FLI1-pLIV. The blue bar shows the genomic scale, which represents kilobases of DNA base pairs. R1 and R2 indicate the sample replicates used.

inspecting some well-known developmentally repressed PcG targets. Analyses of these regions indicated high enrichment of H3K27me3 in both control and EWSR1-FLI1 sample replicates (data not shown), despite the difference of the total number of peaks between the two experimental conditions. Next, we studied the presence of H3K27me3 in enhancers associated with EWSR1-FLI1 that are known to lose H3K27me3 when EWSR1-FLI1 is introduced into stem cell models. We used the more enriched H3K27me3 ChIP-seq samples (R1 replicates) for further analysis. We validated in our data that, following EWSR1-FLI1 introduction into hpMSC, H3K27me3 was lost from the promoter as well as from enhancer regions bound by the oncogene (**Figure IV. 13D**). For instance, analysis of the *NKX2-2* promoter and its related enhancer, which is positioned approximately 40 kb upstream the TSS, showed a loss of H3K27me3 coinciding with EWSR1-FLI1 peaks, which agrees with published data (**Figure IV. 13D**, left). Such alterations were also visible in intronic enhancers, for instance in the KIT proto-oncogene, receptor tyrosine kinase (*KIT*) gene (**Figure IV. 13E**, right). As Boulay et al. (2018) recently analysed H3K27me3 by ChIP-seq with a different antibody than the one we used here, we also included H3K27me3 as well as the FLI1 ChIP-seq tracks (GSM2857578, GSM2857579, GSM2857585, GSM2857586) in our analysis.

To further characterize H3K27me3 positioning after EWSR1-FLI1 introduction, we first intersected the gene-associated peaks of both control replicates and found 1,806 common regions (**Figure IV. 14A**). We next examined the H3K27me3 distribution by setting a 5-kb window upstream and downstream of the TSS in these common gene-associated peaks. Our data revealed that control cells displayed more H3K27me3 around 1.5 kb of the TSS, whereas cells overexpressing EWSR1-FLI1 mainly lost this mark from these regions (**Figure IV. 14B**). These results confirm genome-wide the prominent loss we previously described in the promoter regions bound by EWSR1-FLI1. Among the group of genes that lost H3K27me3 were some EWSR1-FLI1-activated targets, such as the FEZ family zinc finger 1 gene *(FEZF1)* and *HOXD11* (**Figure IV. 14C**).

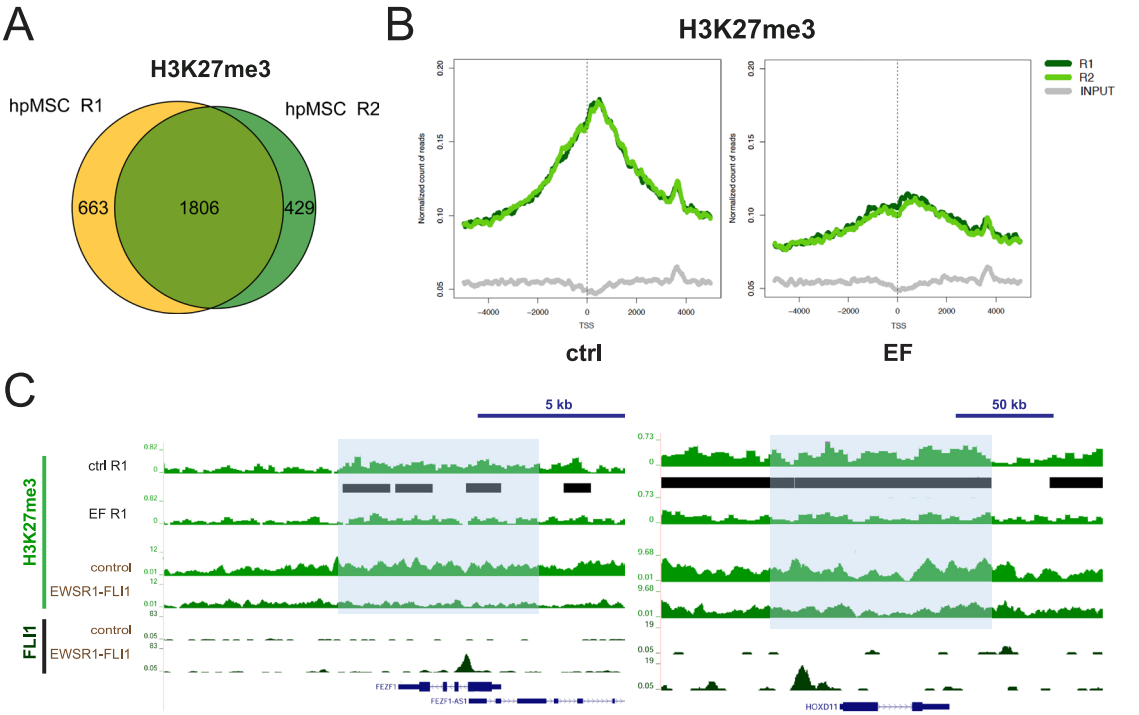

FIGURE IV. 14 ***H3K27me3 is lost from promoters in hpMSC overexpressing the fusion oncogene and correlates with EWSR1-FLI1–activated targets.***
A) Venn diagram of H3K27me3 gene-associated peaks in control R1 and R2 hpMSC ChIP-seq replicates, showing an overlap of 1806 peaks. ***B)*** Metagene plot showing the genomic distribution of H3K27me3 in the subset of 1806 genes shown in ***A)*** in empty pLIV (ctrl) EWSR1-FLI1-pLIV (EF) hpMSC. H3K27me3 peaks are represented in 5 kb upstream and downstream of the TSS. R1 and R2 indicate the sample replicates used. ***C)*** Genome browser visualization of H3K27me3 enrichment in EWSR1-FLI1-activated targets, exemplified in *FEZF1* and *HOXD11* in empty pLIV (ctrl) EWSR1-FLI1-pLIV (EF) hpMSC. Publicly available ChIP-seq tracks of FLI1 and H3K27me3 in control and EWSR1-FLI1-hpMSC from Boulay et al. (2018) were also included in these studies, which are indicated in brown names. Peak distribution is represented as black bars under each track. Grey boxes frame the areas with H3K27me3 loss following EWSR1-FLI1 introduction in hpMSC. The blue bar shows the genomic scale, which represents kilobases of DNA base pairs. R1 and R2 indicate sample replicates used.

In summary, our study unveils a great loss of H3K27me3 in the promoters of a set of genes marked by this histone mark prior to the introduction of EWSR1-FLI1, with most of these genes corresponding to EWSR1-FLI1–activated targets.

3.1.4 The gene body of EWSR1-FLI1–repressed targets gains H3K27me3

We next analysed the genomic distribution of H3K27me3 focusing on the gains of this mark, which, together with the specific losses described previously, could explain the unaltered global levels obtained upon EWSR1-FLI1 introduction in hpMSC. To this end, we plotted the H3K27me3 peaks around 5 kb from the TSS for all genes of the genome in control and EWSR1-FLI1 cells. Global distribution analysis following introduction of the fusion oncoprotein revealed that H3K27me3 was increased genome-wide in regions from 2- to 5-kb downstream of the TSS (**Figure IV. 15A**). Remarkably, among the genes that gained H3K27me3 after introducing EWSR1-FLI1, we found representation of many

EWSR1-FLI1 repressed targets. For instance, a gain of H3K27me3 was clearly observed in the gene body of the transforming growth factor beta induced *(TGFBI)* and *IGFBP3* (**Figure IV. 15B**). Importantly, our analysis of the data on these regions published by Boulay et al. (2018) not only reproduced our observations but showed even stronger gains.

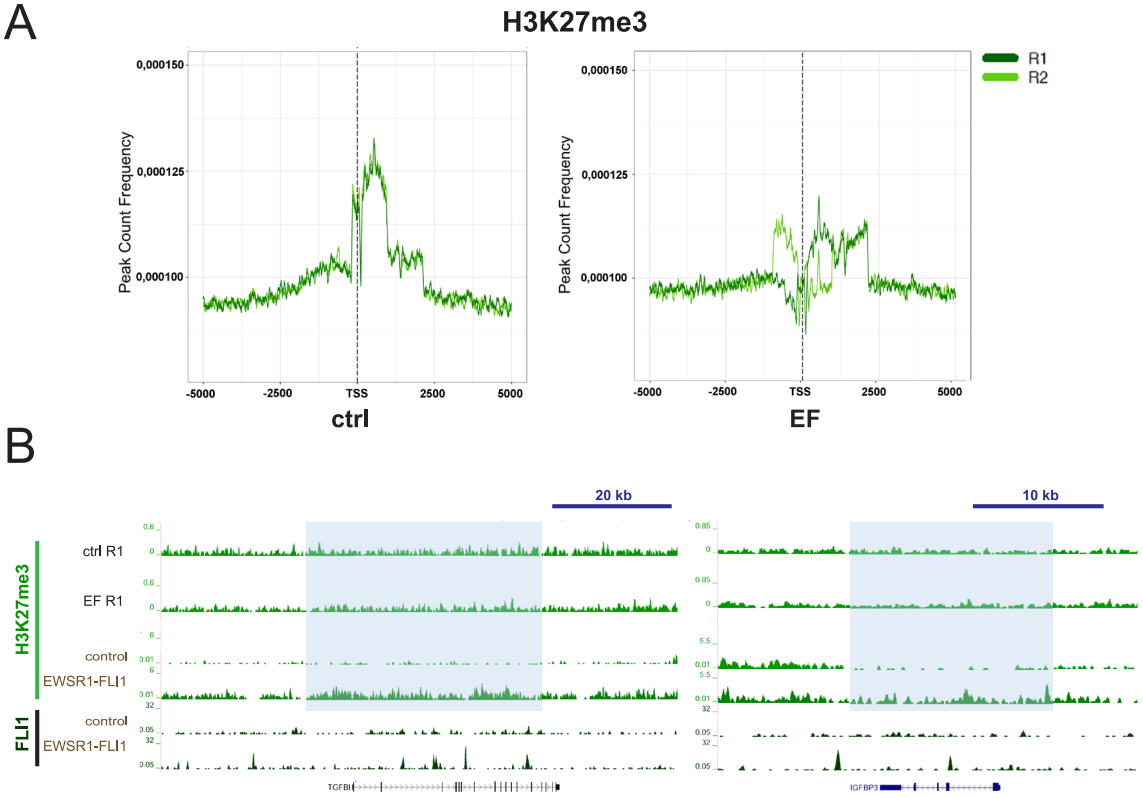

FIGURE IV. 15 ***H3K27me3 is increased at the gene body of EWSR1-FLI1-repressed targets in hpMSC overexpressing the fusion oncogene.***
A) Metagene plot analysis showing the genomic distribution of H3K27me3 in all genes in empty pLIV (ctrl) EWSR1-FLI1-pLIV (EF) hpMSC. H3K27me3 peaks are represented in 5 kb upstream and downstream of the TSS. R1 and R2 indicate the sample replicates used. ***B)*** Genome browser visualization of H3K27me3 enrichment in *IGFBP3* and *TGFBI* (both EWSR1-FLI1-repressed targets), exemplifying the gain of H3K27me3 in the gene body following overexpression of the fusion oncogene in hpMSC. Peak distribution is represented as black bars under each track. Publicly available ChIP-seq tracks of FLI1 and H3K27me3 in control and EWSR1-FLI1-hpMSC from Boulay et al. (2018) were also included in these studies, which are shown in brown names. Grey boxes frame the areas with H3K27me3 gain following EWSR1-FLI1 introduction in hpMSC. The blue bar shows the genomic scale, which represents kilobases of DNA base pairs. R1 and R2 indicates sample replicates used.

To sum up, our study showed a gain of H3K27me3 in the gene body of some genes, including a subset of EWSR1-FLI1–repressed targets. Altogether, we demonstrate that H3K27me3 is redistributed upon overexpression of the oncogene in hpMSC, possibly explaining the unaltered global levels of the histone mark.

3.2 EZH2 and KDM6A drive redistribution of H3K27me3 in ES cells

Due to the loss and gain of H3K27me3 observed upon ectopic expression of EWSR1-FLI1 in hpMSC, we hypothesized that the enzymatic activities of writing and erasing H3K27me3 might also be redistributed and consequently might be relevant for ES transformation. In fact, ES tumours display high levels of the H3K27me3 catalytic subunit EZH2, which is induced upon ectopic overexpression of EWSR1-FLI1 in hpMSC (Riggi et al., 2008; Staege et al., 2004). Also, EWSR1-FLI1 binds the *EZH2* promoter *in vivo* in ES cell lines activating transcription (Richter et al., 2009). Furthermore, EZH2 has been proposed to have a central role in ES pathology, shaping the oncogenity and stem cell phenotype of this tumour by inhibiting endothelial and neuroectodermal differentiation programs and influencing its metastatic potential (Richter et al., 2009). Regarding to the loss of H3K27me3 observed at EWSR1-FLI1-activated targets, enzymes such as demethylases might be involved in the tumorigenic process by helping the oncoprotein erase the repressive mark from promoters that will become active. Removal of methyl groups from K27 in histone H3 is mediated by the KDM6 JmjC-domain histone demethylases, which have not yet been characterized in ES.

3.2.1 KDM6A is highly expressed in ES cell lines and tumours

In order to elucidate whether members of KDM6 demethylase family were behind H3K27me3 loss, we first evaluated by Western blot the expression of KDM6A and KDM6B family members, in a panel of ES cell lines and other developmental tumours. We observed that, as compared to RMS or NB, ES cell lines had higher levels of KDM6A than of KDM6B (**Figure IV. 16A**). Next, we studied the expression of the demethylases in a panel of ES PdX from our laboratory (kindly provided by Dr. Ángel Montero) and found that KDM6A was more abundant as compared to KDM6B, correlating with the results observed in cell lines (**Figure IV. 16B**). To further elucidate if KDM6A was expressed in primary ES tumours, we explored publicly available gene expression data from the Gene Expression Omnibus (GEO2R) of 184 ES tumours at the debut (19 tumour samples from GSE37371, 48 from GSE17679, and 117 from GSE34620). According to *KDM6A* expression, we discriminated two distinct groups of ES patients with a set cut-off of 7.023 log2 on *KDM6A* (high, n=88; low, n=96) and performed a supervised analysis between the two groups (**Figure IV. 16C**). Strikingly, we found that tumours with a lower expression of *KDM6A* were predominantly from male patients (78 vs. 7; 91.76%), whereas those with higher expression of the demethylase were females (58 vs. 22; 72.5%). There was no information with respect to sex in the 19 remaining tumour samples. In this regard, we found a statistically significant association between expression of KDM6A and sex (P-value < 0.0001; Chi-squared test). This might be due to the X-chromosome location of KDM6A, which has been reported to escape X-inactivation, leading to sex-specific

differences (Dunford et al., 2015; Dunford et al., 2017). Moreover, when analysing the differentially expressed genes from the two groups, many X-linked or Y-linked genes were represented (data not shown). Analysis of KDM6A by immunohistochemistry in 18 ES primary tumour specimens from newly diagnosed patients of our institution also revealed two distinct groups with different KDM6A expression pattern, showing a median of positive nuclei of 74.8% (**Figure IV. 16D**).

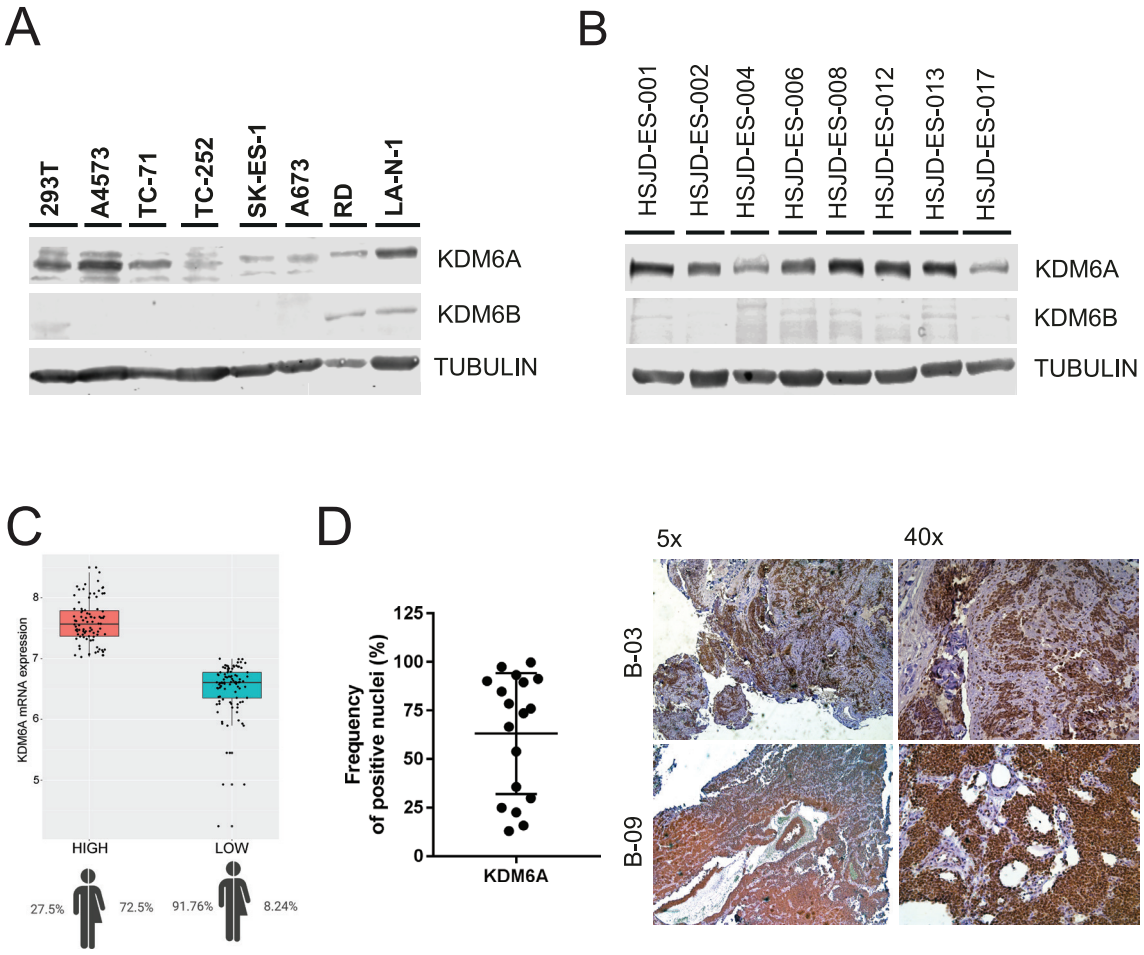

FIGURE IV. 16 ***KDM6A is highly expressed in ES.***
A) Western blot showing KDM6A and KDM6B expression in HEK 293T cells, ES cells (A4573, TC-71, TC-252, SK-ES-1 and A673), a RMS cell line (RD), and a NB cell line (LA-N-1). Tubulin was used as loading control. ***B)*** Western blot showing KDM6A and KDM6B expression in ES PdX generated by our group. Tubulin was used as loading control. ***C)*** Box plot representing KDM6A mRNA levels from 186 ES patients at the debut extracted from GEO2R. Two groups according to high (N=88) or low (N=96) expression of KDM6A are plotted using a cut-off of 7.023, which are statistically associated with sex (*P < 0.05). Sex percentages of each group are shown below the graph. ***D)*** Graph representing the percentage of KDM6A-positive nuclei of the 18 ES tumour samples at the debut (left), and the corresponding immunohistochemistry images from two representative biopsies (B-03 and B-09) (right). Tumour sections were counterstained with H&E and scanned with the Ariol software to analyse the number of positive and negative cells calculated from total nuclei per sample. Images were captured with an optical microscope using 5× and 40××x magnification.

Taken together, RNA expression data and immunohistochemical studies indicate ES cell lines and PdX highly express KDM6A compared to KDM6B. Moreover, we observe a strong correlation between expression of *KDM6A* and sex in ES tumours.

3.2.2 KDM6A and EZH2 have opposite genomic distribution in A673 cells

We analysed the genome-wide positioning of KDM6A and EZH2 enzymes by ChIP-seq in the ES cell line A673. For this purpose, we used two different antibodies against KDM6A (ab1 and ab2), although only one (ab1) displayed evaluable peaks; we obtained a total of 2,455 peaks, corresponding to 1110 genes bound by KDM6A in A673 cells (**Figure IV. 17A**). Genomic distribution of peaks revealed that KDM6A binds with approximately the same frequency to genic and intergenic regions, representing 49.4% and 45.4% of the total peaks, respectively (**Figure IV. 17B**). Of note, only 5.2% of peaks were associated to promoters. Compared to KDM6A, a significant lower number of peaks were obtained for EZH2, with a total of 748 EZH2 peaks associated to 607 genes (**Figure IV. 17C**). Interestingly, a large percentage (66.2%) of EZH2 peaks were condensed in the promoter region, in agreement with the genomic distribution found for H3K27me3. In contrast, only 18.7% and 15.1% of EZH2 peaks were found in the genic and inter genic regions, respectively (**Figure IV. 17D**).

A

	INPUT	KDM6A_ab1	KDM6A_ab2
Barcode	CAGATC	GTTTCG	CCGTCC
Mapped reads	36.595.152	37.553.566	45.249.119
Peaks	-	2455	1
Genes	-	1110	1

B

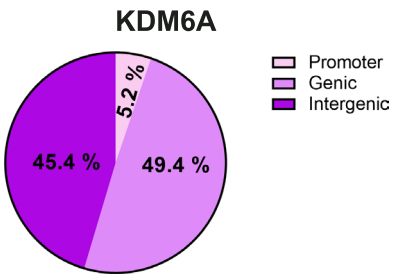

C

	INPUT	EZH2
Barcode	CGATGT	TGACCA
Mapped reads	37.305.618	48.049.939
Peaks	-	748
Genes	-	607

D

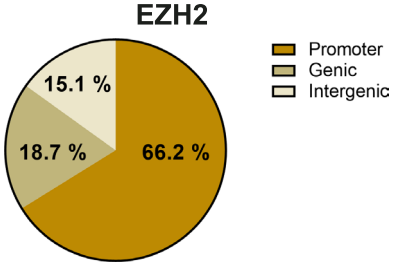

FIGURE IV. 17 ***KDM6A and EZH2 are differently distributed genome-wide in A673 ES cells.***
A) Table showing KDM6A ChIP-seq information in A673 cells related to the barcode used, mapped reads and number of peaks. The number of gene-associated peaks and input information is also shown. ***B)*** Pie chart representing the genomic distribution of the 2455 KDM6A peaks, classifying them into promoter, genic and intergenic peaks. ***C)*** The same information as in ***A)*** but for EZH2 ChIP-seq data in A673 cells. ***D)*** Pie chart representing the same information as in ***B)*** but showing the genomic distribution of the 748 EZH2 peaks.

Altogether, ChIP-seq analysis of KDM6A and EZH2 clearly revealed an opposite genomic distribution of these enzymes, consistent with their distinct roles on H3K27me3. Our results show that while EZH2 is preferentially bound to promoters, KDM6A is more frequently associated to genic and intergenic regions in A673 cells.

3.2.3. KDM6A co-localizes genome-wide with EWSR1-FLI1

In order to understand the functional role of KDM6A in ES, we next investigated if it was recruited to EWSR1-FLI1 target genes. First, we intersected our list of KDM6A gene-associated peaks with a publicly available list of EWSR1-FLI1 gene-associated peaks in A673 cells from Riggi et al. (2014) by ChIP-seq. Notably, we found that 745 of 2469 gene-associated peaks bound by EWSR1-FLI1 (30.17%) were also co-occupied by KDM6A, suggesting a relevant role for this demethylase in ES (**Figure IV. 18A**). Next, we visually inspected some of these co-occupied genes in the Genome Browser. We additionally

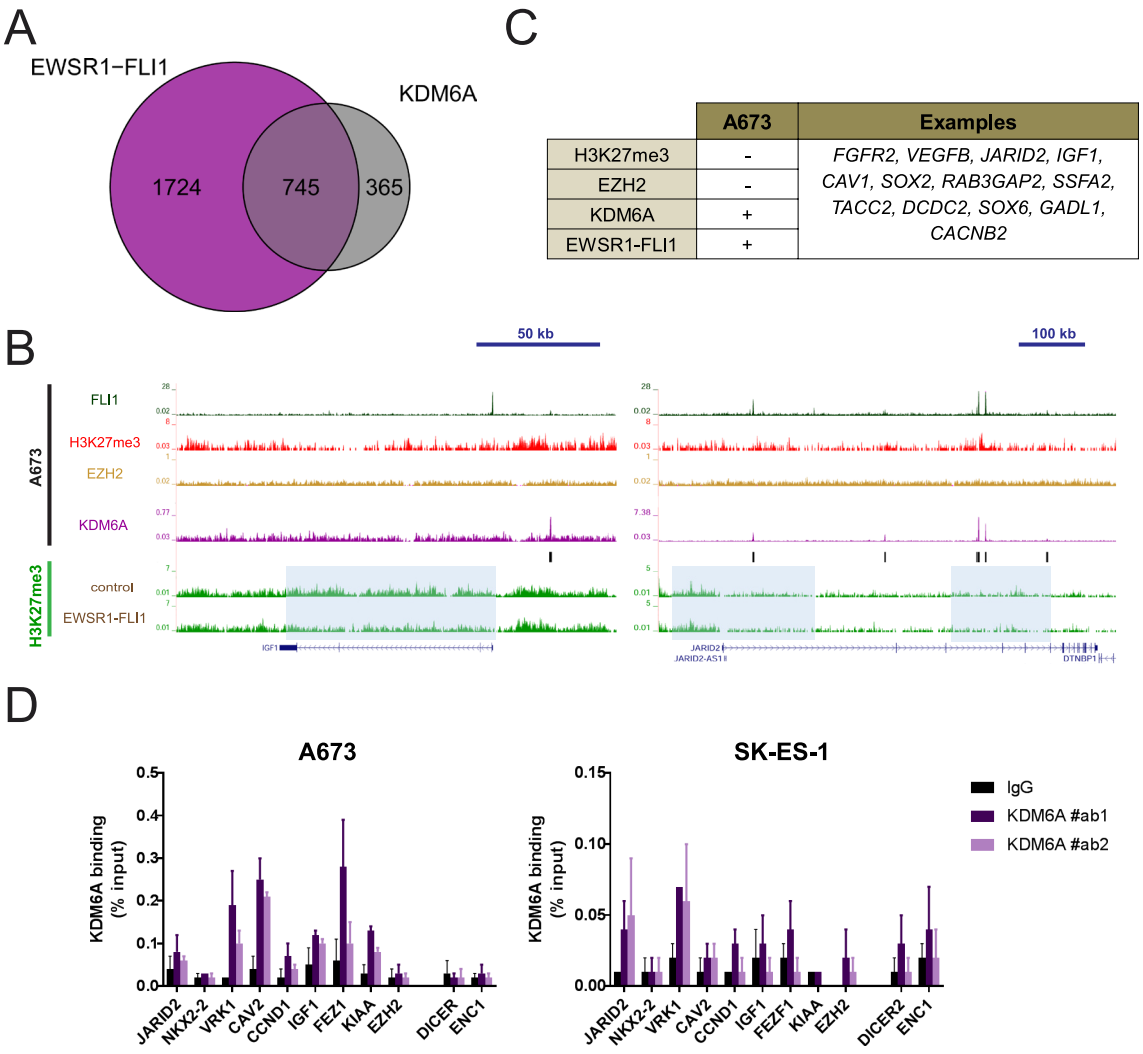

	A673	Examples
H3K27me3	-	*FGFR2, VEGFB, JARID2, IGF1, CAV1, SOX2, RAB3GAP2, SSFA2, TACC2, DCDC2, SOX6, GADL1, CACNB2*
EZH2	-	
KDM6A	+	
EWSR1-FLI1	+	

Figure IV. 18 ***KDM6A peaks colocalize genome-wide with EWSR1-FLI1-activated targets in A673.***
A) Venn diagram of KDM6A and EWSR1-FLI1 ChIP-seq peaks, showing an overlap of 745 common peaks

at gene level in A673 cells. The 2469 EWSR1-FLI1 ChIP-seq peaks in A673 was extracted from Riggi et al. (2014). ***B)*** Genome browser visualization of KDM6A and EZH2 ChIP-seq tracks in two EWSR1-FLI1-activated targets, such as *IGF1* and *JARID2*. Publicly available ChIP-seq tracks of FLI1 and H3K27me3 in A673 from Riggi et al. (2014) were also included. Data from Boulay et al. (2018) H3K27me3 ChIP-seq tracks in hpMSC infected with the oncogene were additionally included and are shown in brown names. Peak distribution is represented as black bars under each track. Grey boxes frame the areas with H3K27me3 loss following EWSR1-FLI1 introduction in hpMSC in data from Boulay et al. (2018). The blue bar shows the genomic scale, which represents kilobases of DNA base pairs. ***C)*** Table showing some of the 745 common genes co-occupied by EWSR1-FLI1 and KDM6A in A673 cells that correlate with a loss of H3K27me3 in hpMSC infected with EWSR1-FLI1. Symbols + and – indicate enrichment or absence of the protein in the ChIP-seq data, respectively. ***D)*** ChIP-qPCR experiments validating enrichment of KDM6A in A673 and SK-ES-1 cell lines using two different antibodies (#ab1 and #ab2). Data represented was calculated with percent input method. *DICER2* and *ENC1* were used as negative regions. All data represent mean ± SEM from a minimum of three biological replicates.

included the tracks from Riggi et al. (2014), corresponding to FLI1 and H3K27me3 in A673 cells (GSM1517562, GSM1517565). We observed that some KDM6A peaks precisely coincided with those for EWSR1-FLI1, for instance in the promoter region of *IGF1* and at the enhancer region of *JARID2* (**Figure IV. 18B**). Notably, EZH2 was not bound to these regions, in agreement with the low levels of enrichment found for H3K27me3 at these EWSR1-FLI1–bound regions. We subsequently introduced the H3K27me3 ChIP-seq tracks from hpMSC overexpressing EWSR1-FLI1 from Boulay et al. (2018) to explore whether the KDM6A-bound regions lost H3K27me3 upon ectopic expression of the fusion protein. We found that KDM6A binding was associated with a loss of H3K27me3 in the hpMSC model overexpressing EWSR1-FLI1, suggesting that H3K27me3 is removed by KDM6A to activate EWSR1-FLI1 targets (summarized in **Figure IV. 18C**). We validated KDM6A binding in EWSR1-FLI1–activated targets with two different antibodies by ChIP-qPCR. Dicer 1, ribonuclease III (*DICER1*) and ectodermal-neural cortex 1 (*ENC1*) were used as negative controls for KDM6A enrichment (**Figure IV. 18D**).

We provide for the first-time evidence that KDM6A co-localizes genome-wide with EWSR1-FLI1. Moreover, we observe that KDM6A binding in the A673 cell line occurs in those genes that lose H3K27me3 in the model of hpMSCs overexpressing EWSR1-FLI1, suggesting that H3K27me3 demethylation by KDM6A might play a role in transcriptional activation during EWSR1-FLI1–induced tumorigenesis.

3.2.4 EZH2 is bound to both direct and indirect EWSR1-FLI1–repressed targets

Given the canonical role of EZH2 as a transcriptional repressor through H3K27me3 deposition, we then asked whether EWSR1-FLI1–mediated repression depended on EZH2 binding. To study this, we first overlapped EZH2 peaks associated to genes with the publicly available data reported by Riggi et al. (2014) on EWSR1-FLI1 gene peaks in the A673 cell line. Only 52 of the 2469 genes bound by EWSR1-FLI1 (2.1%) coincided with EZH2 gene peaks (**Figure IV. 19A**). Indeed, when crossing gene expression data of EWSR1-FLI1–downregulated genes from Smith et al. (2006) with EZH2-repressed

targets from Richter et al. (2009), there was an overlap of 141 common downregulated targets, which accounts for 12% and 20% of the repressed targets, respectively (**Figure IV. 19B**). Collectively, these data suggest that, similar to other indirect repressive elements overexpressed by EWSR1-FLI1, such as *NKX2-2* (Fadul et al., 2015; Owen et al., 2008; Smith et al., 2006), EZH2 mediates part of the repression independently of the fusion oncogene, whereas only a small fraction corresponds to genes repressed concomitantly by EWSR1-FLI1 and EZH2.

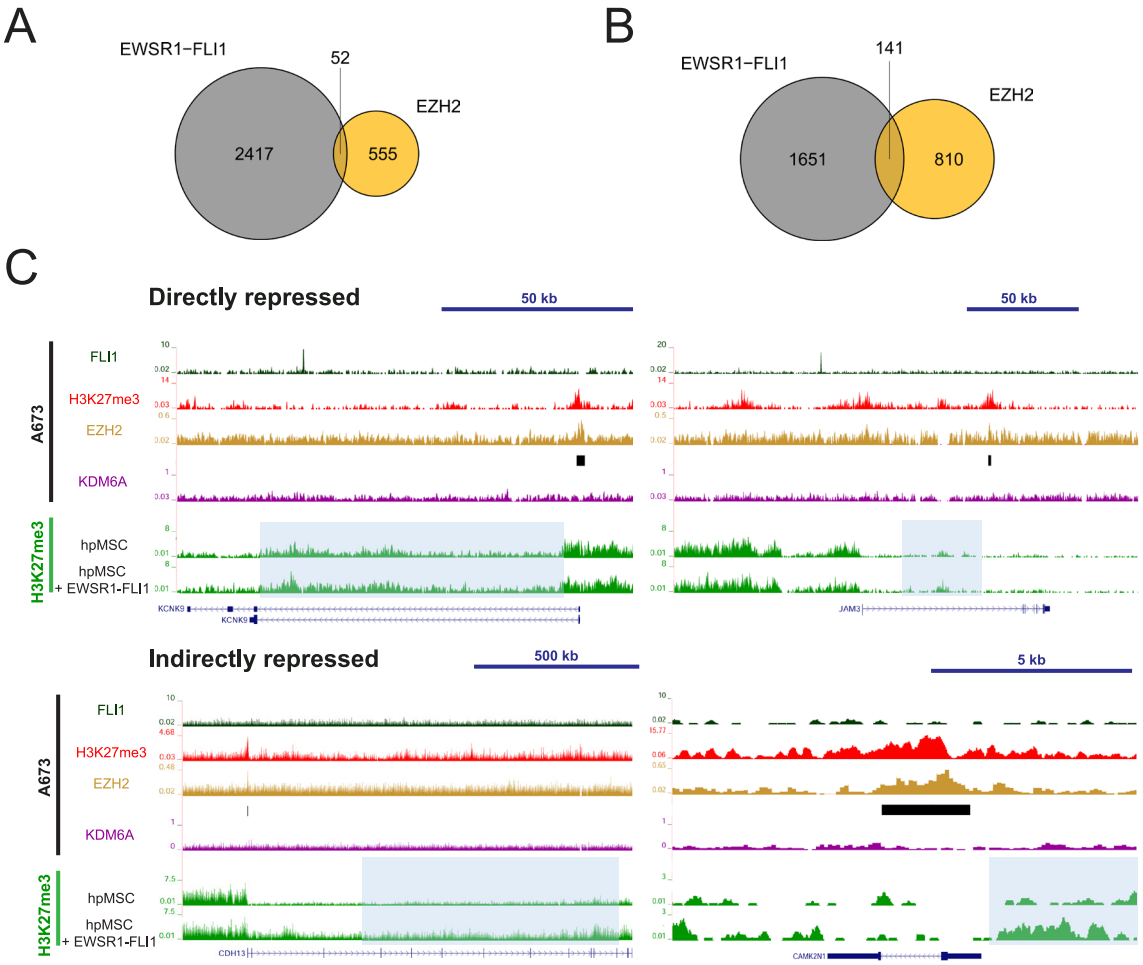

D

		A673	Examples
DIRECTLY REPRESSED	H3K27me3	+	*B4GALT6, HPSE2, JAM3, KCNK9, NRXN1, PTPRN2, SH3RF3, TLE1*
	EZH2	+	
	KDM6A	-	
	EWSR1-FLI1	+	
INDIRECTLY REPRESSED	H3K27me3	+	*CAMK2N1, CDH13, CNIH3, DSP, EGFR, FOXD1, HTRA1, PDGFA, PDLIM3, SIGIRR, TBX2, TPM1*
	EZH2	+	
	KDM6A	-	
	EWSR1-FLI1	-	

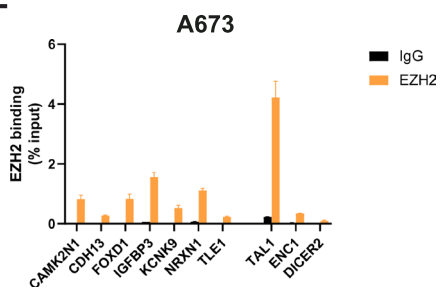

Figure IV. 19 ***EZH2 bounds EWSR1-FLI1-repressed targets in A673 cells.***
A) Venn diagram of ChIP-seq gene-associated peaks of EZH2 and EWSR1-FLI1, showing an overlap of 52 peaks at gene level in A673 cells. Data of 2469 EWSR1-FLI1 ChIP-seq peaks in A673 were extracted from Riggi et al. (2014). ***B)*** Venn diagram representing EWSR1-FLI1 and EZH2-downregulated targets (log FC 0.32 P-value < 0.05) in A673 cells, showing an overlap of 141 commonly repressed genes. Data

from EWSR1-FLI1 downregulated targets in A673 cells were extracted from Smith et al. (2006) and data from EZH2 downregulated targets were from Richter et al. (2009). ***C)*** Genome browser visualization of EZH2 and KDM6A ChIP-seq tracks in directly (up) and indirectly (down) EWSR1-FLI1-repressed targets. *KCNK9* and *JAM3* (up) exemplify these directly bound targets by EWSR1-FLI1, and *CDH13* and *CAMK2N1* (down) those indirectly bound. ChIP-seq tracks publicly available of FLI1 and H3K27me3 in A673 from Riggi et al. (2014) were also included. Data from Boulay et al. (2018) H3K27me3 ChIP-seq tracks in hpMSC infected with the oncogene were additionally included and are indicated in brown names. Peak distribution is represented as black bars under each track. Grey boxes frame the areas with H3K27me3 gain following EWSR1-FLI1 introduction in hpMSC in data from Boulay et al. (2018). The blue bar shows the genomic scale, which represents kilobases of DNA base pairs. ***D)*** Table summarizing the observations shown in ***C)***, showing a list of EZH2 targets repressed directly or indirectly by EWSR1-FLI1 in A673 that gain H3K27me3 in hpMSC following introduction of EWSR1-FLI1. Symbols + and – indicate enrichment or absence of the protein in the ChIP-seq data, respectively. ***E)*** ChIP-qPCR experiments validating enrichment of EZH2 in A673 cells. Data represented was calculated with percent input method. *DICER2* and *ENC1* were used as negative regions and *TAL1* as a known positive region for EZH2. All data represent mean ± SEM from a minimum of three biological replicates.

We subsequently analysed the levels of H3K27me3 in those genes bound by EZH2 that were directly or indirectly bound by EWSR1-FLI1 in A673 cells, as compared to the EWSR1-FLI1–hpMSC overexpressing model. For this, we loaded the publicly available ChIP-seq tracks from Riggi et al. (2014) corresponding to FLI1 and H3K27me3 in A673 cells, as well as the H3K27me3 ChIP-seq tracks from Boulay et al. (2018) in hpMSC overexpressing the fusion oncogene, (as shown in Figure IV. 18B). Analysis of EZH2-repressed regions with EWSR1-FLI1 either directly or indirectly mediating repression revealed that H3K27me3 enrichment in A673 correlated with a gain of this mark in the EWSR1-FLI1–hpMSC model (**Figure IV. 19C**). For instance, potassium two pore domain channel subfamily K member 9 *(KCNK9)* and junctional adhesion molecule 3 (*JAM3*) were EWSR1-FLI1–directly repressed genes with EZH2 bound in A673 cells, which gained H3K27me3 in the gene body in the hpMSC overexpressing EWSR1-FLI1 model. On the other hand, cadherin 13 *(CDH13)* and calcium/calmodulin–dependent protein kinase II Inhibitor 1 *(CAMK2N1)* also gained H3K27me3 in the hpMSC–overexpressing EWSR1-FLI1 model, but with EZH2 bound independently of EWSR1-FLI1, indicating an EWSR1-FLI1–mediated indirect repression through EZH2. In contrast, the opposite enzymatic activity mediated by KDM6A showed no binding in any of those repressed regions. Moreover, in a minority of EZH2 targets, we observed this gain in the promoter rather than in the gene body, such as in *CAMK2N1*. Notably, among the EZH2 targets explored, we found more indirectly repressed genes to be correlated with a gain of H3K27me3 than directly repressed genes, in the hpMSC overexpressing EWSR1-FLI1 model (see summary in **Figure IV. 19D**). We further validated EZH2 enrichment in A673 cells by ChIP-qPCR (**Figure IV. 19E**). TAL BHLH transcription factor 1, erythroid differentiation factor *(TAL1)* was used as a positive control for EZH2 binding and *DICER1* and *ENC1* as negative control regions.

In summary, our data support EWSR1-FLI1 indirectly mediating part of the repression in ES cells through EZH2. Furthermore, we demonstrate that genes with a gain of H3K27me3 along the gene body in the EWSR1-FLI1–hpMSC cells are EZH2 targets in A673 cells,

indicating that EZH2 mediates the redistribution of the histone mark in ES tumorigenesis.

3.3 Modulation of KDM6A and EZH2 reprograms EWSR1-FLI1 targets

3.3.1 Knockdown of KDM6A alters the expression of EWSR1-FLI1 activated target genes

Considering the common genomic distribution of KDM6A and EWSR1-FLI1 in ES target genes, we investigated whether KDM6A might be relevant for EWSR1-FLI1–transactivation activity. To study this, we knocked down the demethylase in ES cell lines. As we were interested in observing the immediate effects produced by the knockdown of KDM6A on gene expression, we used a doxycycline-inducible knockdown model in ES cell lines. A control sequence and two different shRNA sequences targeting KDM6A (named as shRNA#78 and shRNA #99) were used to generate these models. We first optimized the doxycycline concentration that produced a stronger depletion of KDM6A in A673 and SK-ES-1 cells by Western blot upon doxycycline induction with 0.5 and 2 μg/mL at 72 hours (**Figure IV. 20A**). We observed that shRNA#99 was highly efficient in downregulating KDM6A in both ES cell lines, at both the lowest and highest doxycycline concentration tested. However, as shRNA#78 reduced KDM6A protein levels at the highest concentration of doxycycline (and especially in SK-ES-1 cells), we decided to use both shRNA sequences for all experiments. Of note, this high doxycycline concentration did not affect cell viability but altered the expression of many targets (data not shown), as reported by other groups (Ahler et al., 2013). Indeed, as the two shRNA sequences were leaky, especially at the mRNA level (data not shown), we corrected the doxycycline effects by normalizing the shRNA data related to the same doxycycline concentration used in the control sequence.

Because we were interested in determining if KDM6A demethylase activity was relevant enough to alter the expression of EWSR1-FLI1 target genes, we next analysed the expression of these genes upon induction of the shRNA against KDM6A in ES cell lines. Interestingly, RT-qPCR studies indicated strong association between KDM6A knockdown and a downregulation of many EWSR1-FLI1–activated targets that was statistically significant for many of them (**Figure IV. 20B**). *NR0B1* and *IGF1*, for instance, were the most downregulated EWSR1-FLI1 targets in both cell lines upon KDM6A depletion. Moreover, in accordance with protein data, we confirmed *KDM6A* was downregulated in both ES cell lines but had no relevant affect on *KDM6B* expression by RT-qPCR. EWSR1-FLI1 mRNA levels did not change upon KDM6A knockdown in any of the cells tested.

Next, we analysed by Western blot whether the KDM6A demethylating function on H3K27me3 was perturbed upon knockdown of the demethylase. Analysis of the global

levels of H3K27me3 by Western blot revealed that this mark was perturbed with the strongest knockdown (i.e. shRNA#99), showing a slight increase in all cellular models (**Figure IV. 20C**). Thus, these results indicate that only a strong knockdown of KDM6A promotes moderate changes in the global levels of H3K27me3 in ES cells, suggesting compensatory mechanisms (e.g. KDM6B) might be acting.

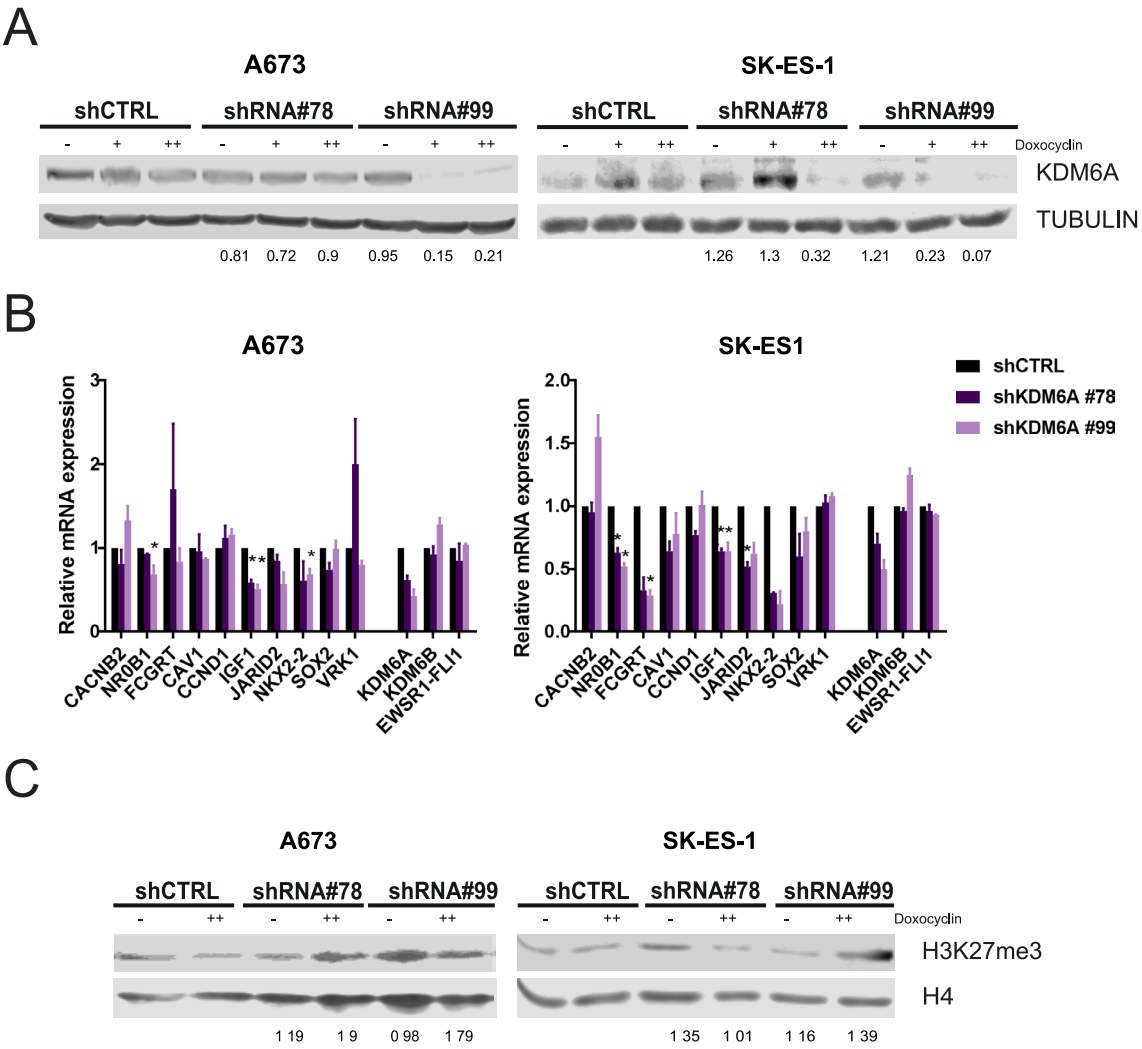

FIGURE IV. 20 ***KDM6A knockdown downregulates EWSR1-FLI1-activated targets in ES cells without altering overall levels of H3K27me3.***

A) Western blot representing KDM6A protein levels upon treatment with 0.5 (+) and 2 (++) μg/mL of doxycycline in A673 and SK-ES-1 ES cells for 72 hours. Tubulin was used as loading control. Numbers below tubulin represent band quantification normalized to tubulin levels and related to shCTRL treated with the same doxycycline concentration. ***B)*** RT-qPCR analysis of mRNA levels of EWSR1-FLI1-activated targets upon induction with 2 μg/mL of doxycycline in A673 and SK-ES-1 cells at 72 hours. mRNA levels of KDM6A, KDM6B and EWSR1-FLI1 were also studied. Data were calculated with ΔΔCT method and normalized to *TBP*. All knockdown data were calculated relative to the control condition (shCTRL) and represents mean ± SEM from a minimum of three biological replicates. *P < 0.05, **P<0.01. ***C)*** Western blot showing H3K27me3 protein levels upon 2 μg/mL (++) doxycycline induction in histone extracts from A673 and SK-ES-1 cells at 72 hours. Histone H4 was used as loading control. Numbers represent band quantification related to shCTRL treated with the same doxycycline concentration. #shRNA79 and #shRNA99 represent different sequences targeting KDM6A.

Overall, our data demonstrate that lower levels of KDM6A affect the expression of many EWSR1-FLI1–activated targets, producing a decrease at the mRNA level in ES cell lines. Because we have shown KDM6A co-localizes genome-wide with EWSR1-FLI1, these data indicate that KDM6A is necessary for EWSR1-FLI1 to mediate its transactivation activity. Alteration of the global levels of H3K27me3 further supports the idea that the demethylating function of KDM6A contributes to the remodelling activity of EWSR1-FLI1 at its target genes.

3.3.2 EZH2 knockdown upregulates EWSR1-FLI1–repressed targets

To elucidate if EZH2 binding in EWSR1-FLI1 target genes is critical to mediate repression, we used ES cell lines with a stable EZH2 knockdown, previously generated by our group. First, we confirmed the knockdown of the enzyme by Western blot, which showed 50% and 30% of EZH2 depletion in A4573 and A673 cells, respectively (**Figure IV. 21A**). Subsequently, we evaluated by RT-qPCR the expression of EWSR1-FLI1-repressed targets (either directly or indirectly) with EZH2 binding in the knockdown cells. By doing this, we observed that following EZH2 knockdown many EWSR1-FLI1-repressed targets were upregulated, including *CAMK2N1*, forkhead box D1 (*FOXD1*), neurexin 1 *(NRXN1)* and TLE family member 1, transcriptional corepressor *(TLE1)* (**Figure IV. 21B**). Importantly,

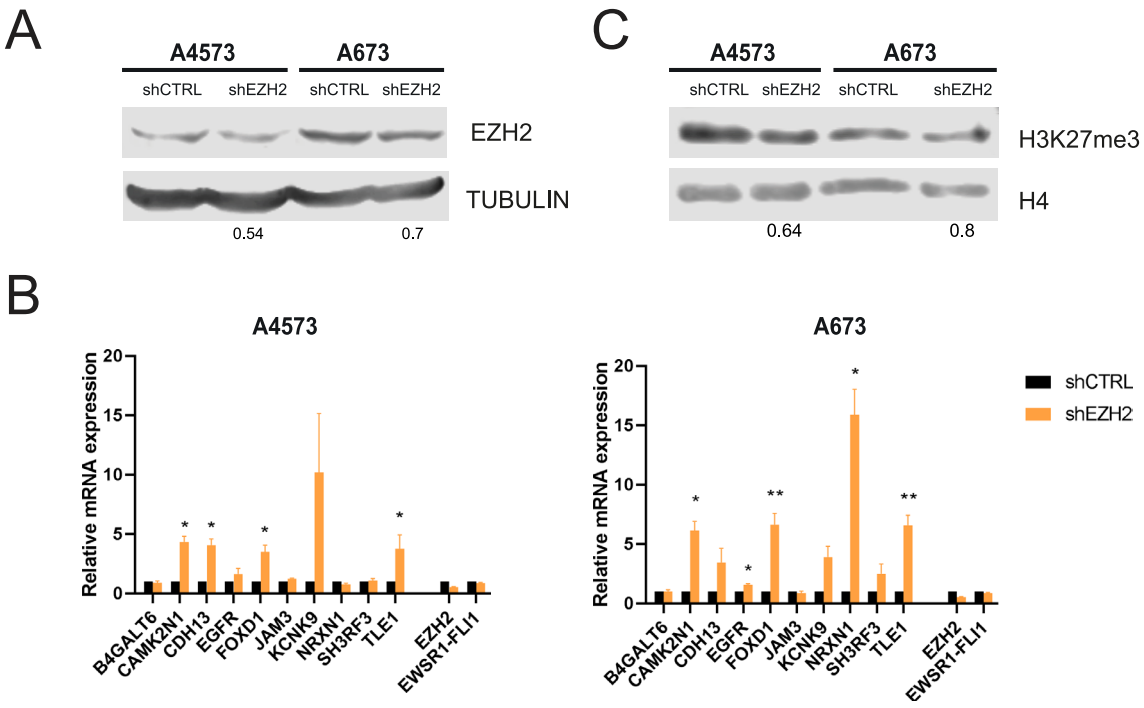

FIGURE IV. 21 ***EZH2 knockdown upregulates EWSR1-FLI1-repressed targets in ES cells with a global loss on H3K27me3.***
A) Western blot representing EZH2 protein levels in control (shCTRL) and EZH2 knockdown (shEZH2) A673 and A4573 ES cells. Tubulin was used as loading control. Numbers below represent band quantification normalized to tubulin levels and related to shCTRL. ***B)*** RT-qPCR analysis of mRNA levels of EWSR1-FLI1-repressed targets upon EZH2 knockdown in A673 and A4573 cells. mRNA levels of EZH2, and EWSR1-FLI1

were also studied. Data were calculated with the ΔΔCT method and normalized to *TBP*. All knockdown data were calculated relative to shCTRL and represent mean ± SEM from a minimum of three biological replicates. *P < 0.05, **P < 0.01.

these genes were associated with a gain of H3K27me3 in the hpMSC overexpressing EWSR1-FLI1 cell model (see **Figure 19D**). Furthermore, analysis of H3K27me3 upon EZH2 knockdown by Western blot revealed a decrease in the overall levels, suggesting that the upregulation of such repressed targets was at least in part associated with a lack of the enzymatic activity (**Figure IV. 21C**).

Collectively, these results demonstrate that knockdown of EZH2 can revert EWSR1-FLI1–mediated repression. Moreover, we show that H3K27me3 global levels are perturbed in these cells, and that some of these targets are associated with a gain of H3K27me3 principally along the gene body in the EWSR1-FLI1–overexpressing hpMSC model. Therefore, we suggest that EZH2-mediated positioning of H3K27me3 is determinant for transcriptional repression in ES cells.

3.4 EWSR1-FLI1 interacts with KDM6A

EWSR1-FLI1 directly interacts in the GGAA repeats with the histone acetyl transferase p300 and the MLL component WDR5 to activate transcription (Riggi et al., 2014). Recent data have identified KDM6A in the complexes constituted by p300 and a member of the MLL complex. While a complex constituted by KDM6A, p300, and MLL4 is present at active enhancers in embryonic stem cells (ESCs) (Wang et al., 2017), other p300-MLL2-KDM6A-containing complexes recruit RING1B to H3K27me3-containing promoters to activate transcription in melanoma (Rai et al., 2015). We have previously shown that EWSR1-FLI1 and KDM6A not only co-occupy the same regions but even have coinciding peaks. Considering all these pieces of evidence, we investigated whether KDM6A physically interacts with EWSR1-FLI1. To study this, we transfected HEK 293T cells with both EWSR1-FLI1-pEGFPN1 and KDM6A-pCIG plasmids and immunoprecipitated the EWSR1-FLI1–associated proteins through its GFP tag, using the GFP-Trap® nanobodies (see Materials and Methods). GFP immunoprecipitation of EWSR1-FLI1 and further detection of KDM6A by Western blot yielded a specific band for KDM6A, indicating that EWSR1-FLI1 physically interacts with KDM6A (**Figure IV. 22A**). Further evidence of such an interaction was observed in co-localization studies of both proteins by immunofluorescence staining. We used HEK 293T cells co-transfected with EWSR1-FLI1-pEGFPN1 and KDM6A-pCIG vectors, with subsequent detection of EWSR1-FLI1 by its GFP tag and further labelling with KDM6A antibody. We found that EWSR1-FLI1-GFP displayed a focal pattern around the cell nuclei, which overlapped in many regions with that of KDM6A. In contrast, in control cells, the GFP staining was diffuse around the cell (**Figure IV. 22B**). Analysis of the confocal images by Image J and further calculation of EWSR1-FLI1 and KDM6A co-localization coefficients with either the Pearson's correlation

method or the Li's intensity correlation method (see Materials and Methods) showed a strong correlation between EWSR1-FLI1–pEGFPN1 and KDM6A, further supporting our hypothesis (**Figure IV. 22C**).

A

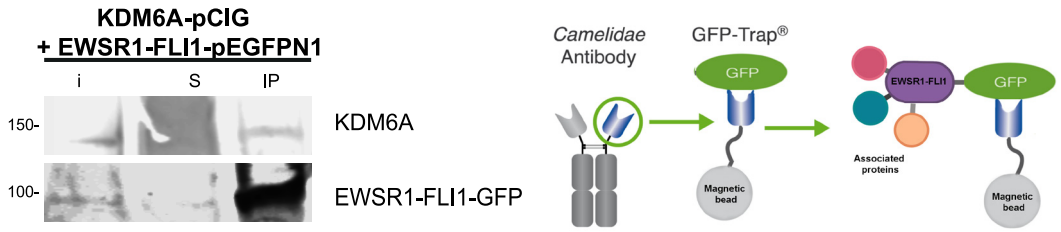

B

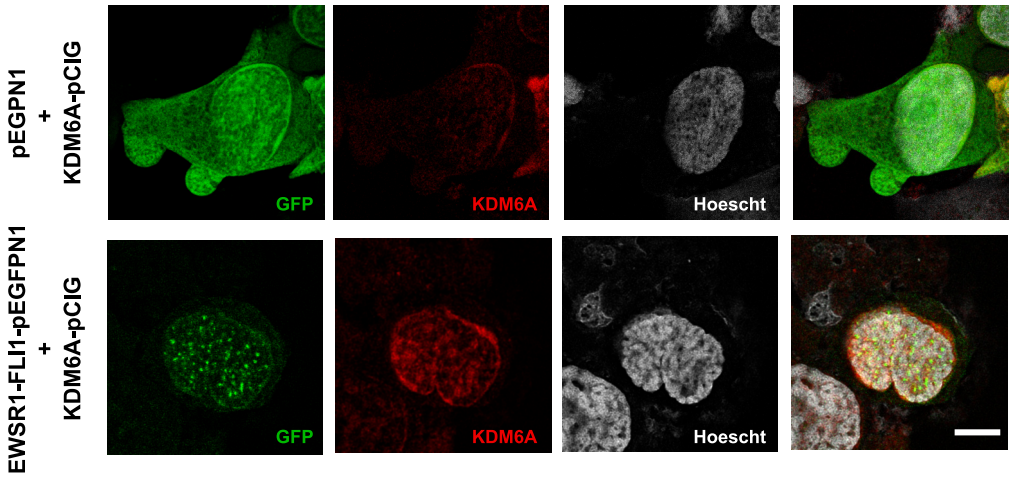

C

	Correlation coefficient between KDM6A and EWSR1-FLI1	
	Pearson's coefficient	Li's coefficient
Mean	0.66	0.36
SEM	0.06	0.03
p-value < 0.05	Yes	No

FIGURE IV. 22 ***KDM6A and EWSR1-FLI1 interact in EWSR1-FLI1-GFP HEK 293T cells.***
A) Western blot of KDM6A and EWSR1-FLI1-GFP in GFP immunoprecipitates of HEK 293T overexpressing EWSR1-FLI1-pEGFPN1 and KDM6A-pCIG. Input, supernatant and GFP immunoprecipitates are indicated as i, S and IP, respectively. The schematic representation of the right shows the mechanistic basis of GFP-trap system to pull-down GFP-tagged proteins. In this case, as EWSR1-FLI1 is coupled to GFP, it can be immunoprecipitated with antibodies targeting GFP to further detect the associated proteins by immunoprecipitation experiments. Images adapted from GFP-Trap for Immunoprecipitation (IP) of GFP-fusion proteins (2018). ***B)*** Confocal microscope images showing KDM6A and EWSR1-FLI1-GFP in HEK 293T cells transfected with EWSR1-FLI1-pEGFPN1 and KDM6A-pCIG. EWSR1-FLI1-GFP was detected in the green channel, KDM6A was detected in the red channel and nuclei were stained with Hoechst and detected in the blue channel. Images were processed in Image J to generate an image composite of all channels. Scale bar represents 5 µm. ***C)*** Table summarizing the results obtained from Image J calculations of Pearson's and Li's intensity coefficient methods to measure colocalization of EWSR1-FLI1 and KDM6A. A minimum of 6 stacks and 6 nuclei were used to study colocalization. A statistical significance of the colocalization is obtained only with the Pearson's correlation method. *P < 0.05.

In summary, we provide further evidence for an EWSR1-FLI1 and KDM6A interaction in an exogenous cellular model that overexpresses the fusion oncoprotein, which is in agreement with the genome-wide co-localization observed by ChIP-seq in A673 cells. These data suggest that KDM6A is part of the EWSR1-FLI1 transcriptional activation complex.

4. COMBINED INHIBITION OF EZH2 AND KDM6A BY GSK126 AND GSKJ4 IN ES CELLS

H3K27me3 dynamics is dysregulated in many cancers (Nichol et al., 2016). We have shown that H3K27me3 positioning is perturbed in ES tumorigenesis, displaying a gain or loss in EWSR1-FLI1–activated or –repressed targets. Moreover, we have demonstrated that single knockdown of the enzymes responsible for its positioning, EZH2 and KDM6A, reverts the transcriptional pattern of many EWSR1-FLI1 targets in ES cells. Consistent with these results, we hypothesized that pharmacological inhibition of the enzymatic activity of EZH2 as well as of KDM6A could be an effective anticancer strategy for this tumour.

To study this, we first considered targeting H3K27me3 deposition with GSK126, a SAM inhibitor of EZH2 methyltransferase activity. We evaluated the response of ES cell lines to GSK126 by MTS cell viability studies as compared to the 1273/99 OSG cell line, which has been shown to be sensitive to EZH2 inhibitors (Xiong et al., 2016). These experiments revealed a low sensitivity for ES cells to GSK-126, as shown by the almost doubled value for the IC50 concentration of these cells as compared to that for the OSG cell line (**Figure IV. 23A**). We next performed the same study with EPZ-6438, another EZH2 inhibitor with a higher selectivity to EZH2, and obtained even higher IC50 concentrations (data not shown). Thus, ES cell lines were apparently resistant to inhibition of EZH2. Subsequently, we evaluated the effects of KDM6A inhibition by GSK-J4 in ES cells, which has been reported to be highly effective in AML (Li et al., 2018), high-risk NB (Lochmann et al., 2018), and DIPG (Hashizume et al., 2014). We observed a high degree of heterogeneity among ES cell lines, with SK-ES-1 and TC-71 highly sensitive (IC50 ≤ 1 μM) and others, such as A673, much more resistant (**Figure IV. 23B**).

As we were interested to deregulate H3K27me3, we considered analysing H3K27me3 levels by Western blot for each treatment. For these experiments, we used the concentration of GSK126 published by Krook et al. (2016) that was shown to remove H3K27me3 from genomic regions in ES cells. Interestingly, we found that a subcytotoxic concentration of 10 μM of GSK126 was sufficient to reduce the overall levels of H3K27me3 in ES cell lines (**Figure IV. 23C**). Indeed, levels of H3K27me3 decreased even more than with depletion of EZH2 (see **Figure IV. 21C**). Moreover, we found stable levels of EZH2 at

such concentrations, indicating that only the enzymatic activity of EZH2 is modified by the inhibitor (data not shown). The same study was subsequently performed with GSK-J4. Analysis of H3K27me3 by Western blot showed that overall levels of H3K27me3 were slightly increased when using two subcytotoxic concentrations of this drug (**Figure IV. 23D**), similar with our previous results with KDM6A knockdown, suggesting that other enzymes (i.e. KDM6B) participate in maintenance of the histone mark.

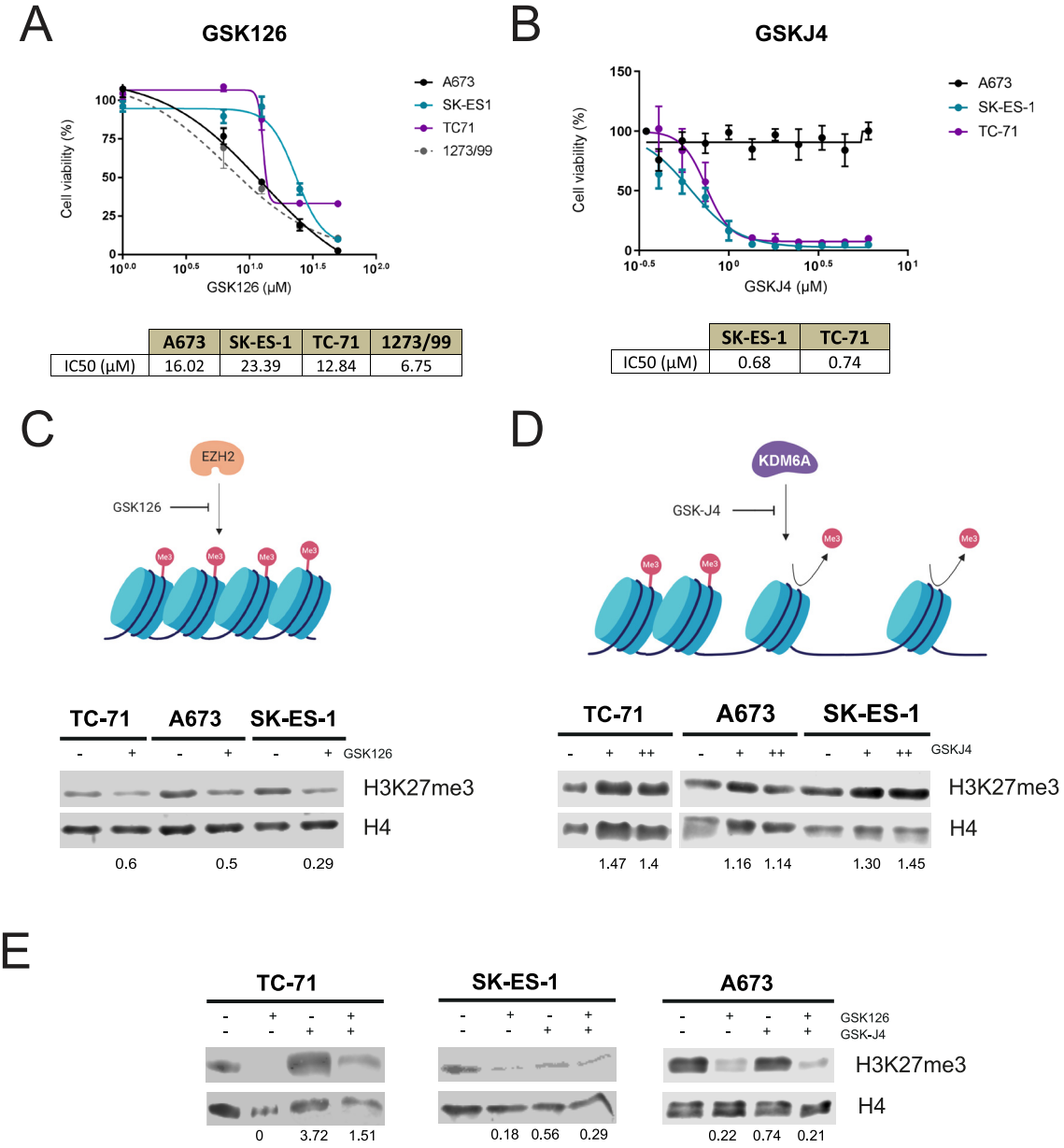

	A673	SK-ES-1	TC-71	1273/99
IC50 (μM)	16.02	23.39	12.84	6.75

	SK-ES-1	TC-71
IC50 (μM)	0.68	0.74

FIGURE IV. 23 ***Inhibition of EZH2 and KDM6A with GSK126 and GSK-J4, respectively, decreases the overall levels of H3K27me3 in ES cells.***
A) MTS cell proliferation curves expressed in percentage of viable cells in A673, SK-ES-1 and TC-71 ES cell lines upon treatment with different concentrations of GSK126 for 72 hours. 1273/99 cells were used as positive control for GSK126. Best-fit curves of three biological replicates were performed in GraphPad Prism. Table below the graph shows IC50 values in micromolar, which were calculated with the same program. ***B)*** Same experiments as in ***A)*** but using GSK-J4 for 72 hours. ***C)*** Western blot showing overall

levels of H3K27me3 in histone extracts from A673, SK-ES-1 and TC-71 cells ES cells treated with 10 μM of GSK126. Histone H4 was used as loading control. Symbols + and – indicate inhibitor or vehicle treatment, respectively. Numbers represent band quantification normalized to histone H4 and related to vehicle. A schematic representation of the mechanistic basis of GSK126 on H3K27me3 is also shown (Created with Biorender.com) ***D)*** Same experiments as in ***C)*** but using different concentrations of GSK-J4 for 72 hours. For A673 5 μM and 8 μM; for SK-ES-1 2.5 μM and 5 μM; for TC-71: 1 μM and 2.5 μM. Symbols ++ and + indicate the highest and lowest concentration of the inhibitor used in each cell line, respectively, while – symbol indicates vehicle treatment. Numbers represent band quantification normalized to histone H4 and related to vehicle. A schematic representation of the mechanistic basis of GSK126 on H3K27me3 is also shown. ***E)*** Western blot of H3K27me3 from histone extracts in A673, SK-ES-1 and TC-71 cells upon GSK126 and GSK-J4 single and combinatorial treatment for 72 hours (GSK126 was fixed to 10 μM; GSK-J4 was used at the lower concentration used in ***D)***. Symbols + and – indicate inhibitor or vehicle treatment, respectively. Numbers represent band quantification normalized to histone H4 and related to vehicle.

Experimental evidence has shown that loss or inactivation of KDM6A sensitizes both *in vivo* and *in vitro* multiple myeloma cells to EZH2 inhibitors (Ezponda et al., 2017). Furthermore, KDM6A-deficient lung cancer tumour cells are more sensitive to EZH2 inhibitors, which suppress tumour growth (Wu et al., 2018). Our previous experiments indicated that ES cell lines displayed a resistant pattern towards EZH2 inhibitors with high sensitivity to GSK-J4. Thus, we hypothesized that a deficient enzymatic activity of KDM6A as a result of GSK-J4 treatment might sensitize ES cells to EZH2 inhibition by GSK126, perturbing H3K27me3 dynamics. First, we studied whether combination treatment using 10 μM of GSK126 and the lower concentration used for GSK-J4 (in **Figure IV. 23D**) changed the overall levels of H3K27me3 by Western blot. Interestingly, we observed that dual targeting of H3K27me3 through GSK126 and GSKJ4 produced a global reduction on the overall levels of this mark in all ES cells, similar to the inhibition of EZH2 by GSK-126 (**Figure IV. 23E**).

We subsequently performed cell cycle experiments to elucidate the effect of GSK126 and GSK-J4 drug combination in ES cells. By propidium iodide staining of treated cells, we clearly observed that dual targeting of H3K27me3 with these inhibitors produced a sub-G1 or apoptotic peak that was significantly higher than single treatments in SK-ES-1 and TC-71 cells (**Figure IV. 24A**). In contrast, the A673 cell line did not show a sub-G1 peak in any experimental condition tested. Based on these results, we next studied apoptosis of these treatments by annexin V staining. In these experiments, SK-ES-1 and TC-71 displayed a higher statistically significant fraction of apoptotic cells as compared to GSK-J4 or GSK-126 treatment alone, confirming our previous results that dual targeting of H3K27me3 caused apoptotic cell death. Furthermore, such cytotoxic effect was apparently synergic for the combination treatment in both cell lines (**Figure IV. 24B**). In contrast, A673, which we showed was resistant to GSK-J4, had no response to any treatment used. Finally, Western blot analysis of programmed cell-death by expression of cleaved PARP-1 (c-PARP1) in single as well as combinatorial treatments showed a c-PARP1 band after GSK-J4 treatment that was stronger after combination treatment in these cells. This further confirms our previous results of a synergic and cytotoxic response of both drugs (**Figure IV. 24C**). A673

cells displayed no sign of programmed cell death after inhibitor treatment. Therefore, these results indicate that combination treatment sensitizes some ES cells to the EZH2 inhibitor. As synergism of the drug combination seems to be dependent on the cytotoxic effect of GSK-J4, and as we used the lowest concentration of GSK-J4 for all cells, it is possible that we might not have sensitized this cell line due to dosing.

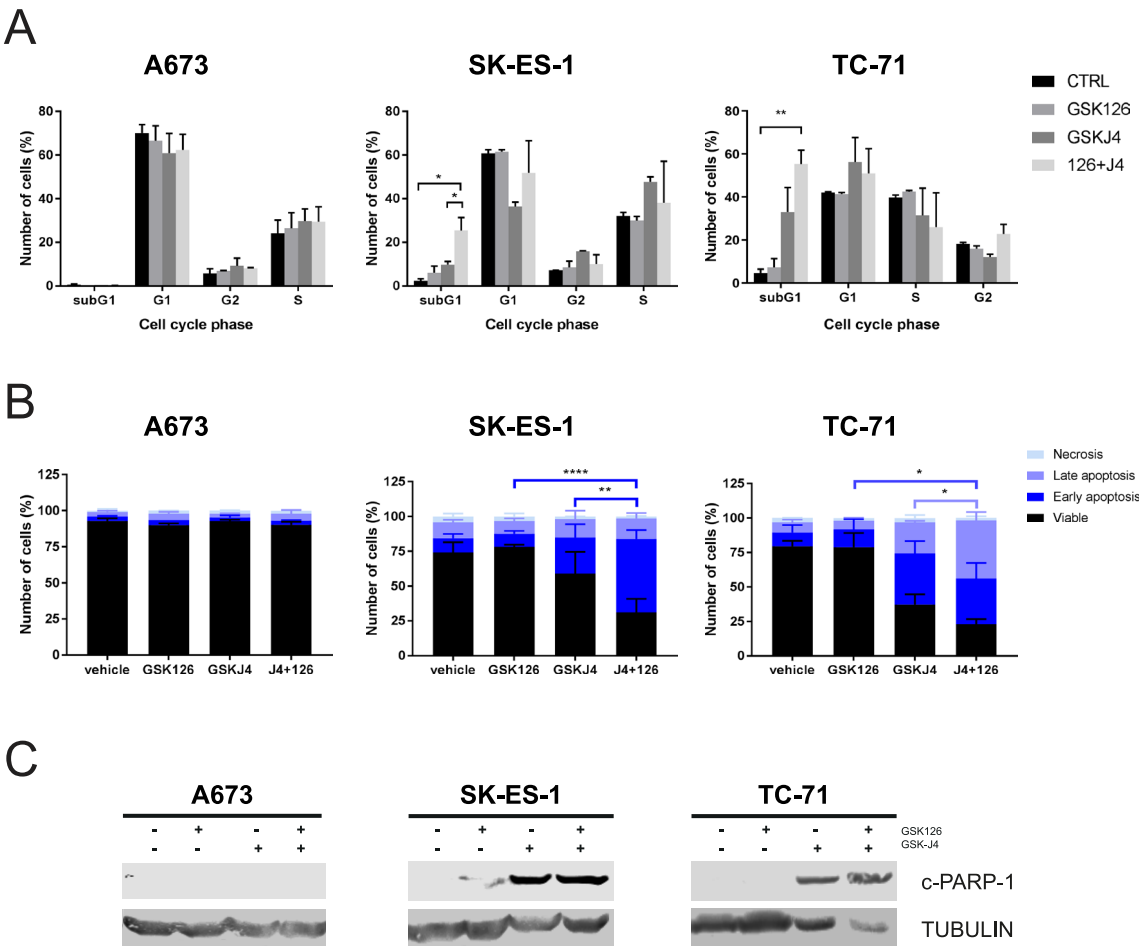

FIGURE IV. 24 ***Dual targeting of H3K27me3 through GSK126 and GSK-J4 combination treatment produces a synergic cytotoxic effect in SK-ES1 and TC-71 ES cell lines.***
A) Bars representing number of cells expressed in percentage in each cell cycle phase from flow cytometry experiments, upon single and combinatorial treatments of GSK126 and GSK-J4 for 72 hours in A673, SK-ES-1 and TC-71 cells. ***B)*** Bars representing percentage of viable, early and late apoptotic and necrotic cells from Annexin V staining analysis by flow cytometry upon single and combinatorial treatments of GSK126 and GSK-J4 for 72 hours in A673, SK-ES-1 and TC-71 cells. A two-way ANOVA test was applied to determine differences between multiple groups. *P < 0.05, **P< 0.01. ***C)*** Western blot showing protein levels of cleaved-PARP1 in A673, SK-ES-1 and TC-71 cells upon GSK126 and GSK-J4 single and combinatorial treatment for 72 hours. Tubulin was used as loading control.

In summary, our data provide evidence of a mechanism of targeting both transcription activation and repression in ES by inhibiting the enzymatic activities responsible for setting H3K27me3 levels. The combinatorial treatment is synergistic in ES cell lines and depends mostly on the inactivation of KDM6A, in agreement with the literature. Indeed,

the efficacy of the dual targeting further suggests that deregulation of H3K27me3 is not trivial in ES tumorigenesis. The translation of these results to preclinical studies has to be elucidated yet.

V. DISCUSSION

Prior to the use of multi-drug systemic therapy, the long-term survival rate of ES following surgery or radiation alone was less than 10% (Iwamoto, 2007). With the addition of a multimodal treatment regimen including intensive multi-agent chemotherapeutics, the 5-year survival rates now range from 70–80% for patients with standard-risk and localized disease yet only 30% for those with metastatic disease (Grunewald et al., 2018). Even when an extensive therapy plan is followed, at least one-fourth of patients with initially localized disease will relapse after completing treatment or within 2 years of initial diagnosis; while for those patients with initially metastatic disease recurrence is still more frequent, accounting for 50-80% (Van Mater and Wagner, 2019). Worse yet, there is no standard management to offer for relapsed patients. Moreover, patients who survive face debilitating and often life-threatening health consequences as a result of the highly toxic therapy (Ginsberg et al., 2010). Therefore, and especially considering the young age and thus potential lifespan of the patients, there is great need for finding new therapies to improve the outcome for these patients.

Considering that ES is a TF-driven disease with paucity of mutations whose biology is highly dependent on EWSR1-FLI1 translocation (Riggi and Stamenkovic, 2007), a first therapeutic strategy that comes to mind is specifically targeting the fusion protein. On this basis, antisense DNA, siRNA and dominant negatives targeting EWSR1-FLI1 markedly impair ES cell growth (Maksimenko and Malvy, 2005). However, the lack of a specific enzymatic activity of TF as well as intrinsically disordered domains that challenges determining its crystal structure, notoriously hinders a targeted pharmacological inhibition (Darnell, 2002).

Alternative strategies currently centre on identifying critical epigenetic partners that interact with EWSR1-FLI1, to reprogram the epigenome. A variety of protein complexes involved in the regulation of chromatin structure have now been described to be dysregulated in ES, including the BAF complex (Boulay et al., 2017). BMI1 and the EZH2 PcG proteins, which constitute the PRC1 and PRC2 complexes respectively, are among such deregulated epigenetic components and are overexpressed with essential roles reported for ES tumorigenesis (Douglas et al., 2008; Hsu and Lawlor, 2011; Riggi et al., 2008). In this thesis, we exemplify the importance of identifying deregulated epigenetic components in ES. Consistently, for the first time, our work reveals that (i) RING1B is crucial for ES tumorigenesis; (ii) EZH2 and KDM6A, the H3K27me3 writer and eraser, respectively, are responsible for the aberrant positioning of this histone modification in ES; and (iii) pharmacological targeting of RING1B, EZH2 and KDM6A are potential new horizons for future preclinical studies in ES.

1. Relevance of RING1B in ES tumorigenesis

Although PRC1 has been classically linked to gene repression, new evidence has identified this complex as facilitating gene transcription (Loubière et al., 2016; Morey et al., 2013; Morey et al., 2015; Rai et al., 2015). Recruitment of RING1B to transcriptionally active regions has been reported for a variety of cancers (Chan et al., 2018; Cohen et al., 2018; Rai et al., 2015). Our group described RING1B as a highly expressed PcG protein in primary ES tumours (Hernandez-Muñoz et al., 2016). According to the new roles published for PRC1 complexes containing RING1B, we have recently unveiled this PcG subunit as an essential partner of EWSR1-FLI1. While we identified a set of regions at which RING1B exerts its canonical repressive function, we also identified a second group of RING1B-bound regions that overlap with those of EWSR1-FLI1 at active enhancers (Sánchez-Molina et al., 2019). These findings are specific for RING1B, as neither BMI1 nor EZH2 are present at active enhancers, despite their clear co-localization at RING1B-repressed regions.

Furthermore, we observed that the occupancy of EWSR1-FLI1 at key enhancer regions decreases upon RING1B knockdown (Sánchez-Molina et al., 2019). The data presented here demonstrate an impaired tumour growth for RING1B knockdown ES xenografts (see **Figure IV. 1 A-B** from Results in Section IV). Consistently, KI67 staining revealed a less proliferative phenotype in RING1B depleted tumours, further confirming an important role in ES tumorigenesis (see **Figure IV. 1 C** from Results in Section IV). Moreover, data from our group show that RING1B knockdown decreases the expression of EWSR1-FLI1 and RING1B co-occupied targets, such as *SOX2* or *NKX2-2* (Sánchez-Molina et al., 2019), whose expression was described to be necessary for ES tumour proliferation (Owen et al., 2008; Riggi et al., 2010; Smith et al., 2006). Therefore, we hypothesize that the delay observed in tumour growth might be related to the novel transcription-activating function of RING1B by means of modulating the recruitment of EWSR1-FLI1 to target regions. This situation would be specific for ES, as although RING1B stimulates proliferation in melanoma through activation of *CCND2*, RING1B promotes an invasive behaviour of the tumour by silencing negative regulators of the transforming growth factor-beta (TGFβ) pathway, such as LTBP2 (Rai et al., 2015).

2. Modulation of RING1B by MLN4924

Our previous observations indicated a crucial role of RING1B in EWSR1-FLI1 chromatin reprogramming that impairs tumour growth of ES xenografts. This provides the rationale to pharmacologically target the activating functions of RING1B. PRT4165 is the only selective inhibitor of the PRC1 complex currently available and has been shown to potently inhibit *in vivo* and *in vitro* the PRC1-mediated ubiquitylation of histone H2A (Ismail et al.,

2013). Studies from our group with this inhibitor demonstrate nevertheless no cytotoxic effect in ES cell lines (data not shown), suggesting that inhibition H2A ubiquitination is not critical for ES cells to survive.

E3 ubiquitin ligases have diverse regulatory mechanisms to control their activity, including for instance PTMs such as phosphorylation, PARylation, autoubiquitination, and non-covalent binding of adaptor proteins (Vittal et al., 2015). A MEK1-mediated phosphorylation of RING1B at serine 41 has been described to enhance its transcriptional activity (Rai et al., 2015). Thus, we considered targeting RING1B with a MEK1 inhibitor, such as trametinib; however, ES cells were highly resistant to the drug (data not shown).

Neddylation has been reported to regulate many E3 ubiquitin ligases (Kawakami et al., 2001; Osaka et al., 2000; Pan et al., 2004). CRL E3 ligases are the most studied examples in the literature showing how important is the NEDD8 modification for regulating not only their enzymatic activity (Pan et al., 2004), but also their stability (Morimoto et al., 2003; Wu et al., 2005). The E3 ligase MDM2, which negatively regulates p53, was reported to be stabilized by neddylation (Watson et al., 2009). Likewise, neddylation of RING1B and other E3 ligases such as RNF168 and RNF8 has been described in the context of DDR (Li et al., 2014). In this work, coinciding with the high sensitivity of ES cells to the NEDD8 inhibitor MLN4924, we observed a decrease of RING1B at the protein level *in vitro* and *in vivo* in a concentration-dependant manner (see **Figures IV. 2 A-B, 6A,** and **9B** from Results in Section IV). We thus propose that lack of neddylation caused by MLN4924 leads to RING1B destabilization via proteasome degradation. This rationale is based on (i) the fact that RING1B is neddylated in ES cells and (ii) the decrease observed of RING1B protein levels upon NEDD8 knockdown, which correlates with the RING1B loss after MLN4924 treatment of ES cells (see **Figure IV. 7 C** and **D** from Results in Section IV, respectively). RING-finger E3 ligases have a self-ubiquitinating activity that is thought to act as a regulatory mechanism to control the abundance of E3 ligases, by marking them for degradation. However, RING1B degradation by UPS does not require its RING finger domain or self-ubiquitinating activity. The association with BMI1 has been reported as one of the mechanisms that protects them for proteasomal degradation (Ben-Saadon et al., 2006). Although mechanistic details explaining how RING1B is targeted to proteasome degradation are missing, it is suspected that a PRC1 exogenous E3 ligase tags it for proteasome degradation. Considering these data, further experiments are needed to elucidate whether RING1B degradation is a direct consequence of the lack of neddylation caused by MLN4924 or an indirect effect of an exogenous E3 regulating its stability that is perturbed by the drug in ES cells.

Our microarray data confirm that MLN4924 rapidly causes DNA damage in the most sensitive ES cell line (e.g. A673), despite using a subcytotoxic concentration of the

inhibitor (see **Figure IV. 3B** from Results in Section IV). These results are consistent with the induction of apoptosis reported for MLN4924 in ES cells (Mackintosh et al., 2012). In fact, ES cells display an impaired homologous recombination DDR, explaining why this tumour is so sensitive to genotoxic agents such as etoposide (Gorthi et al., 2018). Our observations indicating that lack of RING1B sensitizes ES cells to MLN4924, and that DNA damage is one of the main commonly deregulated pathways, further support the dependency of ES cells to RING1B (see **Figures IV. 5 and IV. 4 B, D** from Results in Section IV). In fact, the role of RING1B in the early steps of DDR is well-known, as PRC1 is recruited to sites of DNA double-stranded breaks (Chou et al., 2010; Facchino et al., 2010). At these genomic sites, RING1B exerts its catalytic function to ubiquitylate histone H2Ax, which is required for the efficient formation of γH2Ax (Pan et al., 2011; Wu et al., 2011). Phosphorylation of H2Ax stabilizes most DDR factors at DNA lesions (Stucki and Jackson, 2006); this initiates an ubiquitylation cascade that will ultimately contribute to DNA repair pathway choice (of the homologous recombination or non-homologous end-joining pathway). Genome sites containing γH2Ax colocalize with a poly-NEDD8 chain on histone H4, thus linking neddylation to this process. Structural analyses of such poly-NEDD8 nucleosomes indicate a drastic change on the nucleosome conformation. Thus, neddylation might serve to break nucleosome interactions and to facilitate access of DDR repairing factors to damaged regions (Ma et al., 2013).

On the other hand, the less sensitive cell line tested to MLN4924 treatment, SK-ES-1, displayed IFN and cytokine signalling pathways commonly deregulated by RING1B depletion and the inhibitor, reflecting a cellular stress response (see **Figure IV. 4 C, E** from Results in Section IV). Considering that MLN4924 generates oxidative stress, which leads to DNA damage–induced apoptosis through inactivation of NF-κB (Swords et al., 2010), we argue that most of the sensitivity of ES cells to MLN4924 might be explained by a defective oxidative cell-stress response prior to DNA damage that primes the cells to apoptosis.

Additionally, we described for the first time that RNA levels of RING1B and other E3 ubiquitin ligases were deregulated upon MLN4924 treatment (see **Figures IV. 3 C-D from Results** in Section IV). Even though very little is known about the genetic regulatory loops controlling the activity of E3 ubiquitin ligases, our data agree with that of Lee et al. (2014), who studied the regulation of E3 in the context of the UPS system. Concretely, the authors showed that perturbation of this system leads to an unexpected negative feedback loop that causes downregulation of E3 ubiquitin ligases. This mechanism is believed to shut down the UPS system to prevent abnormal operation. Thus, based on our results, we speculate that MLN4924 causes a negative feedback loop inhibiting transcription of many E3 ligases, including RING1B. However, considering that similar amounts of E3 ubiquitin ligases are upregulated in ES cells upon MLN4924 treatment, we suggest that additional

unknown mechanisms regulating the activity of these proteins might act.

Our results indicate that the E3 ubiquitin ligase activity of RING1B is not altered upon MLN4924 treatment, at least not at a global level (see **Figure IV. 6 B** from Results in Section IV), coinciding with other reports that show steady-state levels of H2Aub mark upon MLN4924 treatment (Kim et al., 2011). Indeed, overall levels of H2Aub remain unchanged upon RING1B knockdown (see **Figure IV. 4 A** from Results in Section IV). We have described similar observations in Sánchez-Molina et al. (2019). In this article, we argue that the ubiquitin ligase activity of RING1B is not its primary role in ES, and that the RING1B paralogue, (i.e. RING1A) might replace the E3 ubiquitin ligase function in this specific context. This hypothesis is reinforced by data reported in other malignancies, for which an uncoupled function of RING1B from its classical role as a repressor has been described. In these cases, it is proposed that RING1A might be enzymatically more active for mono-ubiquitinate histone H2A than for RING1B (Chan et al., 2018). Indeed, the subunits defining the PRC1 complex are determinant for the ubiquitylating activity of histone H2A (Taherbhoy et al., 2015).

Even though EWSR1-FLI1 displays a high protein turnover rate mediated by polyubiquitination at a single lysine residue (Gierisch et al., 2016), we demonstrate that its levels are not altered at low MLN4924 concentrations (see **Figure IV. 2 C** from Results in Section IV). Consistently, the deubiquitinating enzyme USP19 reported to stabilize EWSR1-FLI1 (Gierisch et al., 2019), was not found to be deregulated by MLN4924 in our microarray data (data not shown). We cannot rule out that EWSR1-FLI1 levels might be perturbed at higher concentrations or prolonged exposures of MLN4924. Nevertheless, we observed that following RING1B loss from EWSR1-FLI1-activated target regions by MLN4924, EWSR1-FLI1 was also evicted from these loci with a moderate impact on transcription (see **Figure IV. 8** from Results in Section IV). These results are highly consistent with experiments performed by our group showing that depletion of RING1B impairs EWSR1-FLI1 recruitment to its targets with modest effects on gene expression, indicating high similarities between MLN4924 treatment and RING1B knockdown (Sánchez-Molina et al., 2019). Thus, we propose a model in which lack of active NEDD8 by MLN4924 causes a decrease of RING1B protein levels in ES cells, reducing RING1B binding at EWSR1-FLI1–activated targets. Consequently, EWSR1-FLI1 is evicted from these regions, affecting transcription. More experiments are needed to elucidate whether lack of RING1B alters its binding to canonical repressed regions upon MLN4924 treatment. **Figure V. 1** summarizes these observations.

Experimentally, MLN4924 is an interesting tool that permits RING1B to be modulated, allowing us to gain a better understanding of the early steps in the epigenetics behind ES tumorigenesis. To conclude, MLN4924 represents an attractive drug to further test in preclinical studies of ES.

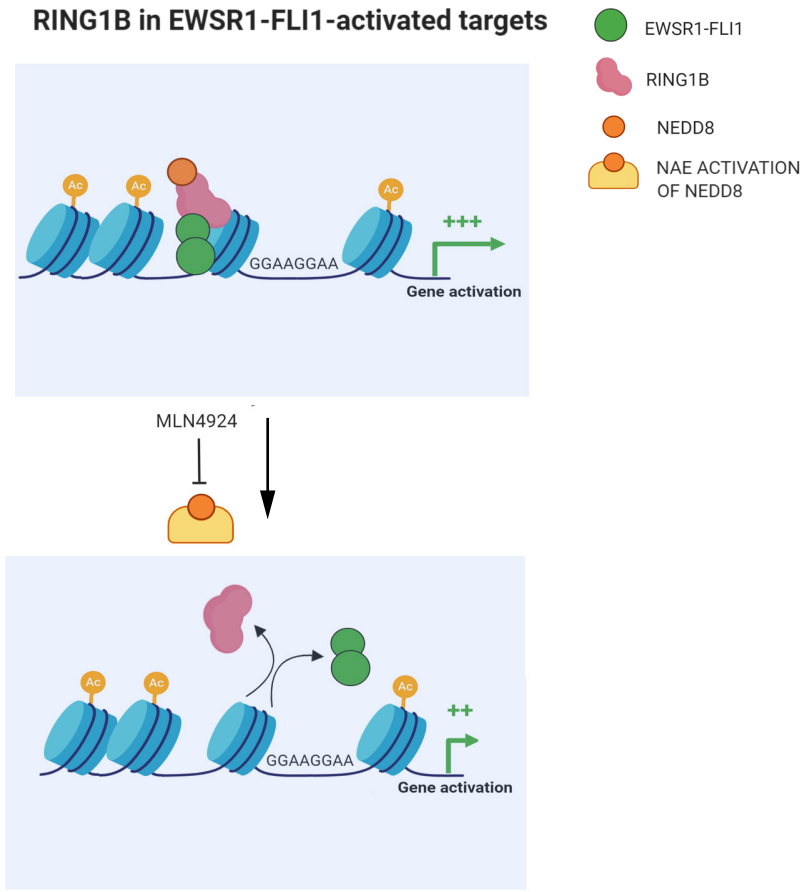

FIGURE V. 1 ***MLN4924 effects on RING1B binding in EWSR1-FLI1-activated targets in ES cells.***
In this model, EWSR1-FLI1–activated regions (GGAA repeats) are initially filled with a neddylated form of RING1B coinciding with active transcription. Treatment of ES cells with MLN4924 triggers an impaired activation of the NEDD8 isoform, leading to loss of RING1B neddylation and causing its loss from EWSR1-FLI1-activated targets. As RING1B might help recruitment of EWSR1-FLI1, EWSR1-FLI1 is consequently evicted upon MLN4924 treatment, with moderate changes on gene transcription. H3K27ac active enhancer marks are represented as yellow buttons. The right legend identifies all the proteins involved in the model. (Created with Biorender.com)

3. EWSR1-FLI1 target regions are previously enriched in H3K27me3

Many paediatric sarcomas are TF-driven diseases with oncogenic fusion genes involved. These tumours display a common epigenetic dysregulated axis inducing *de novo* superenhancers that reprogram the whole transcriptional pattern of the cell. In alveolar RMS, for instance, the PAX3-FOXO1 fusion triggers chromatin remodelling by recruiting p300 and BRD4 to super-enhancers (Gryder et al., 2017). These regulatory regions are defined by active histone modifications, such as H3K27ac, that overlap with the fusion oncoprotein binding sites. In contrast, other fusion proteins, such as the SS18-SSX translocation found in virtually all SS, have acquired the ability to interact with HDAC and SWI/SNF complex components, such as hBRM and hBRG1, to aberrantly activate

transcription (Kadoch and Crabtree, 2013; Nagai et al., 2001; Thaete et al., 1999). Likewise, in ES, EWSR1-FLI1 recruits p300, the WDR5 subunit of the MLL complex, and the BAF component of the SWI/SNF to the GGAA repeats bound by the fusion oncoprotein (Boulay et al., 2017; Riggi et al., 2014). This concurs with strong enrichment of active histone marks, such as H3K27ac, at these regions (Riggi et al., 2014; Tomazou et al., 2015).

Our findings indicate that activated EWSR1-FLI1 binding sites are initially filled with H3K27me3 in both HUVEC and hpMSC (see **Figure IV. 12 C, B** from Results in Section IV), and coincide with recent observations in hpMSC published by Boulay et al. (2018). In fact, genome-wide studies of the GGAA repeats bound by EWSR1-FLI1 reported that in other cellular contexts (e.g. HUVEC and H1 hESC), these regions are highly enriched for H3K27me3 (Patel et al., 2012). Furthermore, a recent study from our group evaluating the chromatin states of H1 hESC, HUVEC and adipose and bone marrow-derived MSC from the Roadmap Epigenomics Consortium (Roadmap Epigenomics et al., 2015) showed that GGAA repeats bound by EWSR1-FLI1 are enriched in repressed PcG chromatin states, defined as highly H3K27me3-bound regions (Sánchez-Molina et al., 2019). Similarly, in SS, the SS18-SSX2 fusion oncoprotein occupies H3K27me3-marked regions (Garcia et al., 2012). Altogether, these data suggest a general mechanism by which fusion oncoproteins do not randomly target regions of open chromatin but rather bind to a subset of PcG loci. Indeed, in SS, the SS18-SSX fusion protein containing the SWI/SNF complex is recruited by the KDM2B demethylase and a PRC1.1 (or BCOR) complex to sites of hypomethylated CGI. This leads to increased gene accessibility and consequent aberrant activation of developmental genes that otherwise should be repressed (Banito et al., 2018). Our findings presented in Sánchez-Molina et al. (2019) indicate that RING1B might recruit EWSR1-FLI1 to target sites enriched in H3K27me3, thereby further supporting a similar model to the one published for SS.

4. Redistribution of H3K27me3 in ES cells

Previous reports indicate a lack of H3K27me3 in EWSR1-FLI1-bound regions in ES cell lines and tumours (Patel et al., 2012; Riggi et al., 2014; Tomazou et al., 2015). Nevertheless, our H3K27me3 ChIP-seq results in hpMSC showed a loss of this mark from EWSR1-FLI1–bound GGAA repeats upon ectopic expression of the oncogene, thus refining our understanding of this mark in the context of ES (see **Figures IV. 13 E and 14** from Results in Section IV). These results are remarkably in agreement with recent data by Boulay et al. (2018). We further confirmed that H3K27me3 loss was more evident at promoters at which this mark was initially present in hpMSC (such as *NKX2-2* and *KIT*) (see **Figure IV. 14** from Results in Section IV). Indeed, the maintenance in overall levels of H3K27me3 that we observed upon EWSR1-FLI1 transformation in hpMSC or HUVEC (see **Figure IV. 11 C** from Results in Section IV) is consistent with previous reports showing unaltered

levels of H3K27me3 following knockdown of EWSR1-FLI1 in ES cells (Tomazou et al., 2015). All these data point to a redistribution process of this histone mark during ES tumorigenesis. Consistently, our findings indicate a genome-wide gain of H3K27me3 in the gene body occurring in some relevant EWSR1-FLI1-repressed targets, e.g. *IGFBP3* and *TGFBR2* (see **Figure IV. 15** from Results in Section IV). The enrichment of H3K27me3 observed across the gene body has been described to be indicative of a strong repression that can extend to flanking regions with little to no correlation with RNAPII, H3K36me3 or H3K4me3 (Young et al., 2011).

In other developmental tumours, such as DIPG, H3K27me3 was described to be globally lost upon introduction of the H3.3K27 mutation in progenitor brain stem cells (Lewis et al., 2013). Similar to ES, this repressive histone mark was found to be elevated or retained at promoters of a particular series of genes enriched in cancer pathways in DIPG cells, for instance by repressing *p16Ink4A* and *CDK6 loci* (Bender et al., 2013; Chan et al., 2013; Mohammad et al., 2017). More recently, new data have demonstrated that PRC2 was redistributed in DIPG cells to poised enhancers contributing to tumorigenesis in part by locally enhancing H3K27me3 and hence silencing tumour suppressor genes (Fang et al., 2018). The importance of a redistribution process of H3K27me3 in cancer is also highlighted by results from another group in melanoma and lymphoma. A recurrent gain-of-function mutation in EZH2 (Y641F) in these tumours has been related to an increased abundance of this mark with a strikingly widespread redistribution. Such aberrant distribution of H3K27me3 in melanoma and lymphoma cells was associated to a perturbed transcription repression, but also activation of some repressed genes that correlates with malignant progression of these tumours (Souroullas et al., 2016).

5. EZH2 contributes to the indirectly mediated repression of EWSR1-FLI1 in ES cells

EZH2 activity has come into the spotlight due to the redistribution process of H3K27me3 during ES tumorigenesis, as described here. This PcG subunit is highly expressed in ES tumours (Staege et al., 2004), and its depletion in ES cells results in a dramatic reduction of tumour growth (Riggi et al., 2008). Consistently, direct binding of EWSR1-FLI1 to the EZH2 promoter region has been reported to stimulate expression of this PcG subunit (Richter et al., 2009). Moreover, EZH2 has been particularly attributed to mediate the stem cell phenotype of this tumour by blocking neural and endothelial differentiation programs in ES cells, with an unfavourable outcome and tumour progression in this tumour as well as other paediatric sarcomas (Ramaglia et al., 2016; Richter et al., 2009).

In this thesis, we contributed to the understanding of how EZH2 participates in the chromatin remodelling process mediated by EWSR1-FLI1. We demonstrated that (i) EZH2

binding regions are associated to promoters of genes that gain H3K27me3 along the gene body in hpMSC overexpressing the fusion protein (see **Figures IV. 17 D** and **19 B-C** from Results in Section IV); and that (ii) EZH2 knockdown triggers an upregulation of critical repressed targets in ES cells (see **Figure IV. 19 D** from Results in Section IV). In fact, we found that EZH2-bound targets are associated to gene ontologies related to developmental or cell differentiation programs of cardiac muscle or epithelial tissues, which arise from the mesoderm germ layer where mesenchyme develops (data not shown).

EZH2 knockdown in ES cells results in a significant delay in tumour development and metastasis in mice (Richter et al., 2009). Expression of PRC2 proteins has been demonstrated to be an independent negative prognostic factor in various sarcomas, including ES (Cho et al., 2018). Altogether, our data reinforce the idea that EZH2 maintains the repressive state in ES (**see Figure IV. 19A-B from Results in section IV**), similar to other repressive factors reported in this tumours that are induced by EWSR1-FLI1 e.g. NKX2-2 (Fadul et al., 2015; Owen et al., 2008; Smith et al., 2006). Parallel mechanisms have been published for other paediatric tumours, such as DIPG, in which EZH2 activity is required for the growth of DIPG cells *in vitro* and *in vivo,* correlating with the H3K27me3 redistribution (Mohammad et al., 2017). A role for EZH2 in NB was also recently suggested (Bate-Eya et al., 2017; Henrich et al., 2016; Tsubota et al., 2017). Similar to ES, high-risk NB with amplification of the MYCN proto-oncogene, BHLH transcription factor (MYCN) overexpress EZH2 (Chen et al., 2018). In this publication authors indicate an essential role for this PcG protein on blocking neuronal differentiation programs, as both genetic and pharmacologic inhibition of EZH2 inhibits tumour growth *in vivo*.

All these pieces of evidence showing perturbed differentiation programs through EZH2 overexpression during tumorigenesis point to this PcG protein as an important deregulated axis for repressing critical developmental programs in various paediatric tumours. This evidence, together with our results showing genetic depletion of EZH2 can revert the expression of important EWSR1-FLI1-repressed targets, provides further rationale for testing EZH2 inhibitors in this tumour.

6. KDM6A as a new partner of EWSR1-FLI1

According to the H3K27me3 loss observed upon ectopic expression of EWSR1-FLI1 in hpMSC, we provide new insights into the activity of KDM6A (also known as UTX), a KDM6 demethylase family member. This demethylase is ubiquitously expressed in tissues, as indicated on its acronym "ubiquitously transcribed tetratricopeptide repeat, X Chromosome" (UTX). In this thesis, we show that KDM6A is highly expressed in ES compared to KDM6B, especially in ES xenografts and PdX tumours (see **Figure IV. 16 A-B, D** from Results in Section IV). In agreement with these data, ES were listed in the twelfth position of different

cancer malignancies harbouring higher mRNA expression of this demethylase (Barretina et al., 2012). In these studies, the KDM6A paralogue UTY was identified as moderately expressed in ES, which has residual demethylating activity (Shpargel et al., 2012).
Among other histone demethylases, KDM6A has been identified as one of the 299 cancer driver genes in the cancer genome atlas project (TCGA) (Bailey et al., 2018). However, its role in cancer development is still ambiguous. While deleterious mutations of KDM6A found in various adult tumours (including bladder urothelial carcinoma, and pancreatic adenocarcinoma) are indicative of a tumour suppressive function (Kandoth et al., 2013; Li et al., 2018; van Haaften et al., 2009), KDM6A appears to support the action of oncogenic factors in other cancer types, like prostrate or breast cancer (Benyoucef et al., 2016; Kim et al., 2014; Xie et al., 2017). KDM6A's role in cancer is thus apparently context-specific and dependent on not only its H3K27me3 demethylating activity, but also its interactions with other epigenetic complexes. In this study, we found 45% of EWSR1-FLI1 gene-associated peaks co-occupied by KDM6A (see **Figure IV. 18 A-B** from Results in Section IV). As a majority of these coinciding peaks in A673 cells correlated with a loss of H3K27me3 upon overexpression of EWSR1-FLI1 in hpMSC (see **Figure IV. 18 B-C** from Results in Section IV), we propose that the demethylating activity of KDM6A at EWSR1-FLI1–activated targets promotes oncogenesis, which agrees with the aforementioned role of this demethylase in some cancers.

In contrast to other KDM6 family members, KDM6A harbours a unique tetratricopeptide (TPR) that permits its interaction with various protein complexes (Chang et al., 2019). On this basis, a substantial number of proteins have been reported to interact with KDM6A to coordinate several biochemical processes associated with gene transcriptional activation, especially in processes associated with H3K4me3 methylation, which marks transcriptionally active regions (Bochyńska et al., 2018; Ford and Dingwall, 2015; Lee et al., 2007; Shilatifard, 2008). In *Drosophila,* for instance, KDM6A is physically associated with BRM, a member of the SWI/SNF complex, and CBP to modulate the H3K27 acetylation activity of the last (Tie et al., 2012). KDM6A is also an integral component of the COMPASS-like complex, which contains the core proteins WDR5, RBBP5, DPY30, and ASH2L as well as the MLL3/KMT2C or MLL2/4/KMT2D methyltransferase, which mono-methylate H3K4 in enhancer chromatin (Cho et al., 2007; Hu et al., 2013; Shilatifard, 2008). In agreement with these data, EWSR1-FLI1 recruits p300 and a member of the MLL complex (such as WDR5) to its GGAA-binding sites to mediate histone acetylation and methylation on H3K27ac and H3K4me3, respectively, and to thereby activate transcription (Riggi et al., 2014). Considering this evidence and our results showing interaction of KDM6A with EWSR1-FLI1 with a high correlation in the cell nuclei (see **Figure IV. 22** from Results in Section IV), we speculate that this demethylase might constitute part of the oncogenic chromatin remodelling complex in ES cells. Therefore, we propose that interactions of KDM6A with other epigenetic factors are fundamental in this tumour for

the chromatin remodelling process imposed by EWSR1-FLI1. Important to note is that KDM6A does not possess a DNA binding domain indicating that interactions with other chromatin partners are essential for its recruitment to chromatin.

In melanoma, KDM6A was identified as part of the p300-MLL2 complex recruited by RING1B at H3K27me3 rich regions leading to chromatin opening to subsequent gene activation (Rai et al., 2015). Our group has shown that RING1B and EWSR1-FLI1 interact and co-localize in active genomic regions in ES cells (Sánchez-Molina et al., 2019). We therefore speculate that RING1B and KDM6A might constitute part of the same complex at active gene regions in ES. According with these data, we postulate a model in which RING1B might recruit an EWSR1-FLI1-containing KDM6A complex to erase H3K27me3 at GGAA repeats. Similar to what has been proposed for p300 and additional acetylating partners recruited by EWSR1-FLI1 to mediate transcription activation (Riggi et al., 2014) and proteins of the SWI/SNF complex involved in chromatin remodelling, e.g. BAF (Boulay et al., 2017), we also propose addition of KDM6A to this scenario (**Figure V. 2**).

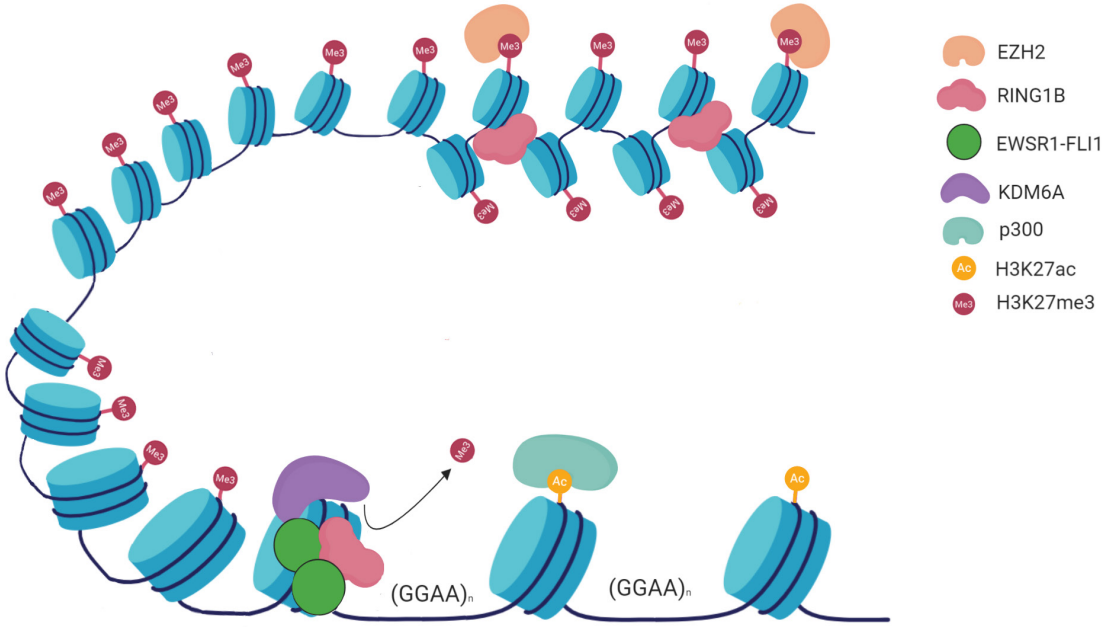

Figure V. 2 ***KDM6A and RING1B in EWSR1-FLI1–activated target regions in ES cells.***
The model presented here shows EWSR1-FLI1 binding to GGAA repeat regions recruiting KDM6A to demethylate histone H3K27me3 at these sites. This would facilitate acetylation of this residue by p300, leading to chromatin opening and transcriptional activation. Although RING1B, is normally enriched together with EZH2 at transcriptionally repressed regions decorated with H3K27me3, in the model presented here is also recruited to active genomic sites, such as in the EWSR1-FLI1–containing KDM6A complexes. Once there, it directly interacts with the fusion oncoprotein and helps its recruitment to these sites. (Created with Biorender.com)

KDM6A, as part of the COMPASS-like complex, mediates transcriptional activation of *HOX* genes during development (Agger et al., 2007; Van der Meulen et al., 2014). Posterior *HOX* genes, and in particular *HOXD13*, are markedly overexpressed in ES cells and maintain the oncogenic phenotype of ES proliferation, invasion and metastasis (Svoboda

et al., 2014; von Heyking et al., 2016). Upon introduction of the fusion oncogene, these sites are reported to lose H3K27me3, followed by a gain in H3K4me3 that correlates with transcriptional activation (Svoboda et al., 2014). MLL1, which is highly expressed in ES, works together with MEN1, a scaffolding protein of the complex, to contribute to the persistent overexpression of the *HOXD* genes (Svoboda et al., 2017). Accordingly, our ChIP-seq data reveal KDM6A enrichment at the *HOXD* loci with EZH2 completely absent from these regions (data not shown); furthermore, the opposite pattern was observed for the anterior *HOX* loci, e.g. *HOXA* (data not shown), which were described to be repressed upon overexpression of EWSR1-FLI1 (Svoboda et al., 2014). These loci were consistently devoid of KDM6A binding but enriched in EZH2. Therefore, our observations suggest that KDM6A might be part of the transcriptional-activating MLL complex described to be recruited at *HOXD* loci to activate transcription in ES.

Our work revealed that genetic targeting of KDM6A through shRNA causes profound defects in the expression of EWSR1-FLI1 targets (see **Figure IV. 20 A-B** from Results in Section IV). Although further studies are needed to elucidate to which extent lack of KDM6A compromises ES cell growth, these results further highlight the importance of inhibiting this demethylase in this tumour.

Emerging evidence has described a demethylase-independent role for KDM6A in stem cell homeostasis and developmental processes (Shpargel et al., 2012; Shpargel et al., 2014; Wang et al., 2012). In ESC, a crosstalk between KDM6A, MLL4 and p300 at enhancers has been reported, where KDM6A might recruit these proteins independently of its demethylating activity. At these regions, KDM6A might facilitate the conversion of an inactive to an active state of the enhancer, i.e. gaining H3K4me1 and H3K27ac marks at these regions (Wang et al., 2017). In this regard, further experiments are needed to address whether demethylation and demethylation-independent roles of KDM6A coexist in ES. We cannot rule out a demethylation-independent role of this demethylase in ES, given that (i) some EWSR1-FLI1–activated targets bound by KDM6A in ChIP-seq still contain H3K27me3 in the hpMSC upon transformation (data not shown); (ii) decreases on gene expression in EWSR1-FLI1–activated targets upon KDM6A knockdown is apparently associated to a moderate gain on the overall levels of H3K27me3 (see **Figure IV. 20 C** from Results in Section IV); and (iii) considering that we observe a prominent loss of H3K27me3 at the promoter regions, and that KDM6A is principally enriched at genic and intergenic regions, this is suggestive of a demethylase-independent role at regulatory regions such as enhancers (see **Figure IV. 14 B and 17 B** from Results in Section IV). In fact, we are currently evaluating whether levels of H3K27me3 are locally gained in EWSR1-FLI1–activated targets upon KDM6A knockdown to elucidate whether downregulation of these targets is related to the demethylating activity of the protein. Furthermore, some EWSR1-FLI1–activated targets that are downregulated upon KDM6A knockdown are not

bound by the demethylase at least on its promoter or enhancer region (see **Figures IV. 18 D** and **20B** from Results in Section IV). RNA-seq data as well as ChIP-seq of H3K27me3 upon KDM6A knockdown might help elucidate this point, which is still an ongoing work.

In summary, all evidence presented here indicates that targeting KDM6A is a promising strategy to test in ES.

7. Modulation of the aberrant H3K27me3 positioning in ES cells by GSK126 and GSK-J4

Deregulated H3K27me3 levels have been demonstrated in a variety of human cancers through genetic hits, altering the machinery responsible for H3K27me3 turnover (Martinez-Garcia and Licht, 2010). In this work, we show a required redistribution of H3K27me3 during ES tumorigenesis that does not occur in a random manner as it leads to a gain or a loss of this mark in important targets of EWSR1-FLI1.

We observed that inhibition of EZH2 alone with either GSK126 or EPZ6438 does not compromise survival of ES cells (see **Figure IV. 23 A** from Results in Section IV), indicating the solely removal of H3K27me3 from enriched regions, e.g. the gene body, does not translate into a cytotoxic response. Emerging evidence in literature reveals a subset of cancers harbouring inactivating mutations in components of SWI/SNF complexes that display epigenetic dependency on EZH2 (Januario et al., 2017; Kim et al., 2014). Thus, targeting EZH2 in these tumours has been reported to be an effective therapeutic strategy. A paradigmatic example in paediatric cancers is found in malignant rhabdoid tumours, where inhibition of EZH2 was shown as a successful cytotoxic strategy, coinciding with an inactivating mutation in a component of the SWI/SNF complex, *SMARCB1*. Moreover, EZH2 in these tumours displays an altered genomic occupancy with high H3K27me3, leading to the repression of lineage-specific targets (Knutson et al., 2013; Unland et al., 2015). Although EZH2 has been reported to repress neuroectodermal lineage genes in ES (Richter et al., 2009), mutations in *SMARCB1* or other members of the SWI/SNF complex have not been identified (Crompton et al., 2014). These tumours indeed depend on recruiting the BAF complex by EWSR1-FLI1 to tumour-specific enhancers to subsequently promote gene activation (Boulay et al., 2017). We thus argue that the failure of EZH2 inhibitors as an effective anticancer strategy in ES is consistent with the necessary activity of components of the SWI/SNF complex reported. Nevertheless, inhibition of EZH2 in ES has been recently demonstrated to be a potentially successful strategy when combined with other therapies. For instance to upregulate the levels of GD2, a cell-

surface ganglioside with restricted and low-level tissue expression, as an immune target for chimeric antigen receptors T cells (Kailayangiri et al., 2019).

Previous studies in T-ALL, urothelial bladder carcinoma, multiple myeloma and lung cancer have described that loss of function mutations in KDM6A lead to higher levels of H3K27me3 compared to wild type tumours and an increased sensitivity to EZH2 inhibitors (Ezponda et al., 2017; Ler et al., 2017; van der Meulen et al., 2015; Wu et al., 2018). In agreement with these data, our work demonstrates that inhibition of KDM6A with GSK-J4 treatment results in an increased sensitivity to EZH2 inhibitors, triggering a synergistic response that is cytotoxic in ES cells (see **Figure IV. 24** from Results in Section IV).

Indeed, in this thesis, we demonstrate that dual targeting of KDM6A and EZH2 causes a decrease of H3K27me3 that is not as profound as compared to GSK126 alone (see **Figure IV. 23 E** from Results in Section IV), further supporting our hypothesis that maintaining H3K27me3 homeostasis is critical in ES. In agreement with this, a recent study has shown that inhibition of the SWI/SNF complex by trabectedin strongly imbalances the distribution of H3K27me3 in ES cells. The study by Harlow et al. (2019), using trabectedin, shows how the eviction of the SWI/SNF complex by the drug causes loss of cell viability and an accumulation of H3K27me3 at the TSS of EWSR1-FLI1 target genes.

Our data suggest H3K27me3 loss in promoters during ES oncogenesis (see **Figure IV. 18 B** from Results in Section IV) is a key event in the chromatin remodelling process infringed by the oncogene. Considering all this evidence, we propose that a proper balance of H3K27me3, maintained by the coordinating activity of EZH2 and KDM6A, is critical for ES cells to survive. In other words, the ES epigenome must retain the enzymatic activity of EZH2 to key repressed promoters, while in transcriptionally active regions (e.g. enhancer-activated EWSR1-FLI1 targets), the demethylating activity of KDM6A is essential. Our results indicate that perturbation of this balance with both GSK126 and GSK-J4 tilts H3K27me3 balance in favour of a global loss of the mark, associated to an increased apoptosis (see **Figure IV. 23 E and IV. 24** from Results in section IV). Accordingly, we suggest that double treatment causes local changes of H3K27me3 distribution on EZH2 and KDM6A target regions that reactivate differentiation genes repressed by EZH2, as well as repress EWSR1-FLI1-activated targets bound by KDM6A, inducing apoptosis. We hence speculate that both targeting of the active and repressive states in ES is fundamental for the cell to survive. These observations are summarized in the model presented in **Figure V. 3**.

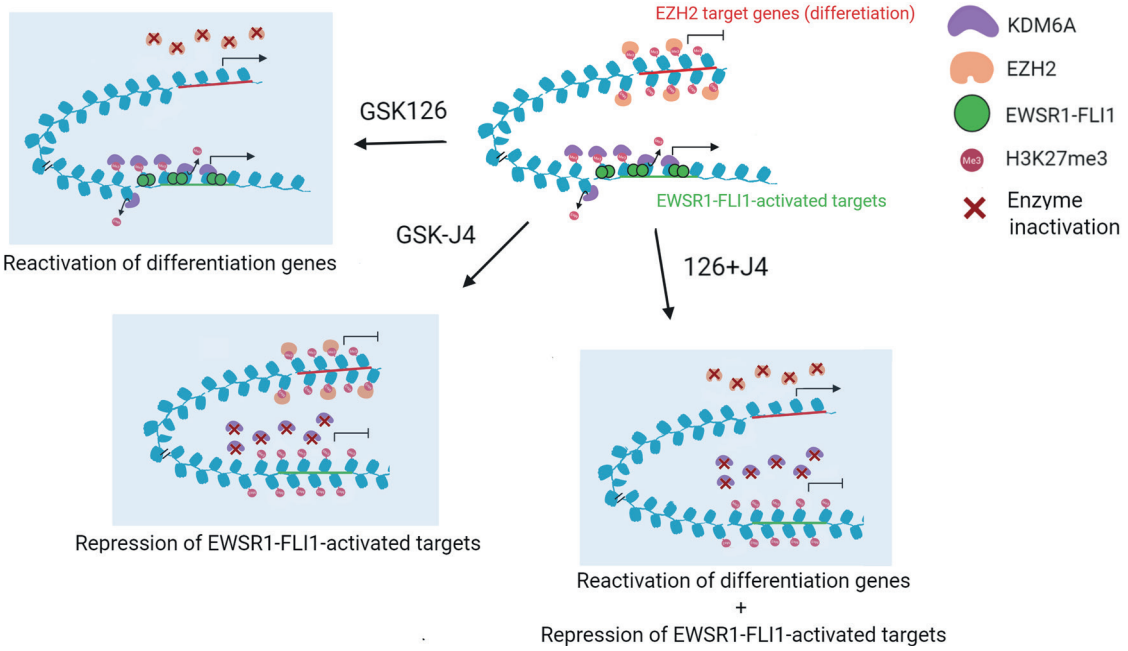

FIGURE V. 3 ***Perturbation of the H3K27me3 balance by GSK126 and GSK-J4 in ES cells.***
We here show a model in which KDM6A and EZH2 maintain a tumorigenic state of ES cells throughout deregulation of H3K27me3 distribution. EZH2-rich regions are repressed differentiation genes decorated with H3K27me3, while EWSR1-FLI1–activated targets are transcriptionally active due to the activity of KDM6A demethylase, and hence these regions lack this histone mark. Inhibition of EZH2 enzymatic activity throughout GSK126 would turn differentiation genes activated, which is associated with reduced global levels of H3K27me3. However, this is not sufficient to induce apoptosis in ES cells; what is critical for ES cells to survive is the inhibition of KDM6A demethylase by GSKJ4, causing repression of EWSR1-FLI1–activated targets with a moderate increase in overall levels of H3K27me3. The combination of the two inhibitors is highly efficient to cause a cytotoxic effect on ES cells, as distribution of H3K27me3 is highly perturbed causing both repression of EWSR1-FLI1-activated targets and reactivation of differentiation genes. This is associated to a decrease in the overall levels of this mark in ES cells (which is not as profound as that of GSK126 alone). Therefore, we suggest that targeting the "tumorigenic distribution" of H3K27me3 is a possible therapeutic strategy in ES. (Created with Biorender.com)

Targeting tumorigenic balance of the H3K27me3 writer and eraser through GSK126 and GSK-J4 inhibitors perturbs the oncogenic advantage of ES cells. Several general inhibitors of the JmjC-containing domain demethylases family, including GSK-J4, have been developed in the last decade. However, these inhibitors are selective against some or all JmjC enzymes but are unable to target one specific JmjC member (Van der Meulen et al., 2014). Even though the antitumor activity of GSK-J4 in preclinical studies in brainstem gliomas correlates with an increase of H3K27me3 levels (Hashizume et al., 2014), this inhibitor additionally perturbs several histone demethylase subfamilies beyond KDM6 family *in vitro* and *in vivo* (Heinemann et al., 2014). In this thesis, we demonstrate a slight increase on the overall levels of H3K27me3 in ES cells treated with GSK-J4, similar to data published by other groups in DIPG or in AML cells treated with this drug (Hashizume et al., 2014; Li et al., 2018). Further experiments are now needed to elucidate whether other histone modifications regulated by other JmjC-subfamilies, e.g. H3K36me3 or H3K79me3, are altered with GSK-J4 in ES cells.

8. KDM6A escapes X-inactivation in ES, rendering differences in ES cell lines to response to GSK-J4

X-inactivation ensures that females have only one functional copy of the genes expressed by this chromosome to produce the same dosage as in males. Genes outside of the pseudoautosomal region of the X-chromosome can escape from X-inactivation, resulting in the expression of two copies in females and one copy in males. Previous reports have identified that mutations in tumour suppressor genes that escape from X-chromosome inactivation (known as EXITS genes) affords females enhanced cancer protection, which substantively contributes to the higher incidence observed for some tumours in males (Dunford et al., 2015; Dunford et al., 2017; Snell and Turner, 2018).

The X-chromosome location of KDM6A has identified this demethylase as one of the genes that escapes from X-chromosome inactivation (Greenfield et al., 1998). Moreover it has been recently shown that KDM6A is implicated in sexual dimorphism diseases, including some cancers and X-linked intellectual disabilities (Dunford et al., 2015; Snell and Turner, 2018). ES has a sex bias, being predominantly more frequent in males than in females (Paulussen et al., 2008). In this thesis, we discerned two groups of ES tumours according to KDM6A expression (see **Figure IV. 16 C-D** from Results in Section IV). Moreover, we observed that sex was statistically associated to KDM6A expression, with males showing a lower expression of KDM6A than females. Therefore, we corroborate the X-inactivation scape for this demethylase in ES tumours and cell lines. In agreement with these observations, we found that only male-derived ES cell lines (i.e. SK-ES-1 and TC-71) responded to the KDM6A inhibitor GSK-J4, triggering an effective synergistic response to EZH2 inhibitors (see **Figure IV. 23 B and 24** from Results in Section IV). Consistently, we observe a complete lack of response to GSK-J4, not only in A673, but also in A4573 and TC252, which are all female-derived ES cell lines (data not shown for the last two cell lines). We therefore speculate that, as male-derived ES cell lines express fewer copies of KDM6A, they are more sensitive to the GSK-J4 inhibitor at lower concentrations than female-derived cell lines, which show a more resistant pattern (**Figure V. 4**). Considering that response to EZH2 inhibitors is highly dependent on the effectiveness of KDM6A inhibition, the aforementioned female ES cell lines were resistant to the dual treatment. Further experiments are needed to explore the extent of this rationale in other male-derived ES cell lines, such as RDES or RW8.

Loss-of-function mutations in KDM6A have been identified in male cancers across multiple subtypes, including urothelial carcinoma, T-ALL, pancreatic cancer, B-cell lymphoma, and medulloblastoma (Andricovich et al., 2018; Li et al., 2018; Robinson et al., 2012; van der Meulen et al., 2015). Moreover, this demethylase was described as a tumour suppressor in the 299-cancer driver list of genes from human cancer genome studies (Bailey et al., 2018).

Furthermore, inactivating mutations of KDM6A have additionally been reported in the context of X-linked intellectual disability (XLID) and the developmental disorder Kabuki syndrome (Adam and Hudgins, 2005), where males harbouring mutations in KDM6A show more severe phenotypes than females (Lederer et al., 2012; Miyake et al., 2013). All these data point the EXITS model for KDM6A as a tumour suppressor gene in these malignancies. Although we observe an X-inactivation escape for this demethylase in ES, KDM6A might not play a tumour suppressive role here, as (i) whole genome sequencing studies published by Crompton et al. (2014) reveal the absence of recurrent mutations in KDM6A in ES tumours or ES cell lines, (ii) in this thesis we describe that EWSR1-FLI1 and KDM6A colocalize genome-wide, and (iii) knockdown of the demethylase downregulates key EWSR1-FLI1-activated targets, possibly due to a lack of H3K27me3 demethylating activity. Thus, we propose that KDM6A has an oncogenic role in ES, although the extent of its tumorigenicity has to be yet elucidated.

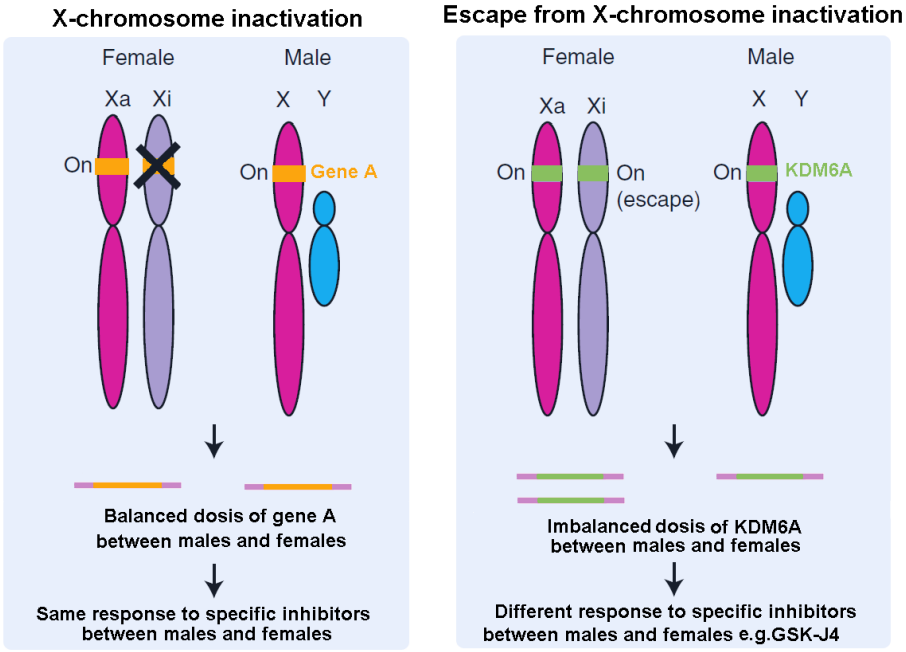

FIGURE V. 4 ***Gender bias association to KDM6A and sensitivity to GSKJ4 explained by an escape from X-inactivation chromosome inactivation in ES.***
X-chromosome inactivation in females ensures dosage compensation of genes located in the X-chromosome (namely gene A (orange)) compared to males. Then, the dose of such gene A might be equal between males and females and thus we would expect no gender effect on the response to inhibitors targeting the underlying gene product (left panel). However, in some situations some genes can escape from such X-chromosome inactivation leading to the opposite scenario. For example, KDM6A (green) has an imbalanced dose in males and females, with females having a highest amount. Thus, we suggest that given the differences on the number of transcripts, these would be also reflected at a protein level leading to sex-related differences on the response to specific inhibitors. Consistent with this hypothesis, we observed that male derived ES cell lines (SK-ES-1 and TC-71) are more sensitive towards GSK-J4 and female-derived cells such as A673 have a more resistant phenotype. Xa (pink chromosome) and Xi (purple chromosome) indicate active and inactive chromosome X, respectively. The Y chromosome is indicated in blue. Framed orange and green area in chromosomes represent location of gene A and KDM6A, respectively. Adapted from Dunford et al. (2017).

9. Thesis main points at a glance

To conclude, ES tumorigenicity is dependent on continued overexpression of PcG members of both PRC1 and PRC2 complexes such as BMI1 and EZH2, respectively (Douglas et al., 2008; Hsu and Lawlor, 2011; Richter et al., 2009; Riggi et al., 2008). The mechanistic basis of such dependency is based on the repressive function of EZH2 on the neuroectodermal and endothelial differentiation (Richter et al., 2009) and the stemness maintenance mediated by BMI1 that is independent of *CDKN2A* repression (Douglas et al., 2008). In this thesis, we have contributed to understanding EZH2-mediated repression in ES. We show this PcG protein exerts most of the repression indirectly from EWSR1-FLI1 with a strong association with the H3K27me3 gain observed in hpMSC overexpressing the fusion oncoprotein. Previous data from our group has shown that RING1B, the enzymatic subunit of PRC1, is highly expressed in ES (Hernandez-Muñoz et al., 2016), and that it also cooperates in an E3-ligase independent manner with EWSR1-FLI1 to activate enhancers (Sánchez-Molina et al., 2019). We show here that RING1B is necessary for ES tumorigenesis and provide a mechanistic insight throughout modulation *in vitro* and *in vivo* of RING1B protein levels by MLN4924. We demonstrate an eviction of EWSR1-FLI1 from activated regions that coincides with a perturbed recruitment of RING1B at these sites by MLN4924 treatment, with moderate transcriptional effects.

In this work, we additionally prove that the KDM6A demethylase might be another interacting partner of EWSR1-FLI1 in transcriptionally active regions. Given the evidence in melanoma that RING1B recruits this demethylase together with p300 to H3K27me3-rich regions (Rai et al., 2015), we speculate that KDM6A is possibly recruited in the same complexes as RING1B in ES cells. In this regard, H3K27me3 is redistributed in ES tumorigenesis in a coordinated manner through the activity of KDM6A and EZH2. Finally, we show that disruption of the enzymatic activities by GSK126 and GSK-J4 deregulates the equilibrium of H3K27me3, triggering a synergistic cytotoxic response especially effective in male-derived ES cell lines. Overall, these data demonstrate the promise of rationally designed combinations of epigenetic-targeted therapy in ES.

VI. CONCLUSIONS

In this thesis, we provide further insight into the importance of studying the epigenetic mechanisms underlying EWSR1-FLI1–mediated transformation in ES to reveal promising therapeutic targets for future clinical trials that could improve patient outcome. Collectively, our results highlight targeting the novel transactivation roles of RING1B in ES with a NEDD8 inhibitor such as MLN4924, as well as blocking the enzymes responsible for the aberrant settling of H3K27me3, i.e. EZH2 and KDM6A. The main conclusions of this work are summarized as follows:

Aim 1:

1. Genetic depletion of RING1B with an shRNA in ES xenografts delays tumour growth and is associated with a less proliferative state.

Aim 2:

1. MLN4924 decreases RING1B, especially at the protein level, *in vitro* and *in vivo*, likely by inhibiting its neddylation and triggering its degradation.
2. MLN4924 treatment is associated with a loss of RING1B binding at EWSR1-FLI1–activated targets and concurs with an eviction of the fusion oncogene from these regions. This correlates with moderate gene expression changes.

Aim 3:

1. Overall levels of H3K27me3 are maintained upon EWSR1-FLI1 transformation in hpMSCs or HUVECs, indicating a redistribution process of this mark during ES tumorigenesis.
2. EWSR1-FLI1–activated targets are largely decorated with H3K27me3 mark in a putative cell-of-origin of ES, such as hpMSCs.
3. hpMSC models that overexpress EWSR1-FLI1 present a redistribution of H3K27me3, with a gain in the promoter and gene body of known repressed targets of the fusion oncoprotein, and a loss in activated targets.
4. KDM6A is highly expressed in ES tumors and is recruited to EWSR1-FLI1–activated targets, likely interacting with EWSR1-FLI1 in ES cell lines.
5. EZH2 shows independent binding of EWSR1-FLI1, mediating part of the indirect repression imposed by the fusion oncoprotein in ES cell lines.
6. EZH2 and KDM6A knockdown revert the repressed and active expression states of EWSR1-FLI1 targets, respectively, with EZH2 depletion causing a severe decrease on the overall levels of H3K27me3.

Aim 4:

1. ES cells show resistance to the EZH2 inhibitor GSK126, despite triggering a profound decrease of the overall levels of H3K27me3.
2. ES cell lines show heterogeneous sensitivity pattern towards GSK-J4, possibly by

the gender bias affecting the amount of KDM6A.

3. GSK-J4 sensitizes ES cell lines to GSK126, causing a synergic cytotoxic effect that is strikingly dependent on cell response towards GSK-J4.
4. Dual targeting of the H3K27me3 writer and eraser throughout GSK126 and GSK-J4, respectively, decreases the overall levels of H3K27me3, which highlights the importance of an unbalanced distribution of this mark in ES.

VII. REFERENCES

Adam, M.P., and Hudgins, L. (2005). Kabuki syndrome: a review. Clin Genet 67, 209-219.
Agger, K., Cloos, P.A.C., Christensen, J., Pasini, D., Rose, S., Rappsilber, J., Issaeva, I., Canaani, E., Salcini, A.E., and Helin, K. (2007). UTX and JMJD3 are histone H3K27 demethylases involved in HOX gene regulation and development. Nature 449, 731-734.

Ahler, E., Sullivan, W.J., Cass, A., Braas, D., York, A.G., Bensinger, S.J., Graeber, T.G., and Christofk, H.R. (2013). Doxycycline alters metabolism and proliferation of human cell lines. PLoS One 8, e64561.

Allfrey, V.G., Faulkner, R., and Mirsky, A.E. (1964). Acetylation and methylation of histones and their possible role in the regulation of RNA synthesis. Proc Natl Acad Sci U S A 51, 786-794.

Allis, C.D., and Jenuwein, T. (2016). The molecular hallmarks of epigenetic control. Nat Rev Genet 17, 487.

Alonso, L., Navarro-Perez, V., Sanchez-Muñoz, A., and Alba, E. (2014). Time to Diagnosis of Ewing Tumors in Children and Adolescents Is Not Associated With Metastasis or Survival. J Clin Oncol 32, 4020-4020.

Ambros, I.M., Ambros, P.F., Strehl, S., Kovar, H., Gadner, H., and Salzer-Kuntschik, M. (1991). MIC2 is a specific marker for Ewing's sarcoma and peripheral primitive neuroectodermal tumors. Evidence for a common histogenesis of Ewing's sarcoma and peripheral primitive neuroectodermal tumors from MIC2 expression and specific chromosome aberration. Cancer 67, 1886-1893.

Amerik, A.Y., and Hochstrasser, M. (2004). Mechanism and function of deubiquitinating enzymes. Biochim Biophys Acta 1695, 189-207.

Anderson, N.D., de Borja, R., Young, M.D., Fuligni, F., Rosic, A., Roberts, N.D., Hajjar, S., Layeghifard, M., Novokmet, A., Kowalski, P.E., et al. (2018). Rearrangement bursts generate canonical gene fusions in bone and soft tissue tumors. Science 361, eaam8419.

Anderson, P.M., Bielack, S.S., Gorlick, R.G., Skubitz, K., Daw, N.C., Herzog, C.E., Monge, O.R., Lassaletta, A., Boldrini, E., Pápai, Z., et al. (2016). A phase II study of clinical activity of SCH 717454 (robatumumab) in patients with relapsed osteosarcoma and Ewing sarcoma. Pediatr Blood Cancer 63, 1761-1770.

Anderton, J.A., Bose, S., Vockerodt, M., Vrzalikova, K., Wei, W., Kuo, M., Helin, K., Christensen, J., Rowe, M., Murray, P.G., et al. (2011). The H3K27me3 demethylase,

KDM6B, is induced by Epstein–Barr virus and over-expressed in Hodgkin's Lymphoma. Oncogene 30, 2037-2043.

Andricovich, J., Perkail, S., Kai, Y., Casasanta, N., Peng, W., and Tzatsos, A. (2018). Loss of KDM6A Activates Super-Enhancers to Induce Gender-Specific Squamous-like Pancreatic Cancer and Confers Sensitivity to BET Inhibitors. Cancer Cell 33, 512-526.e518.

Aranda, S., Mas, G., and Di Croce, L. (2015). Regulation of gene transcription by Polycomb proteins. Sci Adv 1, e1500737.

Ardley, H.C., and Robinson, P.A. (2005). E3 ubiquitin ligases. Essays Biochem 41, 15-30.

Arents, G., and Moudrianakis, E.N. (1995). The histone fold: a ubiquitous architectural motif utilized in DNA compaction and protein dimerization. Proc Natl Acad Sci U S A 92, 11170-11174.

Aubin, S. (2011). What Should the Age Range Be for AYA Oncology? J Adolesc Young Adult Oncol 1, 3-10.

Aurias, A., Rimbaut, C., Buffe, D., Zucker, J.-M., and Mazabraud, A. (1984). Translocation involving chromosome 22 in Ewing's Sarcoma. A cytogenetic study of four fresh tumors. Cancer Genet Cytogenet 12, 21-25.

Ayton, P.M., and Cleary, M.L. (2001). Molecular mechanisms of leukemogenesis mediated by MLL fusion proteins. Oncogene 20, 5695-5707.

Bagatell, R., Norris, R., Ingle, A.M., Ahern, C., Voss, S., Fox, E., Little, A.R., Weigel, B.J., Adamson, P.C., and Blaney, S. (2014). Phase 1 trial of temsirolimus in combination with irinotecan and temozolomide in children, adolescents and young adults with relapsed or refractory solid tumors: a Children's Oncology Group Study. Pediatr Blood Cancer 61, 833-839.

Bailey, M.H., Tokheim, C., Porta-Pardo, E., Sengupta, S., Bertrand, D., Weerasinghe, A., Colaprico, A., Wendl, M.C., Kim, J., Reardon, B., et al. (2018). Comprehensive Characterization of Cancer Driver Genes and Mutations. Cell 173, 371-385.

Bailly, R.A., Bosselut, R., Zucman, J., Cormier, F., Delattre, O., Roussel, M., Thomas, G., and Ghysdael, J. (1994). DNA-binding and transcriptional activation properties of the EWS-FLI-1 fusion protein resulting from the t(11;22) translocation in Ewing sarcoma. Mol Cell Biol 14, 3230-3241.

Banaszynski, L.A., Allis, C.D., and Lewis, P.W. (2010). Histone variants in metazoan development. Dev Cell 19, 662-674.

Banerjee, T., and Chakravarti, D. (2011). A peek into the complex realm of histone phosphorylation. Mol Cell Biol 31, 4858-4873.

Banito, A., Li, X., Laporte, A.N., Roe, J.S., Sanchez-Vega, F., Huang, C.H., Dancsok, A.R., Hatzi, K., Chen, C.C., Tschaharganeh, D.F., et al. (2018). The SS18-SSX Oncoprotein Hijacks KDM2B-PRC1.1 to Drive Synovial Sarcoma. Cancer Cell 33, 527-541.

Bannister, A.J., and Kouzarides, T. (2011). Regulation of chromatin by histone modifications. Cell Res 21, 381-395.

Barkauskaite, E., Jankevicius, G., and Ahel, I. (2015). Structures and Mechanisms of Enzymes Employed in the Synthesis and Degradation of PARP-Dependent Protein ADP-Ribosylation. Mol Cell 58, 935-946.

Barretina, J., Caponigro, G., Stransky, N., Venkatesan, K., Margolin, A.A., Kim, S., Wilson, C.J., Lehár, J., Kryukov, G.V., Sonkin, D., et al. (2012). The Cancer Cell Line Encyclopedia enables predictive modelling of anticancer drug sensitivity. Nature 483, 603.

Bate-Eya, L.T., Gierman, H.J., Ebus, M.E., Koster, J., Caron, H.N., Versteeg, R., Dolman, M.E.M., and Molenaar, J.J. (2017). Enhancer of zeste homologue 2 plays an important role in neuroblastoma cell survival independent of its histone methyltransferase activity. Eur J Cancer 75, 63-72.

Baylin, S.B., Höppener, J.W.M., de Bustros, A., Steenbergh, P.H., Lips, C.J.M., and Nelkin, B.D. (1986). DNA Methylation Patterns of the Calcitonin Gene in Human Lung Cancers and Lymphomas. Cancer Res 46, 2917-2922.

Bayliss, J., Mukherjee, P., Lu, C., Jain, S.U., Chung, C., Martinez, D., Sabari, B., Margol, A.S., Panwalkar, P., Parolia, A., et al. (2016). Lowered H3K27me3 and DNA hypomethylation define poorly prognostic pediatric posterior fossa ependymomas. Sci Transl Med 8, 366ra161.

Beck, R., Monument, M.J., Watkins, W.S., Smith, R., Boucher, K.M., Schiffman, J.D., Jorde, L.B., Randall, R.L., and Lessnick, S.L. (2012). EWS/FLI-responsive GGAA microsatellites exhibit polymorphic differences between European and African populations. Cancer Genet 205, 304-312.

Becker, P.B., and Workman, J.L. (2013). Nucleosome remodeling and epigenetics. Cold Spring Harb Perspect Biol 5, a017905.

Becroft, D., Pearson, A., Shaw, R.L., and Zwi, L.J. (1984). Chromosome Translocation in Extraskeletal Ewing's Tumour. Lancet 2, 324-400.

Ben-Saadon, R., Zaaroor, D., Ziv, T., and Ciechanover, A. (2006). The Polycomb Protein Ring1B Generates Self Atypical Mixed Ubiquitin Chains Required for Its In Vitro Histone H2A Ligase Activity. Mol Cell 24, 701-711.

Bender, S., Tang, Y., Lindroth, A.M., Hovestadt, V., Jones, D.T.W., Kool, M., Zapatka, M., Northcott, P.A., Sturm, D., Wang, W., et al. (2013). Reduced H3K27me3 and DNA Hypomethylation Are Major Drivers of Gene Expression in K27M Mutant Pediatric High-Grade Gliomas. Cancer Cell 24, 660-672.

Benyoucef, A., Palii, C.G., Wang, C., Porter, C.J., Chu, A., Dai, F., Tremblay, V., Rakopoulos, P., Singh, K., Huang, S., et al. (2016). UTX inhibition as selective epigenetic therapy against TAL1-driven T-cell acute lymphoblastic leukemia. Genes Dev 30, 508-521.

Berdasco, M., and Esteller, M. (2013). Genetic syndromes caused by mutations in epigenetic genes. Hum Genet 132, 359-383.

Bernstein, B.E., Mikkelsen, T.S., Xie, X., Kamal, M., Huebert, D.J., Cuff, J., Fry, B., Meissner, A., Wernig, M., Plath, K., et al. (2006). A Bivalent Chromatin Structure Marks Key Developmental Genes in Embryonic Stem Cells. Cell 125, 315-326.

Bernstein, E., and Hake, S.B. (2006). The nucleosome: a little variation goes a long way. Biochem Cell Biol 84, 505-507.

Bid, H.K., Phelps, D.A., Xaio, L., Guttridge, D.C., Lin, J., London, C., Baker, L.H., Mo, X., and Houghton, P.J. (2016). The Bromodomain BET Inhibitor JQ1 Suppresses Tumor Angiogenesis in Models of Childhood Sarcoma. Mol Cancer Ther 15, 1018-1028.

Bilke, S., Schwentner, R., Yang, F., Kauer, M., Jug, G., Walker, R.L., Davis, S., Zhu, Y.J., Pineda, M., Meltzer, P.S., et al. (2013). Oncogenic ETS fusions deregulate E2F3 target genes in Ewing sarcoma and prostate cancer. Genome Res 23, 1797-1809.

Bird, A. (2007). Perceptions of epigenetics. Nature 447, 396-398.

Black, Joshua C., Van Rechem, C., and Whetstine, Johnathan R. (2012). Histone Lysine

Methylation Dynamics: Establishment, Regulation, and Biological Impact. Mol Cell 48, 491-507.

Blanco-García, N., Asensio-Juan, E., de la Cruz, X., and Martínez-Balbás, M.A. (2009). Autoacetylation Regulates P/CAF Nuclear Localization. J Biol Chem 284, 1343-1352.

Bochyńska, A., Lüscher-Firzlaff, J., and Lüscher, B. (2018). Modes of Interaction of KMT2 Histone H3 Lysine 4 Methyltransferase/COMPASS Complexes with Chromatin. Cells 7, 17.

Bosch, A., Panoutsopoulou, K., Corominas, J.M., Gimeno, R., Moreno-Bueno, G., Martín-Caballero, J., Morales, S., Lobato, T., Martínez-Romero, C., Farias, E.F., et al. (2014). The Polycomb group protein RING1B is overexpressed in ductal breast carcinoma and is required to sustain FAK steady state levels in breast cancer epithelial cells. Oncotarget 5, 2065-2076.

Boulay, G., Sandoval, G.J., Riggi, N., Iyer, S., Buisson, R., Naigles, B., Awad, M.E., Rengarajan, S., Volorio, A., McBride, M.J., et al. (2017). Cancer-Specific Retargeting of BAF Complexes by a Prion-like Domain. Cell 171, 163-178.

Boulay, G., Volorio, A., Iyer, S., Broye, L.C., Stamenkovic, I., Riggi, N., and Rivera, M.N. (2018). Epigenome editing of microsatellite repeats defines tumor-specific enhancer functions and dependencies. Genes Dev 32, 1008-1019.

Bowers, E.M., Yan, G., Mukherjee, C., Orry, A., Wang, L., Holbert, M.A., Crump, N.T., Hazzalin, C.A., Liszczak, G., Yuan, H., et al. (2010). Virtual ligand screening of the p300/CBP histone acetyltransferase: identification of a selective small molecule inhibitor. Chem Biol 17, 471-482.

Braun, B.S., Frieden, R., Lessnick, S.L., May, W.A., and Denny, C.T. (1995). Identification of target genes for the Ewing's sarcoma EWS/FLI fusion protein by representational difference analysis. Mol Cell Biol 15, 4623-4630.

Brenner, J.C., Feng, F.Y., Han, S., Patel, S., Goyal, S.V., Bou-Maroun, L.M., Liu, M., Lonigro, R., Prensner, J.R., Tomlins, S.A., et al. (2012). PARP-1 inhibition as a targeted strategy to treat Ewing's sarcoma. Cancer Res 72, 1608-1613.

Brohl, A.S., Solomon, D.A., Chang, W., Wang, J., Song, Y., Sindiri, S., Patidar, R., Hurd, L., Chen, L., Shern, J.F., et al. (2014). The genomic landscape of the Ewing Sarcoma family of tumors reveals recurrent STAG2 mutation. PLoS Genet 10, e1004475.

Brownhill, S.C., Taylor, C., and Burchill, S.A. (2007). Chromosome 9p21 gene copy number and prognostic significance of p16 in ESFT. Br J Cancer 96, 1914-1923.

Burningham, Z., Hashibe, M., Spector, L., and Schiffman, J.D. (2012). The epidemiology of sarcoma. Clin Sarcoma Res 2, 14.

Castillero-Trejo, Y., Eliazer, S., Xiang, L., Richardson, J.A., and Ilaria, R.L. (2005). Expression of the EWS/FLI-1 Oncogene in Murine Primary Bone-Derived Cells Results in EWS/FLI-1–Dependent, Ewing Sarcoma–Like Tumors. Cancer Res 65, 8698-8705.

Cavazzana, A.O., Miser, J.S., Jefferson, J., and Triche, T.J. (1987). Experimental evidence for a neural origin of Ewing's sarcoma of bone. The American journal of pathology 127, 507-518.

Chan, H.L., Beckedorff, F., Zhang, Y., Garcia-Huidobro, J., Jiang, H., Colaprico, A., Bilbao, D., Figueroa, M.E., LaCava, J., Shiekhattar, R., et al. (2018). Polycomb complexes associate with enhancers and promote oncogenic transcriptional programs in cancer through multiple mechanisms. Nat Commun 9, 3377.

Chan, K.M., Fang, D., Gan, H., Hashizume, R., Yu, C., Schroeder, M., Gupta, N., Mueller, S., James, C.D., Jenkins, R., et al. (2013). The histone H3.3K27M mutation in pediatric glioma reprograms H3K27 methylation and gene expression. Genes Dev 27, 985-990.

Chang, S., Yim, S., and Park, H. (2019). The cancer driver genes IDH1/2, JARID1C/ KDM5C, and UTX/ KDM6A: crosstalk between histone demethylation and hypoxic reprogramming in cancer metabolism. Exp Mol Med 51, 66.

Chen, H., Lin, R.J., Schiltz, R.L., Chakravarti, D., Nash, A., Nagy, L., Privalsky, M.L., Nakatani, Y., and Evans, R.M. (1997). Nuclear Receptor Coactivator ACTR Is a Novel Histone Acetyltransferase and Forms a Multimeric Activation Complex with P/CAF and CBP/p300. Cell 90, 569-580.

Chen, L., Alexe, G., Dharia, N.V., Ross, L., Iniguez, A.B., Conway, A.S., Wang, E.J., Veschi, V., Lam, N., Qi, J., et al. (2018). CRISPR-Cas9 screen reveals a MYCN-amplified neuroblastoma dependency on EZH2. J Clin Invest 128, 446-462.

Chi, P., Allis, C.D., and Wang, G.G. (2010). Covalent histone modifications--miswritten, misinterpreted and mis-erased in human cancers. Nat Rev Cancer 10, 457-469.

Cho, Y.J., Kim, S.H., Kim, E.K., Han, J.W., Shin, K.H., Hu, H., Kim, K.S., Choi, Y.D., Kim,

S., Lee, Y.H., et al. (2018). Prognostic implications of polycomb proteins ezh2, suz12, and eed1 and histone modification by H3K27me3 in sarcoma. BMC Cancer 18, 158.

Cho, Y.W., Hong, T., Hong, S., Guo, H., Yu, H., Kim, D., Guszczynski, T., Dressler, G.R., Copeland, T.D., Kalkum, M., et al. (2007). PTIP associates with MLL3- and MLL4-containing histone H3 lysine 4 methyltransferase complex. J Biol Chem 282, 20395-20406.

Chou, D.M., Adamson, B., Dephoure, N.E., Tan, X., Nottke, A.C., Hurov, K.E., Gygi, S.P., Colaiácovo, M.P., and Elledge, S.J. (2010). A chromatin localization screen reveals poly (ADP ribose)-regulated recruitment of the repressive polycomb and NuRD complexes to sites of DNA damage. Proc Natl Acad Sci U S A 107, 18475-18480.

Ciechanover, A. (1998). The ubiquitin-proteasome pathway: on protein death and cell life. EMBO J 17, 7151-7160.

Ciechanover, A., and Schwartz, A.L. (2004). The ubiquitin system: pathogenesis of human diseases and drug targeting. Biochim Biophys Acta 1695, 3-17.

Cironi, L., Riggi, N., Provero, P., Wolf, N., Suvà, M.-L., Suvà, D., Kindler, V., and Stamenkovic, I. (2008). IGF1 Is a Common Target Gene of Ewing's Sarcoma Fusion Proteins in Mesenchymal Progenitor Cells. PLoS One 3, e2634.

Cohen, I., Zhao, D., Bar, C., Valdes, V.J., Dauber-Decker, K.L., Nguyen, M.B., Nakayama, M., Rendl, M., Bickmore, W.A., Koseki, H., et al. (2018). PRC1 Fine-tunes Gene Repression and Activation to Safeguard Skin Development and Stem Cell Specification. Cell Stem Cell 22, 726-739.

Cooper, A., van Doorninck, J., Ji, L., Russell, D., Ladanyi, M., Shimada, H., Krailo, M., Womer, R.B., Hao-ru Hsu, J., Thomas, D., et al. (2011). Ewing Tumors That Do Not Overexpress BMI-1 Are a Distinct Molecular Subclass with Variant Biology: A Report from the Children's Oncology Group. Clin Cancer Res 17, 56-66.

Corujo, D., and Buschbeck, M. (2018). Post-Translational Modifications of H2A Histone Variants and Their Role in Cancer. Cancers (Basel) 10.

Cotterill, S.J., Ahrens, S., Paulussen, M., Jürgens, H.F., VoûteJ, P.A., Gadner, H., and Craft, A.W. (2000). Prognostic Factors in Ewing's Tumor of Bone: Analysis of 975 Patients From the European Intergroup Cooperative Ewing's Sarcoma Study Group. J Clin Oncol 18, 3108-3114.

Cozzio, A., Passegue, E., Ayton, P.M., Karsunky, H., Cleary, M.L., and Weissman, I.L. (2003). Similar MLL-associated leukemias arising from self-renewing stem cells and short-lived myeloid progenitors. Genes Dev 17, 3029-3035.

Cremer, T., and Cremer, C. (2001). Chromosome territories, nuclear architecture and gene regulation in mammalian cells. Nat Rev Genet 2, 292-301.

Creppe, C., Palau, A., Malinverni, R., Valero, V., and Buschbeck, M. (2014). A Cbx8-containing polycomb complex facilitates the transition to gene activation during ES cell differentiation. PLoS Genet 10, e1004851.

Crompton, B.D., Stewart, C., Taylor-Weiner, A., Alexe, G., Kurek, K.C., Calicchio, M.L., Kiezun, A., Carter, S.L., Shukla, S.A., Mehta, S.S., et al. (2014). The Genomic Landscape of Pediatric Ewing Sarcoma. Cancer Discov 4, 1326-1341.

Darnell, J.E. (2002). Transcription factors as targets for cancer therapy. Nat Rev Cancer 2, 740-749.

Dawson, Mark A., and Kouzarides, T. (2012). Cancer Epigenetics: From Mechanism to Therapy. Cell 150, 12-27.

de Alava, E., Lessnick, S.L., and Sorensen, P.H. (2013). Ewing Sarcoma. In WHO Classification of Tumours of Soft Tissue and Bone, C.D.M. Fletcher, J.A. Bridge, and P.C.W. Hogendoorn, et al., eds. (Lyon (France): IARC Press), pp. 305-309.

de Chadarevian, J.P., Vekemans, M., Seemayer, T. A., Whang-Peng, J., Triche, T. J., Knutsen, Miser, J., Israel, M.A. (1984). Reciprocal Translocation in Small-Cell Sarcomas. N Engl J Med 311, 1702-1703.

De Preter, K., Vandesompele, J., Heimann, P., Yigit, N., Beckman, S., Schramm, A., Eggert, A., Stallings, R.L., Benoit, Y., Renard, M., et al. (2006). Human fetal neuroblast and neuroblastoma transcriptome analysis confirms neuroblast origin and highlights neuroblastoma candidate genes. Genome Biol 7, R84.

De Santa, F., Totaro, M.G., Prosperini, E., Notarbartolo, S., Testa, G., and Natoli, G. (2007). The Histone H3 Lysine-27 Demethylase Jmjd3 Links Inflammation to Inhibition of Polycomb-Mediated Gene Silencing. Cell 130, 1083-1094.

Deans, C., and Maggert, K.A. (2015). What do you mean, "epigenetic"? Genetics 199, 887-896.

Delattre, O., Zucman, J., Plougastel, B., Desmaze, C., Melot, T., Peter, M., Kovar, H., Joubert, I., de Jong, P., Rouleau, G., et al. (1992). Gene fusion with an ETS DNA-binding domain caused by chromosome translocation in human tumours. Nature 359, 162-165.

Denslow, S.A., and Wade, P.A. (2007). The human Mi-2/NuRD complex and gene regulation. Oncogene 26, 5433-5438.

Di Croce, L., and Helin, K. (2013). Transcriptional regulation by Polycomb group proteins. Nat Struct Mol Biol 20, 1147-1155.

Dikic, I., Wakatsuki, S., and Walters, K.J. (2009). Ubiquitin-binding domains — from structures to functions. Nat Rev Mol Cell Biol 10, 659-671.

Dorigo, B., Schalch, T., Bystricky, K., and Richmond, T.J. (2003). Chromatin Fiber Folding: Requirement for the Histone H4 N-terminal Tail. J Mol Biol 327, 85-96.

Douglas, D., Hsu, J.H., Hung, L., Cooper, A., Abdueva, D., van Doorninck, J., Peng, G., Shimada, H., Triche, T.J., and Lawlor, E.R. (2008). BMI-1 promotes ewing sarcoma tumorigenicity independent of CDKN2A repression. Cancer Res 68, 6507-6515.

Dunford, A., Schumacher, S.E., Savova, V., Gimelbrant, A.A., Beroukhim, R., Lawrence, M.S., Getz, G., Weinstock, D.M., and Lane, A.A. (2015). Escape from X-Inactivation Tumor Suppressor (EXITS) Genes Are Associated with Excess Incidence of Cancer in Men. Blood 126, 3665-3665.

Dunford, A., Weinstock, D.M., Savova, V., Schumacher, S.E., Cleary, J.P., Yoda, A., Sullivan, T.J., Hess, J.M., Gimelbrant, A.A., Beroukhim, R., et al. (2017). Tumor-suppressor genes that escape from X-inactivation contribute to cancer sex bias. Nat Genet 49, 10-16.

Enchev, R.I., Schulman, B.A., and Peter, M. (2015). Protein neddylation: beyond cullin-RING ligases. Nat Rev Mol Cell Biol 16, 30-44.

Erkizan, H.V., Kong, Y., Merchant, M., Schlottmann, S., Barber-Rotenberg, J.S., Yuan, L., Abaan, O.D., Chou, T.H., Dakshanamurthy, S., Brown, M.L., et al. (2009). A small molecule blocking oncogenic protein EWS-FLI1 interaction with RNA helicase A inhibits growth of Ewing's sarcoma. Nat Med 15, 750-756.

Ernst, J., and Kellis, M. (2010). Discovery and characterization of chromatin states for systematic annotation of the human genome. Nat Biotechnol 28, 817-825.

Ewing, J. (1972). Diffuse endothelioma of bone. CA Cancer J Clin 22, 95-98.

Ezponda, T., Dupéré-Richer, D., Will, C.M., Small, E.C., Varghese, N., Patel, T., Nabet, B., Popovic, R., Oyer, J., Bulic, M., et al. (2017). UTX/KDM6A Loss Enhances the Malignant Phenotype of Multiple Myeloma and Sensitizes Cells to EZH2 inhibition. Cell Rep 21, 628-640.

Facchino, S., Abdouh, M., Chatoo, W., and Bernier, G. (2010). BMI1 Confers Radioresistance to Normal and Cancerous Neural Stem Cells through Recruitment of the DNA Damage Response Machinery. J Neurosci 30, 10096-10111.

Fadul, J., Bell, R., Hoffman, L.M., Beckerle, M.C., Engel, M.E., and Lessnick, S.L. (2015). EWS/FLI utilizes NKX2-2 to repress mesenchymal features of Ewing sarcoma. Genes Cancer 6, 129-143.

Falkenberg, K.J., and Johnstone, R.W. (2014). Histone deacetylases and their inhibitors in cancer, neurological diseases and immune disorders. Nat Rev Drug Discov 13, 673.

Fang, D., Gan, H., Cheng, L., Lee, J.H., Zhou, H., Sarkaria, J.N., Daniels, D.J., and Zhang, Z. (2018). H3.3K27M mutant proteins reprogram epigenome by sequestering the PRC2 complex to poised enhancers. eLife 7, e36696.

Fearon, E.R., and Vogelstein, B. (1990). A genetic model for colorectal tumorigenesis. Cell 61, 759-767.

Felsenfeld, G. (2014). A brief history of epigenetics. Cold Spring Harb Perspect Biol 6, a018200.

Filbin, M., and Monje, M. (2019). Developmental origins and emerging therapeutic opportunities for childhood cancer. Nat Med 25, 367-376.

Flotho, A., and Melchior, F. (2013). Sumoylation: A Regulatory Protein Modification in Health and Disease. Annu Rev Biochem 82, 357-385.

Ford, D.J., and Dingwall, A.K. (2015). The cancer COMPASS: navigating the functions of MLL complexes in cancer. Cancer Genet 208, 178-191.

Foulon, S., Brennan, B., Gaspar, N., Dirksen, U., Jeys, L., Cassoni, A., Claude, L., Seddon, B., Marec-Berard, P., Whelan, J., et al. (2016). Can postoperative radiotherapy be omitted in localised standard-risk Ewing sarcoma? An observational study of the Euro-E.W.I.N.G

group. Eur J Cancer 61, 128-136.

Fraga, M.F., Ballestar, E., Villar-Garea, A., Boix-Chornet, M., Espada, J., Schotta, G., Bonaldi, T., Haydon, C., Ropero, S., Petrie, K., et al. (2005). Loss of acetylation at Lys16 and trimethylation at Lys20 of histone H4 is a common hallmark of human cancer. Nat Genet 37, 391-400.

Franchi A., Pasquinelli, G., Cenacchi, G., Della Rocca, C., Gambini, C., Bisceglia, M., Martinelli, G.N., and Santucci, M. (2001). Immunohistochemical and ultrastructural investigation of neural differentiation in Ewing sarcoma/PNET of bone and soft tissues. Ultrastruct Pathol 25, 219-225.

Frangini, A., Sjöberg, M., Roman-Trufero, M., Dharmalingam, G., Haberle, V., Bartke, T., Lenhard, B., Malumbres, M., Vidal, M., and Dillon, N. (2013). The Aurora B Kinase and the Polycomb Protein Ring1B Combine to Regulate Active Promoters in Quiescent Lymphocytes. Mol Cell 51, 647-661.

Fraumeni, J.J.R., and Glass, A. (1970). Rarity of Ewing's sarcoma among U. S. Negro children. Lancet 295, 366-367.

Funato, K., Major, T., Lewis, P.W., Allis, C.D., and Tabar, V. (2014). Use of human embryonic stem cells to model pediatric gliomas with H3.3K27M histone mutation. Science 346, 1529-1533.

Fyodorov, D.V., Zhou, B.R., Skoultchi, A.I., and Bai, Y. (2018). Emerging roles of linker histones in regulating chromatin structure and function. Nat Rev Mol Cell Biol 19, 192-206.

Gangwal, K., Sankar, S., Hollenhorst, P.C., Kinsey, M., Haroldsen, S.C., Shah, A.A., Boucher, K.M., Watkins, W.S., Jorde, L.B., Graves, B.J., et al. (2008). Microsatellites as EWS/FLI response elements in Ewing's sarcoma. Proc Natl Acad Sci U S A 105, 10149-10154.

Gao, Z., Lee, P., Stafford, J.M., von Schimmelmann, M., Schaefer, A., and Reinberg, D. (2014). An AUTS2-Polycomb complex activates gene expression in the CNS. Nature 516, 349-354.

Garcia, C.B., Shaffer, C.M., Alfaro, M.P., Smith, A.L., Sun, J., Zhao, Z., Young, P.P., VanSaun, M.N., and Eid, J.E. (2012). Reprogramming of mesenchymal stem cells by the synovial sarcoma-associated oncogene SYT-SSX2. Oncogene 31, 2323-2334.

Gaspar, N., Hawkins, D.S., Dirksen, U., Lewis, I.J., Ferrari, S., Le Deley, M.C., Kovar, H., Grimer, R., Whelan, J., Claude, L., et al. (2015). Ewing Sarcoma: Current Management and Future Approaches Through Collaboration. J Clin Oncol 33, 3036-3046.

Geier, B., Kurmashev, D., Kurmasheva, R.T., and Houghton, P.J. (2015). Preclinical Childhood Sarcoma Models: Drug Efficacy Biomarker Identification and Validation. Front Oncol 5, 193.

Geisler, S.J., and Paro, R. (2015). Trithorax and Polycomb group-dependent regulation: a tale of opposing activities. Development 142, 2876.

GFP-Trap for Immunoprecipitation (IP) of GFP-fusion proteins (2018). Available at: https://resources.chromotek.com/gfp-immunoprecipitation-sample?hsCtaTracking=d1034753-43a8-4e7e-adb4-40abd7edd786%7Ce978e964-0a98-4a6c-9657-cf9cec17ef0a [Accessed August 15,2019]

Gierisch, M.E., Pedot, G., Walser, F., Lopez-Garcia, L.A., Jaaks, P., Niggli, F.K., and Schäfer, B.W. (2019). USP19 deubiquitinates EWS-FLI1 to regulate Ewing sarcoma growth. Sci Rep 9, 951.

Gierisch, M.E., Pfistner, F., Lopez-Garcia, L.A., Harder, L., Schäfer, B.W., and Niggli, F.K. (2016). Proteasomal Degradation of the EWS-FLI1 Fusion Protein Is Regulated by a Single Lysine Residue. J Biol Chem 291, 26922-26933.

Giles, K.A., Gould, C.M., Du, Q., Skvortsova, K., Song, J.Z., Maddugoda, M.P., Achinger-Kawecka, J., Stirzaker, C., Clark, S.J., and Taberlay, P.C. (2019). Integrated epigenomic analysis stratifies chromatin remodellers into distinct functional groups. Epigenetics Chromatin 12, 12.

Ginsberg, J.P., Alava, E.d., Ladanyi, M., Wexler, L.H., Kovar, H., Paulussen, M., Zoubek, A., Dockhorn-Dworniczak, B., Juergens, H., Wunder, J.S., et al. (1999). EWS-FLI1 and EWS-ERG Gene Fusions Are Associated With Similar Clinical Phenotypes in Ewing's Sarcoma. J Clin Oncol 17, 1809-1809.

Ginsberg, J.P., Goodman, P., Leisenring, W., Ness, K.K., Meyers, P.A., Wolden, S.L., Smith, S.M., Stovall, M., Hammond, S., Robison, L.L., et al. (2010). Long-term survivors of childhood Ewing sarcoma: report from the childhood cancer survivor study. J Natl Cancer Inst 102, 1272-1283.

Goldman, M. (2001). CpG Islands. In Encyclopedia of Genetics, S. Brenner, and J.H.

Miller, eds. (New York: Academic Press), p. 477.

Gollavilli, P.N., Pawar, A., Wilder-Romans, K., Natesan, R., Engelke, C.G., Dommeti, V.L., Krishnamurthy, P.M., Nallasivam, A., Apel, I.J., Xu, T., et al. (2018). EWS/ETS-Driven Ewing Sarcoma Requires BET Bromodomain Proteins. Cancer Res 78, 4760-4773.

Gordon, F., Luger, K., and Hansen, J.C. (2005). The Core Histone N-terminal Tail Domains Function Independently and Additively during Salt-dependent Oligomerization of Nucleosomal Arrays. J Biol Chem 280, 33701-33706.

Gorthi, A., Romero, J.C., Loranc, E., Cao, L., Lawrence, L.A., Goodale, E., Iniguez, A.B., Bernard, X., Masamsetti, V.P., Roston, S., et al. (2018). EWS-FLI1 increases transcription to cause R-loops and block BRCA1 repair in Ewing sarcoma. Nature 555, 387-391.

Greally, J.M. (2018). A user's guide to the ambiguous word epigenetics. Nat Rev Mol Cell Biol 19, 207-208.

Greaves, M. (2018). A causal mechanism for childhood acute lymphoblastic leukaemia. Nat Rev Cancer 18, 471-484.

Greenfield, A., Carrel, L., Pennisi, D., Philippe, C., Quaderi, N., Siggers, P., Steiner, K., Tam, P.P.L., Monaco, A.P., Willard, H.F., et al. (1998). The UTX Gene Escapes X Inactivation in Mice and Humans. Hum Mol Genet 7, 737-742.

Grobner, S.N., Worst, B.C., Weischenfeldt, J., Buchhalter, I., Kleinheinz, K., Rudneva, V.A., Johann, P.D., Balasubramanian, G.P., Segura-Wang, M., Brabetz, S., et al. (2018). The landscape of genomic alterations across childhood cancers. Nature 555, 321-327.

Gruenbaum, Y., Stein, R., Cedar, H., and Razin, A. (1981). Methylation of CpG sequences in eukaryotic DNA. FEBS Lett 124, 67-71.

Grunewald, T.G.P., Cidre-Aranaz, F., Surdez, D., Tomazou, E.M., de Alava, E., Kovar, H., Sorensen, P.H., Delattre, O., and Dirksen, U. (2018). Ewing sarcoma. Nat Rev Dis Primers 4, 5.

Gryder, B.E., Yohe, M.E., Chou, H.C., Zhang, X., Marques, J., Wachtel, M., Schaefer, B., Sen, N., Song, Y., Gualtieri, A., et al. (2017). PAX3–FOXO1 Establishes Myogenic Super Enhancers and Confers BET Bromodomain Vulnerability. Cancer Discov 7, 884-899.

Guarente, L. (2011). Sirtuins, Aging, and Metabolism. Cold Spring Harb Symp Quant Biol

76, 81-90.

Guillon, N., Tirode, F., Boeva, V., Zynovyev, A., Barillot, E., and Delattre, O. (2009). The oncogenic EWS-FLI1 protein binds in vivo GGAA microsatellite sequences with potential transcriptional activation function. PLoS One 4, e4932.

Hake, S.B., Garcia, B.A., Duncan, E.M., Kauer, M., Dellaire, G., Shabanowitz, J., Bazett-Jones, D.P., Allis, C.D., and Hunt, D.F. (2006). Expression Patterns and Post-translational Modifications Associated with Mammalian Histone H3 Variants. J Biol Chem 281, 559-568.

Han, Z.Y., Richer, W., Freneaux, P., Chauvin, C., Lucchesi, C., Guillemot, D., Grison, C., Lequin, D., Pierron, G., Masliah-Planchon, J., et al. (2016). The occurrence of intracranial rhabdoid tumours in mice depends on temporal control of Smarcb1 inactivation. Nat Commun 7, 10421.

Hancock, J.D., and Lessnick, S.L. (2008). A transcriptional profiling meta-analysis reveals a core EWS-FLI gene expression signature. Cell Cycle 7, 250-256.

Hashizume, R., Andor, N., Ihara, Y., Lerner, R., Gan, H., Chen, X., Fang, D., Huang, X., Tom, M.W., Ngo, V., et al. (2014). Pharmacologic inhibition of histone demethylation as a therapy for pediatric brainstem glioma. Nat Med 20, 1394-1396.

He, H.H., Meyer, C.A., Shin, H., Bailey, S.T., Wei, G., Wang, Q., Zhang, Y., Xu, K., Ni, M., Lupien, M., et al. (2010). Nucleosome dynamics define transcriptional enhancers. Nat Genet 42, 343-347.

Heinemann, B., Nielsen, J.M., Hudlebusch, H.R., Lees, M.J., Larsen, D.V., Boesen, T., Labelle, M., Gerlach, L.O., Birk, P., and Helin, K. (2014). Inhibition of demethylases by GSK-J1/J4. Nature 514, E1-E2.

Henrich, K.-O., Bender, S., Saadati, M., Dreidax, D., Gartlgruber, M., Shao, C., Herrmann, C., Wiesenfarth, M., Parzonka, M., Wehrmann, L., et al. (2016). Integrative Genome-Scale Analysis Identifies Epigenetic Mechanisms of Transcriptional Deregulation in Unfavorable Neuroblastomas. Cancer Res 76, 5523-5537.

Hernandez-Muñoz, I., Figuerola, E., Sanchez-Molina, S., Rodriguez, E., Fernández-Mariño, A.I., Pardo-Pastor, C., Bahamonde, M.I., Fernández-Fernández, J.M., García-Domínguez, D.J., Hontecillas-Prieto, L., et al. (2016). RING1B contributes to Ewing sarcoma development by repressing the NaV1.6 sodium channel and the NF-κB pathway,

independently of the fusion oncoprotein. Oncotarget 7, 46283-46300.

Hernández-Ruiz, E., Toll, A., García-Diez, I., Andrades, E., Ferrandiz-Pulido, C., Masferrer, E., Yébenes, M., Jaka, A., Gimeno, J., Gimeno, R., et al. (2018). The Polycomb proteins RING1B and EZH2 repress the tumoral pro-inflammatory function in metastasizing primary cutaneous squamous cell carcinoma. Carcinogenesis 39, 503-513.

Hinck, L., and Näthke, I. (2014). Changes in cell and tissue organization in cancer of the breast and colon. Curr Opin Cell Biol 26, 87-95.

Hjerpe, R., Thomas, Y., Chen, J., Zemla, A., Curran, S., Shpiro, N., Dick, Lawrence R., and Kurz, T. (2012). Changes in the ratio of free NEDD8 to ubiquitin triggers NEDDylation by ubiquitin enzymes. Biochem J 441, 927-939.

Howlader, N., Noone, A.M., Krapcho, M., Garshell, J., Neyman, N., Altekruse, S.F., Kosary, C.L., Yu, M., Ruhl, J., Tatalovich, Z., et al. (2013). SEER Cancer Statistics Review, 1975-2010 (Bethesda, MD).

Hsu, J.H., and Lawlor, E.R. (2011). BMI-1 suppresses contact inhibition and stabilizes YAP in Ewing sarcoma. Oncogene 30, 2077-2085.

Hu-Lieskovan, S., Zhang, J., Wu, L., Shimada, H., Schofield, D., and Triche, T.J. (2005). EWS-FLI1 Fusion Protein Up-regulates Critical Genes in Neural Crest Development and Is Responsible for the Observed Phenotype of Ewing's Family of Tumors. Cancer Res 65, 4633-4644.

Hu, D., Gao, X., Morgan, M.A., Herz, H.M., Smith, E.R., and Shilatifard, A. (2013). The MLL3/MLL4 branches of the COMPASS family function as major histone H3K4 monomethylases at enhancers. Mol Cell Biol 33, 4745-4754.

Huang, H., Sabari, B.R., Garcia, B.A., Allis, C.D., and Zhao, Y. (2014). SnapShot: histone modifications. Cell 159, 458-458.

Huang, S., Wang, Z., Zhou, J., Huang, J., Zhou, L., Luo, J., Wan, Y.Y., Long, H., and Zhu, B. (2019). EZH2 Inhibitor GSK126 Suppresses Antitumor Immunity by Driving Production of Myeloid-Derived Suppressor Cells. Cancer Res 79, 2009-2020.

Huarte, M. (2015). The emerging role of lncRNAs in cancer. Nat Med 21, 1253-1261.

Hudson, M.M., Link, M.P., and Simone, J.V. (2014). Milestones in the curability of pediatric

cancers. J Clin Oncol 32, 2391-2397.

Huether, R., Dong, L., Chen, X., Wu, G., Parker, M., Wei, L., Ma, J., Edmonson, M.N., Hedlund, E.K., Rusch, M.C., et al. (2014). The landscape of somatic mutations in epigenetic regulators across 1,000 paediatric cancer genomes. Nat Commun 5, 3630.

Huntly, B.J., Shigematsu, H., Deguchi, K., Lee, B.H., Mizuno, S., Duclos, N., Rowan, R., Amaral, S., Curley, D., Williams, I.R., et al. (2004). MOZ-TIF2, but not BCR-ABL, confers properties of leukemic stem cells to committed murine hematopoietic progenitors. Cancer Cell 6, 587-596.

Husnjak, K., and Dikic, I. (2012). Ubiquitin-Binding Proteins: Decoders of Ubiquitin-Mediated Cellular Functions. Annu Rev Biochem 81, 291-322.

Hyun, K., Jeon, J., Park, K., and Kim, J. (2017). Writing, erasing and reading histone lysine methylations. Exp Mol Med 49, e324-e324.

Illingworth, R.S., Moffat, M., Mann, A.R., Read, D., Hunter, C.J., Pradeepa, M.M., Adams, I.R., and Bickmore, W.A. (2015). The E3 ubiquitin ligase activity of RING1B is not essential for early mouse development. Genes Dev 29, 1897-1902.

Ismail, I.H., McDonald, D., Strickfaden, H., Xu, Z., and Hendzel, M.J. (2013). A small molecule inhibitor of polycomb repressive complex 1 inhibits ubiquitin signaling at DNA double-strand breaks. J Biol Chem 288, 26944-26954.

Iwamoto, Y. (2007). Diagnosis and Treatment of Ewing's Sarcoma. Jpn J Clin Oncol 37, 79-89.

Januario, T., Ye, X., Bainer, R., Alicke, B., Smith, T., Haley, B., Modrusan, Z., Gould, S., and Yauch, R.L. (2017). PRC2-mediated repression of SMARCA2 predicts EZH2 inhibitor activity in SWI/SNF mutant tumors. Proc Natl Acad Sci U S A 114, 12249-12254.

Javaheri, T., Kazemi, Z., Pencik, J., Pham, H.T.T., Kauer, M., Noorizadeh, R., Sax, B., Nivarthi, H., Schlederer, M., Maurer, B., et al. (2016). Increased survival and cell cycle progression pathways are required for EWS/FLI1-induced malignant transformation. Cell Death Dis 7, e2419-e2419.

Jawad, M.U., Cheung, M.C., Min, E.S., Schneiderbauer, M.M., Koniaris, L.G., and Scully, S.P. (2009). Ewing sarcoma demonstrates racial disparities in incidence-related and sex-related differences in outcome. Cancer 115, 3526-3536.

Jensen, R.D., and Drake, R.M. (1970). Rarity of Ewing's Tumour in Negroes. Lancet 295, 777.

Jenuwein, T., and Allis, C.D. (2001). Translating the Histone Code. Science 293, 1074-1080.

Jeon, I.S., Davis, J.N., Braun, B.S., Sublett, J.E., Roussel, M.F., Denny, C.T., and Shapiro, D.N. (1995). A variant Ewing's sarcoma translocation (7;22) fuses the EWS gene to the ETS gene ETV1. Oncogene 10, 1229-1234.

Jiang, S., and Mortazavi, A. (2018). Integrating ChIP-seq with other functional genomics data. Brief Funct Genomics 17, 104-115.

Jin, J., Cai, Y., Li, B., Conaway, R.C., Workman, J.L., Conaway, J.W., and Kusch, T. (2005). In and out: histone variant exchange in chromatin. Trends Biochem Sci 30, 680-687.

Jin, Q., Yu, L.R., ., Wang, L., Zhang, Z., Kasper, L.H., Lee, J.E., Wang, C., Brindle, P.K., Dent, S.Y., and Ge, K. (2011). Distinct roles of GCN5/PCAF-mediated H3K9ac and CBP/p300-mediated H3K18/27ac in nuclear receptor transactivation. EMBO J 30, 249-262.

Johnson, K.M., Taslim, C., Saund, R.S., and Lessnick, S.L. (2017). Identification of two types of GGAA-microsatellites and their roles in EWS/FLI binding and gene regulation in Ewing sarcoma. PLoS One 12, e0186275.

Jones, P.A., and Baylin, S.B. (2002). The fundamental role of epigenetic events in cancer. Nat Rev Genet 3, 415-428.

Jones, P.A., and Liang, G. (2009). Rethinking how DNA methylation patterns are maintained. Nat Rev Genet 10, 805-811.

Juergens, C., Weston, C., Lewis, I., Whelan, J., Paulussen, M., Oberlin, O., Michon, J., Zoubek, A., Juergens, H., and Craft, A. (2006). Safety assessment of intensive induction with vincristine, ifosfamide, doxorubicin, and etoposide (VIDE) in the treatment of Ewing tumors in the EURO-E.W.I.N.G. 99 clinical trial. Pediatr Blood Cancer 47, 22-29.

Kadin, M.E., and Bensch, K.G. (1971). On the origin of Ewing's tumor. Cancer 27, 257-273.

Kadoch, C., and Crabtree, G.R. (2013). Reversible disruption of mSWI/SNF (BAF) complexes by the SS18-SSX oncogenic fusion in synovial sarcoma. Cell 153, 71-85.

Kadoch, C., Hargreaves, D.C., Hodges, C., Elias, L., Ho, L., Ranish, J., and Crabtree, G.R. (2013). Proteomic and bioinformatic analysis of mammalian SWI/SNF complexes identifies extensive roles in human malignancy. Nat Genet 45, 592-601.

Kailayangiri, S., Altvater, B., Lesch, S., Balbach, S., Göttlich, C., Kühnemundt, J., Mikesch, J.H., Schelhaas, S., Jamitzky, S., Meltzer, J., et al. (2019). EZH2 Inhibition in Ewing Sarcoma Upregulates GD2 Expression for Targeting with Gene-Modified T Cells. Mol Ther 27, 933-946.

Kandoth, C., McLellan, M.D., Vandin, F., Ye, K., Niu, B., Lu, C., Xie, M., Zhang, Q., McMichael, J.F., Wyczalkowski, M.A., et al. (2013). Mutational landscape and significance across 12 major cancer types. Nature 502, 333-339.

Karlberg, J. (1989). A biologically-oriented mathematical model (ICP) for human growth. Acta Paediatr Scand Suppl 350, 70-94.

Kassis, J.A., Kennison, J.A., and Tamkun, J.W. (2017). Polycomb and Trithorax Group Genes in Drosophila. Genetics 206, 1699-1725.

Kauer, M., Ban, J., Kofler, R., Walker, B., Davis, S., Meltzer, P., and Kovar, H. (2009). A Molecular Function Map of Ewing's Sarcoma. PLoS One 4, e5415.

Kawakami, T., Chiba, T., Suzuki, T., Iwai, K., Yamanaka, K., Minato, N., Suzuki, H., Shimbara, N., Hidaka, Y., Osaka, F., et al. (2001). NEDD8 recruits E2-ubiquitin to SCF E3 ligase. EMBO J 20, 4003-4012.

Kazantsev, A.G., and Thompson, L.M. (2008). Therapeutic application of histone deacetylase inhibitors for central nervous system disorders. Nat Rev Drug Discov 7, 854-868.

Kennedy, A.L., Vallurupalli, M., Chen, L., Crompton, B., Cowley, G., Vazquez, F., Weir, B.A., Tsherniak, A., Parasuraman, S., Kim, S., et al. (2015). Functional, chemical genomic, and super-enhancer screening identify sensitivity to cyclin D1/CDK4 pathway inhibition in Ewing sarcoma. Oncotarget 6, 30178-30193.

Kerscher, O., Felberbaum, R., and Hochstrasser, M. (2006). Modification of Proteins by Ubiquitin and Ubiquitin-Like Proteins. Annu Rev Cell Dev Biol 22, 159-180.

Keshelava, N., Houghton, P.J., Morton, C.L., Lock, R.B., Carol, H., Keir, S.T., Maris, J.M., Reynolds, C.P., Gorlick, R., Kolb, E.A., et al. (2009). Initial testing (stage 1) of vorinostat

(SAHA) by the pediatric preclinical testing program. Pediatr Blood Cancer 53, 505-508.

Kim, J.H., Sharma, A., Dhar, S.S., Lee, S.H., Gu, B., Chan, C.H., Lin, H.K., and Lee, M.G. (2014). UTX and MLL4 coordinately regulate transcriptional programs for cell proliferation and invasiveness in breast cancer cells. Cancer Res 74, 1705-1717.

Kim, K.H., and Roberts, C.W. (2016). Targeting EZH2 in cancer. Nat Med 22, 128-134.

Kim, W., Bennett, E.J., Huttlin, E.L., Guo, A., Li, J., Possemato, A., Sowa, M.E., Rad, R., Rush, J., Comb, M.J., et al. (2011). Systematic and Quantitative Assessment of the Ubiquitin-Modified Proteome. Mol Cell 44, 325-340.

Kinsey, M., Smith, R., and Lessnick, S.L. (2006). NR0B1 Is Required for the Oncogenic Phenotype Mediated by EWS/FLI in Ewing's Sarcoma. Mol Cancer Res 4, 851-859.

Kleer, C.G., Cao, Q., Varambally, S., Shen, R., Ota, I., Tomlins, S.A., Ghosh, D., Sewalt, R.G., Otte, A.P., Hayes, D.F., et al. (2003). EZH2 is a marker of aggressive breast cancer and promotes neoplastic transformation of breast epithelial cells. Proc Natl Acad Sci U S A 100, 11606-11611.

Knutson, S.K., Warholic, N.M., Wigle, T.J., Klaus, C.R., Allain, C.J., Raimondi, A., Porter Scott, M., Chesworth, R., Moyer, M.P., Copeland, R.A., et al. (2013). Durable tumor regression in genetically altered malignant rhabdoid tumors by inhibition of methyltransferase EZH2. Proc Natl Acad Sci U S A 110, 7922-7927.

Kondo, T., Isono, K., Kondo, K., Endo, T.A., Itohara, S., Vidal, M., and Koseki, H. (2014). Polycomb Potentiates Meis2 Activation in Midbrain by Mediating Interaction of the Promoter with a Tissue-Specific Enhancer. Dev Cell 28, 94-101.

Kooistra, S.M., and Helin, K. (2012). Molecular mechanisms and potential functions of histone demethylases. Nat Rev Mol Cell Biol 13, 297.

Kouzarides, T. (2007). Chromatin Modifications and Their Function. Cell 128, 693-705.

Kovar, H. (1998). Ewing's sarcoma and peripheral primitive neuroectodermal tumors after their genetic union. Curr Opin Oncol 10, 334-342.

Krook, M.A., Hawkins, A.G., Patel, R.M., Lucas, D.R., Van Noord, R., Chugh, R., and Lawlor, E.R. (2016). A bivalent promoter contributes to stress-induced plasticity of CXCR4 in Ewing sarcoma. Oncotarget 7, 61775-61788.

Kuleta-Bosak, E., Kluczewska, E., Machnik-Broncel, J., Madziara, W., Ciupińska-Kajor, M., Sojka, D., Rogala, W., Juszczyk, J., and Wilk, R. (2010). Suitability of imaging methods (X-ray, CT, MRI) in the diagnostics of Ewing's sarcoma in children - analysis of own material. Pol J Radiol 75, 18-28.

Kullendorff, C., Mertens, F., Donnér, M., Wiebe, T., Akerman, M., and Mandahl, N. (1999). Cytogenetic aberrations in Ewing sarcoma: Are secondary changes associated with clinical outcome? Med Pediatr Oncol 32, 79-83.

Lamber, E.P., Vanhille, L., Textor, L.C., Kachalova, G.S., Sieweke, M.H., and Wilmanns, M. (2008). Regulation of the transcription factor Ets-1 by DNA-mediated homo-dimerization. EMBO J 27, 2006-2017.

Le Deley, M.C., Delattre, O., Schaefer, K.L., Burchill, S.A., Koehler, G., Hogendoorn, P.C., Lion, T., Poremba, C., Marandet, J., Ballet, S., et al. (2010). Impact of EWS-ETS fusion type on disease progression in Ewing's sarcoma/peripheral primitive neuroectodermal tumor: prospective results from the cooperative Euro-E.W.I.N.G. 99 trial. J Clin Oncol 28, 1982-1988.

Leacock, S.W., Basse, A.N., Chandler, G.L., Kirk, A.M., Rakheja, D., and Amatruda, J.F. (2012). A zebrafish transgenic model of Ewing's sarcoma reveals conserved mediators of EWS-FLI1 tumorigenesis. Dis Model Mech 5, 95-106.

Lederer, D., Grisart, B., Digilio, M.C., Benoit, V., Crespin, M., Ghariani, S.C., Maystadt, I., Dallapiccola, B., and Verellen-Dumoulin, C. (2012). Deletion of KDM6A, a histone demethylase interacting with MLL2, in three patients with Kabuki syndrome. Am J Hum Genet 90, 119-124.

Lee, D., Kim, M., and Cho, K. (2014). A design principle underlying the paradoxical roles of E3 ubiquitin ligases. Sci Rep 4, 5573.

Lee, J., Hoang, B.H., Ziogas, A., and Zell, J.A. (2010). Analysis of prognostic factors in Ewing sarcoma using a population-based cancer registry. Cancer 116, 1964-1973.

Lee, M.G., Villa, R., Trojer, P., Norman, J., Yan, K., Reinberg, D., Di Croce, L., and Shiekhattar, R. (2007). Demethylation of H3K27 Regulates Polycomb Recruitment and H2A Ubiquitination. Science 318, 447-450.

Ler, L.D., Ghosh, S., Chai, X., Thike, A.A., Heng, H.L., Siew, E.Y., Dey, S., Koh, L.K., Lim, J.Q., Lim, W.K., et al. (2017). Loss of tumor suppressor KDM6A amplifies PRC2-regulated

transcriptional repression in bladder cancer and can be targeted through inhibition of EZH2. Sci Transl Med 9, eaai8312.

Lessnick, S.L., Braun, B.S., Denny, C.T., and May, W.A. (1995). Multiple domains mediate transformation by the Ewing's sarcoma EWS/FLI-1 fusion gene. Oncogene 10, 423-431.

Lessnick, S.L., Dacwag, C.S., and Golub, T.R. (2002). The Ewing's sarcoma oncoprotein EWS/FLI induces a p53-dependent growth arrest in primary human fibroblasts. Cancer Cell 1, 393-401.

Lewis, P.W., Müller, M.M., Koletsky, M.S., Cordero, F., Lin, S., Banaszynski, L.A., Garcia, B.A., Muir, T.W., Becher, O.J., and Allis, C.D. (2013). Inhibition of PRC2 activity by a gain-of-function H3 mutation found in pediatric glioblastoma. Science 340, 857-861.

Li, G., and Reinberg, D. (2011). Chromatin higher-order structures and gene regulation. Curr Opin Genet Dev 21, 175-186.

Li, T., Guan, J., Huang, Z., Hu, X., and Zheng, X. (2014). RNF168-mediated H2A neddylation antagonizes ubiquitylation of H2A and regulates DNA damage repair. J Cell Sci 127, 2238-2248.

Li, X., Zhang, Y., Zheng, L., Liu, M., Chen, C.D., and Jiang, H. (2018a). UTX is an escape from X-inactivation tumor-suppressor in B cell lymphoma. Nat Commun 9, 2720.

Li, Y., Zhang, M., Sheng, M., Zhang, P., Chen, Z., Xing, W., Bai, J., Cheng, T., Yang, F.C., and Zhou, Y. (2018b). Therapeutic potential of GSK-J4, a histone demethylase KDM6B/JMJD3 inhibitor, for acute myeloid leukemia. J Cancer Res Clin Oncol 144, 1065-1077.

Li, Z., Godinho, F.J., Klusmann, J.H., Garriga-Canut, M., Yu, C., and Orkin, S.H. (2005). Developmental stage-selective effect of somatically mutated leukemogenic transcription factor GATA1. Nat Genet 37, 613-619.

Lin, P.P., Pandey, M.K., Jin, F., Xiong, S., Deavers, M., Parant, J.M., and Lozano, G. (2008). EWS-FLI1 induces developmental abnormalities and accelerates sarcoma formation in a transgenic mouse model. Cancer Res 68, 8968-8975.

Lin, P.P., Wang, Y., and Lozano, G. (2011). Mesenchymal Stem Cells and the Origin of Ewing's Sarcoma. Sarcoma 2011, 276463.

Lochmann, T.L., Powell, K.M., Ham, J., Floros, K.V., Heisey, D.A.R., Kurupi, R.I.J., Calbert,

M.L., Ghotra, M.S., Greninger, P., Dozmorov, M., et al. (2018). Targeted inhibition of histone H3K27 demethylation is effective in high-risk neuroblastoma. Sci Transl Med 10, eaao4680.

Loubière, V., Delest, A., Thomas, A., Bonev, B., Schuettengruber, B., Sati, S., Martinez, A.M., and Cavalli, G. (2016). Coordinate redeployment of PRC1 proteins suppresses tumor formation during Drosophila development. Nat Genet 48, 1436-1442.

Luger, K., Mäder, A.W., Richmond, R.K., Sargent, D.F., and Richmond, T.J. (1997). Crystal structure of the nucleosome core particle at 2.8 Å resolution. Nature 389, 251-260.

Luger, K., and Richmond, T.J. (1998). DNA binding within the nucleosome core. Curr Opin Struct Biol 8, 33-40.

Ma, T., Chen, Y., Zhang, F., Yang, C.Y., Wang, S., and Yu, X. (2013). RNF111-dependent neddylation activates DNA damage-induced ubiquitination. Mol Cell 49, 897-907.

Ma, X., Liu, Y., Liu, Y., Alexandrov, L.B., Edmonson, M.N., Gawad, C., Zhou, X., Li, Y., Rusch, M.C., Easton, J., et al. (2018). Pan-cancer genome and transcriptome analyses of 1699 paediatric leukaemias and solid tumours. Nature 555, 371-376.

MacAlpine, D.M., and Almouzni, G. (2013). Chromatin and DNA replication. Cold Spring Harb Perspect Biol 5, a010207.

Mackintosh, C., García-Domínguez, D.J., Ordóñez, J.L., Ginel-Picardo, A., Smith, P.G., Sacristán, M.P., and de Álava, E. (2012). WEE1 accumulation and deregulation of S-phase proteins mediate MLN4924 potent inhibitory effect on Ewing sarcoma cells. Oncogene 32, 1441-1451.

Maegawa, S., Hinkal, G., Kim, H.S., Shen, L., Zhang, L., Zhang, J., Zhang, N., Liang, S., Donehower, L.A., and Issa, J.P. (2010). Widespread and tissue specific age-related DNA methylation changes in mice. Genome Res 20, 332-340.

Maksimenko, A., and Malvy, C. (2005). Oncogene-targeted antisense oligonucleotides for the treatment of Ewing sarcoma. Expert Opin Ther Targets 9, 825-830.

Mansour, A.A., Gafni, O., Weinberger, L., Zviran, A., Ayyash, M., Rais, Y., Krupalnik, V., Zerbib, M., Amann-Zalcenstein, D., Maza, I., et al. (2012). The H3K27 demethylase Utx regulates somatic and germ cell epigenetic reprogramming. Nature 488, 409-413.

Mao, X., Miesfeldt, S., Yang, H., Leiden, J.M., and Thompson, C.B. (1994). The FLI-1 and chimeric EWS-FLI-1 oncoproteins display similar DNA binding specificities. J Biol Chem 269, 18216-18222.

Margueron, R., Li, G., Sarma, K., Blais, A., Zavadil, J., Woodcock, C.L., Dynlacht, B.D., and Reinberg, D. (2008). Ezh1 and Ezh2 Maintain Repressive Chromatin through Different Mechanisms. Mol Cell 32, 503-518.

Marshall, G.M., Carter, D.R., Cheung, B.B., Liu, T., Mateos, M.K., Meyerowitz, J.G., and Weiss, W.A. (2014). The prenatal origins of cancer. Nat Rev Cancer 14, 277-289.

Martin, C., and Zhang, Y. (2005). The diverse functions of histone lysine methylation. Nat Rev Mol Cell Biol 6, 838-849.

Martinez-Garcia, E., and Licht, J.D. (2010). Deregulation of H3K27 methylation in cancer. Nat Genet 42, 100-101.

May, W.A., Gishizky, M.L., Lessnick, S.L., Lunsford, L.B., Lewis, B.C., Delattre, O., Zucman, J., Thomas, G., and Denny, C.T. (1993). Ewing sarcoma 11;22 translocation produces a chimeric transcription factor that requires the DNA-binding domain encoded by FLI1 for transformation. Proc Natl Acad Sci U S A 90, 5752-5756.

McBryant, S.J., Klonoski, J., Sorensen, T.C., Norskog, S.S., Williams, S., Resch, M.G., Toombs, J.A., 3rd, Hobdey, S.E., and Hansen, J.C. (2009). Determinants of histone H4 N-terminal domain function during nucleosomal array oligomerization: roles of amino acid sequence, domain length, and charge density. J Biol Chem 284, 16716-16722.

McKinsey, E.L., Parrish, J.K., Irwin, A.E., Niemeyer, B.F., Kern, H.B., Birks, D.K., and Jedlicka, P. (2011). A novel oncogenic mechanism in Ewing sarcoma involving IGF pathway targeting by EWS/Fli1-regulated microRNAs. Oncogene 30, 4910-4920.

Medvar, B., Raghuram, V., Pisitkun, T., Sarkar, A., and Knepper, M.A. (2016). Comprehensive database of human E3 ubiquitin ligases: application to aquaporin-2 regulation. Physiol Genomics 48, 502-512.

Merchant, M.S., Bernstein, D., Amoako, M., Baird, K., Fleisher, T.A., Morre, M., Steinberg, S.M., Sabatino, M., Stroncek, D.F., Venkatasan, A.M., et al. (2016). Adjuvant Immunotherapy to Improve Outcome in High-Risk Pediatric Sarcomas. Clin Cancer Res 22, 3182-3191.

Messner, S., and Hottiger, M.O. (2011). Histone ADP-ribosylation in DNA repair, replication and transcription. Trends Cell Biol 21, 534-542.

Miller, B.J., Gao, Y., and Duchman, K.R. (2017). Does surgery or radiation provide the best overall survival in Ewing's sarcoma? A review of the National Cancer Data Base. J Surg Oncol 116, 384-390.

Minas, T.Z., Surdez, D., Javaheri, T., Tanaka, M., Howarth, M., Kang, H.J., Han, J., Han, Z.Y., Sax, B., Kream, B.E., et al. (2017). Combined experience of six independent laboratories attempting to create an Ewing sarcoma mouse model. Oncotarget 8, 34141-34163.

Miranda, T.B., Cortez, C.C., Yoo, C.B., Liang, G., Abe, M., Kelly, T.K., Marquez, V.E., and Jones, P.A. (2009). DZNep is a global histone methylation inhibitor that reactivates developmental genes not silenced by DNA methylation. Mol Cancer Ther 8, 1579-1588.

Miyagawa, Y., Okita, H., Nakaijima, H., Horiuchi, Y., Sato, B., Taguchi, T., Toyoda, M., Katagiri, Y.U., Fujimoto, J., Hata, J., et al. (2008). Inducible expression of chimeric EWS/ETS proteins confers Ewing's family tumor-like phenotypes to human mesenchymal progenitor cells. Mol Cell Biol 28, 2125-2137.

Miyake, N., Mizuno, S., Okamoto, N., Ohashi, H., Shiina, M., Ogata, K., Tsurusaki, Y., Nakashima, M., Saitsu, H., Niikawa, N., et al. (2013). KDM6A Point Mutations Cause Kabuki Syndrome. Hum Mutat 34, 108-110.

Mohammad, F., Weissmann, S., Leblanc, B., Pandey, D.P., Højfeldt, J.W., Comet, I., Zheng, C., Johansen, J.V., Rapin, N., Porse, B.T., et al. (2017). EZH2 is a potential therapeutic target for H3K27M-mutant pediatric gliomas. Nat Med 23, 483-492.

Monument, M.J., Johnson, K.M., Grossmann, A.H., Schiffman, J.D., Randall, R.L., and Lessnick, S.L. (2012). Microsatellites with macro-influence in ewing sarcoma. Genes 3, 444-460.

Mora, J. (2012). What is a pediatric tumor? Clinical Oncology in Adolescents and Young Adults 2, 7-15.

Mora, J., Castaneda, A., Perez-Jaume, S., Lopez-Pousa, A., Maradiegue, E., Valverde, C., Martin-Broto, J., Garcia Del Muro, X., Cruz, O., Cruz, J., et al. (2017). GEIS-21: a multicentric phase II study of intensive chemotherapy including gemcitabine and docetaxel for the treatment of Ewing sarcoma of children and adults: a report from the Spanish sarcoma group (GEIS). Br J Cancer 117, 767-774.

Mora, J., Cruz, C.O., Parareda, A., and de Torres, C. (2009). Treatment of relapsed/refractory pediatric sarcomas with gemcitabine and docetaxel. J Pediatr Hematol Oncol 31, 723-729.

Morey, L., Aloia, L., Cozzuto, L., Benitah, S.A., and Di Croce, L. (2013). RYBP and Cbx7 Define Specific Biological Functions of Polycomb Complexes in Mouse Embryonic Stem Cells. Cell Rep 3, 60-69.

Morey, L., Santanach, A., Blanco, E., Aloia, L., Nora, Elphège P., Bruneau, Benoit G., and Di Croce, L. (2015). Polycomb Regulates Mesoderm Cell Fate-Specification in Embryonic Stem Cells through Activation and Repression Mechanisms. Cell Stem Cell 17, 300-315.

Morimoto, M., Nishida, T., Nagayama, Y., and Yasuda, H. (2003). Nedd8-modification of Cul1 is promoted by Roc1 as a Nedd8-E3 ligase and regulates its stability. Biochem Biophys Res Commun 301, 392-398.

Morreale, F.E., and Walden, H. (2016). SnapShot: Types of ubiquitin ligases. Cell 165, 248-248.el.

Mugneret, F., Lizard, S., Aurias, A., and Turc-Carel, C. (1988). Chromosomes in Ewing's sarcoma. II. Nonrandom additional changes, trisomy 8 and der(16)t(1;16). Cancer Genet Cytogenet 32, 239-245.

Müller, J., and Kassis, J.A. (2006). Polycomb response elements and targeting of Polycomb group proteins in Drosophila. Curr Opin Genet Dev 16, 476-484.

Nagai, M., Tanaka, S., Tsuda, M., Endo, S., Kato, H., Sonobe, H., Minami, A., Hiraga, H., Nishihara, H., Sawa, H., et al. (2001). Analysis of transforming activity of human synovial sarcoma-associated chimeric protein SYT-SSX1 bound to chromatin remodeling factor hBRM/hSNF2 alpha. Proc Natl Acad Sci U S A 98, 3843-3848.

Nagoshi, N., Shibata, S., Kubota, Y., Nakamura, M., Nagai, Y., Satoh, E., Morikawa, S., Okada, Y., Mabuchi, Y., Katoh, H., et al. (2008). Ontogeny and Multipotency of Neural Crest-Derived Stem Cells in Mouse Bone Marrow, Dorsal Root Ganglia, and Whisker Pad. Cell Stem Cell 2, 392-403.

Nascimento, A.G., Unii, K.K., Pritchard, D.J., Cooper, K.L., and Dahlin, D.C. (1980). A clinicopathologic study of 20 cases of large-cell (atypical) Ewing's sarcoma of bone. Am J Surg Pathol 4, 29-36.

National Institute of Health (2010). Cancer. Fact Sheet. Available at: https://report.nih.gov/nihfactsheets/viewfactsheet.aspx?csid=75 [Accessed July 3, 2019]

National Institute of Health (2019). U.S. National Library of Medicine. ClinicalTrials.gov. Available at: https://clinicaltrials.gov/ct2/results?term=epz6438&age_v=&gndr=&type=&rslt=&phase=0&Search=Apply [Accessed June 4, 2019]

Ng, J.M., Martinez, D., Marsh, E.D., Zhang, Z., Rappaport, E., Santi, M., and Curran, T. (2015). Generation of a mouse model of atypical teratoid/rhabdoid tumor of the central nervous system through combined deletion of Snf5 and p53. Cancer Res 75, 4629-4639.

Ng, T.L., O'Sullivan, M.J., Pallen, C.J., Hayes, M., Clarkson, P.W., Winstanley, M., Sorensen, P.H., Nielsen, T.O., and Horsman, D.E. (2007). Ewing sarcoma with novel translocation t(2;16) producing an in-frame fusion of FUS and FEV. J Mol Diagn 9, 459-463.

Nichol, J.N., Dupéré-Richer, D., Ezponda, T., Licht, J.D., and Miller, W.H., Jr. (2016). H3K27 Methylation: A Focal Point of Epigenetic Deregulation in Cancer. Adv Cancer Res 131, 59-95.

Ntziachristos, P., Tsirigos, A., Van Vlierberghe, P., Nedjic, J., Trimarchi, T., Flaherty, M.S., Ferres-Marco, D., da Ros, V., Tang, Z., Siegle, J., et al. (2012). Genetic inactivation of the polycomb repressive complex 2 in T cell acute lymphoblastic leukemia. Nat Med 18, 298-301.

Ntziachristos, P., Tsirigos, A., Welstead, G.G., Trimarchi, T., Bakogianni, S., Xu, L., Loizou, E., Holmfeldt, L., Strikoudis, A., King, B., et al. (2014). Contrasting roles of histone 3 lysine 27 demethylases in acute lymphoblastic leukaemia. Nature 514, 513-517.

Oberlin, O., Rey, A., Desfachelles, A.S., Philip, T., Plantaz, D., Schmitt, C., Plouvier, E., Lejars, O., Rubie, H., Terrier, P., et al. (2006). Impact of High-Dose Busulfan Plus Melphalan As Consolidation in Metastatic Ewing Tumors: A Study by the Société Française des Cancers de l'Enfant. J Clin Oncol 24, 3997-4002.

Ordóñez, J.L., Amaral, A.T., Carcaboso, A.M., Herrero-Martín, D., del Carmen García-Macías, M., Sevillano, V., Alonso, D., Pascual-Pasto, G., San-Segundo, L., Vila-Ubach, M., et al. (2015). The PARP inhibitor olaparib enhances the sensitivity of Ewing sarcoma to trabectedin. Oncotarget 6, 18875-18890.

Orlowski, R.Z., and Kuhn, D.J. (2008). Proteasome Inhibitors in Cancer Therapy: Lessons from the First Decade. Clin Cancer Res 14, 1649-1657.

Osaka, F., Saeki, M., Katayama, S., Aida, N., Toh, E.A., Kominami, K., Toda, T., Suzuki, T., Chiba, T., Tanaka, K., et al. (2000). Covalent modifier NEDD8 is essential for SCF ubiquitin-ligase in fission yeast. EMBO J 19, 3475-3484.

Ouchida, M., Ohno, T., Fujimura, Y., Rao, V.N., and Reddy, E. (1995). Loss of tumorigenicity of Ewing's sarcoma cells expressing antisense RNA to EWS-fusion transcripts. Oncogene 11, 1049-1054.

Owen, L.A., Kowalewski, A.A., and Lessnick, S.L. (2008). EWS/FLI mediates transcriptional repression via NKX2.2 during oncogenic transformation in Ewing's sarcoma. PLoS One 3, e1965.

Paashuis-Lew, Y.R., and Heddle, J.A. (1998). Spontaneous mutation during fetal development and post-natal growth. Mutagenesis 13, 613-617.

Pan, M.R., Peng, G., Hung, W.C., and Lin, S.Y. (2011). Monoubiquitination of H2AX protein regulates DNA damage response signaling. J Biol Chem 286, 28599-28607.

Pan, Z.-Q., Kentsis, A., Dias, D.C., Yamoah, K., and Wu, K. (2004). Nedd8 on cullin: building an expressway to protein destruction. Oncogene 23, 1985-1997.

Pappo, A.S., Vassal, G., Crowley, J.J., Bolejack, V., Hogendoorn, P.C.W., Chugh, R., Ladanyi, M., Grippo, J.F., Dall, G., Staddon, A.P., et al. (2014). A phase 2 trial of R1507, a monoclonal antibody to the insulin-like growth factor-1 receptor (IGF-1R), in patients with recurrent or refractory rhabdomyosarcoma, osteosarcoma, synovial sarcoma, and other soft tissue sarcomas: Results of a Sarcoma Alliance for Research Through Collaboration study. Cancer 120, 2448-2456.

Patel, M., Simon, J.M., Iglesia, M.D., Wu, S.B., McFadden, A.W., Lieb, J.D., and Davis, I.J. (2012). Tumor-specific retargeting of an oncogenic transcription factor chimera results in dysregulation of chromatin and transcription. Genome Res 22, 259-270.

Pathania, M., De Jay, N., Maestro, N., Harutyunyan, A.S., Nitarska, J., Pahlavan, P., Henderson, S., Mikael, L.G., Richard-Londt, A., Zhang, Y., et al. (2017). H3.3(K27M) Cooperates with Trp53 Loss and PDGFRA Gain in Mouse Embryonic Neural Progenitor Cells to Induce Invasive High-Grade Gliomas. Cancer Cell 32, 684-700.

Paull, T.T., Rogakou, E.P., Yamazaki, V., Kirchgessner, C.U., Gellert, M., and Bonner, W.M. (2000). A critical role for histone H2AX in recruitment of repair factors to nuclear foci after DNA damage. Curr Biol 10, 886-895.

Paulussen, M., Ahrens, S., Dunst, J., Winkelmann, W., Exner, G.U., Kotz, R., Amann, G., Dockhorn-Dworniczak, B., Harms, D., Muller-Weihrich, S., et al. (2001). Localized Ewing tumor of bone: final results of the cooperative Ewing's Sarcoma Study CESS 86. J Clin Oncol 19, 1818-1829.

Paulussen, M., Craft, A.W., Lewis, I., Hackshaw, A., Douglas, C., Dunst, J., Schuck, A., Winkelmann, W., Köhler, G., Poremba, C., et al. (2008). Results of the EICESS-92 Study: Two Randomized Trials of Ewing's Sarcoma Treatment—Cyclophosphamide Compared With Ifosfamide in Standard-Risk Patients and Assessment of Benefit of Etoposide Added to Standard Treatment in High-Risk Patients. J Clin Oncol 26, 4385-4393.

Pengelly, A.R., Kalb, R., Finkl, K., and Müller, J. (2015). Transcriptional repression by PRC1 in the absence of H2A monoubiquitylation. Genes Dev 29, 1487-1492.

Perez-Campo, F.M., Costa, G., Lie-a-Ling, M., Kouskoff, V., and Lacaud, G. (2013). The MYSTerious MOZ, a histone acetyltransferase with a key role in haematopoiesis. Immunology 139, 161-165.

Peter, M., Couturier, J., Pacquement, H., Michon, J., Thomas, G., Magdelenat, H., and Delattre, O. (1997). A new member of the ETS family fused to EWS in Ewing tumors. Oncogene 14, 1159-1164.

Pishas, K.I., Drenberg, C.D., Taslim, C., Theisen, E.R., Johnson, K.M., Saund, R.S., Pop, I.L., Crompton, B.D., Lawlor, E.R., Tirode, F., et al. (2018). Therapeutic Targeting of KDM1A/LSD1 in Ewing Sarcoma with SP-2509 Engages the Endoplasmic Reticulum Stress Response. Mol Cancer Ther 17, 1902-1916.

Pizzo P. A., and Poplack, D.G. (1996). Ewing's sarcoma of bone and soft tissue. In Principles and Practice of Pediatric Oncology Williams, and Wilkins, eds. (Philadelphia: Lippincott), pp. 840-841.

Pogo, B.G., Allfrey, V.G., and Mirsky, A.E. (1966). RNA synthesis and histone acetylation during the course of gene activation in lymphocytes. Proc Natl Acad Sci U S A 55, 805-812.

Postovsky, S., Ash, S., Ramu, I.N., Yaniv, Y., Zaizov, R., Futerman, B., Elhasid, R., Ben Barak, A., Halil, A., and Ben Arush, M.W. (2003). Central nervous system involvement in children with sarcoma. Oncology 65, 118-124.

Potratz, J., Jürgens, H., Craft, A., and Dirksen, U. (2012). Ewing Sarcoma: Biology-Based

Therapeutic Perspectives. Pediatr Hematol Oncol 29, 12-27.

Prieur, A., Tirode, F., Cohen, P., and Delattre, O. (2004). EWS/FLI-1 silencing and gene profiling of Ewing cells reveal downstream oncogenic pathways and a crucial role for repression of insulin-like growth factor binding protein 3. Mol Cell Biol 24, 7275-7283.

Rai, K., Akdemir, K.C., Kwong, L.N., Fiziev, P., Wu, C.J., Keung, E.Z., Sharma, S., Samant, N.S., Williams, M., Axelrad, J.B., et al. (2015). Dual Roles of RNF2 in Melanoma Progression. Cancer Discov 5, 1314-1327.

Raisner, R., Kharbanda, S., Jin, L., Jeng, E., Chan, E., Merchant, M., Haverty, P.M., Bainer, R., Cheung, T., Arnott, D., et al. (2018). Enhancer Activity Requires CBP/P300 Bromodomain-Dependent Histone H3K27 Acetylation. Cell Rep 24, 1722-1729.

Rajagopal, N., Ernst, J., Ray, P., Wu, J., Zhang, M., Kellis, M., and Ren, B. (2014). Distinct and Predictive Histone Lysine Acetylation Patterns at Promoters, Enhancers, and Gene Bodies. G3 (Bethesda) 4, 2051-2063.

Ramaglia, M., D'Angelo, V., Iannotta, A., Di Pinto, D., Pota, E., Affinita, M.C., Donofrio, V., Errico, M.E., Lombardi, A., Indolfi, C., et al. (2016). High EZH2 expression is correlated to metastatic disease in pediatric soft tissue sarcomas. Cancer Cell Int 16, 59.

Ramakrishnan, V., Finch, J.T., Graziano, V., Lee, P.L., and Sweet, R.M. (1993). Crystal structure of globular domain of histone H5 and its implications for nucleosome binding. Nature 362, 219-223.

Ramon, A.L., Bertrand, J.R., de Martimprey, H., Bernard, G., Ponchel, G., Malvy, C., and Vauthier, C. (2013). siRNA associated with immunonanoparticles directed against cd99 antigen improves gene expression inhibition in vivo in Ewing's sarcoma. J Mol Recognit 26, 318-329.

Richter, G.H., Plehm, S., Fasan, A., Rössler, S., Unland, R., Bennani-Baiti, I.M., Hotfilder, M., Löwel, D., von Luettichau, I., Mossbrugger, I., et al. (2009). EZH2 is a mediator of EWS/FLI1 driven tumor growth and metastasis blocking endothelial and neuro-ectodermal differentiation. Proc Natl Acad Sci U S A 106, 5324-5329.

Riggi, N., Cironi, L., Provero, P., Suvà, M.L., Kaloulis, K., Garcia-Echeverria, C., Hoffmann, F., Trumpp, A., and Stamenkovic, I. (2005). Development of Ewing's Sarcoma from Primary Bone Marrow–Derived Mesenchymal Progenitor Cells. Cancer Res 65, 11459-11468.

Riggi, N., Knoechel, B., Gillespie, S.M., Rheinbay, E., Boulay, G., Suvà, M.L., Rossetti, N.E., Boonseng, W.E., Oksuz, O., Cook, E.B., et al. (2014). EWS-FLI1 utilizes divergent chromatin remodeling mechanisms to directly activate or repress enhancer elements in Ewing sarcoma. Cancer Cell 26, 668-681.

Riggi, N., and Stamenkovic, I. (2007). The Biology of Ewing sarcoma. Cancer Lett 254, 1-10.

Riggi, N., Suvà, M.L., De Vito, C., Provero, P., Stehle, J.C., Baumer, K., Cironi, L., Janiszewska, M., Petricevic, T., Suvà, D., et al. (2010). EWS-FLI-1 modulates miRNA145 and SOX2 expression to initiate mesenchymal stem cell reprogramming toward Ewing sarcoma cancer stem cells. Genes Dev 24, 916-932.

Riggi, N., Suva, M.L., and Stamenkovic, I. (2009). Ewing's sarcoma origin: from duel to duality. Expert Rev Anticancer Ther 9, 1025-1030.

Riggi, N., Suvà, M.L., Suvà, D., Cironi, L., Provero, P., Tercier, S., Joseph, J.M., Stehle, J.C., Baumer, K., Kindler, V., et al. (2008). EWS-FLI-1 Expression Triggers a Ewing's Sarcoma Initiation Program in Primary Human Mesenchymal Stem Cells. Cancer Res 68, 2176-2185.

Rikhof, B., de Jong, S., Suurmeijer, A.J., Meijer, C., and van der Graaf, W.T. (2009). The insulin-like growth factor system and sarcomas. J Pathol 217, 469-482.

Rivera, M.N., and Haber, D.A. (2005). Wilms' tumour: connecting tumorigenesis and organ development in the kidney. Nat Rev Cancer 5, 699-712.

Roadmap Epigenomics, C., Kundaje, A., Meuleman, W., Ernst, J., Bilenky, M., Yen, A., Heravi-Moussavi, A., Kheradpour, P., Zhang, Z., Wang, J., et al. (2015). Integrative analysis of 111 reference human epigenomes. Nature 518, 317-330.

Robinson, G., Parker, M., Kranenburg, T.A., Lu, C., Chen, X., Ding, L., Phoenix, T.N., Hedlund, E., Wei, L., Zhu, X., et al. (2012). Novel mutations target distinct subgroups of medulloblastoma. Nature 488, 43-48.

Rodriguez, R., Rubio, R., and Menendez, P. (2012). Modeling sarcomagenesis using multipotent mesenchymal stem cells. Cell Res 22, 62-77.

Ropero, S., and Esteller, M. (2007). The role of histone deacetylases (HDACs) in human cancer. Mol Oncol 1, 19-25.

Rorie, C.J., Thomas, V.D., Chen, P., Pierce, H., O'Bryan, J.P., and Weissman, B. (2004). The Ews/Fli-1 Fusion Gene Switches the Differentiation Program of Neuroblastomas to Ewing Sarcoma/Peripheral Primitive Neuroectodermal Tumors. Cancer Res 64, 1266-1277.

Rothbart, S.B., and Strahl, B.D. (2014). Interpreting the language of histone and DNA modifications. Biochim Biophys Acta 1839, 627-643.

Ryland, K.E., Hawkins, A.G., Weisenberger, D.J., Punj, V., Borinstein, S.C., Laird, P.W., Martens, J.R., and Lawlor, E.R. (2016). Promoter Methylation Analysis Reveals That KCNA5 Ion Channel Silencing Supports Ewing Sarcoma Cell Proliferation. Mol Cancer Res 14, 26-34.

Ryland, K.E., Svoboda, L.K., Vesely, E.D., McIntyre, J.C., Zhang, L., Martens, J.R., and Lawlor, E.R. (2015). Polycomb-dependent repression of the potassium channel-encoding gene KCNA5 promotes cancer cell survival under conditions of stress. Oncogene 34, 4591-4600.

Sánchez-Beato, M., Sánchez, E., González-Carreró, J., Morente, M., Díez, A., Sánchez-Verde, L., Martín, M.C., Cigudosa, J.C., Vidal, M., and Piris, M.A. (2006). Variability in the expression of polycomb proteins in different normal and tumoral tissues. A pilot study using tissue microarrays. Mod Pathol 19, 684-694.

Sánchez-Molina, S., Figuerola-Bou, E., Blanco, E., Sanchez-Jimenez, M., Gomez, S., Ballare, C., Garcia-Dominguez, D.J., Prada, E., Hontecillas-Prieto, L., Montero Carcaboso, A., et al. (2019). RING1B recruits EWSR1-FLI1 and cooperates in the remodeling of chromatin necessary for Ewing sarcoma tumorigenesis. Manuscript submitted for publication.

Sankar, R., Maheswari, R., Karthik, S., Shivashangari, K.S., and Ravikumar, V. (2014). Anticancer activity of Ficus religiosa engineered copper oxide nanoparticles. Mater Sci Eng C Mater Biol Appl 44, 234-239.

Sankar, S., Bell, R., Stephens, B., Zhuo, R., Sharma, S., Bearss, D.J., and Lessnick, S.L. (2013). Mechanism and relevance of EWS/FLI-mediated transcriptional repression in Ewing sarcoma. Oncogene 32, 5089-5100.

Sankar, S., and Lessnick, S.L. (2011). Promiscuous partnerships in Ewing's sarcoma. Cancer Genet 204, 351-365.

Schaaf, C.A., Misulovin, Z., Gause, M., Koenig, A., Gohara, D.W., Watson, A., and Dorsett, D. (2013). Cohesin and polycomb proteins functionally interact to control transcription at

silenced and active genes. PLoS Genet 9, e1003560.

Schleiermacher, G., Peter, M., Oberlin, O., Philip, T., Rubie, H., Mechinaud, F., Sommelet-Olive, D., Landman-Parker, J., Bours, D., Michon, J., et al. (2003). Increased Risk of Systemic Relapses Associated With Bone Marrow Micrometastasis and Circulating Tumor Cells in Localized Ewing Tumor. J Clin Oncol 21, 85-91.

Schuettengruber, B., Bourbon, H., Di Croce, L., and Cavalli, G. (2017). Genome Regulation by Polycomb and Trithorax: 70 Years and Counting. Cell 171, 34-57.

Schuettengruber, B., and Cavalli, G. (2009). Recruitment of Polycomb group complexes and their role in the dynamic regulation of cell fate choice. Development 136, 3531-3542.

Schuettengruber, B., Martinez, A.-M., Iovino, N., and Cavalli, G. (2011). Trithorax group proteins: switching genes on and keeping them active. Nat Rev Mol Cell Biol 12, 799-814.

Scotting, P.J., Walker, D.A., and Perilongo, G. (2005). Childhood solid tumours: a developmental disorder. Nat Rev Cancer 5, 481-488.

Second generation recombinant lentiviral vectors (2019). The Lentivirus - An Introduction,. Available at: https://www.abmgood.com/marketing/knowledge_base/The_Lentivirus_System [Accessed May 3, 2019]

Seligson, D.B., Horvath, S., McBrian, M.A., Mah, V., Yu, H., Tze, S., Wang, Q., Chia, D., Goodglick, L., and Kurdistani, S.K. (2009). Global levels of histone modifications predict prognosis in different cancers. Am J Pathol 174, 1619-1628.

Seto, E., and Yoshida, M. (2014). Erasers of histone acetylation: the histone deacetylase enzymes. Cold Spring Harb Perspect Biol 6, a018713.

Sheffield, N.C., Pierron, G., Klughammer, J., Datlinger, P., Schönegger, A., Schuster, M., Hadler, J., Surdez, D., Guillemot, D., Lapouble, E., et al. (2017). DNA methylation heterogeneity defines a disease spectrum in Ewing sarcoma. Nat Med 23, 386-395.

Shen, X., Liu, Y., Hsu, Y.J., Fujiwara, Y., Kim, J., Mao, X., Yuan, G.C., and Orkin, S.H. (2008). EZH1 mediates methylation on histone H3 lysine 27 and complements EZH2 in maintaining stem cell identity and executing pluripotency. Mol Cell 32, 491-502.

Shi, Y., and Whetstine, J.R. (2007). Dynamic Regulation of Histone Lysine Methylation by Demethylases. Molecular Cell 25, 1-14.

Shilatifard, A. (2008). Molecular implementation and physiological roles for histone H3 lysine 4 (H3K4) methylation. Curr Opin Cell Biol 20, 341-348.

Shpargel, K.B., Sengoku, T., Yokoyama, S., and Magnuson, T. (2012). UTX and UTY demonstrate histone demethylase-independent function in mouse embryonic development. PLoS Genet 8, e1002964.

Shpargel, K.B., Starmer, J., Yee, D., Pohlers, M., and Magnuson, T. (2014). KDM6 Demethylase Independent Loss of Histone H3 Lysine 27 Trimethylation during Early Embryonic Development. PLoS Genet 10, e1004507.

Singer, D.S., and Singer, M.F. (1976). Studies on the interaction of H1 histone with superhelical DNA: Characterization of the recognition and binding regions of H1 histone. Nucleic Acids Res 3, 2531-2548.

Smith, M.A., Maris, J.M., Gorlick, R., Kolb, E.A., Lock, R., Carol, H., Keir, S.T., Reynolds, C.P., Kang, M.H., Morton, C.L., et al. (2012a). Initial testing of the investigational NEDD8-activating enzyme inhibitor MLN4924 by the pediatric preclinical testing program. Pediatr Blood Cancer 59, 246-253.

Smith, R., Owen, L.A., Trem, D.J., Wong, J.S., Whangbo, J.S., Golub, T.R., and Lessnick, S.L. (2006). Expression profiling of EWS/FLI identifies NKX2.2 as a critical target gene in Ewing's sarcoma. Cancer Cell 9, 405-416.

Smith, Z.D., Chan, M.M., Mikkelsen, T.S., Gu, H., Gnirke, A., Regev, A., and Meissner, A. (2012b). A unique regulatory phase of DNA methylation in the early mammalian embryo. Nature 484, 339-344.

Snell, D.M., and Turner, J.M.A. (2018). Sex Chromosome Effects on Male-Female Differences in Mammals. Curr Biol 28, R1313-r1324.

Soucy, T.A., Smith, P.G., and Rolfe, M. (2009). Targeting NEDD8-Activated Cullin-RING Ligases for the Treatment of Cancer. Clin Cancer Res 15, 3912-3916.

Souroullas, G.P., Jeck, W.R., Parker, J.S., Simon, J.M., Liu, J.Y., Paulk, J., Xiong, J., Clark, K.S., Fedoriw, Y., Qi, J., et al. (2016). An oncogenic Ezh2 mutation induces tumors through global redistribution of histone 3 lysine 27 trimethylation. Nat Med 22, 632-640.

Souza, B.K., da Costa Lopez, P.L., Menegotto, P.R., Vieira, I.A., Kersting, N., Abujamra, A.L., Brunetto, A.T., Brunetto, A.L., Gregianin, L., de Farias, C.B., et al. (2018). Targeting

Histone Deacetylase Activity to Arrest Cell Growth and Promote Neural Differentiation in Ewing Sarcoma. Mol Neurobiol 55, 7242-7258.

Spencer, T.E., Jenster, G., Burcin, M.M., Allis, C.D., Zhou, J., Mizzen, C.A., McKenna, N.J., Onate, S.A., Tsai, S.Y., Tsai, M.-J., et al. (1997). Steroid receptor coactivator-1 is a histone acetyltransferase. Nature 389, 194-198.

Srijyothi, L., Ponne, S., Prathama, T., Ashok, C., and Baluchamy, S. (2018). Roles of Non-Coding RNAs in Transcriptional Regulation. In Transcriptional and Post-Transcriptional Regulation, K. Ghedira, ed. (Intech Open).

Staege, M.S., Hutter, C., Neumann, I., Foja, S., Hattenhorst, U.E., Hansen, G., Afar, D., and Burdach, S.E.G. (2004). DNA Microarrays Reveal Relationship of Ewing Family Tumors to Both Endothelial and Fetal Neural Crest-Derived Cells and Define Novel Targets. Cancer Res 64, 8213-8221.

Stark, B., Mor, C., Jeison, M., Gobuzov, R., Cohen, I.J., Goshen, Y., Stein, J., Fisher, S., Ash, S., Yaniv, I., et al. (1997). Additional chromosome 1q aberrations and der(16)t(1;16), correlation to the phenotypic expression and clinical behavior of the Ewing family of tumors. J Neurooncol 31, 3-8.

Steliarova-Foucher, E., Colombet, M., Ries, L.A.G., Moreno, F., Dolya, A., Bray, F., Hesseling, P., Shin, H.Y., Stiller, C.A., Bouzbid, S., et al. (2017). International incidence of childhood cancer, 2001–10: a population-based registry study. Lancet Oncol 18, 719-731.

Stewart, E., Federico, S.M., Chen, X., Shelat, A.A., Bradley, C., Gordon, B., Karlstrom, A., Twarog, N.R., Clay, M.R., Bahrami, A., et al. (2017). Orthotopic patient-derived xenografts of paediatric solid tumours. Nature 549, 96-100.

Stucki, M., and Jackson, S.P. (2006). γH2AX and MDC1: Anchoring the DNA-damage-response machinery to broken chromosomes. DNA Repair 5, 534-543.

Suh, C.-H., Ordóñez, N.G., Hicks, J., and Mackay, B. (2002). Ultrastructure of the Ewing's Sarcoma Family of Tumors. Ultrastruct Pathol 26, 67-76.

Svoboda, L.K., Bailey, N., Van Noord, R.A., Krook, M.A., Harris, A., Cramer, C., Jasman, B., Patel, R.M., Thomas, D., Borkin, D., et al. (2017). Tumorigenicity of Ewing sarcoma is critically dependent on the trithorax proteins MLL1 and menin. Oncotarget 8, 458-471.

Svoboda, L.K., Harris, A., Bailey, N.J., Schwentner, R., Tomazou, E., von Levetzow, C.,

Magnuson, B., Ljungman, M., Kovar, H., and Lawlor, E.R. (2014). Overexpression of HOX genes is prevalent in Ewing sarcoma and is associated with altered epigenetic regulation of developmental transcription programs. Epigenetics 9, 1613-1625.

Swigut, T., and Wysocka, J. (2007). H3K27 Demethylases, at Long Last. Cell 131, 29-32.

Swords, R.T., Kelly, K.R., Smith, P.G., Garnsey, J.J., Mahalingam, D., Medina, E., Oberheu, K., Padmanabhan, S., O'Dwyer, M., Nawrocki, S.T., et al. (2010). Inhibition of NEDD8-activating enzyme: a novel approach for the treatment of acute myeloid leukemia. Blood 115, 3796-3800.

Taherbhoy, A.M., Huang, O.W., and Cochran, A.G. (2015). BMI1–RING1B is an autoinhibited RING E3 ubiquitin ligase. Nat Commun 6, 7621.

Takigami, I., Ohno, T., Kitade, Y., Hara, A., Nagano, A., Kawai, G., Saitou, M., Matsuhashi, A., Yamada, K., and Shimizu, K. (2011). Synthetic siRNA targeting the breakpoint of EWS/Fli-1 inhibits growth of Ewing sarcoma xenografts in a mouse model. Int J Cancer 128, 216-226.

Talbert, P.B., and Henikoff, S. (2010). Histone variants - ancient wrap artists of the epigenome. Nat Rev Mol Cell Biol 11, 264.

Tanaka, M., Yamazaki, Y., Kanno, Y., Igarashi, K., Aisaki, K., Kanno, J., and Nakamura, T. (2014). Ewing's sarcoma precursors are highly enriched in embryonic osteochondrogenic progenitors. J Clin Invest 124, 3061-3074.

Taverna, S.D., Ueberheide, B.M., Liu, Y., Tackett, A.J., Diaz, R.L., Shabanowitz, J., Chait, B.T., Hunt, D.F., and Allis, C.D. (2007). Long-distance combinatorial linkage between methylation and acetylation on histone H3 N termini. Proc Natl Acad Sci U S A 104, 2086-2091.

Taylor, B.S., Barretina, J., Maki, R.G., Antonescu, C.R., Singer, S., and Ladanyi, M. (2011). Advances in sarcoma genomics and new therapeutic targets. Nat Rev Cancer 11, 541-557.

Teschendorff, A.E., Menon, U., Gentry-Maharaj, A., Ramus, S.J., Weisenberger, D.J., Shen, H., Campan, M., Noushmehr, H., Bell, C.G., Maxwell, A.P., et al. (2010). Age-dependent DNA methylation of genes that are suppressed in stem cells is a hallmark of cancer. Genome Res 20, 440-446.

Thaete, C., Brett, D., Monaghan, P., Whitehouse, S., Rennie, G., Rayner, E., Cooper, C.S.,

and Goodwin, G. (1999). Functional Domains of the SYT and SYT-SSX Synovial Sarcoma Translocation Proteins and Co-Localization with the SNF Protein BRM in the Nucleus. Hum Mol Genet 8, 585-591.

Thomas, G.H., and Elgin, S.C. (1988). Protein/DNA architecture of the DNase I hypersensitive region of the Drosophila hsp26 promoter. EMBO J 7, 2191-2201.

Thompson, A.D., Teitell, M.A., Arvand, A., and Denny, C.T. (1999). Divergent Ewing's sarcoma EWS/ETS fusions confer a common tumorigenic phenotype on NIH3T3 cells. Oncogene 18, 5506-5513.

Tie, F., Banerjee, R., Conrad, P.A., Scacheri, P.C., and Harte, P.J. (2012). Histone demethylase UTX and chromatin remodeler BRM bind directly to CBP and modulate acetylation of histone H3 lysine 27. Mol Cell Biol 32, 2323-2334.

Tie, F., Banerjee, R., Fu, C., Stratton, C.A., Fang, M., and Harte, P.J. (2016). Polycomb inhibits histone acetylation by CBP by binding directly to its catalytic domain. Proc Natl Acad Sci U S A 113, E744-E753.

Tirado, O.M., Mateo-Lozano, S., Villar, J., Dettin, L.E., Llort, A., Gallego, S., Ban, J., Kovar, H., and Notario, V. (2006). Caveolin-1 (CAV1) Is a Target of EWS/FLI-1 and a Key Determinant of the Oncogenic Phenotype and Tumorigenicity of Ewing's Sarcoma Cells. Cancer Res 66, 9937-9947.

Tirode, F., Laud-Duval, K., Prieur, A., Delorme, B., Charbord, P., and Delattre, O. (2007). Mesenchymal Stem Cell Features of Ewing Tumors. Cancer Cell 11, 421-429.

Tirode, F., Surdez, D., Ma, X., Parker, M., Le Deley, M.C., Bahrami, A., Zhang, Z., Lapouble, E., Grossetête-Lalami, S., Rusch, M., et al. (2014). Genomic landscape of Ewing sarcoma defines an aggressive subtype with co-association of STAG2 and TP53 mutations. Cancer Discov 4, 1342-1353.

Tomazou, E.M., Sheffield, N.C., Schmidl, C., Schuster, M., Schönegger, A., Datlinger, P., Kubicek, S., Bock, C., and Kovar, H. (2015). Epigenome mapping reveals distinct modes of gene regulation and widespread enhancer reprogramming by the oncogenic fusion protein EWS-FLI1. Cell Rep 10, 1082-1095.

Tsubota, S., Kishida, S., Shimamura, T., Ohira, M., Yamashita, S., Cao, D., Kiyonari, S., Ushijima, T., and Kadomatsu, K. (2017). PRC2-Mediated Transcriptomic Alterations at the Embryonic Stage Govern Tumorigenesis and Clinical Outcome in MYCN-Driven

Neuroblastoma. Cancer Res 77, 5259-5271.

Turc-Carel, C., Phiklip, I., Berger, M.P., Philip, T., Lenoir, G.M. (1983). Chromosomal translocations in Ewings sarcoma. N Engl J Med 309, 497-498.

Uckelmann, M., and Sixma, T.K. (2017). Histone ubiquitination in the DNA damage response. DNA Repair 56, 92-101.

Unland, R., Borchardt, C., Clemens, D., Kool, M., Dirksen, U., and Frühwald, M. (2015). Analysis of the antiproliferative effects of 3-deazaneoplanocin A in combination with standard anticancer agents in rhabdoid tumor cell lines. Anticancer Drugs 26, 301-311.

Unnikrishnan, A., Gafken, P.R., and Tsukiyama, T. (2010). Dynamic changes in histone acetylation regulate origins of DNA replication. Nat Struct Mol Biol 17, 430-437.

Urano, F., Umezawa, A., Yabe, H., Hong, W., Yoshida, K., Fujinaga, K., and Hata, J. (1998). Molecular analysis of Ewing's sarcoma: another fusion gene, EWS-E1AF, available for diagnosis. Jpn J Cancer Res 89, 703-711.

Ushigome, S., Machinami, R., and Sorensen, P.H. (2002). Ewing sarcoma/primitive neuroectodermal tumour (PNET). In World Health Organization Classification of Tumours. Pathology and Genetics of Tumours of Soft Tissue and Bone., C.D.M. Fletcher, Unni, K.K., Mertens, F. , ed. (Lyon (France): IARC Press), pp. 298-300.

van der Meulen, J., Sanghvi, V., Mavrakis, K., Durinck, K., Fang, F., Matthijssens, F., Rondou, P., Rosen, M., Pieters, T., Vandenberghe, P., et al. (2015). The H3K27me3 demethylase UTX is a gender-specific tumor suppressor in T-cell acute lymphoblastic leukemia. Blood 125, 13-21.

Van der Meulen, J., Speleman, F., and Van Vlierberghe, P. (2014). The H3K27me3 demethylase UTX in normal development and disease. Epigenetics 9, 658-668.

van Doorninck, J.A., Ji, L., Schaub, B., Shimada, H., Wing, M.R., Krailo, M.D., Lessnick, S.L., Marina, N., Triche, T.J., Sposto, R., et al. (2010). Current treatment protocols have eliminated the prognostic advantage of type 1 fusions in Ewing sarcoma: a report from the Children's Oncology Group. J Clin Oncol 28, 1989-1994.

van Haaften, G., Dalgliesh, G.L., Davies, H., Chen, L., Bignell, G., Greenman, C., Edkins, S., Hardy, C., O'Meara, S., Teague, J., et al. (2009). Somatic mutations of the histone H3K27 demethylase gene UTX in human cancer. Nat Genet 41, 521-523.

Van Mater, D., and Wagner, L. (2019). Management of recurrent Ewing sarcoma: challenges and approaches. Onco Targets Ther 12, 2279-2288.

Vanden Heuvel, J.P., Maddox, E., and Maalouf, S.W. (2018). Replication Study: Systematic identification of genomic markers of drug sensitivity in cancer cells. eLife 7, e29747.

Varambally, S., Dhanasekaran, S., Zhou, M., Barrette, T.R., ., Kumar-Sinha, C., Sanda, M.G., Ghosh, D., Pienta, K.J., Sewalt, R.G., Otte, A.P., et al. (2002). The polycomb group protein EZH2 is involved in progression of prostate cancer. Nature 419, 624-629.

Verma, V., Denniston, K.A., Lin, C.J., and Lin, C. (2017). A Comparison of Pediatric vs. Adult Patients with the Ewing Sarcoma Family of Tumors. Front Oncol 7, 82.

Vigfusson, N.V., Allen, L.J., Phillips, J.H., Alschibaja, T., and Riches, W.G. (1986). A neuroendocrine tumor of the small intestine with a karyotype of 46,XY,t(11;22). Cancer Genet Cytogenet 22, 211-218.

Vittal, V., Stewart, M.D., Brzovic, P.S., and Klevit, R.E. (2015). Regulating the Regulators: Recent Revelations in the Control of E3 Ubiquitin Ligases. J Biol Chem 290, 21244-21251.

Vitte, J., Gao, F., Coppola, G., Judkins, A.R., and Giovannini, M. (2017). Timing of Smarcb1 and Nf2 inactivation determines schwannoma versus rhabdoid tumor development. Nat Commun 8, 300.

von Heyking, K., Roth, L., Ertl, M., Schmidt, O., Calzada-Wack, J., Neff, F., Lawlor, E.R., Burdach, S., and Richter, G.H. (2016). The posterior HOXD locus: Its contribution to phenotype and malignancy of Ewing sarcoma. Oncotarget 7, 41767-41780.

von Levetzow, C., Jiang, X., Gwye, Y., von Levetzow, G., Hung, L., Cooper, A., Hsu, J.H., and Lawlor, E.R. (2011). Modeling initiation of Ewing sarcoma in human neural crest cells. PLoS One 6, e19305.

Voss, A.K., Collin, C., Dixon, M.P., and Thomas, T. (2009). Moz and Retinoic Acid Coordinately Regulate H3K9 Acetylation, Hox Gene Expression, and Segment Identity. Dev Cell 17, 674-686.

Waddington, C.H. (1942). Canalization of development and the inheritance of acquired characters. Nature 150, 563-565.

Wagner, M.J., Gopalakrishnan, V., Ravi, V., Livingston, J.A., Conley, A.P., Araujo, D.,

Somaiah, N., Zarzour, M.A., Ratan, R., Wang, W.L., et al. (2017). Vincristine, Ifosfamide, and Doxorubicin for Initial Treatment of Ewing Sarcoma in Adults. Oncologist 22, 1271-1277.

Walport, L.J., Hopkinson, R.J., Vollmar, M., Madden, S.K., Gileadi, C., Oppermann, U., Schofield, C.J., and Johansson, C. (2014). Human UTY(KDM6C) Is a Male-specific Nϵ-Methyl Lysyl Demethylase. J Biol Chem 289, 18302-18313.

Wang, C., Lee, J.E., Cho, Y.W., Xiao, Y., Jin, Q., Liu, C., and Ge, K. (2012). UTX regulates mesoderm differentiation of embryonic stem cells independent of H3K27 demethylase activity. Proc Natl Acad Sci U S A 109, 15324-15329.

Wang, H., Wang, L., Erdjument-Bromage, H., Vidal, M., Tempst, P., Jones, R.S., and Zhang, Y. (2004). Role of histone H2A ubiquitination in Polycomb silencing. Nature 431, 873-878.

Wang, S.P., Tang, Z., Chen, C.W., Shimada, M., Koche, R.P., Wang, L.H., Nakadai, T., Chramiec, A., Krivtsov, A.V., Armstrong, S.A., et al. (2017). A UTX-MLL4-p300 Transcriptional Regulatory Network Coordinately Shapes Active Enhancer Landscapes for Eliciting Transcription. Mol Cell 67, 308-321.

Wang, Y., Mandal, D., Wang, S., Hughes, D., Pollock, R.E., Lev, D., Kleinerman, E., and Hayes-Jordan, A. (2009). Inhibiting Platelet-derived Growth Factor β Reduces Ewing's Sarcoma Growth and Metastasis in a Novel Orthotopic Human Xenograft Model. In Vivo 23, 903-909.

Watson, I.R., Li, B.K., Roche, O., Blanch, A., Ohh, M., and Irwin, M.S. (2009). Chemotherapy induces NEDP1-mediated destabilization of MDM2. Oncogene 29, 297-304.

Watson, S., Perrin, V., Guillemot, D., Reynaud, S., Coindre, J.M., Karanian, M., Guinebretiere, J.M., Freneaux, P., Le Loarer, F., Bouvet, M., et al. (2018). Transcriptomic definition of molecular subgroups of small round cell sarcomas. J Pathol 245, 29-40.

Weber, C.M., and Henikoff, S. (2014). Histone variants: dynamic punctuation in transcription. Genes Dev 28, 672-682.

Wei, G.H., Badis, G., Berger, M.F., Kivioja, T., Palin, K., Enge, M., Bonke, M., Jolma, A., Varjosalo, M., Gehrke, A.R., et al. (2010). Genome-wide analysis of ETS-family DNA-binding in vitro and in vivo. EMBO J 29, 2147-2160.

Welstead, G.G., Creyghton, M.P., Bilodeau, S., Cheng, A.W., Markoulaki, S., Young, R.A.,

and Jaenisch, R. (2012). X-linked H3K27me3 demethylase Utx is required for embryonic development in a sex-specific manner. Proc Natl Acad Sci U S A 109, 13004-13009.

Wen, H., Schaller, M.A., Dou, Y., Hogaboam, C.M., and Kunkel, S.L. (2008). Dendritic cells at the interface of innate and acquired immunity: the role for epigenetic changes. J Leukoc Biol 83, 439-446.

Whang-Peng, J., Triche, T.J., Knutsen, T., Miser, J., Douglass, E.C., and Israel, M.A. (1984). Chromosome translocation in peripheral neuroepithelioma. N Engl J Med 311, 584-585.

Whang-Peng, J., Triche, T.J., Knutsen, T., Miser, J., Kao-Shan, S., Tsai, S., and Israel, M.A. (1986). Cytogenetic characterization of selected small round cell tumors of childhood. Cancer Genet Cytogenet 21, 185-208.

Widhe, B., and Widhe, T. (2000). Initial symptoms and clinical features in osteosarcoma and Ewing sarcoma. J Bone Joint Surg Am 82, 667-674.

Womer, R.B., West, D.C., Krailo, M.D., Dickman, P.S., Pawel, B.R., Grier, H.E., Marcus, K., Sailer, S., Healey, J.H., Dormans, J.P., et al. (2012). Randomized controlled trial of interval-compressed chemotherapy for the treatment of localized Ewing sarcoma: a report from the Children's Oncology Group. J Clin Oncol 30, 4148-4154.

Woodcock, C.L., and Dimitrov, S. (2001). Higher-order structure of chromatin and chromosomes. Curr Opin Genet Dev 11, 130-135.

Woodcock, C.L., Skoultchi, A.I., and Fan, Y. (2006). Role of linker histone in chromatin structure and function: H1 stoichiometry and nucleosome repeat length. Chromosome Res 14, 17-25.

Woodcock, D.M., Crowther, P.J., and Diver, W.P. (1987). The majority of methylated deoxycytidines in human DNA are not in the CpG dinucleotide. Biochem Biophys Res Commun 145, 888-894.

Wu, C., Kang, H., Yang, W., Wu, J., Jeong, Y.S., Wang, J., Chan, C., Lee, S., Zhang, X., Lamothe, B., et al. (2011). Critical Role of Monoubiquitination of Histone H2AX Protein in Histone H2AX Phosphorylation and DNA Damage Response. J Biol Chem 286, 30806-30815.

Wu, J., Lin, H., Hu, Y., and Chien, C. (2005). Neddylation and deneddylation regulate Cul1 and Cul3 protein accumulation. Nat Cell Biol 7, 1014-1020.

Wu, Q., Tian, Y., Zhang, J., Tong, X., Huang, H., Li, S., Zhao, H., Tang, Y., Yuan, C., Wang, K., et al. (2018). In vivo CRISPR screening unveils histone demethylase UTX as an important epigenetic regulator in lung tumorigenesis. Proc Natl Acad Sci U S A 115, E3978-E3986.

Wu, S.C., and Zhang, Y. (2010). Active DNA demethylation: many roads lead to Rome. Nat Rev Mol Cell Biol 11, 607-620.

Xia, S.J., Pressey, J.G., and Barr, F.G. (2002). Molecular pathogenesis of rhabdomyosarcoma. Cancer Biol Ther 1, 97-104.

Xie, G., Liu, X., Zhang, Y., Li, W., Liu, S., Chen, Z., Xu, B., Yang, J., He, L., Zhang, Z., et al. (2017). UTX promotes hormonally responsive breast carcinogenesis through feed-forward transcription regulation with estrogen receptor. Oncogene 36, 5497-5511.

Xie, Y., Skytting, B., Nilsson, G., Brodin, B., and Larsson, O. (1999). Expression of Insulin-like Growth Factor-1 Receptor in Synovial Sarcoma: Association with an Aggressive Phenotype. Cancer Res 59, 3588-3591.

Xiong, X., Zhang, J., Liang, W., Cao, W., Qin, S., Dai, L., Ye, D., and Liu, Z. (2016). Fuse-binding protein 1 is a target of the EZH2 inhibitor GSK343, in osteosarcoma cells. Int J Oncol 49, 623-628.

Xu, Y., and Price, B.D. (2011). Chromatin dynamics and the repair of DNA double strand breaks. Cell Cycle 10, 261-267.

Yang, J., Hamid, O., and Carvajal, R.D. (2018). The Need for Neddylation: A Key to Achieving NED in Uveal Melanoma. Clin Cancer Res 24, 3477-3479.

Young, M.D., Willson, T.A., Wakefield, M.J., Trounson, E., Hilton, D.J., Blewitt, M.E., Oshlack, A., and Majewski, I.J. (2011). ChIP-seq analysis reveals distinct H3K27me3 profiles that correlate with transcriptional activity. Nucleic Acids Res 39, 7415-7427.

Zhao, Y., Morgan, M.A., and Sun, Y. (2014). Targeting Neddylation pathways to inactivate cullin-RING ligases for anticancer therapy. Antioxid Redox Signal 21, 2383-2400.

Zhou, L., Jiang, Y., Luo, Q., Li, L., and Jia, L. (2019). Neddylation: a novel modulator of the tumor microenvironment. Mol Cancer 18, 77.

Zhou, V.W., Goren, A., and Bernstein, B.E. (2010). Charting histone modifications and the functional organization of mammalian genomes. Nat Rev Genet 12, 7-18.

Zoubek, A., Dockhorn-Dworniczak, B., Delattre, O., Christiansen, H., Niggli, F., Gatterer-Menz, I., Smith, T.L., Jurgens, H., Gadner, H., and Kovar, H. (1996). Does expression of different EWS chimeric transcripts define clinically distinct risk groups of Ewing tumor patients? J Clin Oncol 14, 1245-1251.

Zucman, J., Melot, T., Desmaze, C., Ghysdael, J., Plougastel, B., Peter, M., Zucker, J.M., Triche, T.J., Sheer, D., and Turc-Carel, C. (1993). Combinatorial generation of variable fusion proteins in the Ewing family of tumours. EMBO J 12, 4481-4487.